

TECHNICAL UNIVERSITY OF CLUJ-NAPOCA
FACULTY OF MACHINE BUILDING



**MEDICAL ROBOTIC SYSTEMS
WITH APPLICATION IN SURGERY,
ONCOLOGY AND REHABILITATION**

HABILITATION THESIS

CĂLIN VAIDA

CLUJ-NAPOCA, 2018

Contents

***“Promise me you’ll always remember:
You’re braver than you believe,
And stronger than you seem,
And smarter than you think.”***

(A good friend of mine)

Title	Page
Introduction	
Chapter 1. Robotics in medicine - From surgery towards cancer treatment and post-stroke rehabilitation	1
Chapter 2. Surgical robotics and devices	27
Chapter 3. Robotic systems for brachytherapy	63
Chapter 4. Advanced systems for minimally invasive percutaneous therapy	107
Chapter 5. Robotic rehabilitation of the upper limb	145
Chapter 6. Some final thoughts	175
References	

"A wise man should consider that health is the greatest of human blessings, and learn how by his own thought to derive benefit from his illnesses." (Hippocrates)

Introduction

Scientific research has always been one of the most difficult but also rewarding fields of work helping humanity to make advancements in knowledge. The ultimate goal of this endeavour is the progress of human kind which is met in every aspect of life. Like many other domains available to a reduced percentage of the population scientific research itself evolved in time on multiple aspects, as pointed out is the work [Nii 15], entitled “Scientific Progress” and integrated in the Stanford Encyclopaedia of Philosophy:

- Economical – *the continuous increase of funding for scientific research;*
- Professional – *the rising status of scientists and their institutions within society;*
- Educational – *the continuous increase of the skill and expertise of scientists;*
- Methodical – *the invention of the research methods along with now scientific instruments;*
- Cognitive – *increase and advancement of scientific knowledge.*

In an abstract approach scientific progress must influence in a positive way *technological progress* (or the overall increase of technology) and *social progress* (with direct influence on the humanity through prosperity, quality of life and justice in society).

With great power comes great responsibility!!! - A simple yet very strong statement which, throughout history has been found in the Bible, later on used in the French Revolution in 1793 and individuals like *Lord Melbourne, Winston Churchill, Teddy Roosevelt, and Franklin D. Roosevelt* can also encompass our role and duty towards society as to use in the most efficient way our time and available resources while delivering advancement. Many times, when facing new challenges, this aspect becomes a burden but also a motivation in the continuous search for answers. This is how I personally perceive our position in today’s society as educated seekers of knowledge and creators of solutions to unanswered questions.

The following work will summarize in a descriptive form my activity as a scientific researcher in the period following my Doctoral Thesis defence. Even though this habilitation thesis has an individual character all the achievements are the result of the joint effort of the team from CESTER (Research Center for Industrial Robots Simulation and Testing). I strongly believe that apart from the occasional geniuses who can provide themselves both unsolvable problems and their solutions it is compelling for us to work in competitive and complementary teams maximizing the output of our effort.

This thesis invites you, the reader, in an evolutionary journey of **Robotics in Medicine** presenting the major achievements to which I have contributed in the last eight years in:

- Minimally invasive robotic assisted surgery;
- Targeted treatment options of cancer using robotic guided instrumentation;
- Robotic assisted rehabilitation of post-stroke patients.

In the end, I state my continuous motivation towards scientific research believing that I have reached the maturity to work alongside younger colleagues and guide their first steps towards their education as scientific researchers through doctoral studies.

Chapter 1. Robotics in medicine

From surgery towards cancer treatment and post-stroke rehabilitation

*“He who knows all the answers has not been asked all the questions.”
(Confucius)*

An overview of the field of robotics in medicine

Robotics has slowly entered every domain where progress imposed activities/ actions that were beyond the natural capabilities of humans. The most relevant example in this sense is the industry with all its branches where the higher and higher level of quality and output capacity have imposed the use of specialised devices that could perform faster and more reliable. From highly repetitive activities to heavy lifting, 24 hours shifts and so on, the responsibilities of the human workers have shifted towards the setup, programming and maintenance of the production lines. Without going into further details, just to emphasize the criticality of these manufacturing lines, the reliability of an industrial robot is over 99,9999%.

However, there are other fields of work, where classical industrial robots cannot be integrated, imposing the development of personalized, dedicated solution which would fit perfectly a certain task. Such case is the medical field where, especially when taking about direct interaction between the robot and the patient, the robot will never act based on pre-defined programs but rather as an advanced, highly capable, accurate and safe device.

In medicine, notable achievements which refer to the use of robotics for different tasks date from the early 80s while in our days there are multiple situation where robotic assisted procedures represent the gold standard for certain medical treatments. As one can state that medical robotics have reached a certain level of maturity the future development has to be achieved in an organized manner identifying the areas where such devices can have a positive impact in an economically feasible context.

Making a generic comparison between an industrial manufacturing process where robots have been introduced to increase the productivity and thus the financial efficiency, in medicine the main purpose of a robotic device is to improve the quality of life for the patient. Nevertheless, as cruel as it may sound, in order to enable the access of the large population to such a better treatment option this must be also economically feasible.

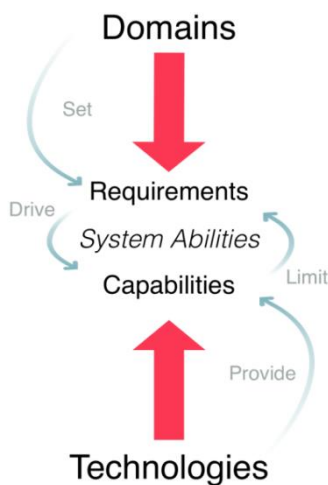
For that, one of the most difficult tasks is to properly identify the medical areas where the need of robotics is most dire and then, to find development solutions that will lead towards efficient devices. At European level, this endeavour has been assumed in the last years by the euRobotics AISBL, a non-profit organization which has been created following the good results of a former EU project. At the moment, all the important European players (universities, research institutes and private companies) which work in robotics have joined this organization, whose main purpose is to define a comprehensive strategy for the future development of EU

robotics, taking into account both the worldwide achievements and the actual needs of the EU population and industry.

To support this, the European Council is launching all the ICT calls with topics based on the strategy defined by euRobotics, namely the Multi Annual Roadmap [MAR 17]. Quoting from euRobotics:

“The goals of the Roadmap are:

- *To provide a common framework of description for robotics within Europe;*
- *To provide a clear set of goals for market relevant technical development;*
- *To illustrate the relevance of these goals with respect to future market opportunity.*



The descriptive framework used within the MAR allows comparison between and within projects when referring to robotics technology and systems and helps to link technology development with user driven market needs. This is a conventional Road-mapping activity with market domains setting requirements and technologies driving capabilities that fulfil those requirements. The approach uses non-domain specific and non-technology specific System Abilities to map market requirements to technology capabilities and vice versa. This common goal approach helps identify the cross cutting technologies that impact on multiple market domains while allowing unforeseen

technology developments to be integrated by referring to System Ability independently of technology.

The roadmap identifies opportunities for innovation, current technical capability and sets out the R&D&I agenda for each domain.”

Our university, through our research center, CESTER, is affiliated to this organization since 2015 and our research topics have been defined in accordance to the European strategic agenda.

European strategic agenda for robotics in healthcare

One of the major changes with multiple implications in the field of healthcare is represented by the demographic changes of the population. More specifically, Europe is facing an increase of the life expectancy whereas, in 2008 the population aged over 65 represented something around 17% this will increase to over 30% by 2060 while the population aged over 80 will shift from 4.4% to over 12% (EUROSTAT projections). Even on national level, a comparison between the last two demographic evaluations there is a reported increase of over 20% of the elderly population (aged over 60).

While it is clear that the elderly population has a greater tendency towards different medical conditions, the healthcare system will slowly become incapable of properly care for all the patients, while aiming towards a continuous increase of the life quality. On one hand this is due to the natural increase in medical costs and on the other hand due to the logical decrease in the number of healthcare givers with respect to the number of existing patients. On the positive side, all the existing studies have already raised these issues and solutions are thought to prepare the society for the future.

The only logical approach is to find ways for improving the overall efficiency of the medical act with economically feasible solutions that will enable (without detailing at this time the targeted diseases):

- Minimization of the “collateral damage” or the side effects of different curative treatments;
- Improvement of long-term diseases management allowing a single caregiver to monitor, advise, treat and support more patients in the same time;
- Develop solutions that allow personalized treatments that will maximize the treatment outcome;
- Develop solutions for “home use” long time treatments that would allow patients to stay in their own environment.

In order to achieve these conceptual needs, the European Commission has identified three major areas of interest where robotics would play an important role:

Clinical robotics: refer to robotic systems that interact directly with the patient supporting the “care” and “cure” processes. Some areas where such robots would apply are: diagnosis, treatment, surgical interventions and medication and also emergency. They would be used by trained medical personnel.

Rehabilitation: refer to robotic system that would be used following a medical condition (traumatic, post-operative or neurological) where their direct physical interaction with the patient would either enhance the recovery process or act as a replacement for a lost function.

Assistive robotics: refer to secondary aspects related to the medical process, providing assistance to the healthcare givers of the patients.

In the research activity within CESTER, the team has developed multiple innovative solutions in two of these areas of interest, which will be detailed in the following chapters of this thesis.

A. Clinical Robotics

As mentioned before, clinical robotics covers three major areas of intervention: surgery, diagnosis and therapy. The overall potential for clinical robotics is huge because their development would bring benefits in virtually all areas medical specialities aiming to boost the overall outcome of the procedures.

Surgical Robots

With respect to surgery, mainly through the da Vinci robotic system, the United States have a very strong intellectual property (IP) coverage and thus, this field imposes the development of radically new strategies (hardware, software and control) together with the initial development costs which are very high imposing also a timely clinical validation.

The main area of intervention where surgical robots fit is minimally invasive surgery (MIS). Considered by many a quite recent surgical approach, in reality, the first documented minimally invasive procedure dates back from 1901 when Kelling [KEL01] reported the results of a procedure performed on a dog model where he attempted to control the blood loss in the abdomen by insufflation of high pressure air in the abdominal area. Later in the same year, a second minimally invasive procedure is reported by Ott [OTT01] who examined the peritoneal cavity of a pregnant woman using a head mirror and a speculum. Ten years later, in 1911, new reports from Sweden, by Jacobeus [JAC11], and United States, by Bernheim [BER11] present new achievement of minimally invasive procedures on humans. Following this pioneering age the 20th century was the birth of minimally invasive surgery with a continuous development of surgical tools, visions systems and along with them techniques that would gradually change the way surgery is performed. Without detailing too much these advancements one must note several great surgeons which contributed to the progress of MIS: Kurt Semm [SEM83], Mouret [MOU96] and Erich Muhe [LIT98]. Like many other pioneering technique it took some time for MIS to be widely accepted in the operating room, but slowly it became the gold standard for most procedures performed in the abdominal area.

The evolution of robotic surgery is somehow similar, with its major milestones and share of criticism during the early stages of development. One of the first documents which describes the idea of robotic surgery and also defines the particularity of the motion of such devices was published by Russel Taylor in 1995 [TAY95]. In his paper Taylor introduces the concept of Remote Center of Motion (RCM), defining the entrance point in the abdomen as a fixed point within the workspace of a surgical robot, through which the instruments are introduced inside the human body (figure 1). Based on figure one, in can be stated that with respect

point B (the entry point in the patient body) the instrument can achieve 4 independent motions:

- **In spherical coordinates:** two rotations that would position the point E on a surface of a “sphere” with radius BE, one translation along the A-B-E segment or the longitudinal axis of the instrument and one rotation around the same axis;
- **In Cartesian coordinates:** three translations which enable the positioning of the point E in space with respect to the point B and one rotation around the longitudinal axis of the instrument.

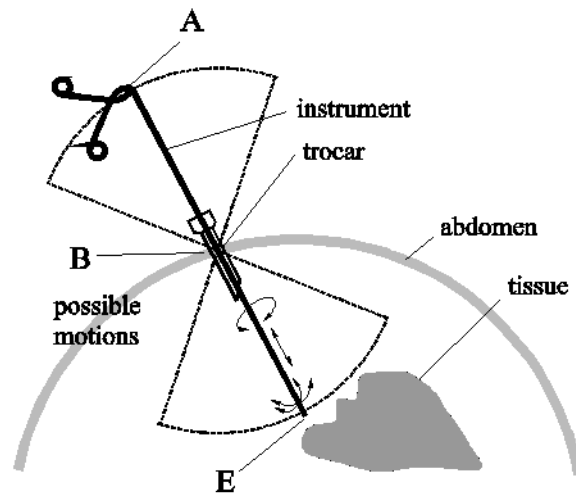


Figure 1.1. The motion of a surgical instrument inside the human body in MIS [VA112]

Furthermore, the instruments used in the MIS can be grouped in two categories:

- The endoscopic camera (the laparoscope, figure 2): which is basically a device which has a set of lenses and a camera on top which with the help of a light source provides intra-operative images during the procedure – this device will not enter into physical contact with the internal organs;
- Surgical instruments (figure 3): surgical tools of different complexity, which have at the distal head a special configuration that allows the performing of a certain procedure and a special handle at the opposite end from which the surgeon operates the instrument.

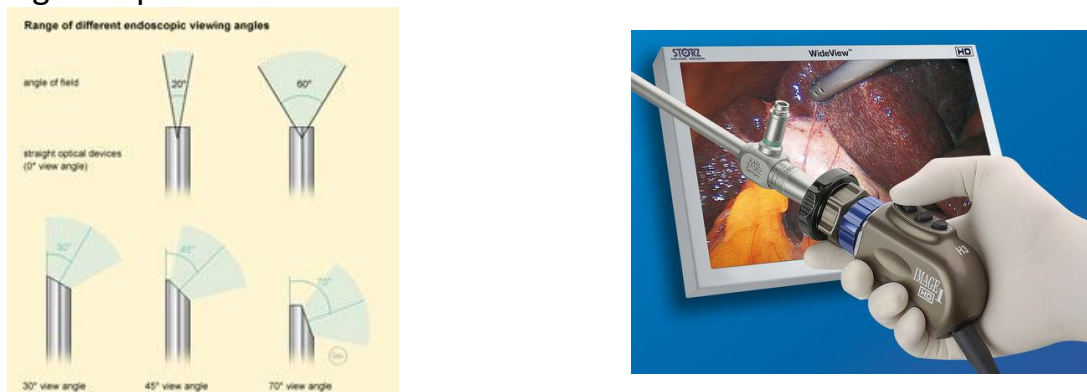


Figure 1.2. Laparoscopic camera (left – viewing angles, right – proximal head)



Figure 1.3. Different types of laparoscopic instruments

While acknowledging the uncontested advantages that the da Vinci system has brought in robotic surgery, imposing even as gold standard in multiple procedures, there is still room for improvement whereas typical requests refer to:

- **improved dexterity** – development of new systems that would allow more freedom in the positioning of the entry ports, improvement of the overall dexterity of the instruments to increase their reach;
- **increased efficiency** – development of new systems that would allow a faster and safer patient – robot relative positioning thus reducing the initial setup phase while allowing the surgeon more freedom in the positioning of the instruments;
- **additional feedback** – development of systems that would provide additional real-time relevant data for the surgeon during the procedure, where one particular aspect is still an open problem for all systems: the force feedback.

Making an overview of the general advantages of robotic surgery the following must be underlined, in comparison to classical minimally invasive procedures:

- faster recovery, reduced scaring and trauma, less tissue damage and lower exposure to radiation. These are determined by the fact that robotic procedures bring additional dexterity and motion scaling;
- access to new, enhanced techniques. These are determined by the development of new instruments, dedicated and optimized towards a certain application.

Overview of the minimally invasive procedures

Advancing hand in hand with technology, minimally invasive robotic assisted procedures have evolved in the last years towards multiple new approaches that can be classified into two main categories:

- Pure minimally invasive surgical procedures that aimed a continuous reduction of scaring and collateral damage while maximizing the surgical outcome;

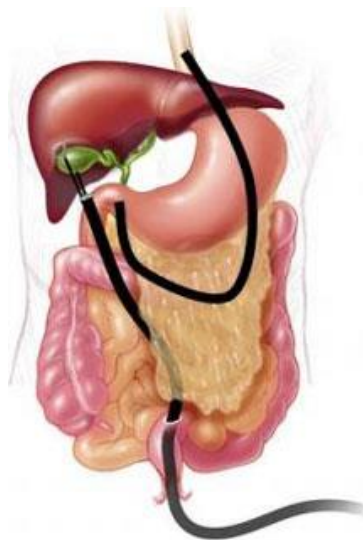
- Minimally invasive non-surgical techniques that provide specific treatments for patients where surgery is not an option, with emphasis here on targeted cancer treatment.

Evolution of minimally invasive surgery (MIS)

As MIS is considered to have approached the maximum level of performance with respect to the patient comfort and post-operative recovery new techniques have been developed to minimize even more the side effects of surgical interventions:

- NOTES (Natural Orifice Transluminal Endoscopic Surgery), and
- SILS (Single- Incision Laparoscopic Surgery).

NOTES (fig. 4) is an experimental surgical technique where operations can be performed with a dedicated specialized instrument (which integrates a camera and two or three instruments that are all integrated in a single, dexterous tube) which is passed through a natural orifice (mouth, urethra, anus, etc.) followed by an internal incision into the stomach, vagina, bladder or colon, thus avoiding any other external incisions [BIN14].



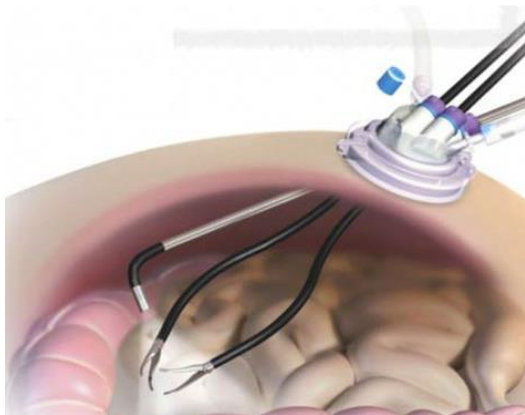
NOTES access routes towards internal organs



ANUBIS – a device for NOTES

Figure 1.4. Access routes and typical devices for NOTES

SILS (fig. 5) as the name suggests, means the introduction of all the surgical tools (camera and instruments) through a narrow port of 15 - 20 mm, or the use of multilumen trocar forcing the surgeon to work in awkward positions, with crossing instruments, etc. Due to the very close positions of the instruments the procedure dexterity is very low and the workspace is decreased, but for certain cases it represents a viable alternative. SILS is also a challenging field for robotic approaches as by using highly dexterous instruments, the natural disadvantages of this technique can be reduced [VAI12].



SILS procedure – concept view



SILS procedure (Courtesy of University Clinical Hospital Barcelona, Spain)

Figure 1.5. Single Incision Laparoscopic Surgery

While the real benefits of NOTES are somehow doubtful, as shown in [BES 10] and [KAM11], SILS already represents a real benefit for patients suitable for this procedure. Compared to classical or MIS procedures, the benefits for patients are: decreased pain, even shorter recovery period (counted in hours), lower morbidity, reduced cost and superior cosmetics. Kamran, Patel and others published a review [KAM11] where they analysed several hundreds of cases before pointing out these advantages.

From a personal perspective, NOTES was a wonderful idea, which aimed to integrate multiple instruments into a single flexible tube. However, even though there are no external scars left by NOTES there are unnecessary internal scars (in the stomach wall, inside the vagina or the colon) which cannot be supervised as an external one, and in time these scars could lead to serious complications even cancer. SILS, as a personal consideration, has a much higher potential but surgeons should choose carefully the patients that can be operated in this way. Furthermore, with adequate research in terms of highly dexterous devices, SILS use can be extended and its benefits maximized.

Minimally invasive non-surgical procedures for cancer

Cancer, considered the disease of the XXI century, is one open problem in which every progress means a step forward in the fight between life and death. The fight against cancer has two main components strongly interconnected: **diagnosis** and **treatment**. An early, accurate diagnosis can provide the means for local targeted treatment of the tumours with excellent life expectancy. Thus, the proper diagnosis and staging of cancer [FIL14, MEE13] is the first step towards a positive prognosis for a cancer patient.

Prostate cancer – diagnosis and treatment. In order to emphasize the importance of accurate diagnosis and treatment a short statement is made regarding prostate cancer. This is the most widely spread type of cancer and because of that extensive research has been done to treat it. Even the most advanced surgical robotic device, Da Vinci, was initially developed for prostate surgery. Prostate cancer has also two extreme characteristics: it is 100% curable but also the 2nd deadliest type of cancer. Statistically it was proven that the 5 years survival rates by stage of diagnosis is nearly 100% for local and regional spread dropping to 28% for distant tumours. This means that if detected early prostate cancer can be cured but when it has spread in the body it will eventually cause the death of the patient. The current gold standard has high percentages of false negative results in early stages supporting the worldwide efforts in finding new, accurate ways of diagnosis for this disease.

Cancer Diagnosis. Described in a very roughly way, cancer diagnosis refers to the identification of malignant tumours that grow inside the body. There are several imagistic, non-invasive methods, (CT and MRI and their derivate) which provide high contrast and high resolution images of the internal structure of the body but they have certain limitations [VER12] (identifying the nature of the tumour, the correct indication of the cancer stage, etc.) whereas the most conclusive investigation remains the biopsy of the tissue.

Cancer treatment. The therapeutic index in the treatment of cancer stands for optimizing the treatment in such a way that the benefit of a therapy for the patient largely exceeds its' toxicity. However, this threshold is seldom obvious. In a **curative** intended scenario, this is due mainly to the need of multiple treatments for the same cancer, i.e. surgery, irradiation or/ and chemotherapy, each one with its own profile of side effects. On the other hand, in a **palliative** setting, for very advanced stages of cancer or for very frail patients, a procedure might be considered too invasive or costly to be justified. From the **spread** point of view cancer treatment can be roughly divided into two main categories: local, targeted treatments (brachytherapy [SHA13, KHA14], radiofrequency ablation [TIL14, KEN13, BIR14, VOG13]) and widespread treatments (external radiation, chemotherapy).

A reasonable conclusion for **the enhancement of cancer treatment** would be **to perform accurate early diagnosis to identify potential malignant tumours in early stages and to perform local targeted treatment to destroy the tumours in both curative and palliative approaches.**

In order to provide a clear view of the targeted procedures, each single one will be shortly defined:

- **Biopsy:** the prelevation of tissue from inside an organ by using a special needle [LEE14] (core biopsy needle or aspiration needle) – schematic view (fig. 6.a);

- **Brachytherapy:** the positioning of radioactive seeds (with high but locally distributed radiation) directly in the tumour without damaging the proximal healthy tissues (fig. 6.b);
- **Radiofrequency ablation:** the ablation of a tumour using the heat generated from a high frequency alternating current [NEA11], (fig. 6.c).

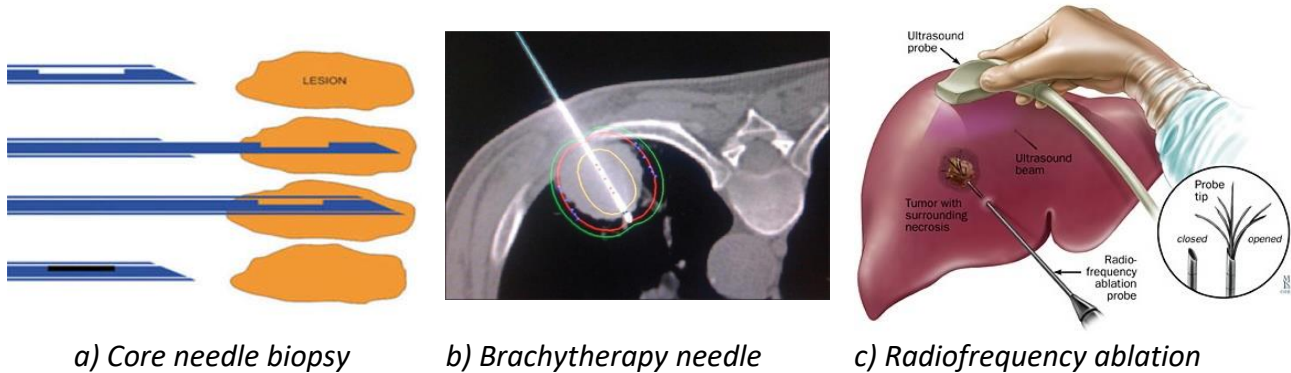


Figure 1.6. Needle guided procedures in the diagnosis and treatment of cancer

The two procedures share a common requirement which restricts their development: the need of a highly accurate targeting solution which could reach a defined point inside the human body with an overall accuracy of 1 mm, which is well beyond the human natural capabilities, as shown in [STR11, POD14]. The first researches in this field proposed robotic solutions which targeted a specific organ (e.g. robots for prostate brachytherapy and biopsy) but no general use solution has been developed so far. A very recent report [POD14] (August 2014) published by AAPM (American Association of Physicists in Medicine) makes a very thorough review of all achievements in robotic brachytherapy presenting 13 robotic solutions (12 for prostate and one for lung cancer) emphasizing the need of additional solutions and proposing also a guideline for their characteristics.

The curative potential of brachytherapy

Brachytherapy, also known as internal radiation, enables the delivery of higher doses of radiation to more-specific areas of the body, compared with the conventional form of radiation therapy (external beam radiation) that projects radiation from a machine outside the body. Basically, **brachytherapy consists of irradiating a tumour from inside it**, by placing in or just next to the tumour one or several miniaturized radioactive sources (1 mm diameter), via plastic or metallic catheters. The **gradient of the radiation dose decreases abruptly** with the distance to the source, according to an inverse square law (i.e. at 10 mm from the source we will have one quart of the 5 mm dose). That means **a very high dose can be delivered to a well-defined area**, without damaging the healthy tissue in the immediate vicinity. However, **the precision of the radioactive placement is crucial**, as a geographical miss of a part of the tumour might cause a recurrence, whereas

inserting the catheters outside the tumour will profoundly and uselessly irradiate healthy tissue, inducing necrosis and severe complications.

Being a procedure which targets a specific, local area of the body (where the tumour or cancerous cells are located) it implies the placement of specific devices inside into the body tissue. Unfortunately, there are many areas of the body, such as the retroperitoneal area (representing the most posterior zone of the abdominal cavity) or the mediastinum where the access to the tumour area imposes a highly invasive surgery that cannot be tolerated by the majority of cancer patients due to the systemic frailty caused by their illness. The procedure is minimally invasive but should be performed by radiotherapists which sometimes tend to avoid this approach because of its “bloody” nature. However, due to its potential both for curative and palliative purposes brachytherapy is one of the therapies widely studied in research centres all over the world, the next decade foreseeing its use on a large scale. New generations of robotic devices could have the technical capabilities to satisfy the accuracy required by the procedure this being one of the topics of interest in this thesis.

To emphasize even more the potential of this procedure, the next table illustrates a set of clinical cases which, with the help of brachytherapy could have evolved differently.

Table 1. Clinical cases which could benefit from brachytherapy

No.	Diagnosis	Therapy	Evolution
Tumours located in the prostate			
1	Prostate adenocarcinoma T3NoMo, G8, iPSA=18 ng/ml (2013)	Hormone Therapy (HT)+External Radiotherapy (RT) 76 Gy	Local recurrence. A complement of brachytherapy seeds in 2013 could have avoided the recurrence.
2	Prostate adenocarcinoma T2NoMo, G6, iPSA=11 ng/ml (2011). Right seminal bladder recurrence.	Permanent implant of iodine 125.	Local recurrence. A complement of brachytherapy seeds would avoid a mutilating surgery that the patient refused.
3	Prostate adenocarcinoma T2aNoMo, G6, iPSA=9 (2012). Prior rectum cancer surgically removed.	Hormone Therapy (HT)	Death. Robotic assisted brachytherapy would have saved the patient.
4	Bladder cancer, T2NoMo	Radical cystectomy	Partial cystectomy and robotic assisted brachytherapy would have avoided the mutilating surgery with a better quality of life.
Tumours located in the liver			
1	Rectosigmoid cancer stage IV (liver and pulmonary metastases), Radio- and Chemotherapy (RCT), surgery.	Palliative chemotherapy. Radiofrequency ablation.	Focal brachytherapy would have performed better on the liver metastases.

2	Oesophagus cancer, stage III, RCT. Local recurrence and liver spread. Cirrhosis.	Supportive care.	Death. Brachytherapy (oesophagus and liver) would have extended the patient survival with good life quality.
3	Unifocal hepatocellular carcinoma over cirrhosis. Inoperable due to comorbidities.	Sorafenib	Death. Local brachytherapy would have extended the patient survival.
4	Hepatic Cholangiocarcinoma, stage IV	Chemotherapy	Death. Focal brachytherapy on the primary tumour and metastases would have extended the patient survival and life quality without complications.
Tumours located at the rectum level			
1	Rectal cancer, RCT, surgery. Local recurrence.	Palliative chemotherapy.	Local and distant recurrence. Brachytherapy would have improved the prognosis avoiding (or delaying) metastases.
2	Rectum (stage III) and prostate Synchronous Adenocarcinoma T3NoMo	RCT + surgery	Prostate brachytherapy would have prevented the surgery and all its complications (incontinence, urinary infection)
3	Epidermoid carcinoma anal canal. T4N2Mo, RCT. Local recurrence. Surgery (rectum amputation)	Surgery	Initial brachytherapy would have avoided the recurrence and thus the amputation.
4	Inferior rectum adenocarcinoma T2NoMo	Rectum amputation	Local excision and brachytherapy would have avoided the second, mutilating, surgery.
Thoracic tumours (lungs and breast)			
1	Pulmonary metastases following testicle cancer, multiple recurrences.	Chemotherapy, surgeries (testicle, ganglions, lungs) External pulmonary radiotherapy	Death. Brachytherapy would have avoided the recurrences.
2	Epidermoid pulmonary cancer. Local inoperable recurrence.	Chemotherapy, palliative radiotherapy	Death. Brachytherapy would have, at least, extended the survival.
3	Thoracic sarcoma	Surgery, radiotherapy	Brachytherapy would have provided the same outcome with much lower toxicity.
4	Retroperitoneal sarcoma, positive margins resection, irradiated	Surgery, RT, CHT	Local recurrence. Brachytherapy could have complemented the external dose of radiation to avoid recurrences, without the increase of intestinal toxicity.

Fundamental characteristics of minimally invasive robotic systems

The development of robotics devices as advanced minimally invasive tools for the physicians must integrate a set of fundamental characteristics (or properties) in order to provide a real benefit for the therapy (fig. 7).

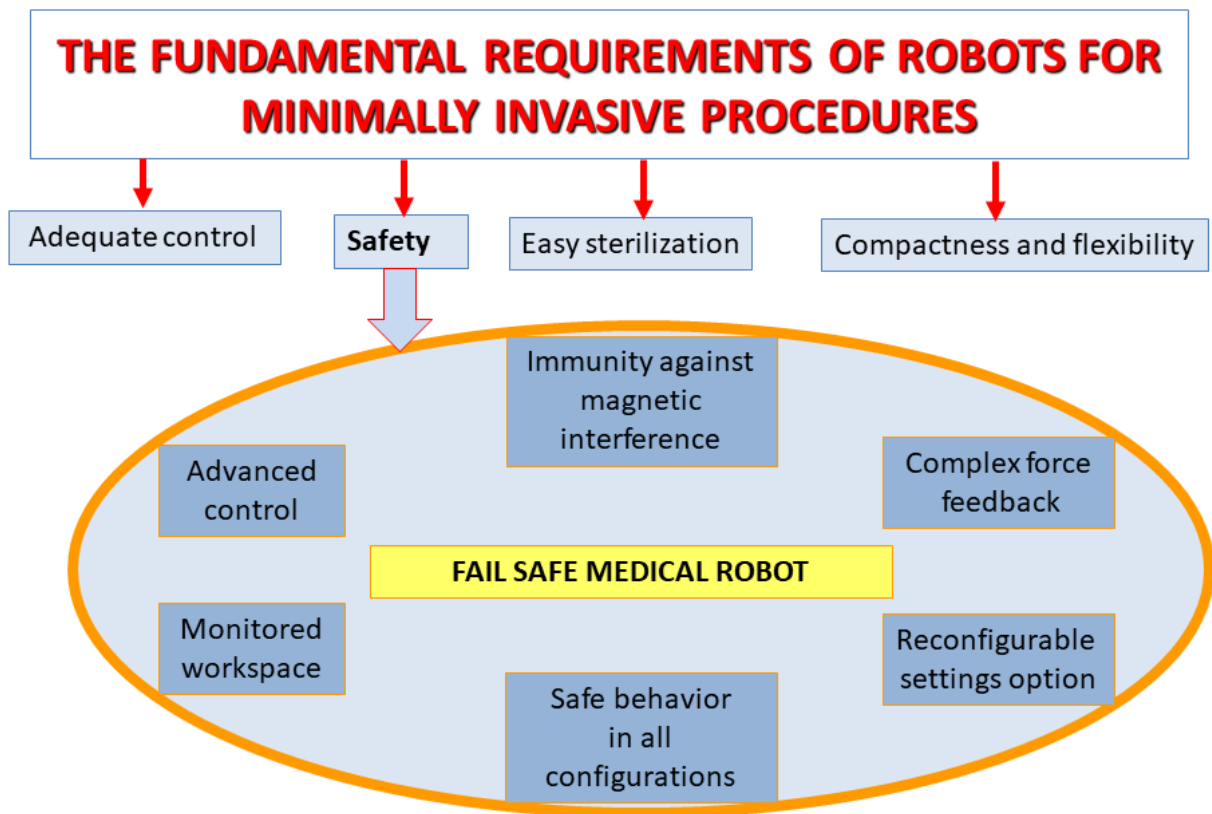


Figure 1.7. Fundamental characteristics of minimally invasive robotic systems

Adequate control. Minimally invasive devices along with pure surgical robots are entering into direct contact with the internal organs of the patient making them very demanding in terms of control. While the system must perform as efficient as possible with respect to the given task it must also provide a comfortable operating way for the physician while preventing, as much as possible, any misuse that would endanger the patient. Also, it must integrate motion scaling to provide specific delicate / micro positioning of the tools and specific user interfaces that would ensure maximum ergonomics for the doctors.

Easy sterilization. Minimally invasive procedures (surgical or non-surgical) impose the introduction and manipulation of tools inside and in the close vicinity of a human body imposes the use of sterile/single use instruments but this would have to naturally extend at least to the end module of the robot that handles those instruments. While the robot itself can be covered in a sterile sheet isolating it, the end module that handles the active instruments must be made in such a way (in terms of materials and design) to support sterilization.

Compactness and flexibility. Most of the procedures that involve in insertion of an instrument inside the body have to be performed inside an operating room (OR) where besides there are a lot of additional equipment and physicians inside monitoring the patient, assisting the procedure which limits a lot the access points and the available space in the OR. Also, in case the patient condition deteriorates, the robot must be removed very fast to allow the conversion of the procedure or to provide quick access to the patient.

Safety. For the invasive procedures, safety is more than a requirement because it integrates multiple “must have” characteristics:

Safe 1. *Immunity against magnetic interference.* Inside the OR there are multiple electronic equipment which should not interfere one with the other affecting their behaviour.

Safe 2. *Complex force feedback.* Whereas force feedback cannot be provided yet for classical surgical robotic devices, it becomes a must for the robotic devices that handle instruments like biopsy guns, needles for brachytherapy or ablation probes.

Safe 3. *Reconfigurable setting options.* As the human anatomy is unique for each individual and taking into account that any instrument inserted in the body must use a RCM for the guiding of the tools the setting options must be adjustable for different procedures.

Safe 4. *Safe behaviour in all configurations.* Every robotic system has a slightly different behaviour in terms of positioning accuracy, stiffness and dexterity within its entire workspace. However, these variations should not be very high such to have volumes or zones that cannot be used this being achieved by efficient mechanism design.

Safe 5. *Monitored workspace.* The motion parameters along with accuracy, stiffness and dexterity should be known and controlled within the robot workspace while the initial relative positioning between the robot and the patient should exploit the workspace volume that presents the best possible combination of these aforementioned parameters.

Safe 6. *Advanced control.* The control system should be properly designed to fit the specific parameters of the procedure taking into account also the information from the force feedback on the active instruments and the specific functions that have to be integrated to user interface.

B. Rehabilitation robotics

According to the same strategic document, Multi-Annual Robotics Roadmap [MAR 17], the second field of robotics in medicine covers devices developed as rehabilitation devices used to train/retrain the functions of an impaired/damaged limb and prosthetics where a robotic device would replace a lost limb in order to provide the user a functional regain as close as possible to the natural human

capabilities. As shown in figure 8, in the first group, of rehabilitation devices there can be integrated three major categories of devices:

- **Rehabilitation aids:** developed to be used following a trauma or a surgical procedure, the role of these devices is to enable a faster recovery and healing;
- **Functional replacement aids:** the robotic systems are conceived to replace a lost function of the body, due to either ageing or a traumatic event. Based on their specific purpose, these robotic devices will be worn as a prosthetic or an exoskeletal or orthotic device;
- **Neuro-rehabilitation:** a specific type of trauma refers to diseases that cause a certain damage to the neural connections between the brain and the limb itself, which causes a functional degradation without any musculoskeletal injury.

Prosthetic devices come as a different category of devices as these robots would replace a lost limb. The latest efforts in this field aim towards the development of smart devices able to integrate cognitive awareness with increased dexterity and control.

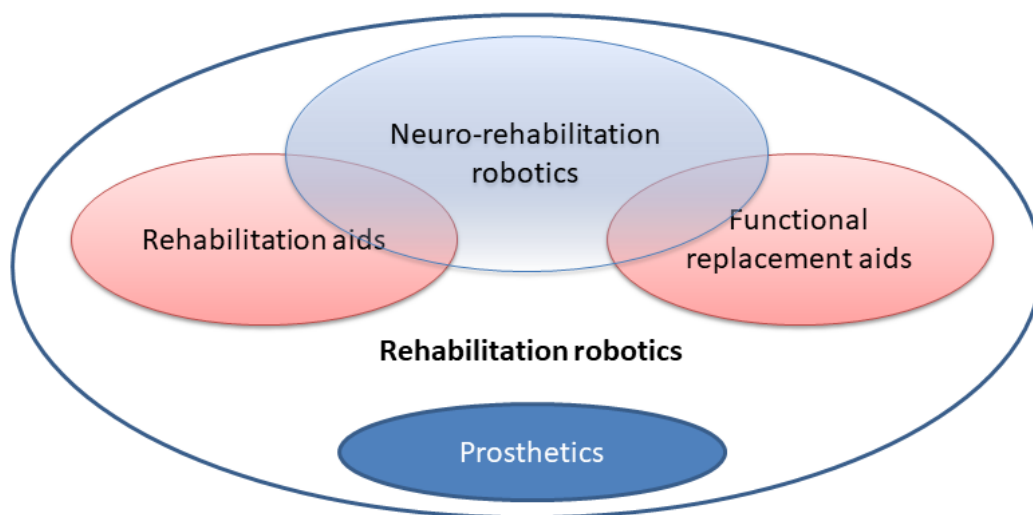


Figure 1.8. Overview of the field of rehabilitation devices

Within CESTER research has focused on the field of neuro-rehabilitation with emphasis on the development of new parallel robotic structures for the post-stroke rehabilitation the international and national context being illustrated below.

Post-stroke robotic assisted rehabilitation – a new paradigm in patient management

Stroke, as defined by World Health Organization (WHO), is a "*neurological deficit of cerebrovascular cause that persists beyond 24 hours or is interrupted by death within 24 hours*". Strokes are produced by cardiovascular diseases (CVD), which are a form on non-communicable diseases (NCD) that are responsible for the deaths of

around 17.5 million people annually out of which approximately 8 million deaths in Europe with the same number of people suffering from permanent disabilities, according to WHO. Instances of cerebrovascular disease have been recorded in people as young as 15 years old, the risk increasing with age. These diseases are driven by ageing, unplanned urbanization, and the globalization of unhealthy lifestyles.

After a stroke, patients that survive will suffer from several secondary effects. One such effect is hemiplegia, paralysis to one side of the body often occurring on the opposite side of the brain disorder. Another such effect is hemiparesis which represents weakness on one side of the body, this being the lesser form of hemiplegia.

The patients that suffer from such side effects can undergo physical rehabilitation, which is the process of helping patients recover control of part of their body through mainly repetitive physical exercises of the impaired limb. Since an entire part of a patient's body gets damaged, it is usually necessary for more than one therapist to help with the rehabilitation process. Unfortunately in today's society where the ageing population is increasing, the number of therapists will also increase.

National level

Based on the statistical data of the Ministry of Health, illustrated in the National Health Strategy, in 2012 there was an increase of 20.8% of the percentage of elderly population (over 60) with respect to the last demographic evaluation. Even though Romania is trailing behind Europe with respect to the medical services provided, especially towards the lower income population, a continuous mortality decrease has been recorded on every major disease, as shown in **table 2** [SNS 14]. This means that more people which survive an acute episode will require medical assistance for rehabilitation.

Table 2. Standardized mortality on the main death causes in Romania 2006-2010
(number of death / 100.000 persons)

Disease	2006	2007	2008	2009	2010	2006-2010 (%)
Cardiovascular episodes	618.7	578.07	558.3	548.6	539.7	-12.8%
<i>Ischaemic</i>	<i>213.5</i>	<i>200.9</i>	<i>194.2</i>	<i>188.8</i>	<i>187.2</i>	<i>-12.3 %</i>
<i>Stroke</i>	<i>205.2</i>	<i>186.4</i>	<i>173.5</i>	<i>169.9</i>	<i>167.0</i>	<i>-18.6 %</i>
Malignant tumors	179.8	178.02	179.7	181.4	180.1	0.2 %

In Romania, the healthy age expectancy remains inferior to the one of the member states EU 27 (age of 57.1 with respect to 62.2 in EU). The SILC¹ investigations point out that even though the life expectancy at birth increased the healthy age expectancy decreased in Romania, in opposition with the situation in EU 27, based on the study by EHLEIS [EHL 13]. This report shows that the expectancy of healthy ageing at the age of 65 has decreased between 2007-2010 for men – from 7.7 to 5.9 years and for women – from 7.8 to 5 years. In reality this data shows that after 65, women will live, on average 5 more years without medical conditions which determine a limitation of activities, 7.5 more years with moderate limitations and 4.8 years with severe limitations, while men will spend in the same categories 5.9, 5.6 and respectively 2.5 years.

Another important aspect refers to another statistical study which evaluates the *Years of Life Lost (YLL)* where a statistic performed by the Institute for Health Metrics and Evaluation² is presented in the table below.

Table 3. The potential years of life lost per cause of death for women and men in Romania 2010 (thousands of YLL and YLL / 1000 persons)

<i>Cause of death</i>	Women		Men	
	<i>YLL ‰</i>	<i>thousands YLL</i>	<i>YLL ‰</i>	<i>thousands YLL</i>
Ischaemic cardiac disease	39.4	432.9	57.3	598.2
Stroke	39.5	434.5	42.3	441.7
Cirrhosis	8.2	90.3	17.3	180.4

On the first place within the women population and second place within men, far higher than the other death causes, stroke represents an outstanding adversary which can be fought against only with adequate methodologies. As shown in table 1, **the medical efficiency in the acute phase reaction shows an amazing decrease of 20% of death following a stroke, however the following rehabilitation steps which will lead towards higher life quality and expectancy still need an answer.**

International level

Healthcare is one of the strategic domains for the development of robotics for the period 2014-2020 as shown in the European documents Strategic Research Agenda (SRA) 2014-2020 issued by euRobotics AISBL and the MAR [MAR 14].

¹ Statistics on Income and Living Conditions

² <http://www.healthdata.org/>, 2013

Quoting from MAR :” It is estimated that in the EU the proportion of the population aged over 65 will rise from 17.1% in 2008 to 30% in 2060 and that the proportion of persons aged over 80 will rise from 4.4% to 12.1% over the same period (EUROSTAT population projections). Neurological conditions, especially stroke, are a major cause of disability among older people. Incidence of a first stroke in Europe is about 1.1 million and prevalence about 6 million. Currently, about 75% of stroke sufferers survive one year after...approximately 80% of stroke patients experience long-term reduced manual dexterity and half of all patients with neurological conditions are unable to perform everyday tasks.”

The above statement underlines one critical aspect which must be dealt with to ensure the survival of our society. By 2060 the number of elderly people will be equal with the employable ones, which shows that the number of caregivers acting by the current healthcare strategies cannot be reached in future. Thus, it is compulsory to develop tools which can replace human medical assistance assuring, in the same time, a good life quality for elderly people their self-management in own environments and social inclusion.

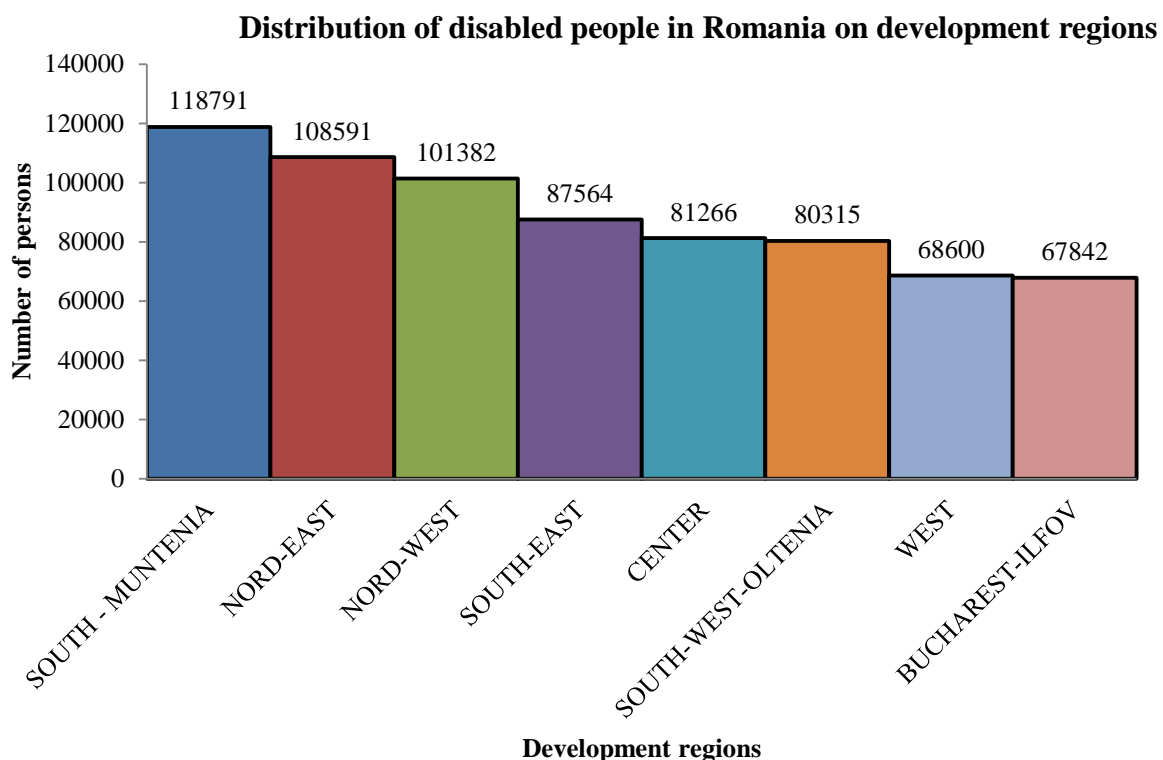


Figure 1.9. The number of persons with disabilities and their distribution on development regions in Romania (study published by the Ministry of Labour, Family, Social Protection and Elderly)

Stroke has been classified by World Health Organization (WHO) in 2008 as one of the five main chronic diseases with an amplified incidence with respect to ageing.

With an annual incidence of over 1.5 million new cases just in Europe (over 1 million) and United States (over 500.000) the potential market of new rehabilitation devices in ensured and judging by the current number of implemented devices it becomes a greater necessity with each year that passes.

On national level, the statistical data [PDP 14] published by the Ministry of Labour, Family, Social Protection and Elderly on the 30th of June 2014 reports a number of **714.891 persons with disabilities**. Among these, **97.6% are under the care of families and/or live independently and 2.4% (17.129) are institutionalized**. However there is no relevant data showing the percentage of disabled people which benefit from healthy ageing and social inclusion and respectively the number of persons which are immobilized in bed or inside their living environment without interaction with the society. The statistical data illustrates also the regional distribution of disabled persons, this information being graphically represented below.

In the next figure, the disability type is illustrated divided between adults and children. It can be seen that the physical and somatic disabilities are the ones with the highest incidence, representing the target groups for the development of rehabilitation devices.

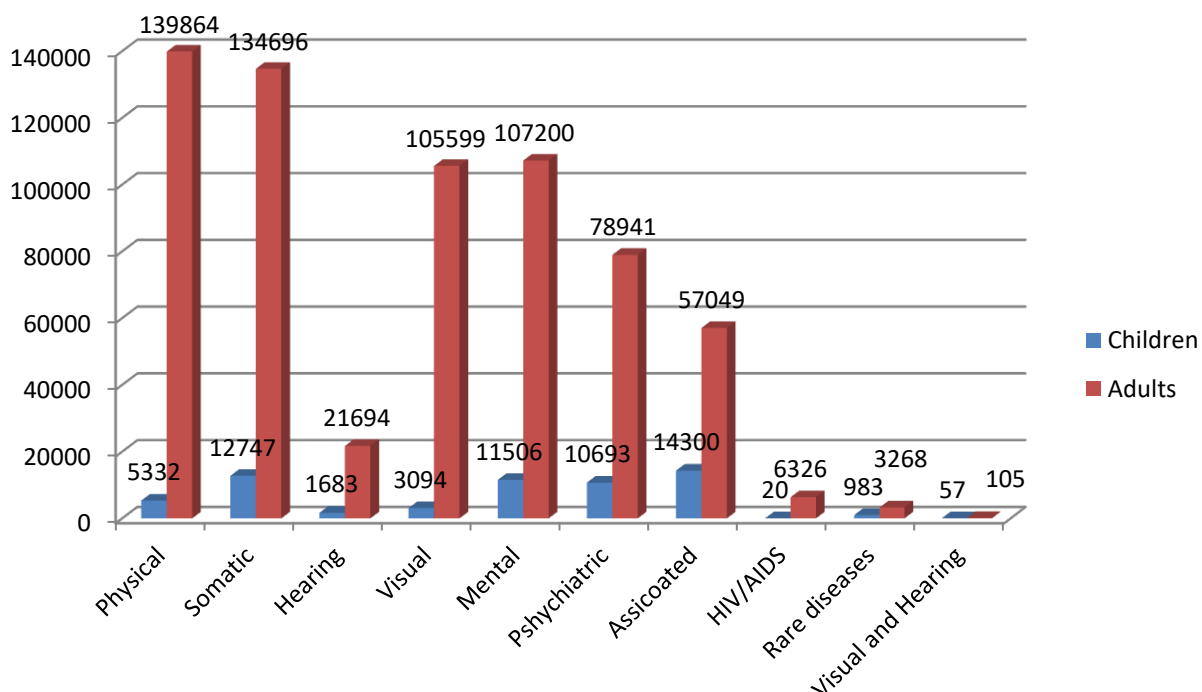


Figure 1.10. Number of persons with different disabilities/impairments

Furthermore, the same study [PDP 14] emphasises that the number of persons with disabilities aged over 50 represent 66.34% of the total adult persons with

disabilities, which underlines even more the necessity of technologies which can contribute to the quality life increase of these persons.

The number of public institutions for social services (assistance) for the adults with disabilities which are coordinated by the Ministry of Labour, Family, Social Protection and Elderly through its Office for the Protection of Persons with Disabilities reaches a total of 398 units out of which 342 offer permanent residency, the rest being day care centres. Compared to 2013 there was an increase of 11 day care centres, whereas in 2014 there were only 3 specialized centres for training elderly people towards an independent life. Unfortunately, at the publishing date of this study in Romania there existed no centre for neuro-rehabilitation and social integration. All this data is alarming as the resources available for persons with disabilities are clearly insufficient. Furthermore, Romania faces a crisis with the medical personnel which often choose to work in other European countries for better income and work conditions. This situation has to be changed and AgeWell can bring an important contribution towards a positive evolution by providing efficient and cost effective equipment which can increase the number of persons that can benefit from neuro-rehabilitation.

Based on the statistical data which are supported also by doctor Dafin Muresanu, the president of the Romanian Society of Neurology, in Romania annually over 65000 people have a stroke of which a third suffer a certain disability. For these people, neuro-rehabilitation represents the best chance of partial/total recovery of the deficits and their return to a normal life. Referring to the age, the statistical studies demonstrate that the maximum incidence of strokes appear, in 75% of the cases, after the age of 65, age which is associated also with a more difficult post-stroke rehabilitation.

On the positive side the Romanian government acknowledged that actions must be taken to prevent a social crisis which might appear in the next 10 years when the increasing average age of the population will lead also to a higher number of strokes and thus people that will need medical and rehabilitation care. Thus, for the next period of technological development (2014-2020), Romania has defined healthcare as one of the priority fields for research placing rehabilitation among the top subjects of interest along cancer research.

On international level, reference is made to the documents which define the critical domains where the development of robotics represents a necessity in the next years. As in Romania, healthcare is among the most important areas where robotics systems can enhance the level of medical care that can be provided for patients.

With reference to neuro-rehabilitation the Multi-Annual Roadmap² shows an increase in the implementation of robotic solutions which is however insufficient. Their report makes reference to statistical data which forecast very important demographics changes in the next decades. Nowadays the ratio between elderly, retired people and the active (working) population is around 26.8% (one elderly person for every four working persons) whereas in 2060 this ratio will increase to 52.6% (one elderly person for every two working persons). These demographic changes will generate automatically modifications of the expenses in population healthcare (higher number of pensions and people requiring medical services, increased number of medical personnel and so on) which will put pressure upon the economic development and sustainability of economies worldwide. Furthermore, EUROSTAT³ studies shown that in 2011 20.5% of the elderly European population (EU 27) live in poverty at the border of social exclusion (Bulgaria – 61.1%, Romania – 35.3%, Greece – 29.3%, Portugal – 24.5%, Italy – 24.2%) which shows that a decrease of the funding allocated for healthcare or an increase in the healthcare costs, this category of people will suffer even more leading to economic crises which will not be sustainable causing a domino effect with global implications. This data demonstrates once more that reaction must be taken before it is too late.

The same European document, the Multi-Annual Roadmap², points out the fact that the utilization of robotic systems in post-stroke rehabilitation along other neurologic pathologies (Parkinson, Multiple Sclerosis, ataxia) proved to have positive effects (in many cases higher than traditional therapies). The same document illustrates also some of the necessary characteristics of these robotic systems: sustainable production costs, clinical validation, proper protocols for the evaluation of patients' progress, large scale implementation strategies.

A Systematic Overview of the Critical Elements of a Robotic Assisted Rehabilitation System

One drawback of the early rehabilitation systems refer to their closed and independent loop control. In order to achieve better results the patient must become an integral, active part of the system supplying real-time data that can be used to adapt the robot behavior to the particular needs of each patient. Thus, a generalized overview of the main components of an efficient rehabilitation system is proposed.

³ http://ec.europa.eu/eurostat/statistics-explained/index.php/Children_at_risk_of_poverty_or_social_exclusion

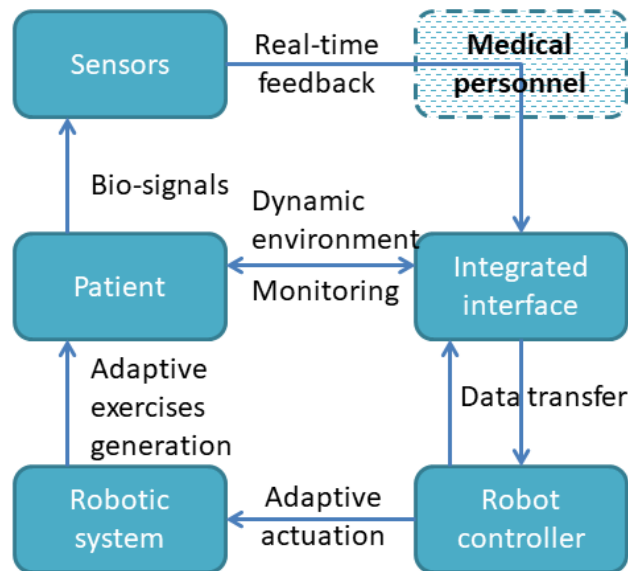


Figure 1.11. The conceptual overview of the robotic assisted rehabilitation system

A. The main components of the rehabilitation system

Figure 11 illustrates the main system components: Patient, Sensors, Medical Personnel, Integrated interface, Robot controller and the Robotic system itself.

Patient: The patient becomes an active component of the rehabilitation system supplying real-time data through the system of sensors. It also receives continuous information from the integrated interface as additional stimuli and motivation.

Sensors: The sensors are grouped in two main categories: **the external ones** which monitor in real-time multiple relevant parameters: dynamic motion amplitudes, electromyography, pulse, oxygen levels; **the internal ones** which belong directly to the robotic system: encoders, inductive sensors for homing and so on.

Integrated interface: represents the decision maker or the “brain” of the system. Designed on multiple access levels (patient, physician, and engineer) the interface allows the definition of personalized exercise plans combined with different audio-visual virtual reality environments to stimulate the patient neural activity on multiple levels. Within the interface patient data must be stored (securely) enabling the continuous monitoring of the patient progress on the overall and on specific exercises. This allows physicians to personalize the rehabilitation process to achieve maximum results. Another important aspect is that such systems are to be used in hospitals in the first weeks after the incident after which the patient will be treated in specialized centres or at home. In such cases the patient must be able to work daily while being monitored from a distance.

Robot controller: contains the control architecture of the robotic system, incorporating a real-time PLC, input output ports and drivers for the actuation

system. The controller communicates directly with the *Integrated interface* to load the desired motion parameters. The system must support multiple working modes which range for the performing simple motions to assistive ones when the patient will partially perform a motion with the robot being just an aid.

Robotic system: represents the mechanical structure of the robot and the actuation system. Using the data supplied by the controller the robotic system will perform the actual motions upon the targeted patient limb.

Medical personnel: the rehabilitation process includes continuous patient assessment from kineto-therapists and neurologists. However the system can perform exercises, based on predefined protocols without their direct involvement sending relevant recorded patient data at regular intervals or warnings whenever a medical parameter exceeds its pre-set limits.

B. The bio-signals of interest in robotic assisted rehabilitation

To have an objective quantification of the efficiency of the robot-assisted rehabilitation in stroke patients, several physiological parameters might offer reliable guidance.

First, by using **real-time heart-rate monitoring**, one can fine-tune the intensity of the applied forces and frequency of motion. If the paretic limb is passively moved, venous return is enhanced, a higher volume of blood is sent to the heart, increasing slightly the heart-rate. If the assistance is not entirely passive, but requires also the patient to participate with his residual power during the exercise, the heart-rate might show a further increase, and this should be monitored for example in the condition of heart-failure and consecutive tachyarrhythmia, frequently a pre-existing condition in stroke. If the applied forces are higher than tolerated or required, the patient might experience a sympathetic overflow, having producing a further increase in heart-rate, this being potentially a dangerous condition.

Along with the mobilization of venous blood, **better oxygenation** of the peripheral tissue might occur, which can be easily monitored using pulseoxymetry. This is beneficial for the paretic tissue, mostly from the point of view of maintaining a good trophicity. Awareness should be imposed, if the preload increases significantly, a degree of failure might be triggered by the exercise itself, which in turn decreases the peripheral blood and oxygen supply.

By applying repetitive exercises, on one hand the mobility increases by passive enhancement of the joint range of motion, on the other hand this can be increased by the gradual return of the **active movements** of the patient. This effect is objectively assessed by goniometry.

The residual forces are usually increased by exercises. A motor unit is composed of the nerve terminal and the muscle fibres innervated by it. **Motor unit action potential recording**, an EMG technique, monitors volitional muscle activity.

Individual fiber contractions are summed in a single potential and recorded as a potential change either by using a needle electrode, or on the surface of the muscle. The second method is not as precise, but is less invasive. By exercising, the amplitude of the MUAPs shows a gradual increase, a good measure for the efficiency of the rehabilitation method.

Besides the valuable information that is provided during the exercise times, as rehabilitation is a very long time process the recording of the bio-signals data is of critical importance to assess the patient progress, evaluate his active involvement in the exercises and as the authors intent also to assess its mood. It has been shown in numerous studies and synthesized in [VAI 17] that better results are obtained during exercises when multiple stimuli are applied. However, each individual has different perceptions about these stimuli and it is very hard to develop a solution that would comfort everyone. **Visual aids**, like virtual reality or augmented reality can be useful but depending on the patient background what can be very entertaining for a person might have the opposite effect on another one. Also, it is well-known that most stroke patients which suffer mild to severe limb control loss have a certain level of depression. Why is this relevant? It has been shown [BAS 14] that an uninvolved, bored, uninterested patient will benefit extremely less from the physical exercises. This is why a long term analysis of the bio-signals, their variation during exercises and their comparison with normal data will reveal critical information also about the patient mental involvement in the process. Furthermore, referring to the monitoring of the motion amplitudes a faster progress can be achieved by gradually increasing the dynamic parameters (angles, speeds, number of repetitions) while monitoring the other data to evaluate the patient response to the changes. As severe affected patients might not experience any pain when a certain articulation is stretched to its limits, the authors will attempt to detect it based on the combined variation of the bio-signals and robot sensors information.

Prospective conclusions regarding robotic assisted rehabilitation

Robotic assisted rehabilitation is a critical field of research which will become increasingly integrated as a common therapeutic practice in the next decade due to the natural age shifting of the population, **imposing a new paradigm**, where the role of the physical therapist will shift from the performing of the exercises with each patient to the development, programming and setup of personalized treatment plans for the post-stroke patients.

Due to the very large number of devices developed in research centres all over the world some standardization must be achieved in terms of Human – Robot Interaction strategies, patient progress monitoring and scoring.

New Trends in Medical and Service Robots

In 2012 an ambitious idea arose in CESTER, based on all the work and achievements in the field of Medical Robotics: the setup of an international event that would gather scientists from all over the world that share a common passion for research in the field of Medical Robotics.

This is how the International Workshop **New Trends in Medical and Service Robots** was born and to my personal satisfaction it grew beyond our initial imagination. It had travelled around Europe, growing from one edition to another and I hope it will never stop:

- 2012 – Cluj-Napoca, Romania;
- 2013 – Belgrade, Serbia;
- 2014 – Lausanne, Switzerland;
- 2015 – Nantes, France;
- 2016 – Graz, Austria;
- 2018 – Cassino, Italy.

Closing introductory remarks

All the research results presented in this thesis have been achieved within CESTER - **Research Centre for Industrial Robots Simulation and Testing** under the scientific coordination of Prof. Doina Pisla and Prof. Nicolae Plitea.

I will not state here the names of all the projects that have funded the research in this thesis as I don't consider them relevant in that particular way.

I will state that what is presented in this thesis is the result of the team effort, of the struggles and dedication of a group of people, which slowly became from colleagues, to friend and family and to all of them I express my gratitude and this is dedicated to everyone who believes in me as a person and as a researcher.

I will also address my apologies towards everyone affected by this with respect to the time I invested in research in the detriment of other things which one way or another influenced their lives.

Chapter 2. Surgical robotics and devices

“Whenever the art of medicine is loved, there is also a love of humanity.”
(Hippocrates)

A flexible multi-bend instrument for minimally invasive surgery

Without minimizing the exceptional benefits and progress in many surgical procedures brought by the most advanced surgical robotic system, da Vinci, one must also acknowledge some of its drawbacks [RAJ17]: affordability, use of dedicated, expensive instrumentation, lack of tactile feedback and collisions between the robot arms [MOR09]. Collisions between the robot arms are one of the biggest problems in robotic surgery, as the surgeon cannot complete the desired motion, the robotic arms can be damaged, and the increased surgical time. Many authors proposed solutions such as planning simulation and supervision systems, [ADH03] or port preplanning [TRE07]. These collisions appear due to the fact that the surgeon, sitting at the main robot console (figure 2.1) is trying to align the surgical instruments tips would force the motion of the arms on intersecting trajectories.

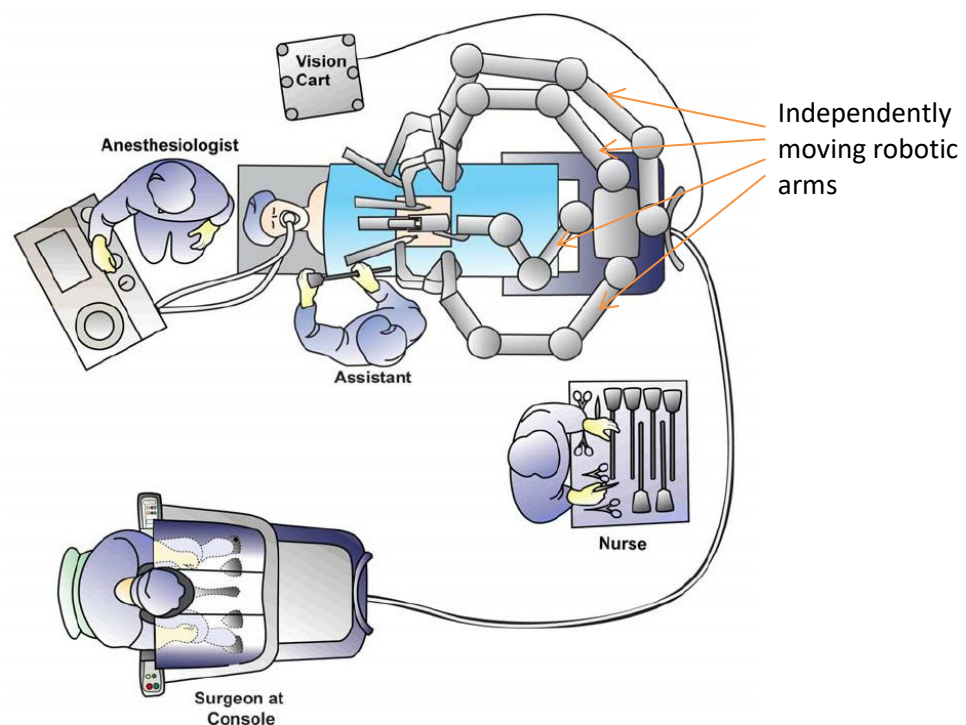


Figure 2.1. The setup of the da Vinci robot in the operating room

One of the solutions to this problem is to increase the instruments flexibility so that certain alignments could be done without actually moving the robotic arms. Of course, this idea is not limited to the da Vinci robot, as it is equipment independent, but this robotic system has been used in sufficient procedures to allow both physicians and engineers to express documented opinions in its behalf. The classical surgical robotic instruments have already a good dexterity as the instrument tip allows complete orientations of the active tool (fig. 2.2). Furthermore, another challenge in the design of tools for minimally invasive procedures, instruments that are used inside the patient body, is the size versus complexity. Nowadays, the trend

in MIS aims towards instruments of 10, 5 and 2 millimetres in which case adding a function to a classical instrument becomes a real challenge. Up to a certain dimension classical mechanical solutions can be used but beyond that point other approaches are needed, e.g. the use of shape memory alloys, [DAG10]. Clarke makes a critical survey in [CLA09] pointing out multiple aspects related to safety in surgical procedures, one of them stressing the idea that high complexity instruments can sometimes cause damage to the patient.

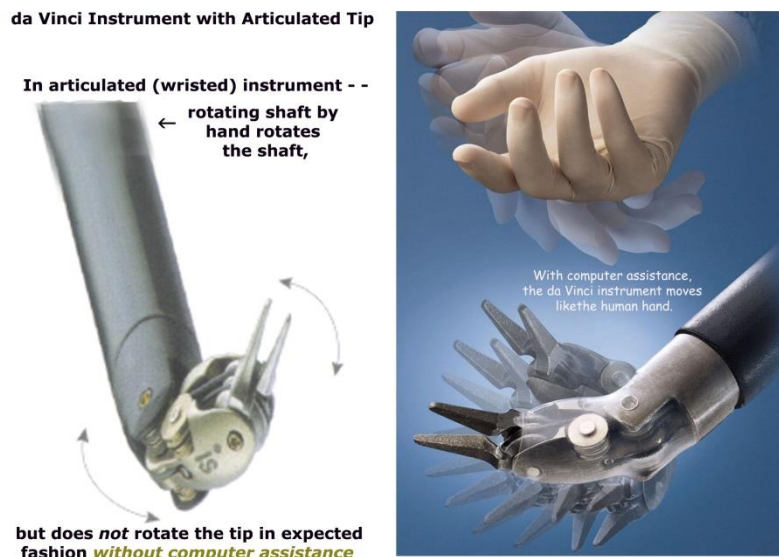


Figure 2.2. The dexterity of the da Vinci instruments with the articulated tip

Analysing the dexterity of the instruments one can easily compare it (as seen in figure 2.2) with the one of the human wrist. However, in a given generic activity the dexterity of the human arm is not solely determined by the wrist but by the entire set of articulations between the arm segments. Taking this into account, instead of criticising something that is good (the distal instrument wrist), one can attempt to add to the instruments additional dexterity.

Thus an innovative modular solution is proposed, which transforms any classical instrument into an articulated tool, and allows customisation based on the procedure special needs. Besides that, the new concept proposes the use of multiple curvatures (bends) which can prove very useful in MIS procedures for avoiding frontal objects, to allow lateral approach and in SILS to set the tips of the instruments apart. Used in a robotic setup the solution proposed reduces to a minimum the collision problem by allowing the instrument tips to work close one to another while keeping the robotic arms at a safe distance. The presented approach provides a solution which offers multiple configurations without the need of redesign [VAI11]. The new concept can be integrated in any type of instrument, from classical manually handed ones, to the most complex instruments used in robotic surgery.

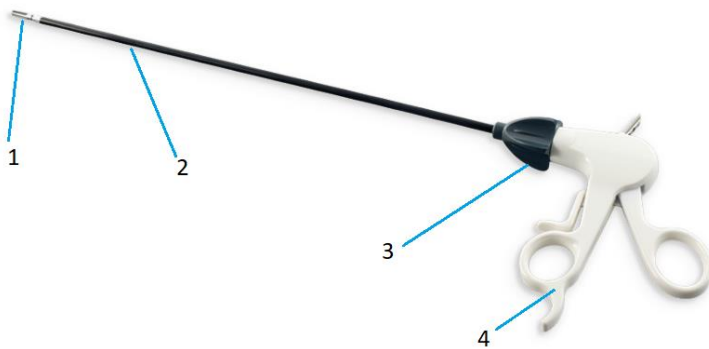


Figure 2.3. Classical MIS instrument

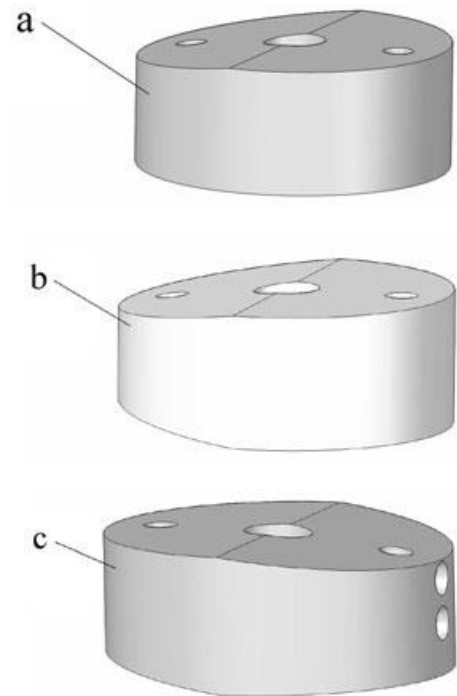


Figure 2.4. Components of the orientation module for the flexible tools

Design and dimensioning of the module

An example of a classical laparoscopic tool, manually operated, is presented in Fig. 1. It consists of 4 main parts (from the distal to the proximal end): 1 - distal head (instrument tip), 2 - rigid rod, 3 - rotational knob, 4 - handle. The handle allows the surgeon to perform the active function of the instrument: cutting, grasping, clamping etc., while the rotation knob allows the orientation of the distal head around its longitudinal axis, with 360° (free rotation).

In order to increase the dexterity of the instrument an orientation mechanism will be added in the distal third of the rigid rod. As the instrument must also maintain its stiffness the bending should be made between straight and bended for each curvature, ensuring simplicity in both design and use.

The modular approach proposes the use of 3 different components which allow the setup of multiple configurations, both in terms of bending angles and in number of bends [VAI11]. These three elements are (fig. 2.4.): the end parts (a) (the module extremities), the curvature change parts (b) and the intermediary parts (c). The solution can be applied to multiple dimensional models of laparoscopic instruments (10 and 5 mm in diameter) and allows the development of particular solutions, without the need of redesign.

The dimensional parameters are generalised, as the user can select/set any desired values, the final number of elements being imposed by these parameters. Each module will consist of:

- two end parts, positioned in the extremities of the module,

- a number of intermediary parts which depend on the desired curvature angle for each bend of the module, and the inclination angle of the element surface;
- (optional), if more than one curvature is needed, the component (c) presented in Fig. 2.4 will be used as an intermediary part to change the curvature direction.

Theoretically, using a certain combination of the components (a, b and c) one can achieve any orientation setup for the orientation module. For a surface angle of $\alpha = 7.5^\circ$, an example is proposed to demonstrate the possible configurations of a module with two different orientations in opposite directions. The value of the angle α will have a direct influence on the number of intermediary parts needed to achieve a certain inclination angle and, of course, the thickness of the elements. Fig. 2.5 illustrates the dimensions for the elements:

- **L** – the thickness of an element;
- **d** – the diameter of an element;
- α – the surface angle;
- β – the angle that determines the angle between two separate curvatures (which normally is 180°), for other values β , the angle between the normal planes of the inferior and superior surfaces of the element c.

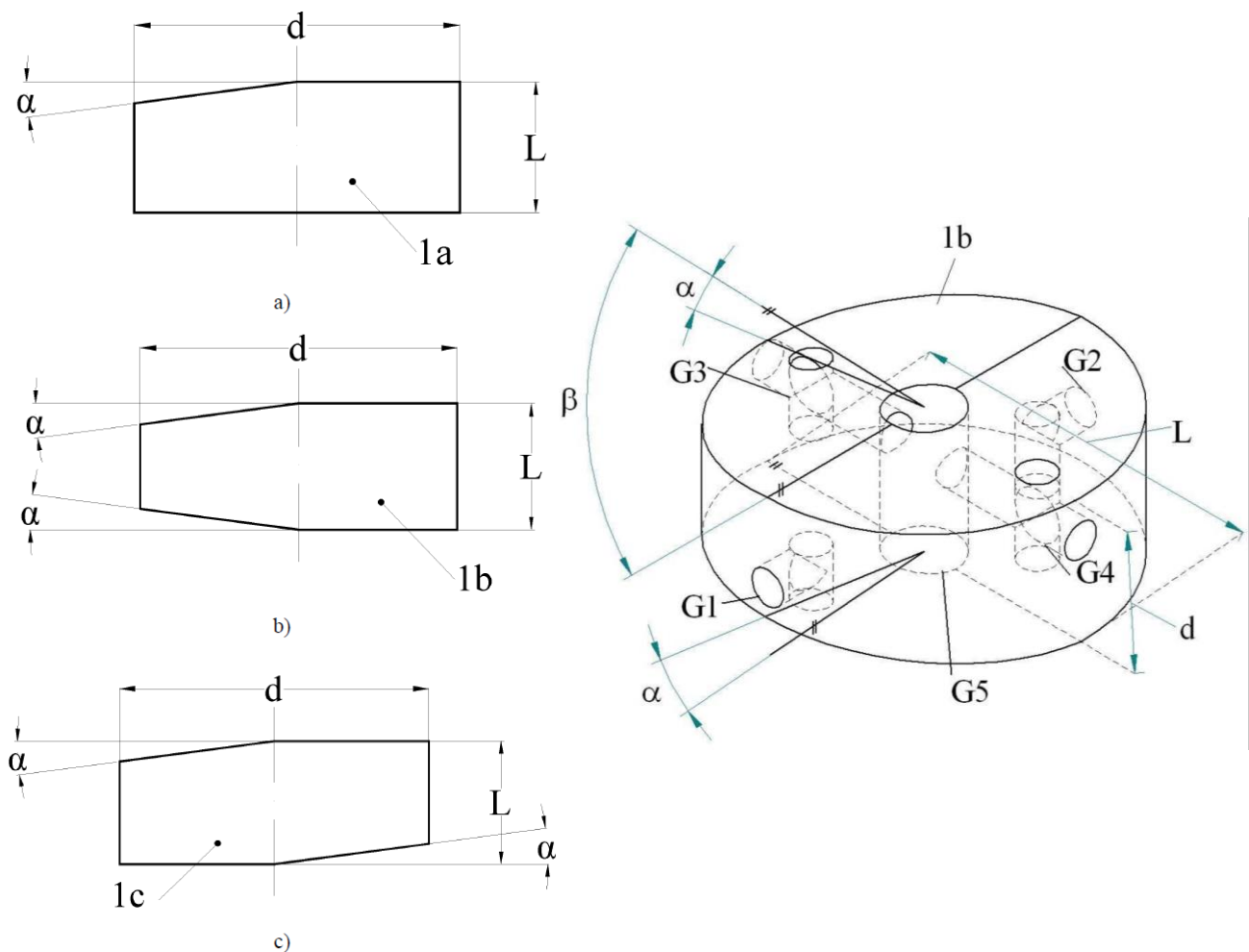


Figure 2.5. The general dimensions of the orientation module

The proposed example will combine two bending in opposite directions, with angles of 45° and respectively 90°. Thus, the orientation module will have four possible configurations (in each bend the number of intermediary parts used will determine the total angle), as shown in fig. 2.6:

- straight position (a);
- first curvature bent (b);
- second curvature bent (c);
- both curvatures bent (d).

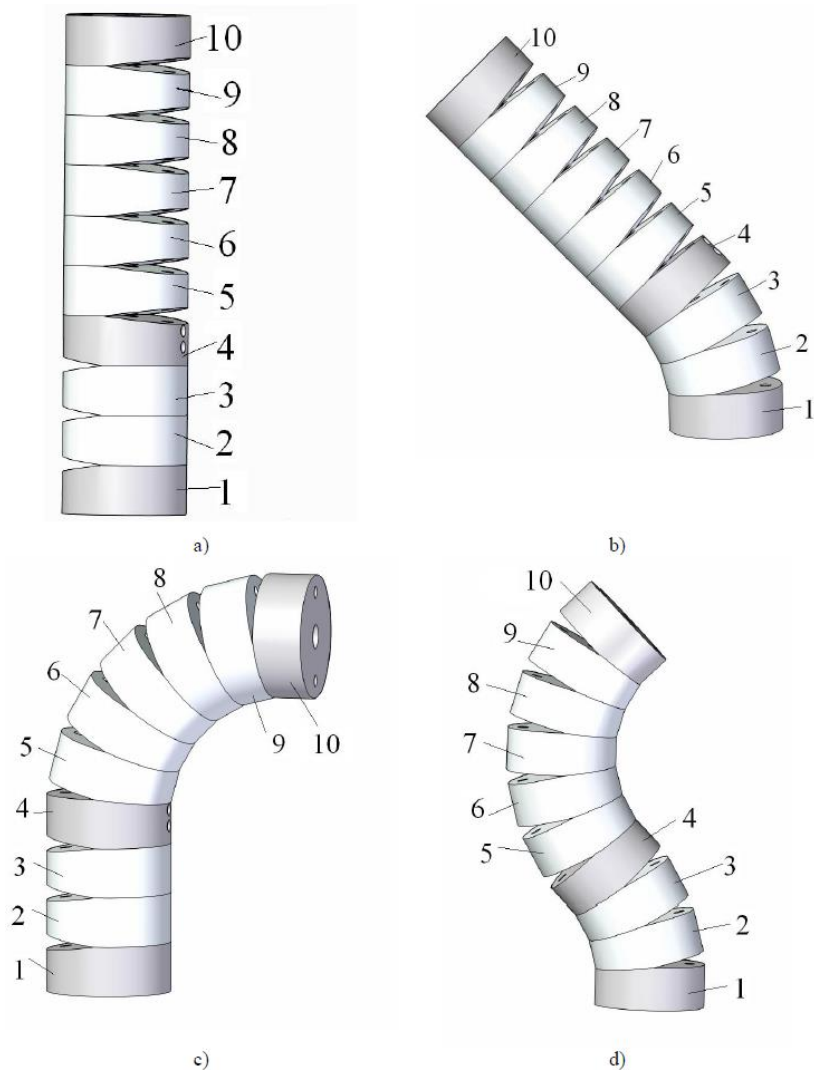


Figure 2.6. The possible configurations of the orientation module with two bends

In this way, during the procedure, the surgeon can select a classical approach or an angular/lateral one, the fourth configuration being of great help when he needs to avoid an obstacle situated in the instrument path. The bending/unbending of the module is achieved by wires which are passing through each element and are actuated: (I) by means of two circular knobs positioned near the instrument handle to facilitate easy access for *manual instruments*, and (II) by means of two motors

which rotate two wheels on which the wire is positioned, for *instruments used as tools for surgical robots*. A schematic representation of the cross-section through the module is illustrated in Fig. 2.7, pointing out the functioning of the orientation module presented as numerical example before.

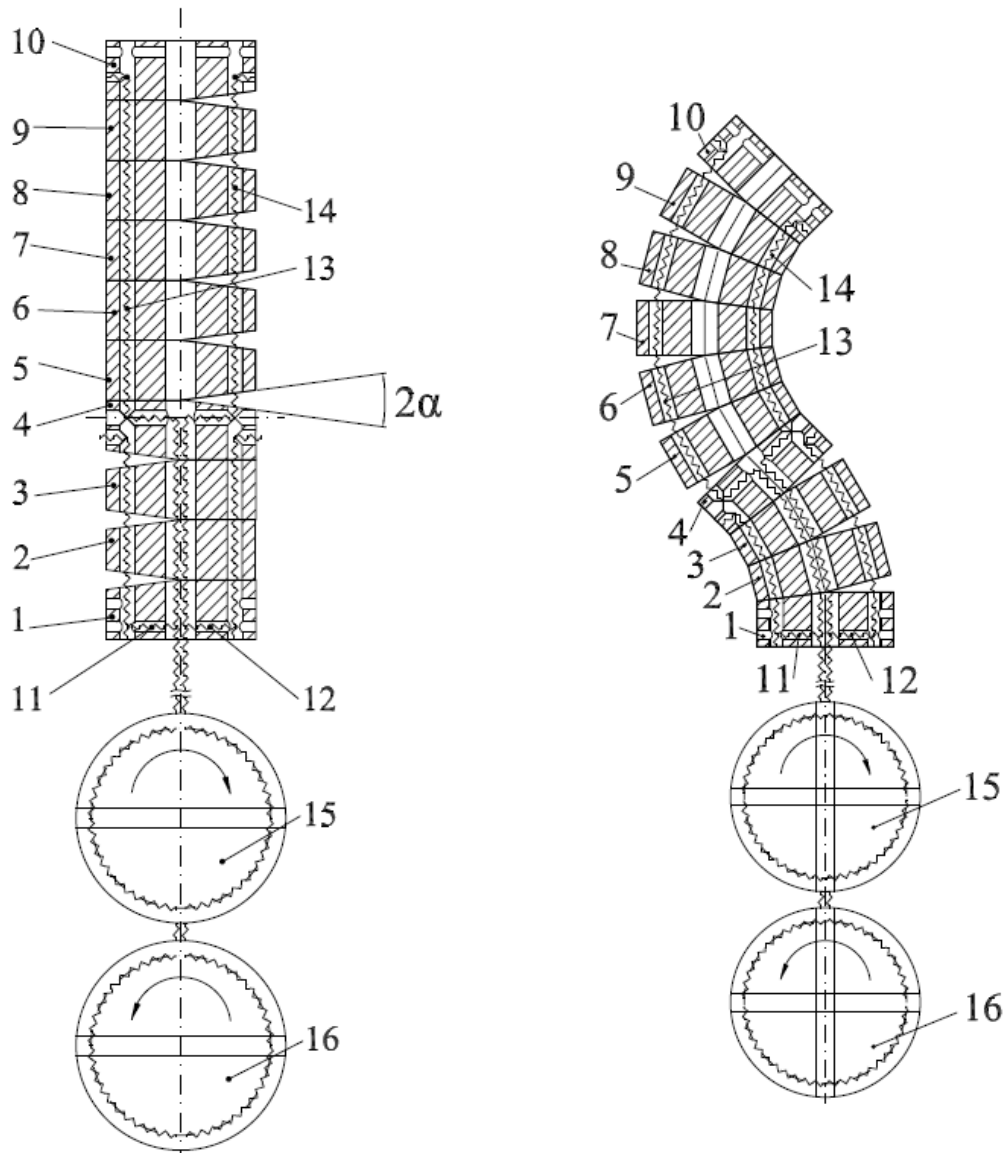


Figure 2.7. Wiring of the orientation module elements

In fig. 2.7 elements (1) and (10) represent the end parts, (4) is the curvature modification part while elements (2) and (3), respectively (5) to (9) are intermediary parts which generate the two bends. The wires (11) and (12), actuated by the knob (16) are used to achieve the first bend, while the wires (13) and (14) together with the knob (15) achieve the second bend. Each knob has to be rotated in the direction of the bend and during the computation it is assumed that there is no slip between the wire and the driving wheel. The only part with a slightly more complicated design is the curvature switch part, see figure 2.5. Besides the normal through holes for the cables it has two pairs of lateral holes used for the cables guiding. As one

bend ends, a set of wires has the ends fixed in the first pair of holes, as seen in Fig. 2.7 on the part (4) while the second pair is used to pass the wires from the middle channel to the lateral through holes. The length of the wires has to be determined with respect to the dimensions of the module, number of elements and curvatures. In order to establish some general calculation rules, all the dimensions have been denoted as generic parameters, a general formula being obtained. The following notations are introduced representing the geometrical parameters of the orientation module:

- **n** - total number of elements;
- **k** - number of bends;
- **m_i** - number of intermediary parts for bend “i”;
- **D₀** - diameter of the circle on which the leading holes are placed on;
- **h** - height of the fixing holes for the wire ends;
- **d_{dk}** - the diameter of the driving knob.

The total number of elements can be written as the following sum:

$$n = \sum_{i=1}^k m_i + 2_{ep} + k_{cs} \quad (2.1)$$

where: 2_{ep} represents the number of end parts, which is 2, and k_{cs} represents the number of curvature switch elements. Considering that all the elements of the module have the same surface inclination (α is constant), the angles for each bend can be determined as follows:

$$\varphi_i = 2 \cdot \alpha \cdot m_i \quad (2.2)$$

In the straight/non-actuated position (fig. 2.6-a) the lengths of the wires on each side of the orientation module are respectively equal namely the lengths of wires (11) and (12) and correspondingly (13) and (14). The following notations are introduced:

- ***l_{ii}*** - the length of the wire on the inner curvature side for bend “i”;
- ***l_{io}*** - the length of the wire on the outer curvature side for bend “j”.

Without any simplification hypothesis or influence on the calculus accuracy, the wire lengths are computed from the first module element onward, eliminating the length between the module and the driving knob, which is constant and will be separately determined. Thus, for the segment which is measured from the orientation module towards the distal head (active tip) of the instrument, the wire length is:

$$l_{ii} = l_{io} = L \cdot \sum_{i=1}^k m_i + 1_{ep} + k_{cs} + h + D_0 \quad (2.3)$$

Taking into account that the length of the wires used for the bend “i” is not influenced by the state of the previous segments (as the wires pass through the centre holes of the elements), the equations which define the variation of the wire length for the inner and outer side of the bend “i” are:

$$l_{i_{act}} = l_{ii} - (m_i + 1) \cdot D \cdot \sin(\alpha) \quad (2.4)$$

$$l_{i_{oact}} = l_{io} + (m_i + 1) \cdot D \cdot \sin(\alpha) \quad (2.5)$$

Taking into account that for the successful achievement of each curvature (bend) the actuation knob will be rotated with 90° (suggesting also the on/off positions), the diameter of the wheel on which the wire is wound on, can be calculated:

$$d_i = \frac{4 \cdot (m_i + 1) \cdot D \cdot \sin(\alpha)}{\pi} \quad (2.6)$$

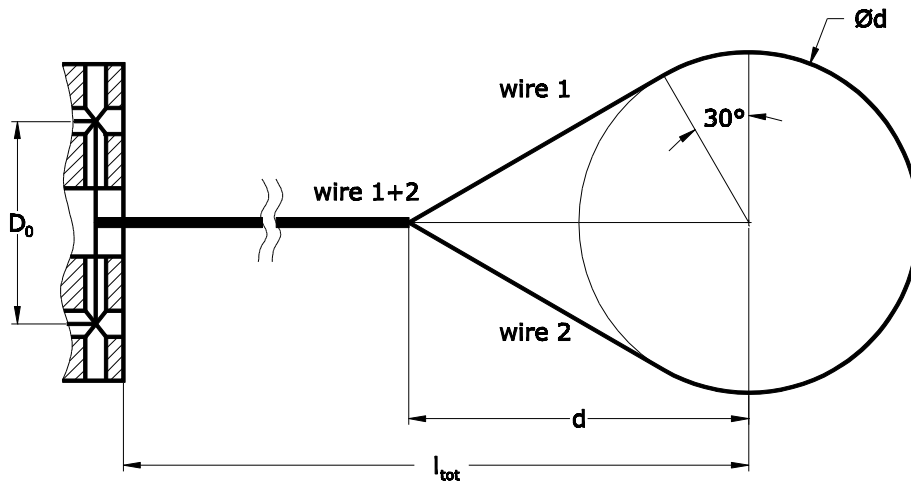


Figure 2.8. Wire length for the segment outside the orientation module

For the second segment, used to determine the length of the wire outside the orientation module, as shown in fig. 2.8., the following equation can be written:

$$l_{out_i} = 2 \cdot \left[l_{tot} - d + d \cdot \cos\left(\frac{\pi}{6}\right) \right] + \frac{\pi \cdot d}{3} \quad (2.7)$$

Thus, the total length of the actuation wire for each bend is:

$$l_{tot_i} = l_{out_i} + 2 \cdot l_{ii} \quad (2.8)$$

Workspace analysis for different surgical tasks

The equations which characterise the orientation module have been described for a general case having “*i*” bends but even though, at least theoretically any number of bends can be achieved, two bends are generally sufficient in order to satisfy the surgeon’s needs. The first bend is useful when a better approach must be attained towards a certain surface, or when the instruments have to be set apart, generally in SILS procedures. The second bend is very useful when an object must be avoided without putting any pressure on it. Having the two bends in opposite directions (180 degrees rotated) a bend in the same direction can be achieved for both the left hand and right hand instrument, following a lateral approach. A study is proposed analysing the instrument reach in different situations, to establish the performance, or the added value which the orientation module brings for the surgical act. This study assesses the benefits of the orientation module compared to a rigid classical instrument in three different medical (surgical) tasks:

- *touching/palpation* - the instrument must be able to touch a given surface;
- *grasping* - the instrument must touch the surface under an angle of at least 45°;
- *cutting* - the instrument must touch the surface under an angle of at least 60°.

For the first task, only the capability to reach a certain point in the surgical field is studied. For the second one when a tissue must be grasped, a supplementary constraint is imposed (in terms of the allowed contact angle between the instrument and the tissue surface) which is increased even more in the third case when cutting/dissection must be applied. Considering that the perfect contact angle is 90°, a limit value of 45° is imposed for grasping to avoid a superficial contact and 60° to prevent the cutting of the tissue in an unwanted direction, as shown in [SUC11]. Figure 2.9(a) illustrates the range of motions of a surgical instrument in minimally invasive surgery. Actuated by the motions of the surgeon hand, the instrument has 4 DOF, one translation along its longitudinal axis, and three rotations, which are achieved with respect to the entry point (Remote Centre of Motion) in the body. In order to study the workspace of surgical instruments properly, there are several constraints that must be taken into consideration:

1. the instrument must always pass through a fixed point in space (the insertion point – the Remote Centre of Motion), denoted here with B;
2. the angle between a normal axis on the insertion surface and the instrument must not exceed 60°;
3. denoting with A the outer extremity and with E the tip of the instrument, the following restrictions apply: $AB \geq 50$ mm and $BE \geq 80$ mm, which are imposed by the dimension of the trocar¹.

¹ The trocar is a medical device through which the instruments are inserted inside the human body, having a double purpose of protecting the tissue walls against the motions of the instrument and for maintaining the gas used for creating an empty cavity where the instruments can move on top of the surgical field.

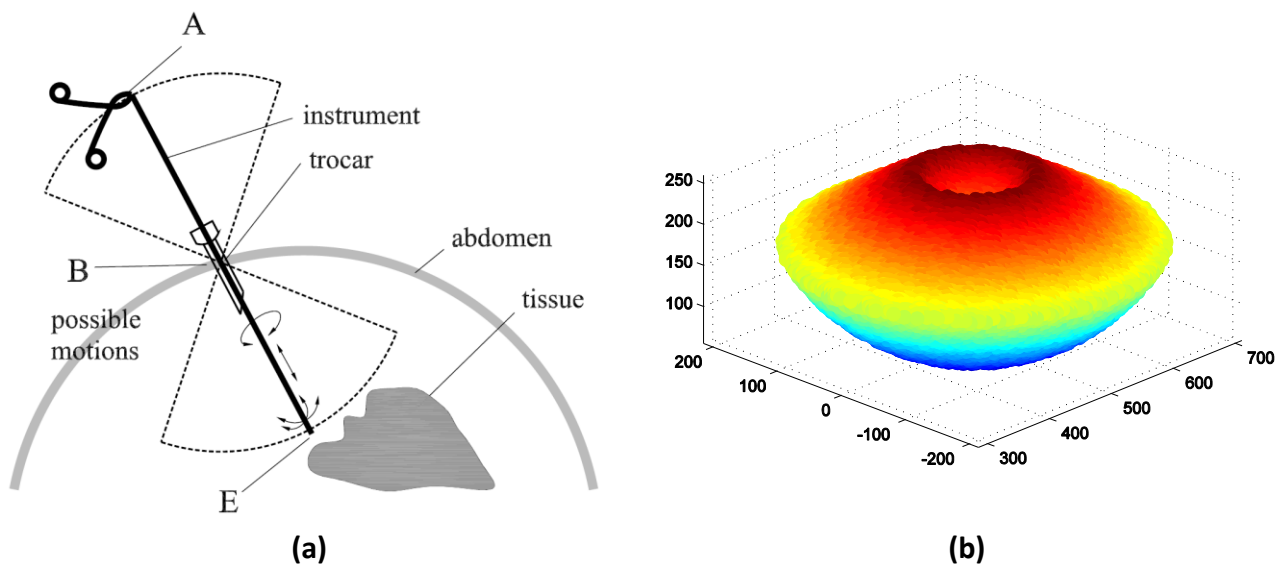


Figure 2.9. The mobility degrees (a) and the total workspace (b) for a classical surgical instrument

The workspace analysis is made starting from a general view, detailing then the differences between the three studied actions. Figure 2.8(b) shows the general workspace of an instrument, pointing out the constraints imposed. The insertion point B is marked on the figure to illustrate the reachable area of the instrument.

A discussion regarding the empty volume below point B is presented in [VAI09] denoting the remaining volume with “active workspace”. This is due to the presence of the trocar, through which the instruments are inserted. An instrument cannot be used when its distal end is situated inside the trocar, a comparison between the total workspace and the active one being presented in [GHE10]. The study proposes the assessment of the following aspects:

- The workspace gain between classical MIS instruments and the ones that use the orientation module;
- The influence of the instrument total length upon the workspace gain;
- The workspace variation due to the value of the bend angles;
- The influence of the module position with respect to the distal end of the instrument.

In order to achieve the study, the following numerical data is used, illustrating the instrument parameters in Fig. 2.10:

- A fixed coordinate system OXYZ is introduced, representing the surgeon position, considering the OZ axis vertical, oriented upwards; the OY axis represents the left/right positioning of the instrument, while the OX axis is the extension/retraction of the instrument; the 0 value for the vertical axis is considered at the level of the operating table;
- The coordinates of point B: $X_B = 500$ mm, $Y_B = 0$ mm, $Z_B = 300$ mm; They represent a possible configuration of the insertion point inside the patient body of one of the instruments, having a height of 300 mm (the average height of the body of a normal 80–90 kg person), and a distance of 500 mm

- with respect to the surgeon; The values themselves do not influence the overall quality of the results but enable a numerical study;
- The values are selected to define the length of the instruments $h_1 = 350$ mm and $h_2 = 450$ mm in accordance with existing surgical instruments; The longer instruments are used in special cases, but in order to enable a proper comparison between figures, the point B was kept unchanged thus allowing the longer instrument type to reach negative values;
 - The orientation module is positioned proximal to the distal end, representing the last part of the instrument;
 - The length of the orientation module is $l = 50$ mm, with the first bend at $l_{12} = 20$ mm;
 - The instrument tip is denoted with E for both instrument types;
 - The point G is introduced representing the origin of the orientation module, meaning that the segment AG represents the rigid part of the instrument;
 - The orientation module has two bends, for the first curvature two angles are chosen, $\alpha_{1a} = 45^\circ$ and $\alpha_{1b} = 60^\circ$, for the second one a bend of 90° is imposed, in the same plane with the first one, in opposite sense;
 - Between the last element of the module and the distal end of the instrument, a length l_e is introduced, with two values: $l_{e1} = 15$ mm (for the case when the orientation module is near the instrument tip) and $l_{e2} = 50$ mm (when the orientation module is situated at a certain distance with respect to the instrument tip).

In [VAI09] and [GHE11] the workspace was generated by calculating the coordinates of the instrument tip based on the achievable positions of point A, which proved to supply an un-uniformly distributed set of points with negative consequences upon the workspace representation. The explanation for the different view of the point cloud is the following: when one uses the direct kinematic model to compute the positions of the end-effector (the instrument tip), within the active joints that determine the motion of the end-effector constant increments will be used which will reflect, normally, into an uneven distribution of the point cloud which will be more sparse as the instrument tip will be further away from the entry point. So, because in this study the interest is to study and compare the volume covered inside the body by different instrument configurations, another approach will be used: an initial volume which surely integrates the real instrument workspace is considered. By using a constant increment, each point is verified to supply valid positions of point A. Thus, the workspace is achieved by eliminating the invalid points from the initial considered volume. Analysing the shape of the instrument workspace presented in Fig. 7, and taking into account that no restrictions are applied for its motion, the comparative analysis can be achieved by studying the workspace section view by a plane which contains the symmetry axis of the volume, namely the vertical axis which passes through point B. The simplest way to achieve that is to consider the X coordinate fixed, $X_E = X_B = 500$ mm. By this simplification, no points

are lost, but the computation time is significantly reduced. In order to determine the workspace, the coordinates of point E are considered known, and by computing the corresponding point A these positions are validated, based on the following equations:

$$l_{BE} = \sqrt{(Y_B - Y_E)^2 + (Z_B - Z_E)^2} \quad (2.9)$$

The orientation of the instrument is determined by two angles, ϕ and θ :

$$\phi = \text{atan2} \left(\sqrt{\frac{(X_G - X_B)^2 + (Y_G - Y_B)^2}{l_{BE}}}, \frac{Z_B - Z_G}{l_{BE}} \right) \quad (2.10)$$

$$\theta = \text{atan2}(Y_B - Y_E, X_B - X_E) \quad (2.11)$$

where $|\theta| = 0$ because of the restriction $X_E = X_B$, but the angle cannot be eliminated from the equations, as its sign changes with the relative position between Y_E and Y_B . For the classical, rigid instrument, the equations that characterise the coordinates of the instrument tip are:

$$\begin{cases} X_A = X_E - h_i \cdot \sin(\phi) \cdot \cos(\theta) = 0 \\ Y_A = Y_E - h_i \cdot \sin(\phi) \cdot \sin(\theta) \\ Z_A = Z_E + h_i \cdot \cos(\phi) \end{cases} \quad (2.12)$$

Due the condition imposed for the X coordinate, the following equations are presented with only the coordinates of Y and Z. The four possible configurations of the instrument with the orientation module determine four locations of point E for each point A. As the first one is similar to the rigid instrument, only the later three are calculated and the new points saved. Two vectors are introduced:

$$\begin{cases} a_1[3] = [0 \ 1 \ 1] \\ a_2[3] = [1 \ 0 \ 1] \end{cases} \quad (2.13)$$

where a_1 and a_2 are the two bends, value 0 representing the non-actuated state and 1 the actuated state. Knowing the coordinates of point E from the non-actuated state of the two bends, the coordinates of points A and G are easily computed:

$$\begin{cases} Y_A = Y_E - h_i \cdot \sin(\phi) \cdot \sin(\theta) \\ Z_A = Z_E + h_i \cdot \cos(\phi) \end{cases} \quad (2.14)$$

$$\begin{cases} Y_G = Y_E - (l_i + l) \cdot \sin(\phi) \cdot \sin(\theta) \\ Z_G = Z_E + (l_i + l) \cdot \cos(\phi) \end{cases} \quad (2.15)$$

In order to have a clear view on the equations used to compute the workspace for the instrument with the orientation module, the following notations are used:

- **G₁** and **G₂** - the centres of the last modules for each bend;
- **j** - the index for each of the three possible module configurations $j = 1, 2, 3$;
- **k** - the index for the face inclination angle for the first bend, as in the calculus two different values are used (45° and 60°), with $k = 1, 2$;
- **sgn** - the transport variable for the sign of $\sin(\theta)$, being 1 for $\sin(\theta) > 0$ and -1 for $\sin(\theta) < 0$.

Using the above notations, the length of the first bend can be determined based on the inclination angle and the actuation state:

$$GG_1 = \begin{cases} d \cdot \frac{\alpha_{1k}}{\alpha_{01}} & \text{if } a[j] = 0 \\ d \cdot \sin\left(\frac{\alpha_{1k}}{2}\right) \cdot \frac{1}{\tan\left(\frac{\alpha_{01}}{2}\right)} & \text{if } a[j] = 1 \end{cases} \quad (2.16)$$

Using (2.16) the coordinates of the point G_1 can be calculated with the equation:

$$\begin{cases} Y_{G_1} = Y_G + GG_1 \cdot \sin(\phi_1) \cdot \sin(\theta) \\ Z_{G_1} = Z_G - GG_1 \cdot \cos(\phi_1) \end{cases} \quad (2.17)$$

Where the angle ϕ_1 is equal with:

$$\phi_1 = \phi + a1[j] \cdot \frac{\alpha_{1k}}{2} \cdot \text{sgn} \quad (2.18)$$

Using the same approach the coordinates of the point G_2 can be calculated as shown in the next equations, determining first the actuation state and the bending angle:

$$GG_2 = \begin{cases} d \cdot \frac{\alpha_2}{\alpha_{02}} & \text{if } a[j] = 0 \\ d \cdot \sin\left(\frac{\alpha_2}{2}\right) \cdot \frac{1}{\tan\left(\frac{\alpha_{02}}{2}\right)} & \text{if } a[j] = 1 \end{cases} \quad (2.19)$$

$$\phi_2 = \phi + \text{sgn}\left(a1[j] \cdot \alpha_{1k} - a2[j] \cdot \frac{\alpha_2}{2}\right) \quad (2.20)$$

$$\begin{cases} Y_{G_2} = Y_{G_1} + GG_2 \cdot \sin(\phi_2) \cdot \sin(\theta) \\ Z_{G_2} = Z_{G_1} - GG_2 \cdot \cos(\phi_2) \end{cases} \quad (2.21)$$

Having computed the coordinates for the point G2, the coordinates of the instrument tip, E, can be calculated:

$$\begin{cases} Y_{E_j} = Y_{G_2} + (d + le_i) \cdot \sin(\phi_3) \cdot \sin(\theta) \\ Z_{E_j} = Z_{G_2} - (d + le_i) \cdot \cos(\phi_3) \end{cases} \quad (2.22)$$

Where the angle ϕ_3 is calculated with the equation:

$$\phi_3 = \phi + \text{sgn}(a1[j] \cdot \alpha_{1k} - a2[j] \cdot \alpha_2) \quad (2.23)$$

Equation (2.22) defines the positions for the instrument tip in the four considered configurations. Figure 2.10 illustrates the four possible positions of the instrument equipped with the orientation module. In the figure the four possible configurations were denoted with pairs of 0 and 1, 0 standing for the non-actuated state while 1 is for the bent state for each curvature. Thus result the four possible configurations (0, 0), (0, 1), (1, 0) and (1, 1) with (0, 0) representing the instrument in pure linear position with both curvatures non-actuated. This configuration must be used when inserting the instrument inside the body.

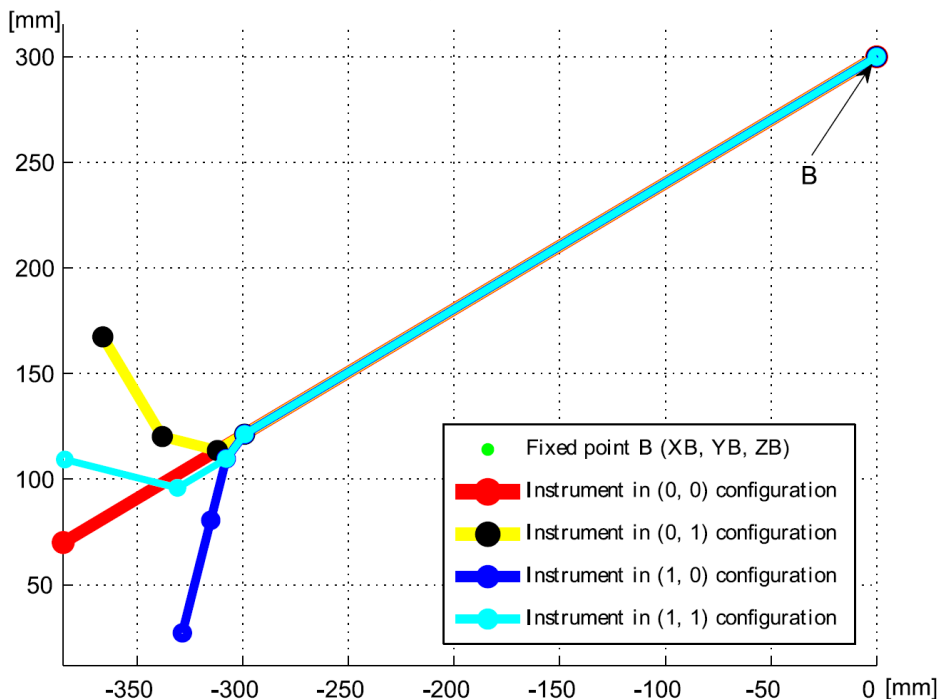


Figure 2.10. The four possible configurations of the two bends orientation module

Numerical analysis for the first case, of touching/palpation

In order to assess the performance increase of an instrument equipped with the orientation module with respect to a rigid one the workspace gain has been analysed. Three simulation parameters were considered as variable, as presented above: the length of the instrument tip, the angle of the first bend and the overall length of the instrument. Having two values for each parameter, a total number of 8 runs were performed, based on an algorithm implemented in MATLAB. By using a section view representation, in a OYZ plane, at $X_E = 500$ mm the workspace of each configuration can be represented on the same graph, together with the classical instrument workspace allowing a better view of the gains in different scenarios. The results are graphically presented in two representations, the first one showing the areas covered by the classical instrument and the one with the orientation module and the second one showing the contours for each instrument configuration. The gain is determined analytically by computing the ratio between the two areas of the graphic, as shown in the table.

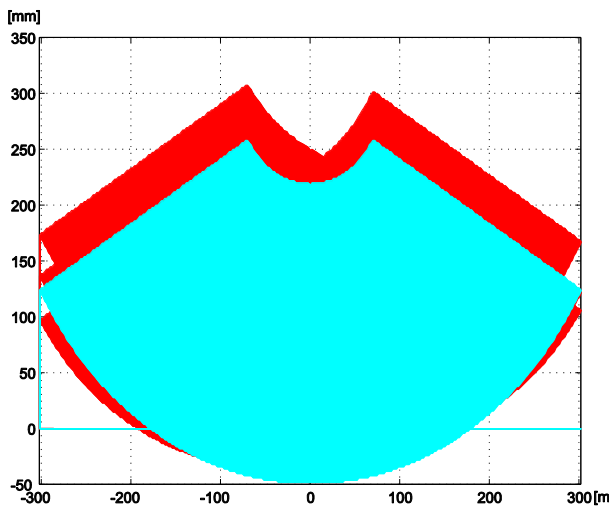


Figure 2.11. Graphical comparison for case 1

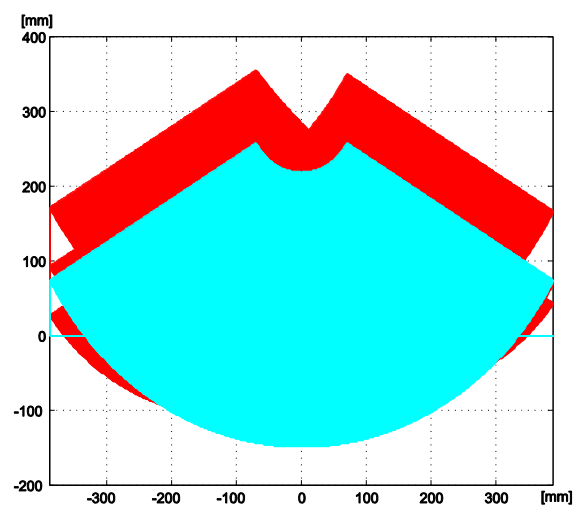


Figure 2.12. Graphical comparison for case 8

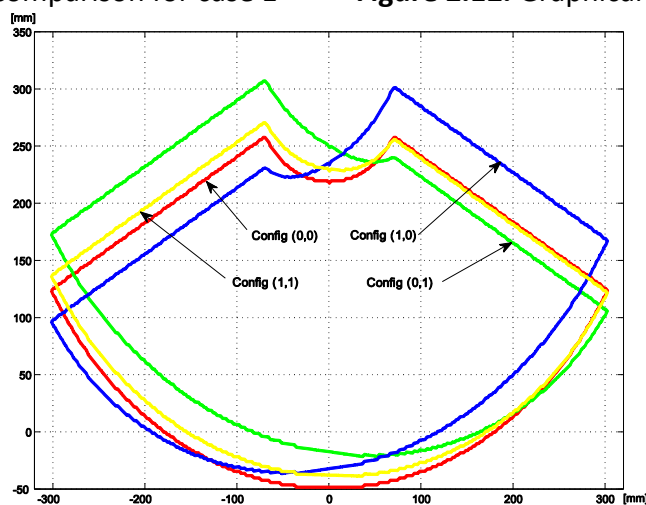


Figure 2.13. Workspace contours for the first case for touching/palpation

Table 2.1. Numerical results for instruments assessment for touching/palpatation

No.	l_e [mm]	α_1 [°]	l [mm]	Area increase	Working area [mm ²]
1	15	45	350	24.79 %	$1.50 \cdot 10^5$
2	50	45	350	44.68 %	$1.74 \cdot 10^5$
3	15	60	350	27.90 %	$1.53 \cdot 10^5$
4	50	60	350	49.32 %	$1.79 \cdot 10^5$
5	15	45	450	18.90 %	$2.42 \cdot 10^5$
6	50	45	450	34.09 %	$2.73 \cdot 10^5$
7	15	60	450	21.33 %	$2.47 \cdot 10^5$
8	50	60	450	37.66 %	$2.80 \cdot 10^5$

Numerical analysis for the second case, of grasping

The angle between the instrument and the contact surface must be over 45° for the second case, where the grasping operation is assessed. The geometrical parameters for the instruments are similar with the ones used in the first case. Figure 2.14 presents a comparison between the contours of the areas covered by the rigid instrument (similar to the (0, 0) configuration) and the instrument which uses the orientation module having the following parameters: $l_e = 15$ mm, $\alpha_1 = 45^\circ$ and $l = 350$ mm. Two additional graphical evaluations are presented with respect to the areas covered by the two types of instruments (Figs. 2.15 and 2.16) for two different combinations of parameters. With respect to the first case one can observe that the field of operation for the (0, 0) configuration becomes narrower and the gain generated by the orientation module increases. This is also reflected in Table 2 which shows the complete set of numerical determinations for the workspace comparison between the two types of instruments.

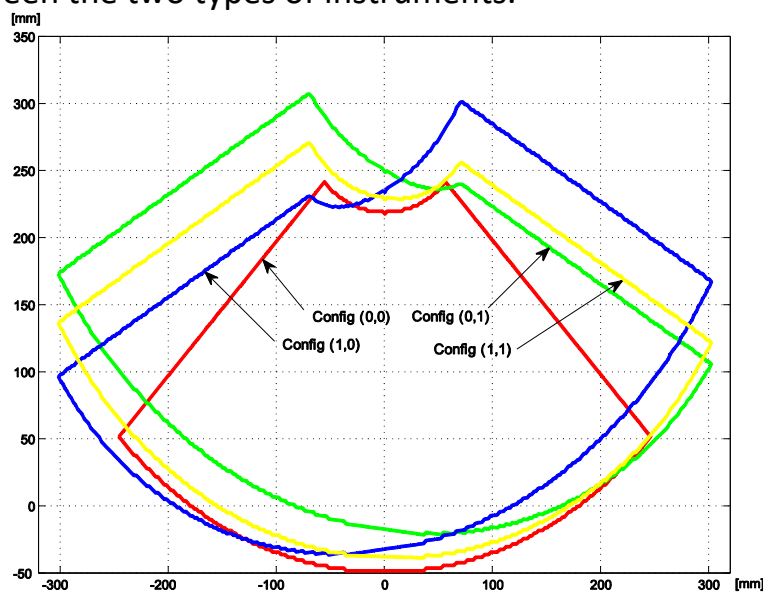


Figure 2.14. Workspace contours for the first case for grasping

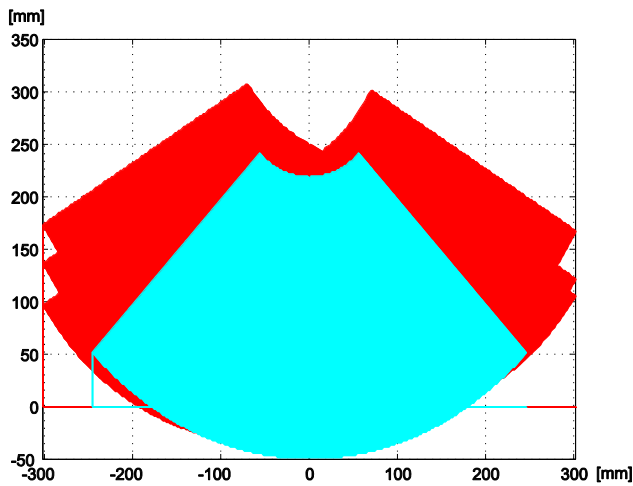


Figure 2.15. Graphical comparison for case 1

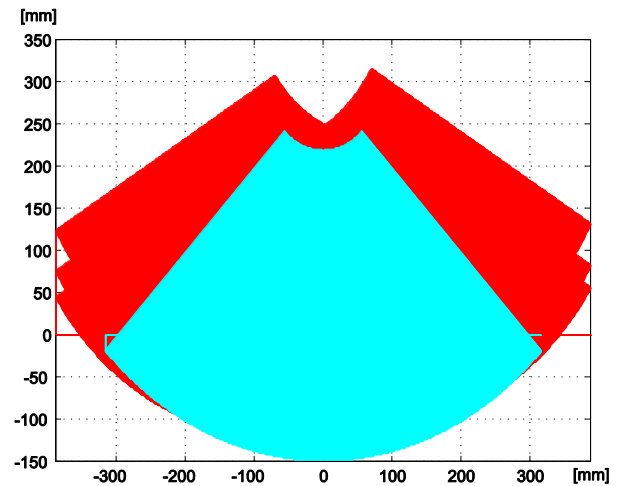


Figure 2.16. Graphical comparison for case 7

Table 2.2. Numerical results for instruments assessment for grasping

No.	l_e [mm]	α_1 [°]	l [mm]	Area increase	Working area [mm ²]
1	15	45	350	67.22%	$1.50 \cdot 10^5$
2	50	45	350	93.88%	$1.74 \cdot 10^5$
3	15	60	350	71.39%	$1.53 \cdot 10^5$
4	50	60	350	100.01%	$1.79 \cdot 10^5$
5	15	45	450	59.27%	$2.42 \cdot 10^5$
6	50	45	450	79.53%	$2.73 \cdot 10^5$
7	15	60	450	62.45%	$2.47 \cdot 10^5$
8	50	60	450	84.30%	$2.80 \cdot 10^5$

Numerical analysis for the second case, of cutting

The third task chosen for evaluation represents the most complex task, as it refers not only to the contact with the human tissue, but also to its alteration. The dexterity of the instrument is critical in this case to provide maximum handling comfort for the surgeon. Continuing the numerical experiments, Fig. 2.17 presents the contours which define the workspace for each instrument configuration, using the same parameters as in the first two cases: $l_e = 15$ mm, $\alpha_1 = 45^\circ$ and $l = 350$ mm. Figure 2.18 illustrates the comparative areas covered by the classical instrument and the one with the orientation module using the following parameters: $l_e = 50$ mm, $\alpha_1 = 60^\circ$ and $l = 350$ mm. In both numerical cases it is clear that one of the configurations, (0, 1) corresponding with the bending of the instrument head at 90° has no points that would fulfil the imposed condition. Figure 2.19 presents a comparison between the computed areas (marked with cyan or light colour if printed in grayscale) and the contours given by each configuration to illustrate the computational precision of the calculated areas. In Table 3 are given the data obtained for all the numerical simulations for the third studied case.

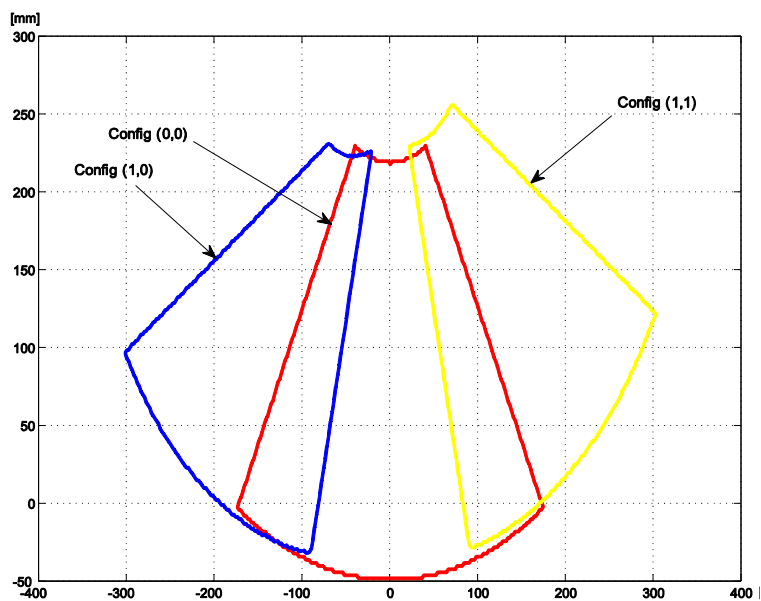


Figure 2.17. Workspace contours for the first case for cutting

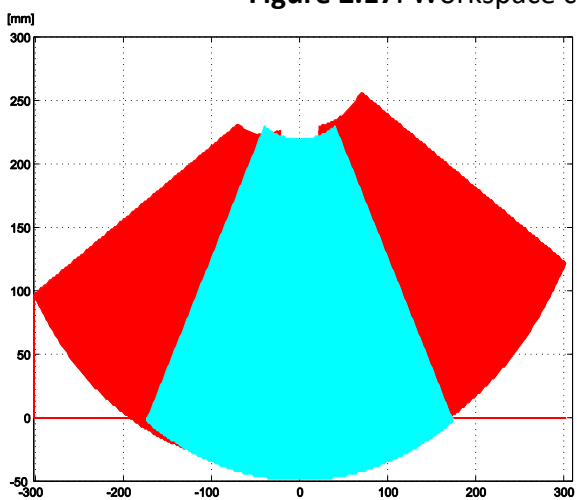


Figure 2.18. Graphical comparison for case 1

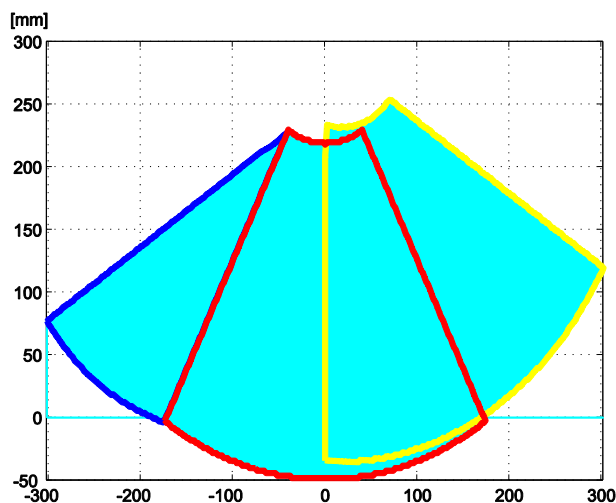


Figure 2.19. Area calculus example

Table 2.3. Numerical results for instruments assessment for cutting

No.	l_e [mm]	α_1 [°]	l [mm]	Area increase	Working area [mm ²]
1	15	45	350	91.86%	$1.52 \cdot 10^5$
2	50	45	350	82.63%	$1.09 \cdot 10^5$
3	15	60	350	93.53%	$1.16 \cdot 10^5$
4	50	60	350	84.62%	$1.10 \cdot 10^5$
5	15	45	450	93.35%	$1.96 \cdot 10^5$
6	50	45	450	85.84%	$1.89 \cdot 10^5$
7	15	60	450	94.83%	$1.98 \cdot 10^5$
8	50	60	450	87.40%	$1.90 \cdot 10^5$

Discussion

Due to the fact that for each (0, 0) configuration the orientation module provided an additional three tip orientations it was clear for the beginning that there **will be a certain workspace increase** but the real question is how much is that gain and how useful will it be for the surgical procedures. Table 2.1 with the numerical data for the first case, touch/palpation reveals an average gain of over 25 % in workspace with a maximum peak of 49 % for the fourth set of numerical data. Even though the gain is considerable, the rigid instrument can satisfy pretty well the requirements of the task. Switching to the second case, there is a dramatic change with respect to the workspace covered by each type of instrument, the one equipped with the orientation module having gains with an average of over 70 % and a peak of 100.1 % registered again in the fourth data set. The second critical aspect that has to be pointed is that comparing the areas covered by the instrument with the orientation module there is no shrinkage, which means that more procedures can be easily executed in the entire surgical field. The third set of numerical data, Table 2.3, reveals higher gains in workspace for the instrument with the orientation module with an average of over 80 % and a peak of 95 %. Here as it can be seen in Fig. 2.17 one configuration has no valid points in the workspace. This is due to the fact that this configuration (where the instrument tip is bent at 90 % with respect to the rod) is suitable for lateral approach. Figure 2.20 underlines this aspect showing the lateral approach ability for the instrument with the orientation module. An important fact is that there are no valid points for the (0, 0) configuration which means that classical instruments are not suitable for this approach.

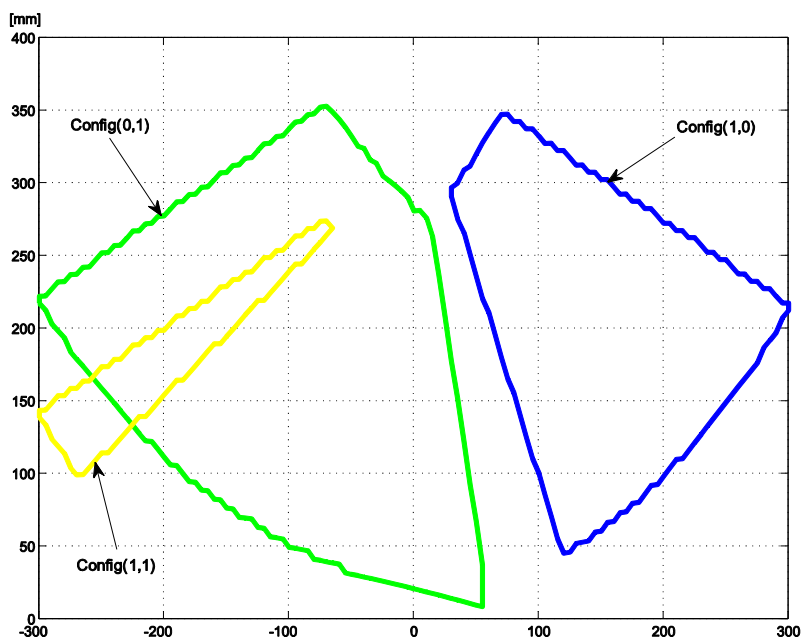


Figure 2.20. Workspace contours for lateral approach using the orientation module

The use of an orientation module for instruments in robotic assisted procedures can reduce the collision problems allowing the left and right instrument tips to work close one to the other while keeping the robotic arms apart. Analysing the gain obtained for different instrument lengths it can be concluded that the gain increases for shorter instruments and for larger angle values for each bend. In terms of instrument tip length, for the first two cases a longer tip means higher workspace gain and for the third one the opposite. The numerical data points out that while keeping the solution very simple several configurations can be set up to provide optimal tools for different tasks (figure 2.21).

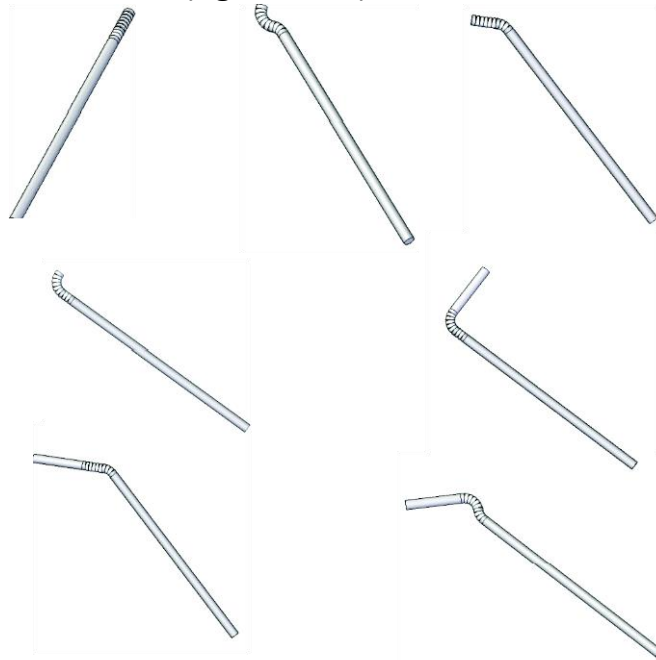


Figure 2.21. Different instrument configurations integrating the orientation module

The numerical results point out several key aspects with regard to the use of the orientation module for surgical instruments:

- ✓ The workspace of the instrument is very wide for any type of approach which reduces the need of supplementary incisions during complicated procedures;
- ✓ The instrument provides better ergonomics for the surgeon with positive effects upon the patient safety and procedure duration;
- ✓ The instrument provides lateral approach which eliminates the need of new incisions for those specific areas;
- ✓ The orientation module is completely modular, the computational tools enabling the definition of any configuration without the need of redesign;
- ✓ From the economical point of view the existence of a single solution usable in a wide area of configurations while keeping a very simple structure provides the necessary means for developing affordable, cost-effective solutions;
- ✓ The orientation module can be integrated in surgical instrument in different locations and using single module a lot of useful instrument configurations can be obtained, as illustrated in Fig. 2.21.

A demonstrative experimental model of the orientation module



Figure 2.22. The components of the mechanism



Figure 2.23. Manufacturing of the experimental model

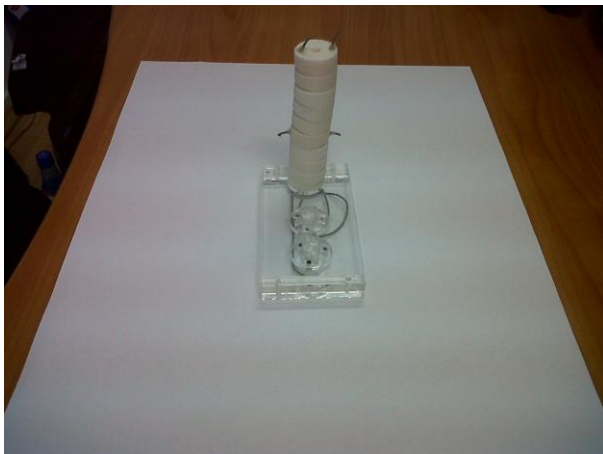


Figure 2.24. Module in the straight position

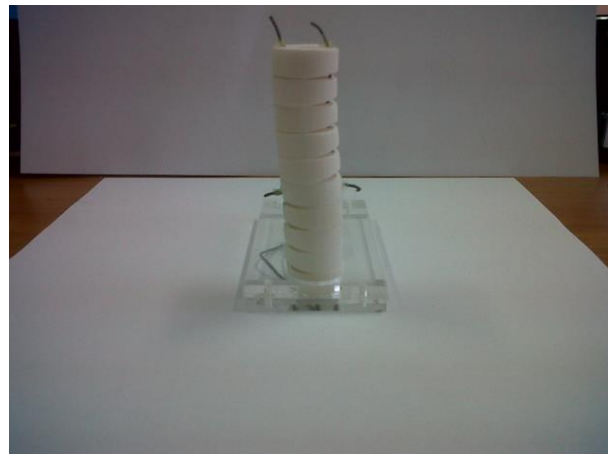


Figure 2.25. Module in the straight position – details of the components and bends



Figure 2.26. Module with first bend actuated and second one straight



Figure 2.27. Module with first bend non-actuated and second one actuated



Figure 2.28. Module with both bends actuated

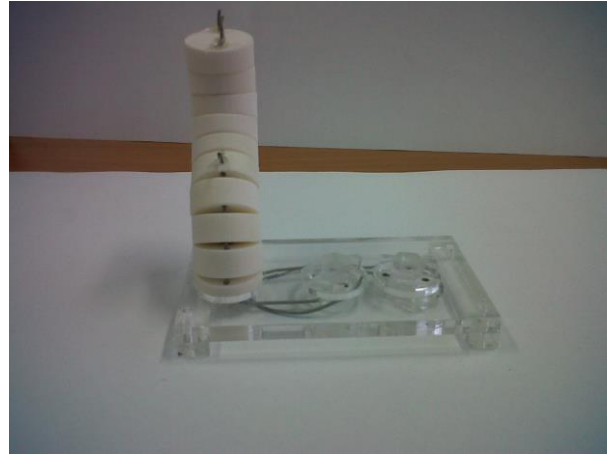


Figure 2.29. Module with both bends actuated
– lateral view

A simple spherical mechanism for robotic assisted surgical applications

The following kinematic scheme which is illustrated in Fig. 2.30 presents a classic spherical robotic arm with three active joints: q_1, q_2, q_3 . The first motor achieves the rotational motion around the X axis, the second one achieves a circular displacement along a curve of radius R while the third motor achieves a linear displacement along the radius of the sphere. Considering a combined motion between these three motors, the instrument tip can reach any point of the surgical field. Besides its kinematic simplicity, this structure presents another characteristic that in its fixed coordinate system the “virtual” fixed point is always the same: $B(R, 0, 0)$, where R is the radius of the sphere.

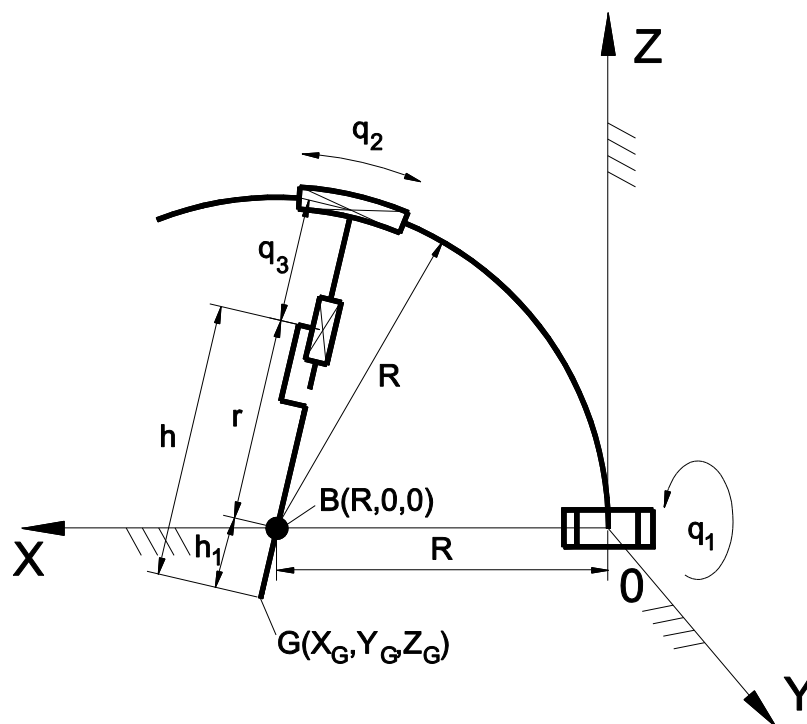


Figure 2.30. The kinematic scheme of the robotic arm

Geometric Modelling

For the geometrical modelling of the robotic arm, a fixed coordinate system OXYZ is defined with the origin in the centre of the first active joint and the positive direction of X towards the centre of the sphere as it can be seen in Fig. 3.

The following parameters are known for the geometric modelling of this structure:

- The radius, R of the mechanism;
- The length, h of the endoscopic instrument;
- The coordinates of point B, which can be defined with respect to OXYZ coordinate system, $B(R, 0, 0)$.

With respect to the fixed coordinate system, the following matrices are introduced:

Rotation around the X axis with q_1 :

$$R_{x_{-}q_1} = \begin{bmatrix} 1 & 0 & 0 \\ 0 & \cos(q_1) & -\sin(q_1) \\ 0 & \sin(q_1) & \cos(q_1) \end{bmatrix}. \quad (2.24)$$

Rotation around the Y axis with q_2 :

$$R_{y_{-}q_2} = \begin{bmatrix} \cos(q_2) & 0 & \sin(q_2) \\ 0 & 1 & 0 \\ -\sin(q_2) & 0 & \cos(q_2) \end{bmatrix}. \quad (2.25)$$

Translation on the Z axis with $-q_3-h$:

$$T_{z_{-}q_3-h} = \begin{bmatrix} 0 \\ 0 \\ -q_3-h \end{bmatrix}. \quad (2.26)$$

The authors have adopted the XY Euler convention for the rotational matrices which has led to the following data:

Rotation around the X axis with ψ :

$$R_{x_{-}\psi} = \begin{bmatrix} 1 & 0 & 0 \\ 0 & \cos(\psi) & -\sin(\psi) \\ 0 & \sin(\psi) & \cos(\psi) \end{bmatrix}. \quad (2.27)$$

Rotation around the Y axis with θ :

$$R_{y_{-}\theta} = \begin{bmatrix} \cos(\theta) & 0 & \sin(\theta) \\ 0 & 1 & 0 \\ -\sin(\theta) & 0 & \cos(\theta) \end{bmatrix}. \quad (2.28)$$

Where the two angles ψ and θ have the expressions:

$$\psi = a \tan 2(Y_G - Y_B, Z_B - Z_G). \quad (2.29)$$

$$\theta = a \tan 2 \left(X_B - X_G, \frac{(Z_B - Z_G)}{\cos(\psi)} \right). \quad (2.30)$$

Replacing the coordinates of the point B with the known values, it results:

$$\psi = a \tan 2(Y_G, -Z_G). \quad (2.31)$$

$$\theta = a \tan 2 \left(R - X_G, \frac{-Z_G}{\cos(\psi)} \right). \quad (2.32)$$

The inverse geometrical model

In the case of the inverse geometrical model, the parameters of the structure and the coordinates of the instrument tip (point G) are considered known and the coordinates of the active joints q_1, q_2, q_3 should be determined.

Using equations (2.24) – (2.32) it results:

$$\begin{cases} q_1 = a \tan 2(\sin(\psi) \cdot \cos(\theta), \cos(\psi) \cdot \cos(\theta)) \\ q_2 = a \tan 2(\sin(\theta) \cdot \cos(q_1), \cos(\psi) \cdot \cos(\theta)) \\ q_3 = R - (h - h_1) \end{cases} \quad (2.33)$$

Where:

$$h_1 = \sqrt{(X_G - R)^2 + Y_G^2 + Z_G^2}. \quad (2.34)$$

The direct geometrical model

In the case of the direct geometrical model, the parameters and the position of the active joints are known and the coordinates of the instrument tip must be determined.

The expressions for the angles ψ and θ are determined using the known values of q_1 and q_2 :

$$\psi = a \tan 2(\sin(q_1), \cos(q_1)). \quad (2.35)$$

$$\theta = a \tan 2(\sin(q_2), \cos(q_2)). \quad (2.36)$$

The length of the instrument situated inside the patient body is:

$$h_1 = q_3 - R + h. \quad (2.37)$$

Using the known coordinates of point B, it results:

$$\begin{cases} X_G = X_B - h_1 \cdot \sin(q_2) \\ Y_G = h_1 \cdot \sin(q_1) \cdot \cos(q_2) \\ Z_G = -h_1 \cdot \cos(q_1) \cdot \cos(q_2) \end{cases} . \quad (2.38)$$

Workspace Analysis

For the generation of the robot workspace, the following parameters have been used with the values below:

- Radius R = 300 mm;
- Instrument length h = 270 mm;

The workspace of the structure is illustrated in Fig. 2.31. In addition, a schematic representation of the robot dimensions for the arm is also illustrated, to suggest the ratio between the dimensions of the structure and the achievable workspace. The condition that must be imposed in order to have a functional solution, is $R > h$ meaning that the radius of the structure must be greater than the instrument length so that the system is capable of insertion and extraction of the instrument from the surgical field.

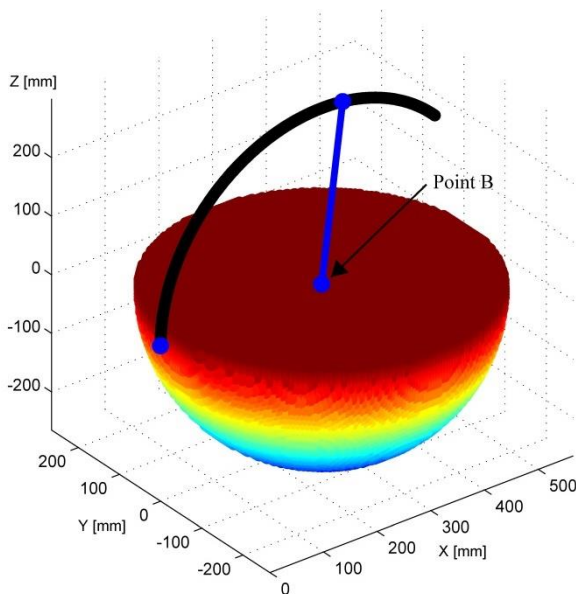


Figure 2.31. Theoretical maximum robot workspace

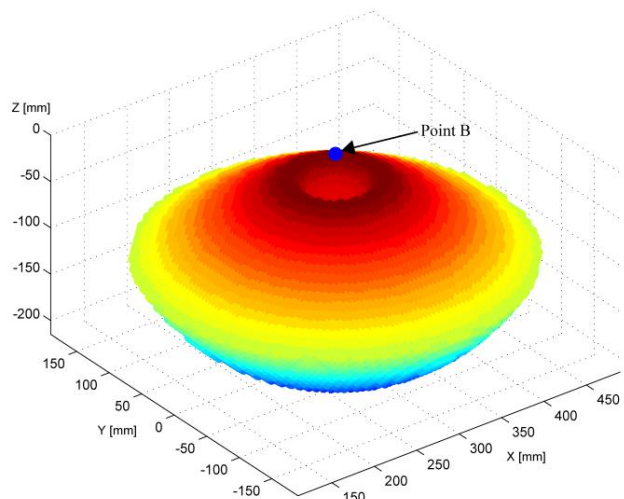


Figure 2.32. The robot workspace restricted by the surgical conditions

There are a set of conditions [PIS10] imposed by the surgical act such as:

- ✓ The laparoscope should be inside the patient at least 50 mm, due to the thickness of the skin;
- ✓ The angle between the laparoscope and the normal axis to the patient skin should not exceed 60° (Fig. 2.32).

Another very important aspect that needs to be taken into consideration is the precision in positioning of the robot. This can be studied in terms of capability, by determining a relation between positioning precision of the actuators and the motion of the instrument tip. Considering a variation of 1 displacement unit achieved by the actuator, in Fig 2.33. can be seen the uniform radial precision variation which decreases with the distance increase with respect to point B. The proportionality between the motions of at the actuator level and the end-effector displacement is maintained below one and with no sudden changes in its value. As the value of the proportionality factor is below one, the positioning precision of the instrument tip will be always higher than the actuator increment, and it can be stated that the mechanism has a very good precision level in any point of the workspace.

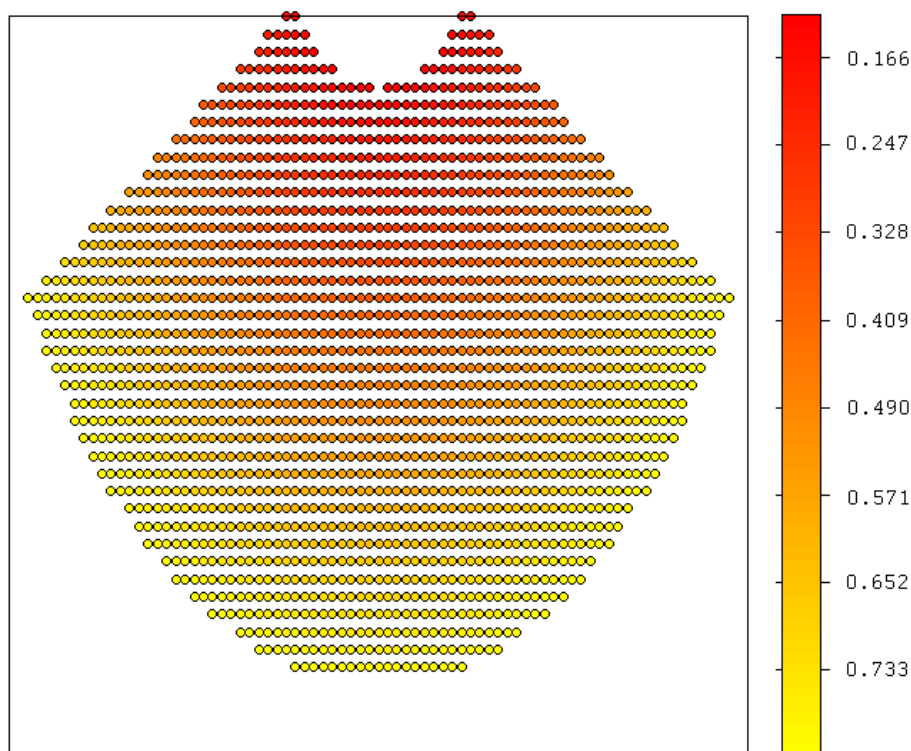


Figure 2.33. Precision mapping of the robot

Kinematic model and singularities analysis of the spherical robotic arm

The kinematic model is solved with the equations which characterize the relationship between the active coordinates and the ones of the instrument tip (point G). Those equations are used as input data for the solving of the model.

$$\left\{ \begin{array}{l} f_1(q_1, Y_G, Z_G) \equiv \frac{\sin(q_1)}{\cos(q_1)} + \frac{Y_G}{Z_G} = 0 \\ f_2(q_1, q_2, X_G, Z_G) \equiv \\ \equiv \frac{\sin(q_2)}{\cos(q_2)} + \cos(q_1) \cdot \frac{R - X_G}{Z_G} = 0 \\ f_3(q_3, X_G, Y_G, Z_G) \equiv q_3 - R + h - h_1 = \\ = q_3 - R + h - \sqrt{(R - X_G)^2 - Y_G^2 - Z_G^2} = 0 \end{array} \right. \quad (2.39)$$

Using the above system of equations, (2.39), the Jacobi matrices are determined. Matrix A is presented in (2.40) :

$$A = \begin{pmatrix} 0 & \frac{1}{Z_G} & -\frac{Y_G}{Z_G^2} \\ -\frac{\cos(q_1)}{Z_G} & 0 & -\cos(q_1) \cdot \frac{R - X_G}{Z_G^2} \\ \frac{R - X_G}{h_1} & \frac{-Y_G}{h_1} & \frac{-Z_G}{h_1} \end{pmatrix} \quad (2.40)$$

And the Jacobi matrix B is presented in (2.41):

$$B = \begin{pmatrix} \frac{1}{\cos^2(q_1)} & 0 & 0 \\ -\sin(q_1) \cdot \frac{R - X_G}{Z_G} & \frac{1}{\cos^2(q_2)} & 0 \\ 0 & 0 & 1 \end{pmatrix} \quad (2.41)$$

Singularities analysis

With the Jacobi matrices taken into account, the singularities of the spherical robot can be studied and based on eq. (2.40) the determinant of matrix A is:

$$\det(A) = \frac{\cos(q_1) \cdot h_1}{Z_G^3} \quad (2.42)$$

Three cases of singularities can be distinguished:

1. $q_1 = \pm \frac{\pi}{2}$. This corresponds to the case where the robot arm is located horizontally on any of its sides, a position that can never be attained in the applications. In this case point G would be situated in the OXY plane with $Z=0$, which represents the boundary of the workspace. Analysing the above figure 2.33 it results that these points are outside the robot workspace.
2. $h_1 = 0$. From the equation 2.34. it results that $G \equiv B$. In this case, when the tip of the instrument is located in the centre of the sphere, the modification of values of q_1 and q_2 is irrelevant because the position of the instrument remains the same. This means that after the instrument insertion with the initial orientation defined, only q_3 requires actuation in order to insert the instrument inside the patient. But this situation is a boundary one and during a medical procedure, the instrument will never reach point B.
3. $Z_G = 0$. This case refers again to the boundary surface of the robot workspace and it results to be outside the operational robot workspace.

The determinant of matrix B is:

$$\det(B) = \frac{1}{\cos^2(q_1) \cdot \cos^2(q_2)} \quad (2.43)$$

Two cases can be distinguished:

1. $q_1 = \pm \frac{\pi}{2}$. This corresponds to the first case analysed for matrix A.
2. $q_2 = \pm \frac{\pi}{2}$. The same situation is created when the second actuator reaches the extreme positions that place the tip of the instrument on the OXY plane at $Z_G=0$.

With the above singularities presented and analysed it can be concluded that there are no singular points in the operational workspace of the robot. Still one should be careful during the instrument insertion procedure as the coordinates of q_1 and q_2 must be correctly defined before introducing the instrument inside the patient.

The kinematic model of the robotic arm

The derivatives of the two Jacobi matrices lead towards simple expressions. The derivative of matrix A is:

$$\dot{A} = \begin{pmatrix} 0 & -\frac{\dot{Z}_G}{Z_G^2} & \frac{2 \cdot Y_G \cdot \dot{Z}_G - Z_G \cdot \dot{Y}_G}{Z_G^2} \\ AA_{21} & 0 & AA_{23} \\ AA_{31} & AA_{32} & AA_{33} \end{pmatrix} \quad (2.44)$$

Where:

$$\begin{aligned} AA_{21} &= \frac{\sin(q_1) \cdot \dot{q}_1 \cdot (R - X_G) + \cos(q_1) \cdot \dot{Z}_G}{Z_G^2} \\ AA_{23} &= \frac{\sin(q_1) \cdot \dot{q}_1 \cdot (R - X_G) + \cos(q_1) \cdot \dot{X}_G}{Z_G^2} + \frac{2 \cdot \cos(q_1) \cdot (R - X_G) \cdot \dot{Z}_G}{Z_G^3} \\ H_1 &= \frac{(X_G - R) \cdot \dot{X}_G + Y_G \cdot \dot{Y}_G + Z_G \cdot \dot{Z}_G}{h_1} \\ AA_{31} &= -\frac{h_1 \cdot \dot{X}_G + (R - X_G) \cdot H_1}{h_1^2} \\ AA_{32} &= -\frac{h_1 \cdot \dot{Y}_G + Y_G \cdot H_1}{h_1^2} \\ AA_{33} &= -\frac{h_1 \cdot \dot{Z}_G + Z_G \cdot H_1}{h_1^2} \end{aligned} \quad (2.45)$$

The derivative of matrix B has the expression:

$$\dot{B} = \begin{pmatrix} \frac{2 \sin(q_1) \cdot \dot{q}_1}{\cos^3(q_1)} & 0 & 0 \\ BB_{21} & \frac{2 \sin(q_2) \cdot \dot{q}_2}{\cos^2(q_2)} & 0 \\ 0 & 0 & 0 \end{pmatrix} \quad (2.46)$$

Where:

$$BB_{21} = \frac{\cos(q_1) \cdot \dot{q}_1 \cdot (R - X_G) + \sin(q_1) \cdot \dot{X}_G}{Z_G} + \frac{\sin(q_1) \cdot (R - X_G) \cdot \dot{Z}_G}{Z_G^2} \quad (2.47)$$

The notations (2.48) are introduced:

$$\begin{aligned} X &= [X_G \quad Y_G \quad Z_G]^T; \dot{X} = [\dot{X}_G \quad \dot{Y}_G \quad \dot{Z}_G]^T \\ \ddot{X} &= [\ddot{X}_G \quad \ddot{Y}_G \quad \ddot{Z}_G]^T \\ Q &= [q_1 \quad q_2 \quad q_3]^T; \dot{Q} = [\dot{q}_1 \quad \dot{q}_2 \quad \dot{q}_3]^T \\ \ddot{Q} &= [\ddot{q}_1 \quad \ddot{q}_2 \quad \ddot{q}_3]^T \end{aligned} \quad (2.48)$$

Using (2.44-2.48) the direct (2.49) and inverse (2.50) kinematic models of the spherical robot are determined:

$$\dot{X} = -A^{-1} \cdot B \cdot \dot{Q}; \quad \ddot{X} = -A^{-1} (\dot{A} \cdot \dot{X} + B \cdot \ddot{Q} + \dot{B} \cdot \dot{Q}) \quad (2.49)$$

$$\dot{Q} = -B^{-1} \cdot A \cdot \dot{X}; \quad \ddot{Q} = -B^{-1} (\dot{B} \cdot \dot{Q} + A \cdot \ddot{X} + \dot{A} \cdot \dot{X}) \quad (2.50)$$

With the same input data for the sphere radius and instrument length, a trajectory simulation was made to study the behaviour of the robot. The trajectory is a straight line in space which forces the robot to travel the workspace from one side to another. The motion is clearly larger than usual commands given in medical applications but it is more suitable for the study of the robot capabilities and behaviour.

The input data for the simulation is:

$$\begin{aligned} X_{Ginit} &= 216.96 \text{ mm}; \quad X_{Gfinal} = 240 \text{ mm}; \\ Y_{Ginit} &= -21.46 \text{ mm}; \quad Y_{Gfinal} = 50 \text{ mm}; \\ Z_{Ginit} &= -58.96 \text{ mm}; \quad Z_{Gfinal} = -150.75 \text{ mm}; \\ v_{\max} &= 10 \text{ mm/s}; \quad a_{\max} = 5 \text{ mm/s}^2. \end{aligned} \quad (2.51)$$

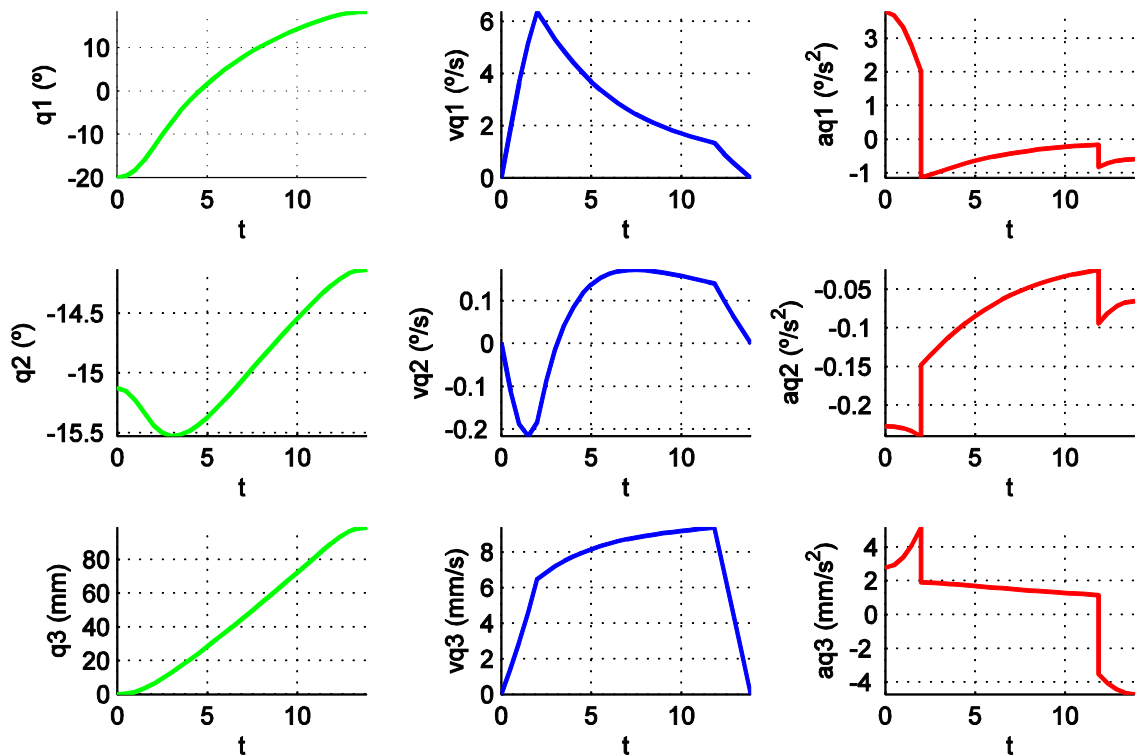


Figure 2.34. Time history diagrams for driving coordinates, velocities and accelerations

Displacements, speeds and accelerations at the level of each individual actuator are presented in Fig. 2.34. The total computational time of the trajectory was 0.06 s (0.000184 s for one set of points) on a Intel Quad Core 2.66 GHz, showing the real-time behaviour capabilities of the developed mathematical model.

Robot Adaptability in Different Minimally Invasive Medical Scenarios

Due to the architectural properties, the spherical robotic structure can be used in different scenarios without any alteration or modification to the kinematic complexity [VAI12a].

I. Laparoscope / instrument holder

The simplest task that the robot can achieve is the one responsible for the laparoscope holder (Fig. 2.35). In this case, the system aids and assists the surgeon by positioning the endoscopic camera at his command.

This configuration can also be used in other minimally invasive scenarios where the only condition is the presence of the fixed point in space.

In this case, the robot has applications in;

- Biopsies prelevation in interventional medicine;
- Needle positioning in deeply located tumours for brachytherapy;
- Exploratory investigations for patients whose condition may endanger the authorized personnel.

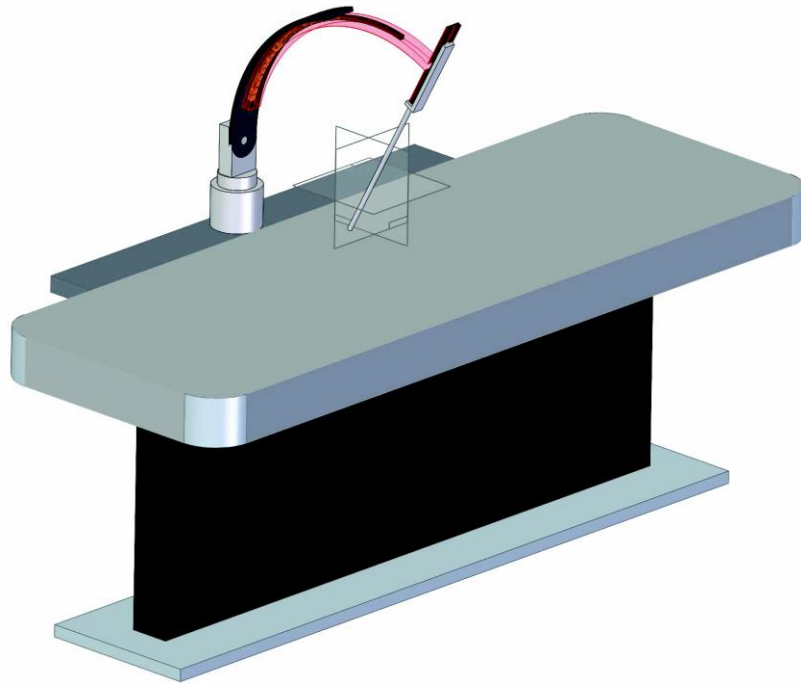


Figure 2.35 One robotic arm functioning as a laparoscope holder for minimally invasive surgery

II. Surgical system with 3 or 4 individual arms

The second configuration (Fig 2.36) can be obtained with no structural modification and represents a surgical system with three or four arms: one for the laparoscopic camera, two for the main surgical instruments and an optional arm for side tasks such as: suction, internal organs displacement etc.

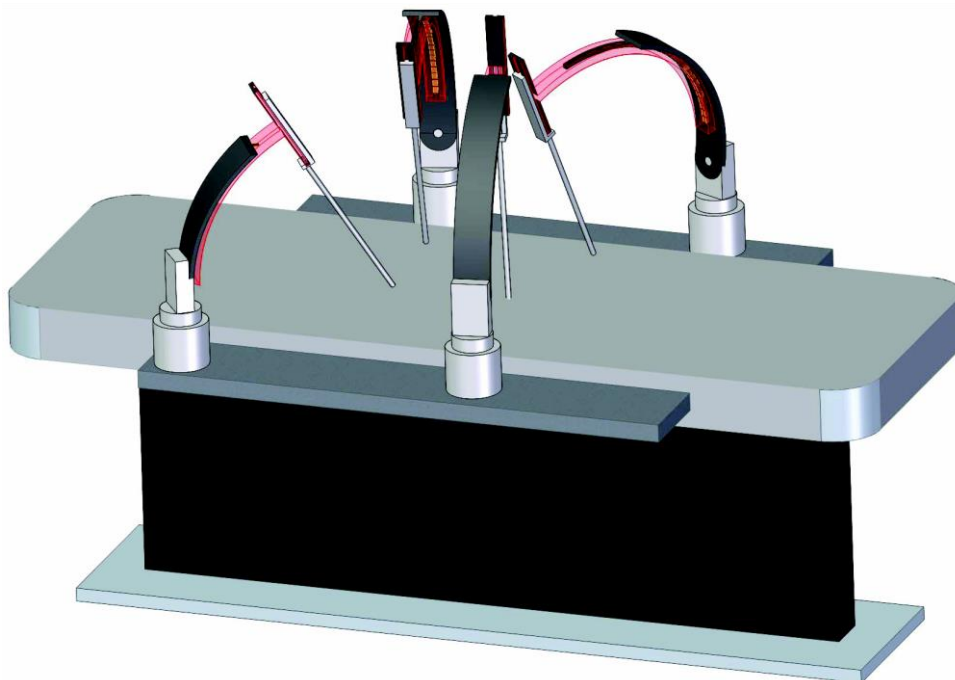


Figure 2.36. Four robotic arms functioning as a robotic system for minimally invasive surgery

III. Robotic arms with multiple instruments for SILS

The most difficult task for surgical systems is the achievement in manipulation of surgical instruments in a confined space imposed by the SILS procedure. As it can be seen in figure 2.37 in the SILS procedure, a multilumen trocar is used through which all the instruments are introduced. For this robotic structure this can be transformed into an advantage because it can be interpreted that all instruments converge towards a point situated along the longitudinal axis of the endoscopic camera.

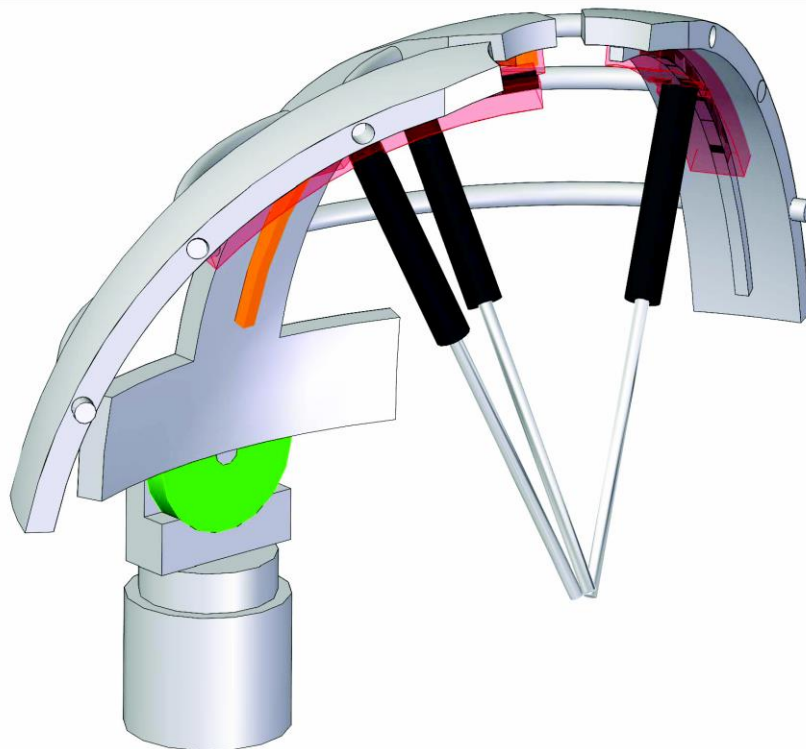


Figure 2.37 Robotic arm configured for SILS

This configuration is achieved by taking into consideration the following criteria:

- ✓ Because of the confined space, the motion of the camera generates the motion of the instruments.
- ✓ The instruments intersect inside the trocar and they cannot crossover the laparoscopic camera.
- ✓ The instrument length is the same, or in a close range.
- ✓ The robot can manipulate the instruments over the head.
- ✓ Only three instruments can be manipulated.
- ✓ The endoscopic camera is always kept in the middle.

Chapter 3. Robotic systems for brachytherapy

“The good physician treats the disease; the great physician treats the patient who has the disease.” (William Osler)

Brachytherapy – evolution and current limitations

Needle placement techniques cover a wide area of medical applications, where the task can be described, in a very simple way, as the insertion of a needle (fig. 3.1) on a certain trajectory, from outside up to a target point situated in the patient body. Needle placement covers applications like biopsies, fluid extraction from internal organs (cardiac tamponade, lungs) or placement of radioactive seeds in different body organs in minimally invasive cancer therapy [STR11, BOC08].

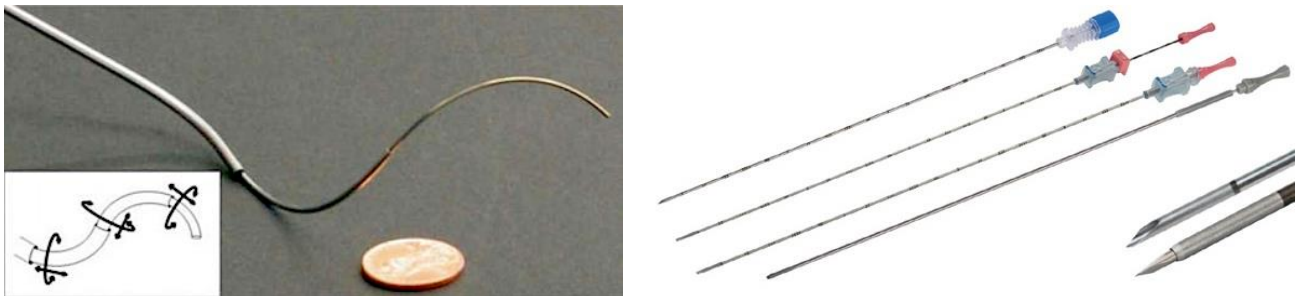


Figure 3.1. Different needles for medical applications

In [STR11] it is shown that a robotic device enhances the needle placement precision beyond the natural human capabilities. This is, on one hand because a device holding the needle is much steadier than the human hand and, on the other hand such a device can use additional information like force measurement, real-time visual monitoring and motion scaling.

Classification of malignant tumours

A very important aspect in the management of cancer (malignant tumours) is the staging of the disease, whereas different therapeutic decisions should be considered based on the survival chances, body frailty and available clinical trials. One of the worldwide recognized such staging systems is the TNM Classification of Malignant Tumours, which was developed by Pierre Denoix over a period of 10 years (1942-1953) [DEN46]. The TNM Classification is continuously updated by the Union for International Cancer Control (UICC) [BRI17] and currently it holds specific classifications for each solid tumours (as it is not applicable to leukaemia and tumours of the central nervous system). Specifically, the TNM Classification has the following codification:

- The letter “**T**” characterizes the size and extent of the main (primary) tumour;
- The letter “**N**” describes the number of nearby lymph nodes that are affected by cancer;
- The letter “**M**” indicates whether the cancer has metastasized (the cancer has spread from the primary tumour of other parts of the body).

When characterizing cancer using the TNM system, for each letter there will be an associated number detailing the cancer spread (e.g. T2N1MX). The specific values that can be used for each of the three TNM parameters are:

Primary tumor (T)

- TX: Main tumor cannot be measured.
- T0: Main tumor cannot be found.
- T1, T2, T3, T4: Refers to the size and/or extent of the main tumor.

The higher the number after the T, the larger the tumor or the more it has grown into nearby tissues. T's may be further divided to provide more detail, such as T3a and T3b.

Regional lymph nodes (N)

- NX: Cancer in nearby lymph nodes cannot be measured.
- N0: There is no cancer in nearby lymph nodes.
- N1, N2, N3: Refers to the number and location of lymph nodes that contain cancer.

The higher the number after the N, there exist more lymph nodes that contain cancer.

Distant metastasis (M)

MX: Metastasis cannot be measured.

M0: Cancer has not spread to other parts of the body.

M1: Cancer has spread to other parts of the body.

There exist other staging classifications, some of them less complicated which try to classify the cancer spread (from local, regional to distant) but they are used mainly to allow patients to have a simple understanding of their disease.

Cancer patient management has two main areas of application with respect to the proposed therapeutic goal:

- Curative – mainly applied in the early stages of cancer (MX, M0), when, by applying different treatments the malignancy can be eradicated from the body leading to the cure of the cancer;
- Palliative – mainly applied in the advanced stages of cancer (M1), when due to location or spread, there is no option of curing the disease but treatments aim to improve the patient survivability time and its quality of life.

Brachytherapy (introduced in chapter 1), also known as internal radiotherapy, sealed source radiotherapy, curietherapy or endocurietherapy, **is a form of radiotherapy** that involves the placement of tiny radioactive miniaturized sources very precisely in the tumour area, delivering high dosage of radiation in the

cancerous cells. Its effectiveness is clearly demonstrated, its side effects are reduced to a minimum, but it involves an important condition: the catheters delivering the radioactive sources must be placed precisely as the radiation dose decreases abruptly from the base and incorrect positioning causes the necrosis of healthy tissue without affecting the tumour.

While in case of curative approach the primary tumours could be located in almost all regions of the body having specific needle/patient relative approaches, for the palliative treatment of cancer patients there are two organs of interest: the liver and the lungs. This is due to the fact that these two organs are filtering the entire blood and once the malignant tumours start to migrate they will become the first locations for metastasis. However, even in such advanced cases with proper care a patient can gain even 5 years of survival with good quality of life which is very important.

As a final comment onto the therapeutic advantages of brachytherapy it must be stated that due to the local nature of effect and the non-destructive way of delivering the medicine this technique has far less side effects compared to open surgery external radiation or chemotherapy.

Accuracy problem

The brachytherapy needles are inserted from outside the body up to the targeted point with an accepted positioning error of 1 mm. This is not hard to achieve for tumours close to the body surface but for the deeper located tumours this becomes a problem. While the different tissue densities, the elasticity and the anatomical motion of the body (due to respiration and heartbeat) have a negative influence on the positioning accuracy also any error in the needle orientation will lead to negative results.

An analysis of the maximum acceptable orientation error with respect to the targeted point depth is presented in figure 3.2. The following parameters are defined: d – the needle insertion depth (between 50 and 250 mm), α_{\max} – the angular deviation, e – maximum acceptable error, which are all integrated in the following equation:

$$\alpha_{\max} = 2 \cdot \arcsin\left(\frac{1}{2} \cdot \frac{e}{d}\right) \cdot \frac{180}{\pi} \quad (3.1)$$

In the figure 3.2 it can be seen that for an error of 1 mm, which is the desired value for a successful treatment, the maximum angular allowable error varies from 1.1459° for a depth of 50 mm to 0.2292° for 250 mm. Even for higher acceptable errors, the angular positioning errors have to be small: 2.2920° for 50 mm depth and

up to 0.4584° at 250 mm depth for an error of 2 mm and respectively 3.483° for 50 mm depth and up to 0.6876° at 250 mm depth for an error of 3 mm.

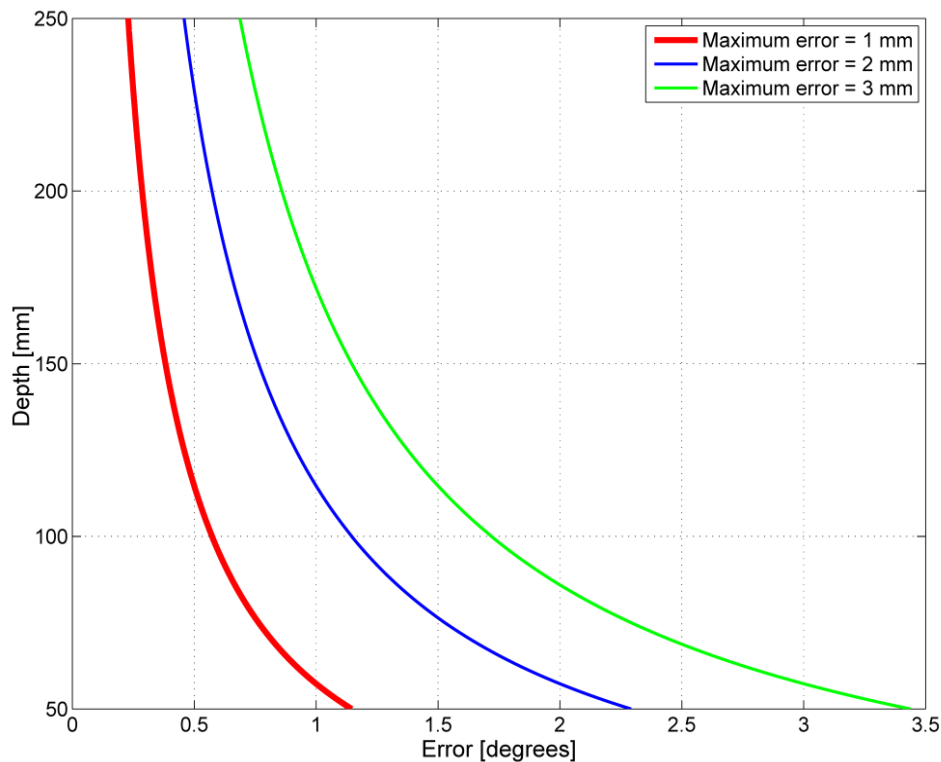


Figure 3.2. The maximum angular allowable positioning error for a given maximum positioning error of the needle tip at different depths

Application definition

The robotic structure should introduce, based on radiologic data, rigid needles of diameter varying from 0.6 mm up to 2 mm and a length from 50 mm up to 250 mm inside the patient body following a linear trajectory. Due to the long distances, the variable tissue density one can define the first requirement for the robot: **the needle is introduced**, in a linear trajectory **by an independent mechanism**, to ensure constant precision for the entire displacement and to avoid any deviations from the predefined trajectory.

Some of the areas of interest for needle placement in different medical applications where the use of a robotic device is justified cover the human thoracic and abdominal area where the target point can be situated in close vicinity to different structures (blood vessels, ganglions, other organs) whereas an error can cause a cataclysmic event leading up the death of the patient. Several applications require the placement of multiple needles in a regular (circular or rectangular matrix) or irregular display thus defining the second requirement for the robot: **it should be capable of placing multiple needles on parallel or independent trajectories**. Thus an advantage would be to be able to fix the robot orientation after its initial setup

and modify only the insertion point from one needle to the other for the situation where parallel trajectories are needed.

Besides emergency situations where the intervention must be performed very fast, needle placement is carried out following a set of imagistic investigations ranging from simple radiologic exams to echography, computer tomography (CT) and/or magnetic resonance imaging (MRI). These techniques provide a set of images enabling the preplanning of the procedure where the physicist defines the desired locations for the radioactive seeds (computing also the amount of radiation that will be delivered by each seed) while the physician defines safe linear trajectories to reach the targeted point(s).

Nevertheless, in order to increase the safety of the procedure it is desired to have a real-time visual feedback of the needle placement during the procedure to reduce the risk of damaging any internal body structures [BOC08]. During the first steps of introducing robotic systems in medical arena, the imagistic methods that can be used during the needle placement were defined [SAU18, EVA18]: High Intensity Focal Ultrasound (HIFU), CT, MRI and Positron Emitted Tomography (PET Scan). Each of these techniques has advantages and limitations. The best option as image quality is the use of MRI but due to the high magnetic fields generated by the machine there are a lot of restrictions for both patient and robot. The ultrasound machines have a low image quality and a limited use especially for deep targets.

CT can be considered at the moment as the most versatile option even though the image quality is lower compared to MRI machines but it is still good enough for real-time needle placement procedures. Fig. 3.3 illustrates an example of a CT machine equipped with supplementary laser sensors (the lasers were enhanced in the figure to provide better contrast) for position calibration. This type of CT scanners is designed especially for fast real-time image feedback but they cannot be used in diagnostics [PLA05]. Fig. 3.4 shows a CT image with a needle inserted inside the human body [GUP05].



Figure 3.3. CT-Sim scan with laser positioning system

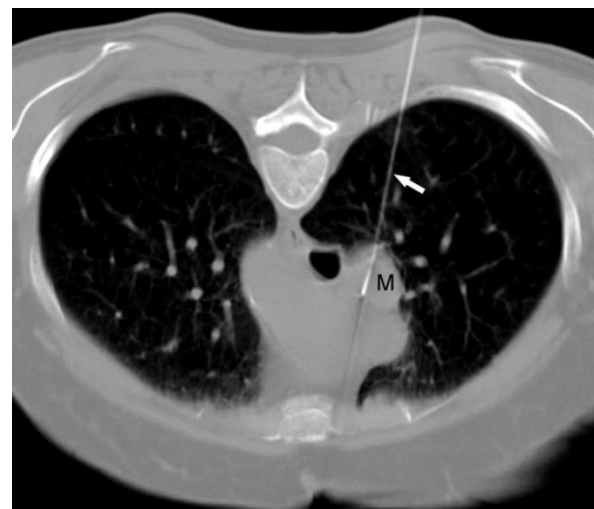


Figure 3.4. CT scan with needle placement (arrow) for transpulmonary biopsy [GUP05]

The need to provide real-time visual feedback for the needle position during its insertion defines the next technical characteristic of the robotic system: **it must be small enough to fit inside the CT gantry in the patient proximity.**

Two systems will be presented as viable robotic solutions for real-time CT guided brachytherapy:

- ATEN – A robotic device with spherical architecture, which has been developed only up to conceptual design;
- PARA-BRACHYROB – A robotic device with parallel architecture, which has been developed up to the level of experimental model and tested in relevant environment.

ATEN – a modular robotic device for minimally invasive needle placement applications

ATEN [VAI13] was developed based on a concept with origins in minimally invasive surgery, namely the use of a remote centre of motion - RCM (a fixed point in space through which the end-effector will pass always). This can be achieved (based on the first definition) in two ways, either by using the tissue around the insertion point as guidance (this simple solution can be used for applications where there is no direct contact between the end-effector and the internal organs, e.g. positioning of the laparoscopic camera) or by constraining mechanically that point in space (this solution will impose the use of two supplementary active joints, but can perform any task inside the body). In addition one could add a third category of RCM, which combines the simplicity of the first with the capabilities of the second, namely architecturally constrained. However, one must acknowledge the fact that in the case of this specific application (brachytherapy), there is no absolute need of the RCM for its original purpose because the trajectory inside the body is linear. However, an architecturally constrained RCM will ensure that the needle will always pass through that point in space which will improve the accuracy modifying the depth parameter (detailed in fig. 3.2) reducing its length between the RCM and the needle tip.

Fig. 3.5 illustrates the kinematic scheme of a spherical robotic arm with three active joints, where the first actuated joint (q_1) achieves a rotation around the X axis, the second one (q_2) achieves a translation along a curve of radius R while the third motor (q_3) achieves a linear displacement along the radius of the sphere. The centre of the sphere becomes the second control point (or the RCM) through which the needle will always pass. From the kinematic point of view the only functional parameter which determines the robot size is the radius R. From the spherical mechanism point of view, the centre of the sphere is fixed, thus when the orientation is achieved the needle will be situated on a parallel line with the defined needle trajectory.

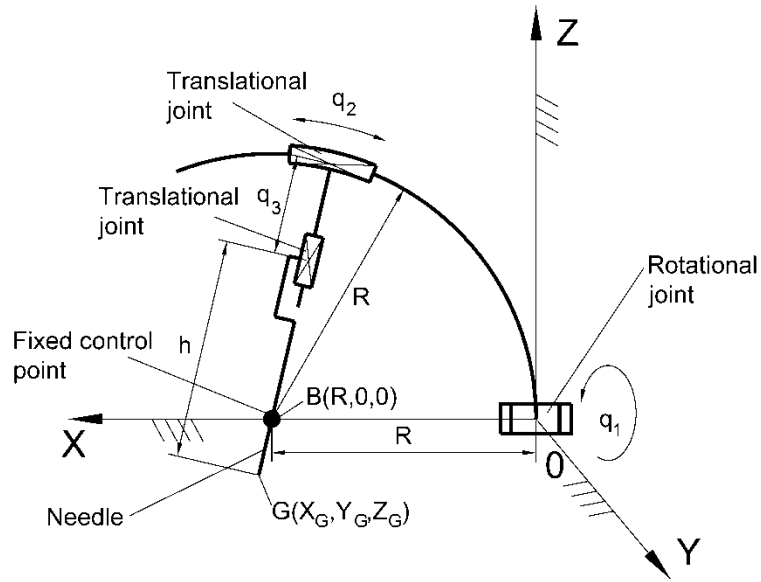


Figure 3.5 The kinematic scheme of the spherical structure

This means that this line must be superposed over the real trajectory and this can be achieved with an XY positioning system on which the spherical mechanism is positioned on. Thus, in Fig. 3.6 is presented the kinematic scheme of the innovative 5-DOF robotic arm, called ATEN, optimized for needle placement interventions, consisting in a 2-DOF planar mechanism with intersecting axis which achieves the displacement with constant orientation of the mobile platform in a plane with $Z=0$. A fixed coordinate system OXYZ is attached to the robot with the origin in the middle of the platform where the coordinates of the planar mechanism are ($q_4=0$ and $q_5=0$). On top of the mobile platform it is positioned the 3-DOF spherical mechanism which has a mobile coordinate system oxyz with the origin in the centre of the rotational joint (q_1) and the axes parallel with the ones of the fixed coordinate system.

The inverse geometrical model

For the inverse geometrical model the geometrical parameters of the structure and the coordinates of the needle tip (point G) are considered known and the coordinates of the active joints should be determined. Furthermore, the insertion point in the body, denoted with A is given in absolute coordinates.

From the kinematic scheme in figure 3.6, the condition for the correct needle positioning can be defined as the collinearity of the points G, B and A. This means that the angles ψ and θ can be calculated with the following expressions:

$$\psi = \text{atan2}(Y_G - Y_A, Z_A - Z_G) \quad (3.2)$$

$$\theta = \text{atan2}\left(X_A - X_G, \frac{(Z_A - Z_G)}{\cos(\psi)}\right) \quad (3.3)$$

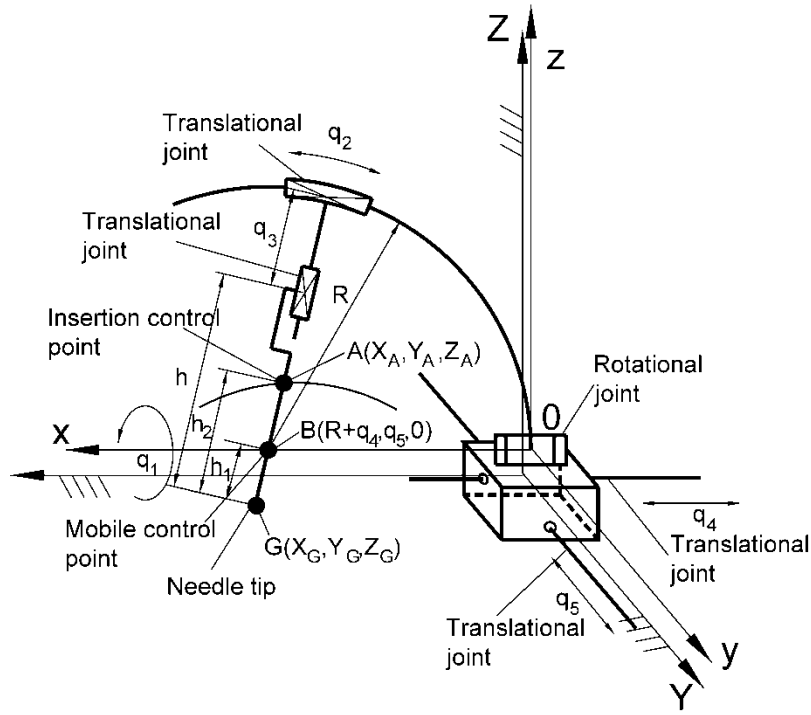


Figure 3.6 The kinematic scheme of the 5-DOF robotic arm ATEN

The coordinates of the active joints of the spherical mechanism can be easily computed with the following equations:

$$\begin{cases} q_1 = \text{atan2}(\sin(\psi) \cdot \cos(\theta), \cos(\psi) \cdot \cos(\theta)) \\ q_2 = \text{atan2}(\sin(\theta) \cdot \cos(q_1), \cos(\psi) \cdot \cos(\theta)) \\ q_3 = R - (h - h_1) \end{cases} \quad (3.4)$$

Where h_1 is:

$$h_1 = \left| \frac{Z_B - Z_G}{\cos(\psi)} \right| = \left| \frac{-Z_G}{\cos(\psi)} \right| \quad (3.5)$$

As the distance between points B and G is known ($\overline{BG} = h_1$) the coordinates of point B can be computed and used to determine the values for the active joints q_4 and q_5 :

$$\begin{cases} X_B = X_G + h_1 \cdot \sin(q_2) \\ Y_B = Y_G - h_1 \cdot \sin(q_1) \cdot \cos(q_2) \end{cases} \quad (3.6)$$

$$\begin{cases} q_4 = X_B - R \\ q_5 = Y_B \end{cases} \quad (3.7)$$

The direct geometrical model

For the direct geometrical model the input parameters are the coordinates of the active joints while the coordinates of the needle tip and its orientation should be computed. For solving the equations the same G – B – A collinearity condition will be used.

Knowing the coordinates of the XY positioning system the coordinates of point B can be expressed as follows:

$$\begin{cases} X_B = R + q_4 \\ Y_B = q_5 \\ Z_B = 0 \end{cases} \quad (3.8)$$

Using the known value of the active joints q_1 and q_2 the needle orientation angles are:

$$\begin{cases} \psi = \text{atan2}(\sin(q_1), \cos(q_1)) \\ \theta = \text{atan2}(\sin(q_2), \cos(q_2)) \end{cases} \quad (3.9)$$

The distance between the points B and G is:

$$h_1 = q_3 - R + h \quad (3.10)$$

Using the coordinates of point B and the equation (3.10) the coordinates of point G can be calculated:

$$\begin{cases} X_G = X_B - h_1 \cdot \sin(q_2) \\ Y_G = Y_B - h_1 \cdot \sin(q_1) \cdot \cos(q_2) \\ Z_G = -h_1 \cdot \cos(q_1) \cdot \cos(q_2) \end{cases} \quad (3.11)$$

Workspace generation

The workspace of the ATEM robot is strictly related to the dimension of the radius R which is also conditioned by the application parameters, namely the dimensions of the CT scan:

- Gantry opening diameter: 800mm;
- Vertical laser positioning: 110 mm in front of the gantry (see figure 3.3);
- Lateral, horizontal lasers, in the plane passing through the gantry centre;
- The mobile couch 110 mm below the median plane of the gantry.

In order to take full benefit from the space inside the CT gantry taking into account also the fact that the patient will also be positioned on the mobile coach, the first rotation axis of the robot (q_1) should be kept in the plane defined by the horizontal axis. Based on that the radius of the spherical mechanism will be concentric with the gantry which would ensure the free motion of the mechanism without the danger of accidental damaging of the CT Scan. The radius of the mechanism should not be too large, but also it cannot be too small because it must also provide space for the patient. Based on the virtual design of the entire application a radius of 300 mm has been selected. For the needle length a value of 200 mm has been imposed.

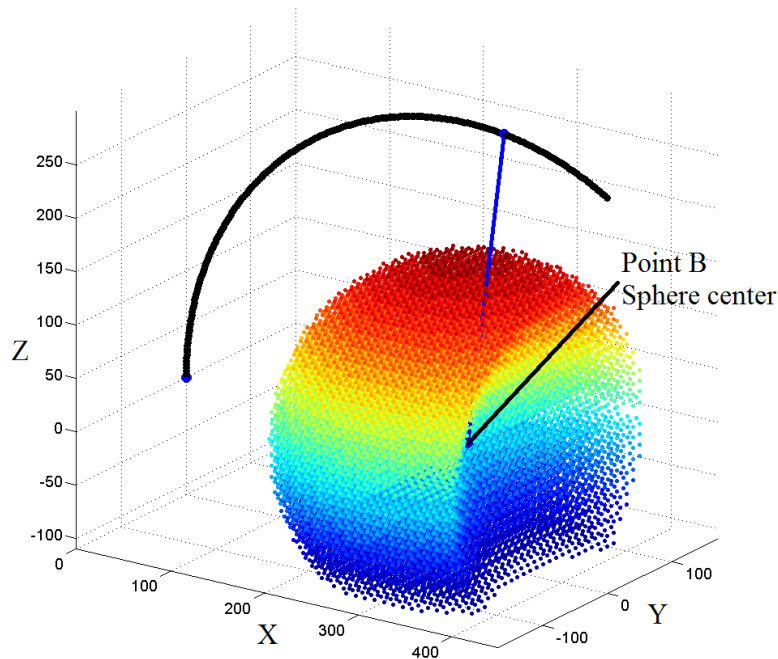


Figure 3.7. Robot workspace for a fixed location of the point B

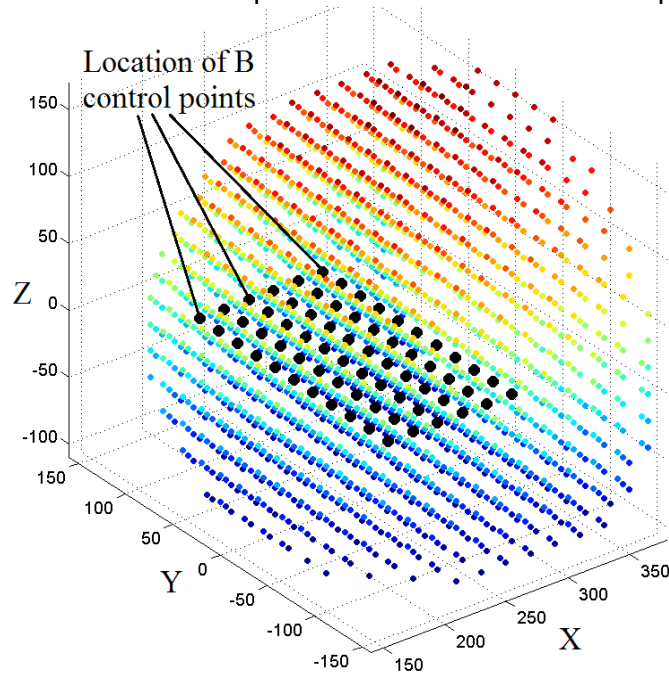


Figure 3.8. Total robot workspace

Figure 3.7 illustrates the robot workspace for a fixed position of the point B (without any actuation on q_4 and q_5). In figure 3.8, analysing the robot workspace it can be easily seen that it covers properly the entire half of the patient situated in the robot proximity, meaning that the robot has to be mounted proximal to the patient side where the targeted tumour is located. Figure 3.8 represents the total workspace of the robot with a displacement of 100 mm for q_4 and 200 mm for q_5 , values selected accordingly to the space inside the CT-Sim gantry.

Singularities analysis and discussion

The singularities analysis is performed by computing the determinants of the Jacobi matrices A and B.

The axes q_4 and q_5 modify only the position of the sphere centre, without any influence on the singularities of the mechanism so the analysis can be performed without any loss of generalization for a fixed value of these two active joints, which will be treated as constants in the matrices. Thus, the Jacobi matrices will have 3x3 dimensions. The implicit equations which determine the relation between the active joints and the coordinates of the needle tip are:

$$\left\{ \begin{array}{l} f_1(q_1, q_5, Y_G, Z_G) \equiv \frac{\sin(q_1)}{\cos(q_1)} + \frac{Y_G - q_5}{Z_G} = 0 \\ f_2(q_1, q_2, q_4, X_G, Z_G) \equiv \frac{\sin(q_2)}{\cos(q_2)} + \cos(q_1) \cdot \frac{R + q_4 - X_G}{Z_G} = 0 \\ f_3(q_3, q_4, q_5, X_G, Y_G, Z_G) \equiv q_3 - R + h - h_1 = \\ \quad = q_3 - R + h - \sqrt{(R + q_4 - X_G)^2 + (q_5 - Y_G)^2} + Z_G^2 = 0 \end{array} \right. \quad (3.12)$$

Where: $h_1 = \sqrt{(X_B - X_G)^2 + (Y_B - Y_G)^2 + (Z_B - Z_G)^2}$

Using the Eq. 3.12, through partial derivation the Jacobi matrices are defined:

$$A = \begin{pmatrix} 0 & \frac{1}{Z_G} & -\frac{Y_G - q_5}{Z_G^2} \\ -\frac{\cos(q_1)}{Z_G} & 0 & -\cos(q_1) \cdot \frac{R + q_4 - X_G}{Z_G^2} \\ \frac{R + q_4 - X_G}{h_1} & \frac{q_5 - Y_G}{h_1} & \frac{Z_G}{h_1} \end{pmatrix} \quad (3.13)$$

$$B = \begin{pmatrix} \frac{1}{\cos^2(q_1)} & 0 & 0 \\ -\sin(q_1) \cdot \frac{R + q_4 - X_G}{Z_G} & \frac{1}{\cos^2(q_2)} & 0 \\ 0 & 0 & 1 \end{pmatrix} \quad (3.14)$$

The determinant of matrix A, computed from 3.13 is:

$$\det(A) = \frac{\cos(q_1) \cdot h_1}{Z_G^3} \quad (3.15)$$

Three cases are distinguished:

1. $q_1 = \pm \frac{\pi}{2}$. This corresponds to the case when the spherical robot arm is placed horizontally on any of its sides, position that is improper for needle placement applications, which means that this conditions has no negative influence on the robot performance.
2. $h_1 = 0$. Geometrically, this means that $G \equiv B$. In this case, when the tip of the needle is exactly in the centre of the sphere no matter how one modifies the values of q_1 and q_2 , the position of the needle tip will remain the same. For needle placement applications, the needle is driven on a linear trajectory so this case has no effect on the robot manoeuvrability. In addition as the point B will be kept, through the relative robot positioning with respect to the patient (and the targeted tumour), when this point is reached the active joints q_1 and q_2 would have to be kept fixed.
3. $Z_G = 0$. This situation refers again to the boundary surface analysed in the first case, and due to the nature of the application in hand the robot will never even approach those conditions.

The determinant of matrix B is:

$$\det(B) = \frac{1}{\cos^2(q_1) \cdot \cos^2(q_2)} \quad (3.16)$$

Two cases are distinguished:

1. $q_1 = \pm \pi/2$. This corresponds to the first case analysed for the matrix A.

2. $q_2 = \pm\pi/2$. The same situation is created when the second actuator reaches the extreme positions that places the tip of the instrument on the OXY plane at $Z_G = 0$.

Based on the conditions that were determined analytically one can state that the ATEN robotic system can be used safely for the brachytherapy task as the operational workspace (conditioned by the CT Scan) has no singular points inside it.

A stepwise procedure for needle insertion applications under CT – Scan real time monitoring.

The last aspects regarding the ATEN structure will cover a step by step procedure describing the achievement of the medical application in relevant environment and a representation of the robot size and its integration in the CT

The ATEN robot is developed as a structure dedicated for needle placement applications, and in this paragraph the procedure description is presented as a sequence of logical and safety proof steps.

1. The medical data is received from the physicians defining the target points locations and the desired linear trajectories.
2. The patient is placed in the CT-Sim device and immobilized in a predefined position, then calibrated with respect the laser system of the machine.
3. The robot is rigidly fixed in the CT-Sim table and calibrated with respect to the laser system. After this step the robot must remain fixed until the procedure ends.
4. Base on the medical data provided, the needle is oriented parallel with the linear trajectory to be achieved. This is done using only the active joints q_1 and q_2 .
5. The needle is superposed over the imposed trajectory, by means of the active joints q_4 and q_5 .
6. The needle is driven along the trajectory by means of the active joint q_3 . When the needle touches the skin, due to the additional control point (the sphere centre) the position is checked.
7. If needed, corrections are applied and then, the needle is inserted partially.
8. The needle position is checked again using the CT Sim device. If validated the needle is driven to the target point otherwise it is retracted and step 7 is repeated.
9. If multiple needles must be inserted, if the trajectories are pure parallel, steps 5-8 are repeated, otherwise steps 4-8 must be performed.

An illustration of the ATEN 5-DOR robotic arm placed in the CT-Sim device is presented in the figure 7 to show its dimensional relation to the machine and the patient as well as a detail showing its position inside the gantry, in figure 8.

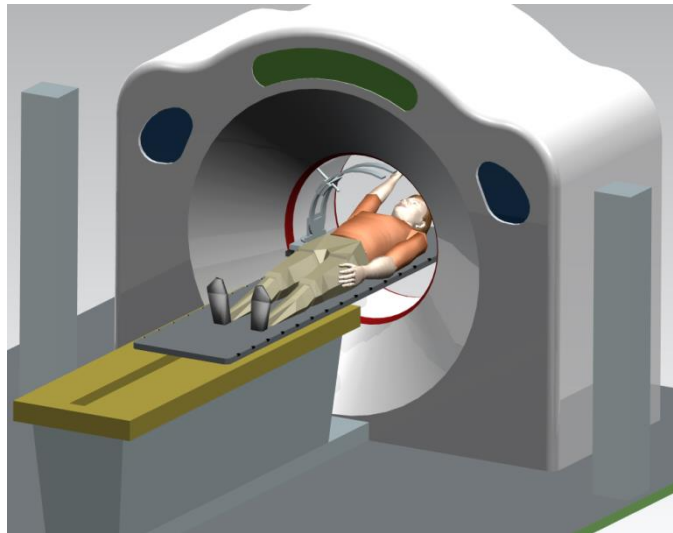


Figure 3.9. The ATEN robot in the CT-Sim environment

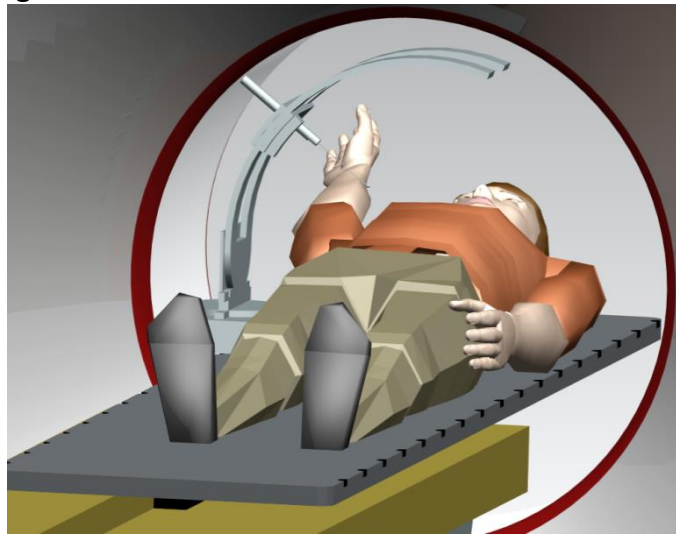


Figure 3.10. Detail showing the ATEN robot position inside the CT-Sim gantry

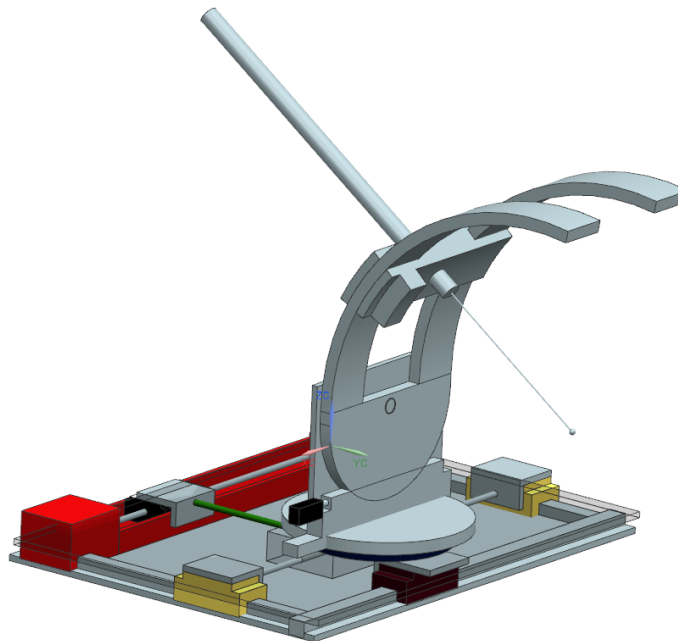


Figure 3.11. Detailed design of the ATEN robot

PARA-BRACHYROB

The second system developed for brachytherapy, initially named **BR3**, has a modular structure with two modules with 3 DOF working in cylindrical coordinates interconnected at the level of the last joint through two sets of Cardan joints. The kinematic scheme of the initial solution is illustrated in figure 3.12.

The definition of the medical specifications and system requirements were made together with a team of oncologists from the “Ion Chiricuta” Oncology Hospital in Cluj-Napoca:

General requirements:

- compatibility with radiation X environment from 50 to 150 kV;
- teleoperation from a safe distance, (over 5 m);
- portable;
- mounting options in fixed positions relative to the CT table;

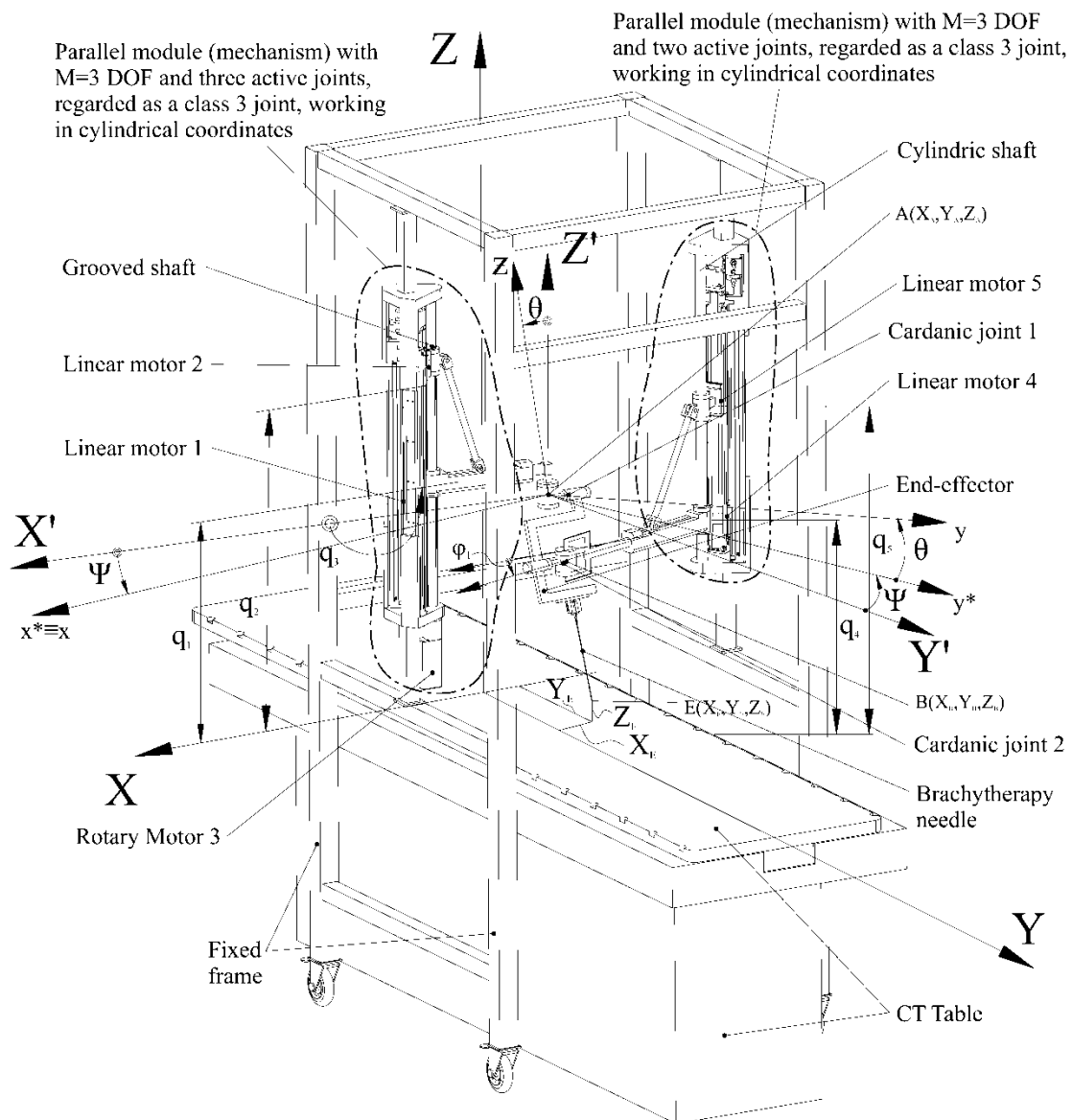


Figure 3.12. Parallel robot with $M=5$ DOF and family $F=1$ with modular construction

Technical requirements:

- DOFs: 5 (translations on X, Y and Z, rotations around X and Y);
- orientation angles: +/- 45°;
- Sterilisable fixed support for needles of diameter from 1.6 to 2 mm and lengths of 50 to 250 mm;
- Detection system with adjustable upper limit of the penetration force;
- Vessels pulsations detection system;
- Contact precision less than 3 mm.

Each module of the BR3 robot has two active translational joints consisting of ball-screws actuated by motors 1, 2 respectively motors 4 and 5 (figure 3.12). For the first module, with three actuated joints, the translational active joints move two bushings on the grooved shaft which represents an active revolute joint actuated by the motor 3. The bushings move linear with the translational joints and rotate with the grooved shaft. For the second module, which has only two active joints, the grooved shaft is replaced by a cylindrical shaft which acts as a passive, driven, revolute joint. Both modules work in cylindrical coordinates. Making reference also to the coordinate system the two cylindrical modules are interconnected using a pair of Cardan joints having each the first axis parallel with the OZ axis of the coordinate system (or parallel with the translation axis of the linear actuator). At the ends of the second axis of each of the Cardan joints the needle module was connected. As the original design (figure 3.12) was unable to fit the needle holder inside the CT a table mountable solution (to be positioned on the mobile couch of the CT Scan) was achieved (figure 3.13).



Figure 3.13. The second design of BR3

Further analysis and optimizations – the development of the final version of PARABRACHYROB

The interconnection of the cylindrical modules

The initial design proposed the use of individual fixtures on the sides of the mobile couch for the two cylindrical modules which does not provide sufficient stiffness for the structure and also has a negative impact on the mounting of the robot. Thus, a flat plate was introduced in the design that would fit below the patient, having the cylindrical modules attached to it and, by using a set of calibrated hole the plate would be than attached to the CT Scan mobile couch.

The addition of a redundant 6th actuator

From a purely geometrical point of view the motion that must be performed by the robotic system (not taking into account the preparations) has two phases, that will be described in detail later on: having two control points, the insertion and the target, knowing that between them there is a linear trajectory, the first phase refers to the positioning of the needle tip in the insertion point with its final orientation while the second phase would represent the insertion of the needle on the linear trajectory until the needle tip moves from the Insertion point to the Target one. By adding the 6th, redundant actuator (meaning that the number of degrees of freedom of the robot will not increase) the following advantages are generated:

- ✓ The workspace of the robot increases as with the use of its 5 original actuators the robot must achieve only the positioning (with the final orientation) of the needle in the insertion point as the insertion itself will be achieved using the 6th actuator;
- ✓ The needle can be held in the needle insertion module in a retracted position which increases the stiffness and the accuracy of the procedure reducing also the unwanted needle bending during the insertion;
- ✓ As the needle is inserted using a single actuator which drives the needle in linearly, the tissue resistance force can be measured in a simple way using a force sensor mounted at the proximal end of the needle allowing a simple yet relevant force monitoring.

The repositioning of the fixed coordinate system

During the initial study of the robot the fixed coordinate system (see figure 3.12) has been positioned to have the Y axis in the same vertical plane with the laser system of the CT-Scan which means the median plane of the mobile couch. However, when solving the kinematic model of the robot, the equation resulted in very complicated formulas making it difficult to achieve a definite analysis of the singularities due to the complex form of the Jacobi matrices. In order to simplify these matrices multiple “zeroes” should be obtained, which can be achieved by repositioning the fixed

coordinate system with the Z axis similar to the axis of motion of the actuated joints of the first module of the robot (the one with three active joints).

The final version of the brachytherapy parallel robot PARA-BRACHYROB

Based on the new kinematic scheme illustrated in figure 3.14, the PARA-BRACHYROB cylindrical parallel robot consists of three modules, the first one having 3-DOF and 3 active joints, denoted with q_1, q_2, q_3 , a second module with 3-DOF and 2 active joints, q_4, q_5 and a third module used for the needle insertion which is a 1-DOF module with one active joint, q_6 . The first two joints of each cylindrical module are translational joints, while the third motion, a rotational one around the motion axes of the linear joints, is obtained in the first module using an active joint while in the second one it is achieved through a passive joint. The modules end points are denoted with A_1 and A_2 . The new fixed coordinate system is introduced, namely OXYZ, with the Z axis along the active rotational axis of the first module. The second module is positioned through a translation along the X axis, at a distance d_{12} from the origin. The first two modules are interconnected with two passive Cardan joints having the first rotation axis around the Z axis and the second one perpendicular on it. The second rotational axes of each of the two Cardan joints are connected and they guide the needle insertion module.

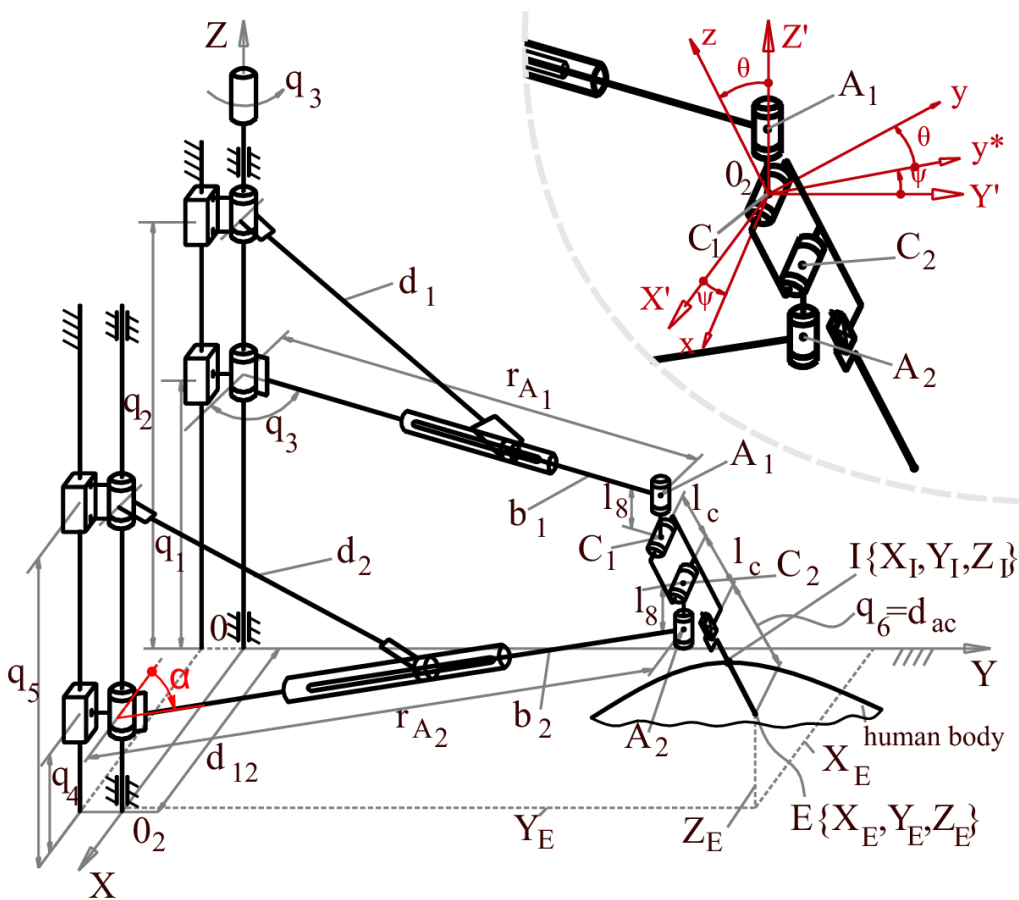


Figure 3.14. The final kinematic scheme of the PARA-BRACHYROB parallel robot

The final module integrates a translational actuator, q_6 which has a redundant motion (with respect to the robotic structure) enabling the needle insertion to the target point with all the other actuators fixed (blocked). Besides the two passive Cardan joints, the robot has also six passive rotational joints and two passive translational joints.

Before presenting the kinematic modelling of this structure, a detailed analysis of the robot required motions is presented, as the data provided by this medical task will be used as input values for the motion generation of the structure.

The medical task for brachytherapy

The robot should introduce, based on radiologic data, needles with diameters varying from 0.6 mm up to 2 mm and lengths from 100 mm up to 250 mm, on distances up to 200 mm, following a linear trajectory.

Following the calibration between the robot – patient – CT Scan (in order to be able to work with the coordinates of points located inside the human body, defined with respect to the highly accurate external lasers of the CT Scan), the robotic system receives a set of two points: point I (X_I, Y_I, Z_I) - the insertion point and point T (X_T, Y_T, Z_T) - the target point. In addition, a third point is introduced in the algorithm, the current robot position, point C $(X_C, Y_C, Z_C, \psi_C, \theta_C)$. One side note is made with reference to the point C, which has five parameters as these are the five independent parameters that characterize a pose of the robot. Based on this data, the final needle orientation is computed, based on the relative positions of the insertion and target points:

$$\begin{aligned}\psi_{IT} &= \text{atan2}(Y_T - Y_I, X_T - X_I) \\ \theta_{IT} &= \text{atan2}\left(\sqrt{(Y_I - Y_T)^2 + (X_I - X_T)^2}, Z_I - Z_T\right)\end{aligned}\quad (3.17)$$

For the first stage of the motion PARA – BRACHYROB will move from point C to point I with the following set of initial and final parameters:

$$X_C, Y_C, Z_C, \psi_C, \theta_C \Rightarrow X_I, Y_I, Z_I, \psi_{IT}, \theta_{IT} \quad (3.18)$$

The second stage, the needle insertion will be performed using the third module of PARA-BRACHYROB, where the active joint q_6 will drive the needle linearly on a distance equal with:

$$d_{insertion} = \sqrt{(X_I - X_T)^2 + (Y_I - Y_T)^2 + (Z_I - Z_T)^2} \quad (3.19)$$

Introducing the notations:

- **M** – the degree of freedom of the parallel robot;
- **F** – the mechanism family (the number of simple motions restricted for all the elements of the parallel mechanism out of the six possible ones);
- **N** – the number of mobile elements of the parallel mechanism;
- **C_i** – the number of class “i” joints, with, i=5,4,3,2,1 where the joint class represents the number of restricted DOF,

For a parallel mechanism of family F, the structural synthesis equations are [PLI06]:

$$M = (6 - F) \cdot N - (5 - F) \cdot C_5 - (4 - F) \cdot C_4 - (3 - F) \cdot C_3 - (2 - F) \cdot C_2 - (1 - F) \cdot C_1$$

or, in compact form

$$M = (6 - F) \cdot N - \sum_{i=1..5} (i - F) \cdot C_i \quad (3.20)$$

The terms $(6 - F) \cdot \dots \cdot (1 - F)$ cannot have negative values.

Considering the first two modules as joints of class 3 (having 3 DOF) and the family of the mechanism $F = 1$, the parameters for (eq. 3.20) are $N = 3, C_5 = 0, C_4 = 2, C_3 = 2$ which means that:

$$M = 5 \cdot N - 4 \cdot C_4 - 2 \cdot C_3 = 5 \quad (3.21)$$

Equation 3.21 validates the structure of PARA-BRACHYROB from the structural point of view.

The kinematic model [PLI14, PIS14] introduces a set of geometrical parameters which are considered known and used as constants in the equations, namely: $d_1, b_1, l_1, d_2, b_2, l_2, l_c, h$.

The inverse geometrical model of PARA-BRACHYROB. For the inverse geometrical model (IGM) the needle tip (target point) coordinates, the needle orientation and the needle length inside the patient are known, namely:

- The coordinates of point $E(X_E, Y_E, Z_E)$;
- The needle orientation angles ψ and θ ;
- The needle depth d_{ac} .

Using the input data the values for the active joints have to be computed. As a note, the sixth actuated joint, q_6 will be treated as a constant as it does not influence the behaviour of the other joints.

For solving the IGM of PARA-BRACHYROB a simple geometrical constraint is used, namely the “architectural” collinearity of the points $E - C_1 - C_2$. This conditions allow, based on the known position of one the points, the fixed distance between the joints and the orientation of the segment defined by three points to determine simply the coordinates of points C_1 and C_2 :

$$\begin{cases} X_{C1} = X_E - (d_{ac} + 2 \cdot l_c) \cdot \sin(\theta) \cdot \cos(\psi) \\ Y_{C1} = Y_E - (d_{ac} + 2 \cdot l_c) \cdot \sin(\theta) \cdot \sin(\psi) \\ Z_{C1} = Z_E + (d_{ac} + 2 \cdot l_c) \cdot \cos(\theta) \end{cases} \quad (3.22)$$

$$\begin{cases} X_{C2} = X_E - (d_{ac} + l_c) \cdot \sin(\theta) \cdot \cos(\psi) \\ Y_{C2} = Y_E - (d_{ac} + l_c) \cdot \sin(\theta) \cdot \sin(\psi) \\ Z_{C2} = Z_E + (d_{ac} + l_c) \cdot \cos(\theta) \end{cases} \quad (3.23)$$

The displacement between the pairs of points $A_i - C_i$ represents a simple translation on an axis parallel with the OZ axis, which means that the points A_1 and A_2 will have the following equations:

$$\begin{aligned} X_{A1} &= X_{C1} \\ Y_{A1} &= Y_{C1} \end{aligned} \quad (3.24)$$

$$\begin{aligned} Z_{A1} &= Z_{C1} + l_1 \\ X_{A1} &= X_{C1} \\ Y_{A1} &= Y_{C1} \end{aligned} \quad (3.25)$$

$$Z_{A1} = Z_{C1} + l_1$$

In case of the use of a pure Cardan joint the values for l_1 and l_2 would be zero, as the centres of the two sequential rotations would be common. However, using these two parameters allows, in the design phase, to study also the possibility of using pairs of rotations joints with perpendicular axis instead of Cardan joints. From the points A_i the distances to the main axis of displacement of the translations active joints of each module can be calculated:

$$r_{A1} = \sqrt{X_{A1}^2 + Y_{A1}^2} \quad (3.26)$$

$$r_{A2} = \sqrt{(X_{A2} - d_{12})^2 + Y_{A2}^2} \quad (3.27)$$

Based on the equations 3.22 ÷ 3.27 the equations of the active joints of PARABRACHYROB are:

$$q_1 = Z_{A1} \quad (3.28)$$

$$q_2 = q_1 + \sqrt{d_1^2 - (r_{A1} - b_1)^2} \quad (3.29)$$

$$q_3 = a \tan 2(Y_{A1}, X_{A1}) \quad (3.30)$$

$$q_4 = Z_{A2} \quad (3.31)$$

$$q_5 = q_4 + \sqrt{d_2^2 - (r_{A2} - b_2)^2} \quad (3.32)$$

$$q_6 = d_{ac} \quad (3.33)$$

The direct geometrical model. For the direct geometrical model (DGM) the coordinates of the active joints are known, namely, $q_1, q_2, q_3, q_4, q_5, q_6$ along with all the geometric parameters of the robot defined before. The unknowns are the end-effector (needle's tip) coordinates $E(X_E, Y_E, Z_E)$ and the orientation angles ψ and θ . Based on the kinematic scheme in figure 3.14, knowing the coordinates of the active joints q_1, q_2, q_4, q_5 the lengths of the two horizontal arms r_{Ai} can be calculated:

$$r_{A1} = b_1 + \sqrt{d_1^2 - (q_2 - q_1)^2} \quad (3.34)$$

$$r_{A2} = b_2 + \sqrt{d_2^2 - (q_5 - q_4)^2} \quad (3.35)$$

In the case of the first module, the active rotational joint q_3 enables the determination of the coordinates of the points A_1 and respectively C_1 :

$$\begin{aligned} X_{A1} &= r_{A1} \cdot \cos(q_3) \\ Y_{A1} &= r_{A1} \cdot \sin(q_3) \end{aligned} \quad (3.36)$$

$$\begin{aligned} Z_{A1} &= q_1 \\ X_{C1} &= X_{A1} \\ Y_{C1} &= Y_{A1} \\ Z_{C1} &= Z_{A1} - l_1 \end{aligned} \quad (3.37)$$

However, in the case of the second module, due to the passive rotational joint, a double solution will be obtained for the points A_2 and respectively C_2 which determines the two working modes of the PARA-BRACHYROB system and as later demonstrated a singularity inside the robot workspace. Two quadratic equations can be written using the geometric properties of circles, namely:

$$\begin{aligned} (X_{C2} - X_{C1})^2 + (Y_{C2} - Y_{C1})^2 &= a^2 \\ (X_{C2} - d_{12})^2 + Y_{C2}^2 &= r_{A2}^2 \end{aligned} \quad (3.38)$$

Where:

$$a = \sqrt{l_c^2 - (Z_{C2} - Z_{C1})^2}$$

The two quadratic equations are solved classically, and to shorten the final results the following notations are introduced:

$$rr_1 = \sqrt{(X_{C1} - d_{12})^2 + Y_{C1}^2 - (a - r_{A2})^2} \cdot \sqrt{(a + r_{A2})^2 - (X_{C1} - d_{12})^2 - Y_{C1}^2} \quad (3.39)$$

$$rr_2 = X_{c1}^2 + Y_{c1}^2 - a^2 - d_{12}^2 + r_{A2}^2$$

$$rr_3 = Y_{c1} \cdot \left((X_{c1} - d_{12})^2 + Y_{c1}^2 - a^2 + r_{A2}^2 \right)$$

The solutions for the quadratic equation (3.38) are:

$$X_{c2-1} = \frac{1}{2(X_{c1} - d_{12})} \cdot \frac{1}{(X_{c1} - d_{12})^2 + Y_{c1}^2} \cdot \left\{ rr_2 - Y_{c1} \cdot \left[rr_1 \cdot (d_{12} - X_{c1}) + rr_3 \right] \right\}$$

$$Y_{c2-1} = \frac{1}{2(X_{c1} - d_{12})^2 + Y_{c1}^2} \cdot \left[rr_1 \cdot (d_{12} - X_{c1}) + rr_3 \right]$$

Respectively:

$$X_{c2-2} = \frac{1}{2(X_{c1} - d_{12})} \cdot \frac{1}{(X_{c1} - d_{12})^2 + Y_{c1}^2} \cdot \left\{ rr_2 - Y_{c1} \cdot \left[rr_1 \cdot (X_{c1} - d_{12}) + rr_3 \right] \right\}$$

$$Y_{c2-2} = \frac{1}{2(X_{c1} - d_{12})^2 + Y_{c1}^2} \cdot \left[rr_1 \cdot (X_{c1} - d_{12}) + rr_3 \right]$$
(3.40)

The value of the Z coordinate of the point C is unique, $Z_{c2} = q_4 + l_2$ which will provide a unique solution for the orientation angle θ :

$$\theta = \text{atan2} \left(\sqrt{l_c^2 - (Z_{c1} - Z_{c2})^2}, (Z_{c1} - Z_{c2}) \right)$$
(3.41)

The angle ψ on the other hand will have a double solution:

$$\psi_i = \text{atan2} \left((Y_{c2-i} - Y_{c1}), (X_{c2-i} - X_{c1}) \right) \quad i = 1..2$$
(3.42)

The final expressions for the coordinates of the needle tip are presented below:

$$X_{E_i} = X_{c1} + (q_6 + 2 \cdot l_c) \sin(\theta) \cos(\psi_i), \quad i = 1, 2$$
(3.43)

$$Y_{E_i} = Y_{c1} + (q_6 + 2 \cdot l_c) \sin(\theta) \sin(\psi_i), \quad i = 1, 2$$
(3.44)

$$Z_E = Z_{c1} - (h + l_c) \cos(\theta)$$
(3.45)

The existence of the two working modes for the robot is not a drawback with respect to the task in hand as during the medical procedure the robot is not moving freely but on a set of trajectories which are defined prior to the procedure. These values being known, the coordinates of the point C (the location from which the

robot will perform the sets of motions for each needle) can be defined and validated in order to avoid the working mode change during the procedure.

The kinematic model of PARA-BRACHYROB. As stated before, because the 6th actuator is redundant and will not be used when the other 5 active joints are moving, it can be treated as a constant parameter. This is important because, for solving the kinematic model using the Jacobi matrices we need square matrices (this is given by the case when the number of independent motions of the needle tip is equal with the number of active joints). Using the previous equations determined for the geometrical model, five closure equations can be written:

$$f_1 : Z_E + l_1 + (q_6 + 2 \cdot l_c) \cdot \cos(\theta) - q_1 = 0 \quad (3.46)$$

$$f_2 : X_E - (q_6 + 2 \cdot l_c) \cdot \sin(\theta) \cdot \cos(\psi) - \left[b_1 + \sqrt{d_1^2 - (q_2 - q_1)^2} \right] \cdot \cos(q_3) = 0 \quad (3.47)$$

$$f_3 : Y_E - (q_6 + 2 \cdot l_c) \cdot \sin(\theta) \cdot \sin(\psi) - \left[b_1 + \sqrt{d_1^2 - (q_2 - q_1)^2} \right] \cdot \sin(q_3) = 0 \quad (3.48)$$

$$f_4 : Z_E - l_2 + (q_6 + l_c) \cdot \cos(\theta) - q_4 = 0 \quad (3.49)$$

$$\begin{aligned} f_5 : & d_{12}^2 + X_E^2 + Y_E^2 + (q_6 + l_c)^2 \cdot \sin^2(\theta) - \\ & - 2 \cdot (q_6 + l_c) \cdot \sin(\theta) \cdot \left[(X_E - X_{O_2}) \cdot \cos(\psi) + Y_E \cdot \sin(\psi) \right] - \\ & - 2 \cdot d_{12} \cdot X_E - b_2^2 - d_2^2 + (q_5 - q_4)^2 - 2 \cdot b_2 \cdot \sqrt{d_2^2 - (q_5 - q_4)^2} = 0 \end{aligned} \quad (3.50)$$

In equation 3.50, the value of d_{12} which represents the distance between the vertical motion axes of the first two modules has been replaced with X_{O_2} , or the X coordinate of the point O_2 in order to allow a better representation of the singularities. In order to write the following matrix equations in a compact form, a set of notations is introduced:

$$\begin{aligned} \text{Velocities: } \dot{X} &= [\dot{X}_E, \dot{Y}_E, \dot{Z}_E, \dot{\psi}, \dot{\theta}]^T, \quad \dot{q} = [\dot{q}_1, \dot{q}_2, \dot{q}_3, \dot{q}_4, \dot{q}_5]^T \\ \text{Accelerations: } \ddot{X} &= [\ddot{X}_E, \ddot{Y}_E, \ddot{Z}_E, \ddot{\psi}, \ddot{\theta}]^T, \quad \ddot{q} = [\ddot{q}_1, \ddot{q}_2, \ddot{q}_3, \ddot{q}_4, \ddot{q}_5]^T \end{aligned} \quad (3.51)$$

The Jacobi matrices are then calculated as representing the partial derivatives of the closure functions with respect to the independent motion parameters, namely the elements of the vectors \dot{X} and \dot{q} . As mentioned before the ideas of modifying the original location of the fixed coordinate system was to simplify the expression of the Jacobi matrices. Thus, the results are presented next. The matrix A has the following terms:

$$A = \begin{pmatrix} 0 & 0 & 1 & 0 & \frac{\partial f_1}{\partial \theta} \\ 1 & 0 & 0 & \frac{\partial f_2}{\partial \psi} & \frac{\partial f_2}{\partial \theta} \\ 0 & 1 & 0 & \frac{\partial f_3}{\partial \psi} & \frac{\partial f_3}{\partial \theta} \\ 0 & 0 & 1 & 0 & \frac{\partial f_4}{\partial \theta} \\ \frac{\partial f_5}{\partial X_E} & \frac{\partial f_5}{\partial Y_E} & 0 & \frac{\partial f_5}{\partial \psi} & \frac{\partial f_5}{\partial \theta} \end{pmatrix} \quad (3.52)$$

Where the “non-zero” terms are as follows:

$$\frac{\partial f_1}{\partial \theta} = -(q6 + 2 \cdot l_c) \cdot \sin(\theta) \quad (3.53)$$

$$\frac{\partial f_2}{\partial \psi} = (q6 + 2 \cdot l_c) \cdot \sin(\theta) \cdot \sin(\psi) \quad (3.54)$$

$$\frac{\partial f_2}{\partial \theta} = -(q6 + 2 \cdot l_c) \cdot \cos(\theta) \cdot \cos(\psi) \quad (3.55)$$

$$\frac{\partial f_3}{\partial \psi} = -(q6 + 2 \cdot l_c) \cdot \sin(\theta) \cdot \cos(\psi) \quad (3.56)$$

$$\frac{\partial f_3}{\partial \theta} = -(q6 + 2 \cdot l_c) \cdot \cos(\theta) \cdot \sin(\psi) \quad (3.57)$$

$$\frac{\partial f_4}{\partial \theta} = -(q6 + l_c) \cdot \sin(\theta) \quad (3.58)$$

$$\frac{\partial f_5}{\partial X_E} = 2 \cdot (X_E - X_{02}) - 2 \cdot (q6 + l_c) \cdot \sin(\theta) \cdot \cos(\psi) \quad (3.59)$$

$$\frac{\partial f_5}{\partial Y_E} = 2 \cdot Y_E - 2 \cdot (q6 + l_c) \cdot \sin(\theta) \cdot \sin(\psi) \quad (3.60)$$

$$\frac{\partial f_5}{\partial \psi} = 2(q6 + l_c) \cdot \sin(\theta) \cdot [(X_E - X_{02}) \cdot \sin(\psi) - Y_E \cdot \cos(\psi)] \quad (3.61)$$

$$\frac{\partial f_5}{\partial \theta} = 2 \cdot (q6 + l_c)^2 \cdot \sin(\theta) \cdot \cos(\theta) - \cos(\theta) \cdot [(X_E - X_{02}) \cdot \cos(\psi) - Y_E \cdot \sin(\psi)] \quad (3.62)$$

The reason for displaying the expressions of each term is to show that through proper selection of functions and arrangements in kinematic structure of the robot even a complex structure can be modelled in a fully analytical way, which will allow a proper setup of the control system and a full analysis of the singularities.

Moving on to the matrix B, its expression is:

$$B = \begin{pmatrix} -1 & 0 & 0 & 0 & 0 \\ \frac{\partial f_2}{\partial q_1} & \frac{\partial f_2}{\partial q_2} & \frac{\partial f_2}{\partial q_3} & 0 & 0 \\ \frac{\partial f_3}{\partial q_1} & \frac{\partial f_3}{\partial q_2} & \frac{\partial f_3}{\partial q_3} & 0 & 0 \\ 0 & 0 & 0 & -1 & 0 \\ 0 & 0 & 0 & \frac{\partial f_5}{\partial q_4} & \frac{\partial f_5}{\partial q_5} \end{pmatrix} \quad (3.63)$$

Where the “non-zero” terms are as follows:

$$\frac{\partial f_2}{\partial q_1} = \frac{q_1 - q_2}{\sqrt{d_1^2 - (q_2 - q_1)^2}} \cdot \cos(q_3) \quad (3.64)$$

$$\frac{\partial f_2}{\partial q_2} = \frac{q_2 - q_1}{\sqrt{d_1^2 - (q_2 - q_1)^2}} \cdot \cos(q_3) \quad (3.65)$$

$$\frac{\partial f_2}{\partial q_3} = \left[b_1 + \sqrt{d_1^2 - (q_2 - q_1)^2} \right] \cdot \sin(q_3) \quad (3.66)$$

$$\frac{\partial f_3}{\partial q_1} = \frac{q_1 - q_2}{\sqrt{d_1^2 - (q_2 - q_1)^2}} \cdot \sin(q_3) \quad (3.67)$$

$$\frac{\partial f_3}{\partial q_2} = \frac{q_2 - q_1}{\sqrt{d_1^2 - (q_2 - q_1)^2}} \cdot \cos(q_3) \quad (3.68)$$

$$\frac{\partial f_3}{\partial q_3} = - \left[b_1 + \sqrt{d_1^2 - (q_2 - q_1)^2} \right] \cdot \cos(q_3) \quad (3.69)$$

$$\frac{\partial f_5}{\partial q_4} = 2 \cdot (q_4 - q_5) \cdot \left[1 + \frac{b_2}{\sqrt{d_2^2 - (q_5 - q_4)^2}} \right] \quad (3.70)$$

$$\frac{\partial f_5}{\partial q_5} = 2 \cdot (q_5 - q_4) \cdot \left[1 + \frac{b_2}{\sqrt{d_2^2 - (q_5 - q_4)^2}} \right] \quad (3.71)$$

For the determination of the kinematic model the following, well-known, matrix equation will be used [MERO6]:

$$A \cdot \dot{X} + B \cdot \dot{q} = 0 \quad (3.72)$$

Thus at the level of the kinematic model for speeds we have the two vectors \dot{X} and \dot{q} each acting as an input value for the other. Thus, for the inverse kinematic model, \dot{X} is considered known, so \dot{q} is:

$$\dot{q} = -B^{-1} \cdot A \cdot \dot{X} \quad (3.73)$$

For the direct kinematic model, in a logical way, the following equation results:

$$\dot{X} = -A^{-1} \cdot B \cdot \dot{q} \quad (3.74)$$

For the kinematic model for accelerations the first step consists in calculating the time derivative of eq. 3.72 and then, computing the two models:

$$A \cdot \ddot{X} + \dot{A} \cdot \dot{X} + B \cdot \ddot{q} + \dot{B} \cdot \dot{q} = 0 \quad (3.75)$$

Thus, for the inverse kinematic model the final equation is:

$$\ddot{q} = -B^{-1} \cdot (\dot{A} \cdot \dot{X} + A \cdot \ddot{X} + \dot{B} \cdot \dot{q}) \quad (3.76)$$

For the direct kinematic model, in a logical way, the following equation results:

$$\ddot{X} = -A^{-1} \cdot (\dot{A} \cdot \dot{X} + B \cdot \ddot{q} + \dot{B} \cdot \dot{q}) \quad (3.77)$$

Singularities analysis. Due to the importance of safety in the medical act the singularities of PARA-BRACHYROB have been analysed using both an analytical method (which will be presented next) and an algebraic method (which was achieved in cooperation with prof. Manfred Husty and his team). As the algebraic approach will represent as the final chapter of this thesis a future direction of development for the author the algebraic method will not be detailed as the main contribution belongs to other authors.

The algebraic method for the singularities analysis will evaluate each determinant of the two Jacobi matrices, whereas in case one of them is null for a certain combination of parameters, this will represent a singular pose of the robot.

The determinant of the matrix A is:

$$\det(A) = -2 \cdot l_c^2 \cdot \sin^2(\theta) \cdot [(X_{O_2} - X_E) \cdot \sin(\psi) + Y_E \cdot \cos(\psi)] \quad (3.78)$$

Case 1: $l_c = 0$

This situation corresponds to the case when the distance between the two Cardan joints is zero, meaning that the points C_1 and C_2 superpose; this situation cannot

materialize in practice and can be discarded. **However**, a more in depth discussion can be made. As the determinant is used in the computation of the kinematic model (when the inverse matrices are calculated) the parameter l_c which is even squared should be as large as possible to provide better robot behaviour. Thus, in the final robot design it was considered almost equal with the length of the needle.

Case 2: $\sin^2(\theta) = 0$

This equation characterizes the vertical position of the needle module, when the two Cardan joints are positioned on a vertical axis (parallel with the OZ axis). In this configuration the robot gains one degree of freedom, allowing the rotation of the needle positioning module around the axis defined by the points C_1 and C_2 . In the robot control algorithm this situation will be avoided by imposing that $\theta_{IT} \neq \frac{\pi}{2}$.

However, the sine of θ appears squared in the equation so, just by avoiding the value of 90° ($\frac{\pi}{2}$) the problem is not solved. In order to ensure the safety of the procedure a safety margin of at least 5° should be considered.

Case 3: $(X_{O2} - X_E) \cdot \sin(\psi) + Y_E \cdot \cos(\psi) = 0$

This equation can be written as: $\tan(\psi) = -\frac{Y_E}{X_{O2} - X_E}$

Considering the fact that the needle tip coordinates (point E) will be always located between the two robot arms, the ratio $\frac{Y_E}{X_{O2} - X_E}$ will be always positive, meaning

that the angle ψ will take values in the domain $\psi \in \left[\frac{\pi}{2}, \pi \right] \cup \left[\frac{3\pi}{2}, 2 \cdot \pi \right]$. The

configuration corresponds to the case when the coordinates of q_4, q_5, C_1, C_2 and E are located in the same plane or when the two solutions of the direct kinematic model will be similar. As this condition can occur in any area of the workspace it must be handled with special care. A geometric representation of the singular points achieved with sufficient number of values will reveal (as shown in figure 3.15) **not** a big number of points **but the lines** corresponding to the multiple instances when this condition occurs and the separation between the two working modes of the robot. Again, in order to be on the safe side a margin of at least 5° must be imposed in the control algorithm to avoid any unwanted situations during the robot actuation.

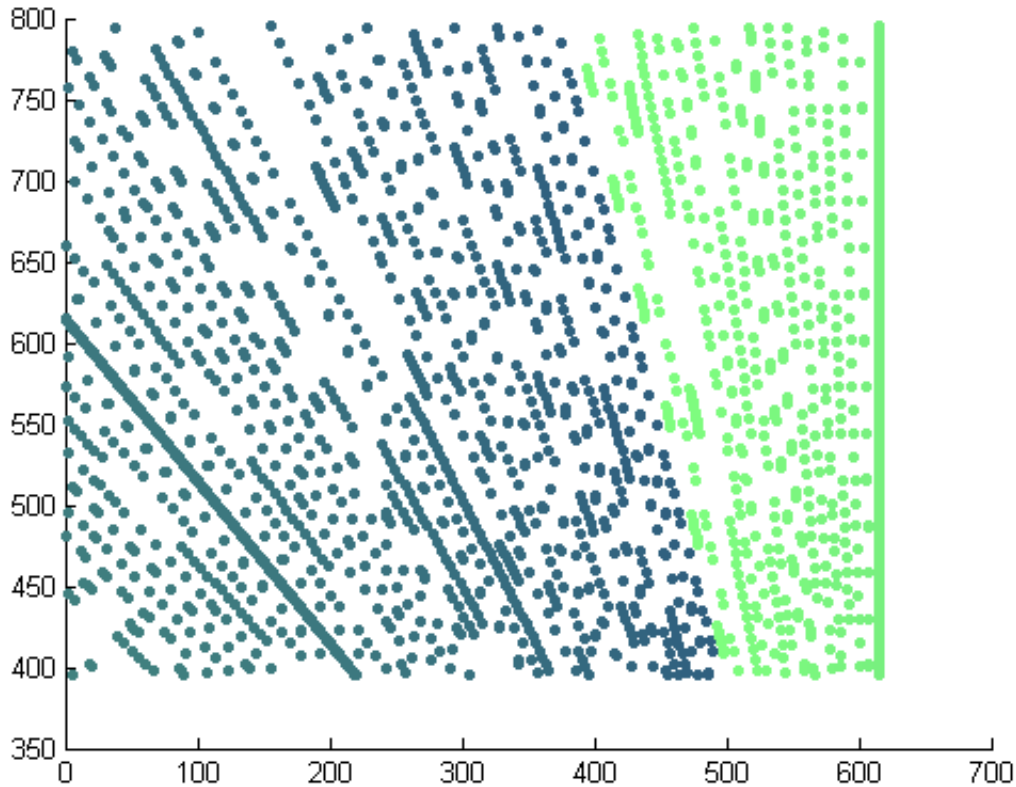


Figure 3.15. A geometric representation of the third singularity of the robot

The determinant of the matrix B is:

$$\det(B) = \frac{(q_2 - q_1) \cdot (q_5 - q_4) \cdot \left[b_1 + \sqrt{d_1^2 - (q_2 - q_1)^2} \right] \cdot \left[b_2 + \sqrt{d_2^2 - (q_5 - q_4)^2} \right]}{\sqrt{d_1^2 - (q_2 - q_1)^2} \cdot \sqrt{d_2^2 - (q_5 - q_4)^2}} \quad (3.79)$$

Case 1: $q_1 = q_2$, respectively $q_4 = q_5$

These configurations define the case when one of the two pairs of translational active joints of the PARA-BRACHYROB modules superpose. In a real scenario this case cannot appear, the experimental model of the robot having limit switches which avoid this situation.

Case 2: $d_1 = q_2 - q_1$, respectively $d_2 = q_5 - q_4$

These configurations define the maximum distance between the two pairs of translational active joints which corresponds to the case when the rod will be positioned vertically. This second case defines an extreme configuration which is avoided in the robot control system.

The singularities identified within the determinant of matrix B are all situated at the boundary of the motion domain of the robot and they do not represent a problem during the robot actuation.

Due to the fact that, as stated before, safety is the most critical issue in this therapy, PARA-BRACHYROB was subjected to a parallel analysis using a method based on a theory developed by Edward Study at the brink of the 20th century [STU1903] and further implemented in the study of robot singularities by Manfred Husty, who became the first scientist to develop a method for the complete analysis of singular robot poses [HUS07]. It is possible to give a complete global description of the manipulators kinematic characteristics using an algebraic approach. This is due to the fact that Study's parametrization of the 3-dimensional Euclidean motion group is free of parametrization singularities. The complete kinematic description is inherent in the constraint equations, derived by using the linear implicitization algorithm (LIA), introduced by Walter and Husty [WAL10], as well as the geometric description of the manipulator. The paper uses Study's parametrization of the Euclidean motion group, the ideals belonging to mechanism constraints and methods to solve polynomial equations are the mathematical equivalents of the mechanism constraints. The challenge of this method is to achieve a Groebner basis (which will provide all the singular conditions) while preserving all the geometric parameters as variables. The analysis of the PARA-BRACHYROB robot using this method is presented in [VAI 15] and [SCH 18]. The method itself will not be presented here as there will be a chapter dedicated to this method within this thesis, but the final result supplied a polynomial equation which resulted in a supplementary condition that, added in the control algorithm, ensures the robot safe behaviour during the procedure.

Workspace analysis of PARA-BRACHYROB

Two approaches will be illustrated here, an analytical one developed based on the geometrical model of the robot and a geometrical one developed using the Siemens NX software applied on the modelled structure of PARA-BRACHYROB. The second approach is interesting because it proposes an approach which enables the visualisation of all the 5-DOFs of the robot within a three-dimensional representation.

For the study of the robot workspace (as this cannot be non-dimensional) numeric values have been assigned to all the geometrical parameters, values that were then used as design parameters for the experimental model.

The robot workspace has to be generated taking into account the coordinates of an insertion point $I(X_I, Y_I, Z_I)$ and then using the inverse geometrical model the geometrical loci of all the validated target points $E(X_E, Y_E, Z_E)$, can be obtained. Besides the obvious results this analysis will also point out the importance of efficient positioning of the robot with respect to the patient and the location of the pairs of Insertion and Target points in order to obtain the best possible dynamic results.

The geometrical parameters used in this study are:

- $d_1 = 400\text{ mm}, b_1 = 400\text{ mm}, l_1 = 65\text{ mm}, d_2 = 400\text{ mm}, b_2 = 500\text{ mm},$
- $l_2 = 65\text{ mm}, l_c = 200\text{ mm}, h = 187\text{ mm}, d_{12} = 500\text{ mm}.$

For the active joints the following limits were defined:

- $q_{i_{\min}} = 0\text{ mm}, q_{i_{\max}} = 950\text{ mm}, i = 1, 2, 4, 5, q_{3_{\min}} = 0, q_{3_{\max}} = 2\pi.$

In figure 3.16 the maximum workspace of PARA-BRACHYROB is displayed, generated for a set of coordinates for the insertion point where all the active joints are located close to the midway of their strokes.

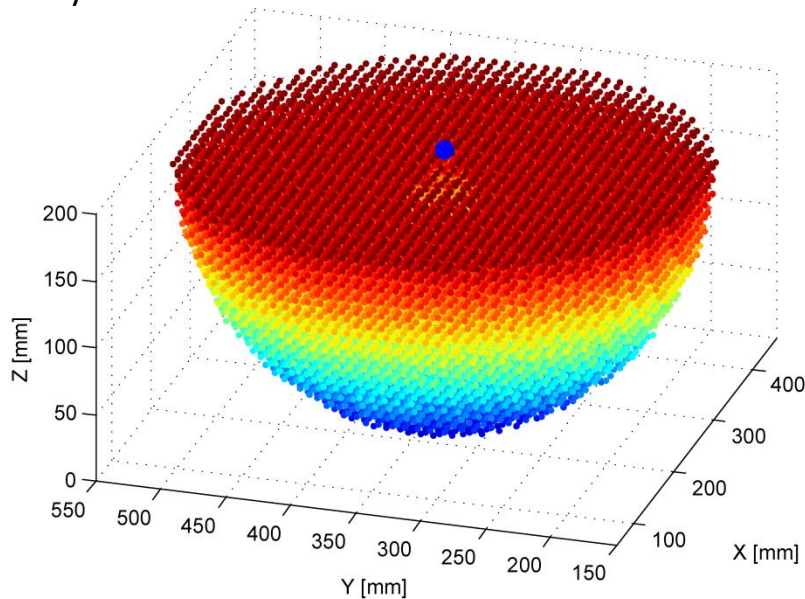
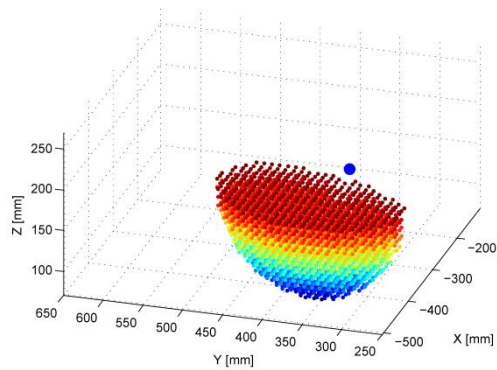


Figure 3.16. The maximum theoretical workspace of the cylindrical parallel robot BR3

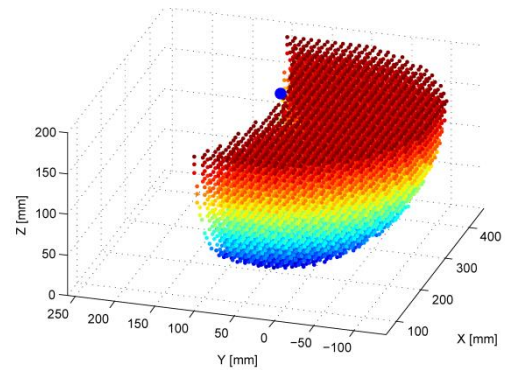
Figures 3.16 a) – f) illustrate the workspace volumes determined for different insertion points coordinates illustrating the importance of the proper definition of the robot positioning with respect to the patient and the targeted organ. For the workspace generation using the inverse geometrical model, a volume which integrates the robot workspace is initially defined. One considers that all the points in that volume are within the robot workspace, and for each point of the needle tip, the values of the active joints are determined. When a valid combination for the active joints is obtained the set of coordinates which defined the target point is saved. The matrix of the validated needle tip coordinates represents the robot workspace. For the validation, a set of conditions were imposed as follows:

- $q_{i_{\min}} < q_i < q_{i_{\max}} \quad i = 1..5$ - the values of the active joints must be located between the lower and upper limits of their strokes;
- $q_1 < q_2, q_4 < q_5$ - this pair of conditions imposes for each of the two translational joints of the cylindrical modules the relative positioning of the actuators which cannot pass one over the other;
- $q_1 > q_4 + l_1 + l_2$ - this condition imposes that the point C1 will always be located on top of the points C2 (with respect to the Z coordinate) as the needle will always be inserted from a higher position, downwards;

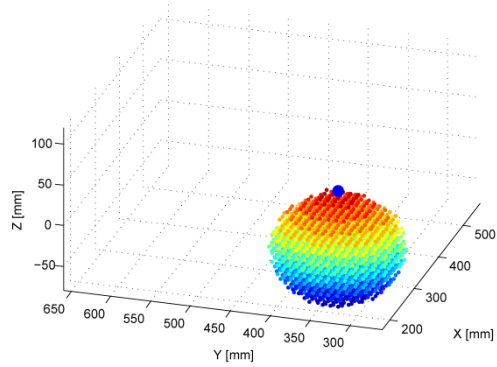
- $q_2 - q_1 < d_1$ and $q_5 - q_4 < d_2$ - these last two conditions limit the maximum distance between the pairs of active joints of each cylindrical module.



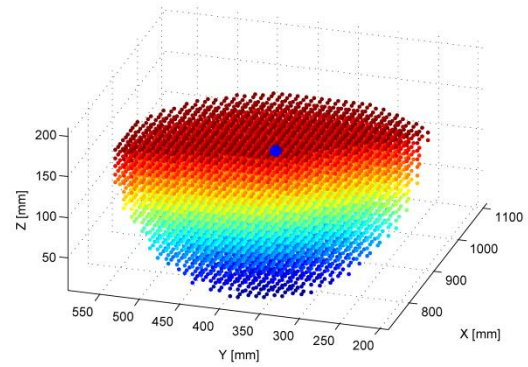
a) $X_I = -345\text{mm}, Y_I = 340\text{mm}, Z_I = 200\text{mm}$



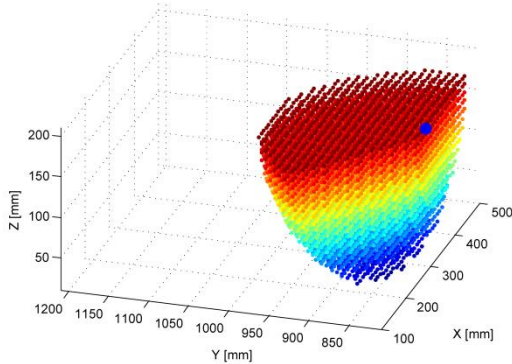
b) $X_I = 250\text{mm}, Y_I = 50\text{mm}, Z_I = 200\text{mm}$



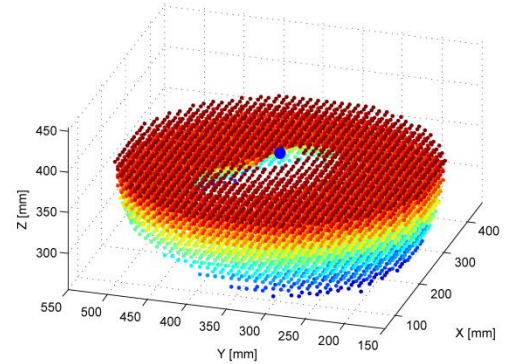
c) $X_I = 250\text{mm}, Y_I = 340\text{mm}, Z_I = 50\text{mm}$



d) $X_I = 745\text{mm}, Y_I = 340\text{mm}, Z_I = 200\text{mm}$



e) $X_I = 250\text{mm}, Y_I = 800\text{mm}, Z_I = 200\text{mm}$



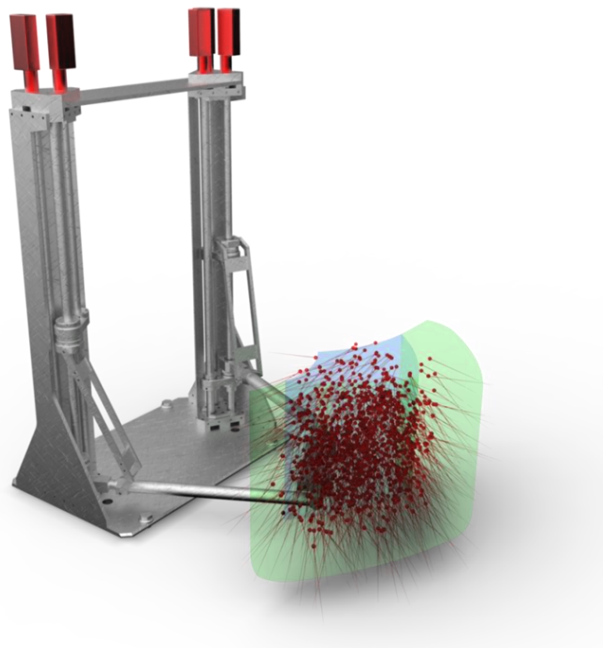
f) $X_I = 250\text{mm}, Y_I = 340\text{mm}, Z_I = 370\text{mm}$

Figure 3.17. PARA-BRACHYROB workspace for different insertion points

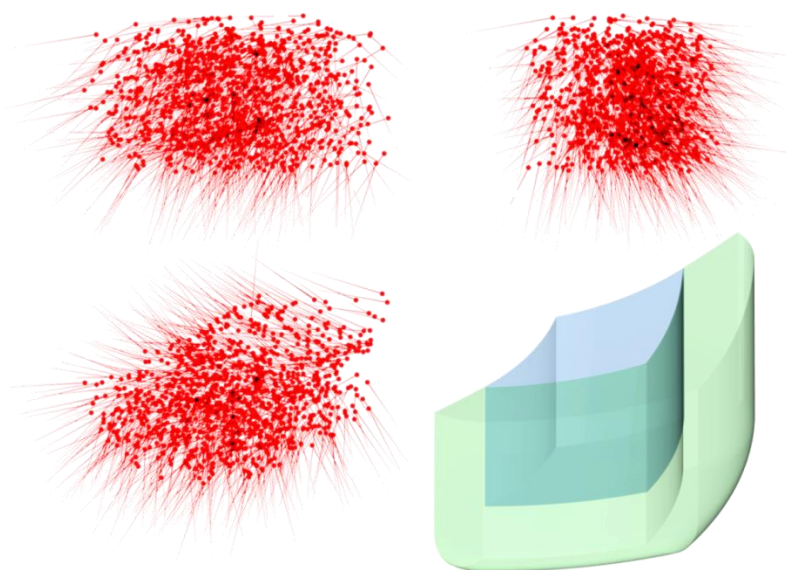
Analysing the robot workspace modifications based on the coordinates of the insertion point, one can conclude that for optimum performance the values for the coordinates of point I should not vary with more than ± 150 mm on X axis, ± 50 mm on Y and Z axis with respect to the values obtained for the maximum robot workspace.

As this type of application requires a careful preplanning, the best relative positioning between the patient and the robot can be easily determined before the actual procedure avoiding any misbehaviours during the actual procedure.

The geometrical modelling of the workspace, detailed for several structures in the PhD thesis of Dragos Cocorean [COC16], proposes the generation of the workspace using a random function that will generate a suitable configuration of the robot and tracing the coordinates of the needle tip, drawn as a sphere. This of course generates a point cloud where the needle orientation is not known, but knowing the values of all the robot coordinates this can be represented as a line that passes through the sphere, thus obtaining a 5-dimensional representation of the workspace. This idea is not fully studied yet and because each trace represent an actual body in the modelling software the analysis is limited to several thousands of points (depending on the computation power of the computer) but the potential of the solution is quite high and will be further investigated in the future. Some of the results on the analysis on PARA-BRACHYROB are illustrated in figure 3.18.



a) The robot workspace with respect to the mechanical structure



b) Detailed view of the robot workspace in 5-dimensional representation
Figure 3.18. Geometrical modelling of the PARA-BRACHYROB workspace

The trajectory generation algorithm and mechanical structure validation

The kinematic equations determined before are used in the robot control for the actuation of the active joints with respect to a given medical task. Using the simulation package from Siemens NX, namely the RecurDYN solver, a motion will be simulated both using the mathematical model and the output data in terms of variations at the levels of the active joints will be inserted in the NX solver which will actuate the structure. Comparing the resulting data, both the mathematical model and the mechanical design will be validated.

In the NX simulation model, the following simplifications are used:

- It neglects gravity forces and the masses of the bodies in motion;
- The external and inertia forces do not affect the motion;
- The bodies and joints are considered to be perfectly rigid.

A real situation was defined for the robot motion as follows:

- The robot has a current arbitrary position which is known with respect to the fixed coordinates system;
- The robot will receive two sets of coordinates for the insertion point and the target point inside the patient;
- The robot motion is decomposed into two parts: in the first, the robot will move from its current location to the insertion point, achieving, in the same time the final orientation for the needle; in the second part, the robot will drive the needle, along a linear path to the target point.

The geometric parameters used for this simulation represent the final dimensions of the robot which have been slightly modified in comparison with the ones used to study the workspace generation:

$$\begin{aligned}
 d_1 &= 400\text{ mm}; & b_1 &= 395\text{ mm}; & l_1 &= 67\text{ mm}; \\
 d_2 &= 400\text{ mm}; & b_2 &= 495\text{ mm}; & l_2 &= 67\text{ mm}; \\
 l_c &= 170\text{ mm}; & d_{ac} &= -112.5\text{ mm}; & d_{12} &= 615\text{ mm};
 \end{aligned}
 \tag{3.80}$$

The negative value of the parameter d_{ac} shows that at the beginning of the procedure the needle is fully retracted. In the current (starting) position of the robot the coordinates of the needle tip (point C) are:

$$\begin{cases} X_c = 307.5\text{ mm}; \\ Y_c = 800\text{ mm}; \\ Z_c = 400\text{ mm}; \end{cases} \begin{cases} \psi_c = 90^\circ \\ \theta_c = 60^\circ \end{cases}
 \tag{3.81}$$

For the motion simulation a real scenario has been selected, namely the treatment of a tumour located in the liver. The patient is positioned lying on his back with the robot targeting the tumour from above.

The two sets of coordinates defining the insertion point and the target point inside the patient are given:

$$\begin{cases} X_I = 360 \text{ mm}; \\ Y_I = 750 \text{ mm}; \\ Z_I = 350 \text{ mm}; \end{cases} \begin{cases} X_T = 380 \text{ mm}; \\ Y_T = 810 \text{ mm}; \\ Z_T = 280 \text{ mm}; \end{cases} \quad (3.82)$$

The orientation angle of the needle is calculated using the equations:

$$\begin{aligned} \psi_{IT} &= \text{atan2}(Y_T - Y_I, X_T - X_I); \\ \theta_{IT} &= \text{atan2}\left(\sqrt{(Y_I - Y_T)^2 + (X_I - X_T)^2}, Z_I - Z_T\right); \end{aligned} \quad (3.83)$$

As motion parameters the following maximum speed and acceleration were imposed for the needle tip, values considered safe for the medical procedure:

$$v_{\max} = 20 \text{ mm/s}; \quad a_{\max} = 10 \text{ mm/s}^2 \quad (3.84)$$

The simulation results are illustrated in the next figures, which validate both the kinematic model and the structure design.

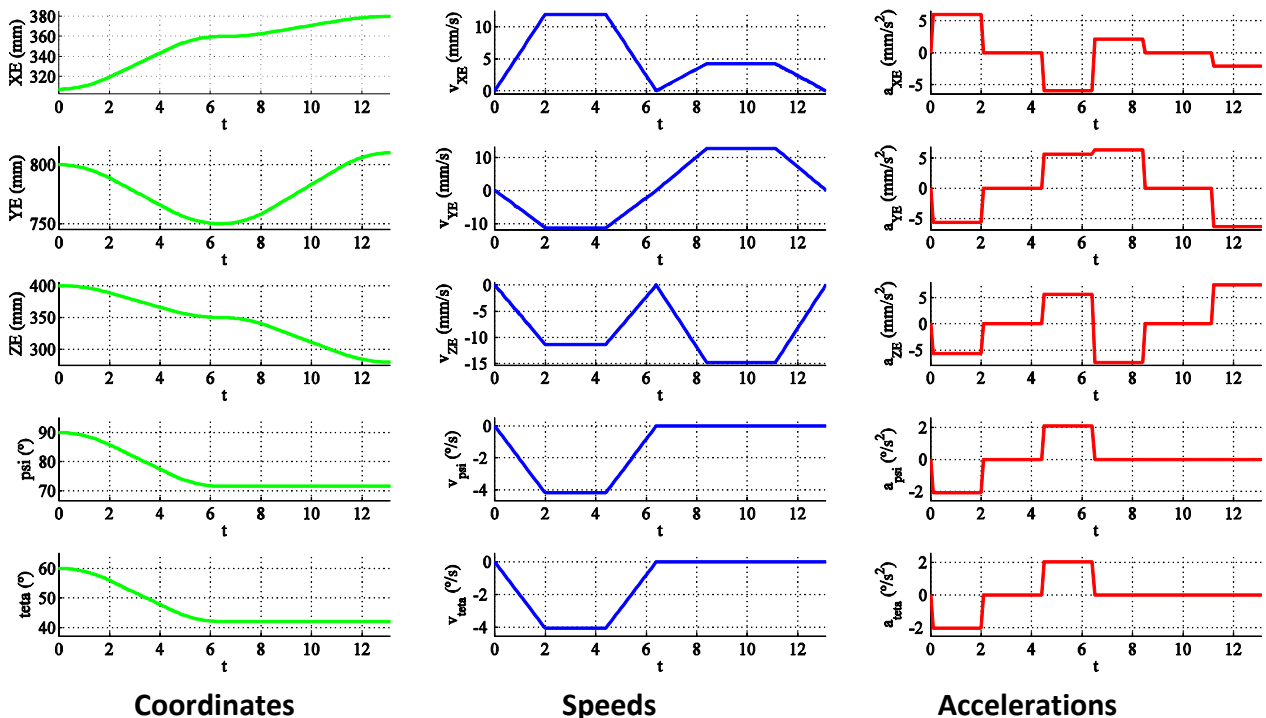


Figure 3.19. The needle tip trajectory (two steps motion)

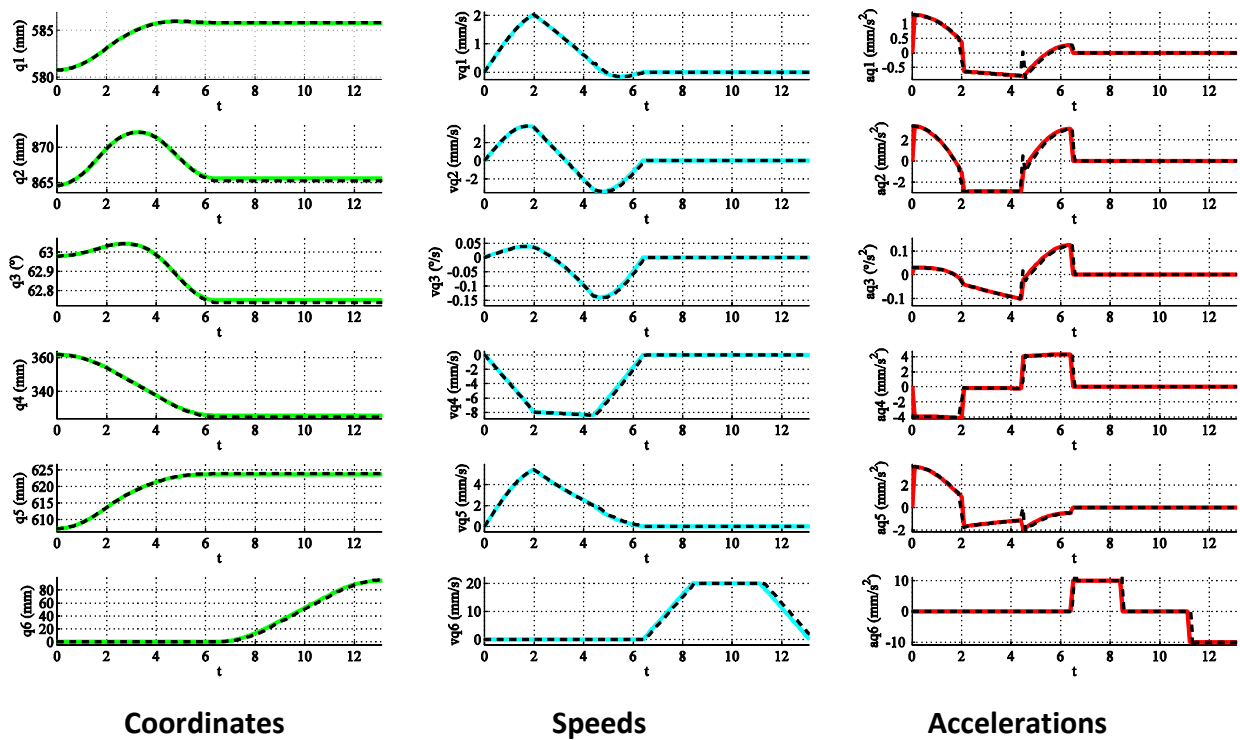


Figure 3.20. The variation of the coordinates, speeds and accelerations at the level of the active joints (Dotted line represents the Siemens NX simulations)

PARA-BRACHYROB experimental model

All the achievements with respect to the development of PARA-BRACHYROB from an idea up to an experimental model were achieved within the project no. 173/2012, code PN-II-PCCA-2011-3.2-0414, entitled “Robotic assisted brachytherapy, an innovative approach of inoperable cancers - CHANCE”, financed by UEFISCDI, and represent the joint work of a large interdisciplinary team. The achievement itself illustrates the importance of teamwork as a single scientist cannot cover all the necessary interconnected fields of work to achieve by himself such results.

The design of the mechanical structure of PARA-BRACHYROB is presented in detail in [COC16]. From the constructive point of view, the robotic structure is positioned on an aluminium plate frame which can be fixed to the CT Scan using the calibrated locations of the mobile couch, with the main 5 active joints (motors) fixed to the top of the frame from where these are referenced (figure 3.21). The needle insertion module motion is obtained by rotating the ball screws and/or grooved shaft held by bearings connected to the fixed frame, necessary for a smooth motion at the active joints. All passive revolute joints are being designed with friction plastic bushings for attenuating the possible vibrations. The frame is supported by the ball screws, cylindrical and grooved shafts as well as the aluminum support plates that transfer the generated forces and vibrations to the CT table. For additional precision both columns will be connected on top by a structural bridge which will both stabilize the robotic structure and provide a viable electrical connection path. The two arms will determine a specific workspace which varies with their length.

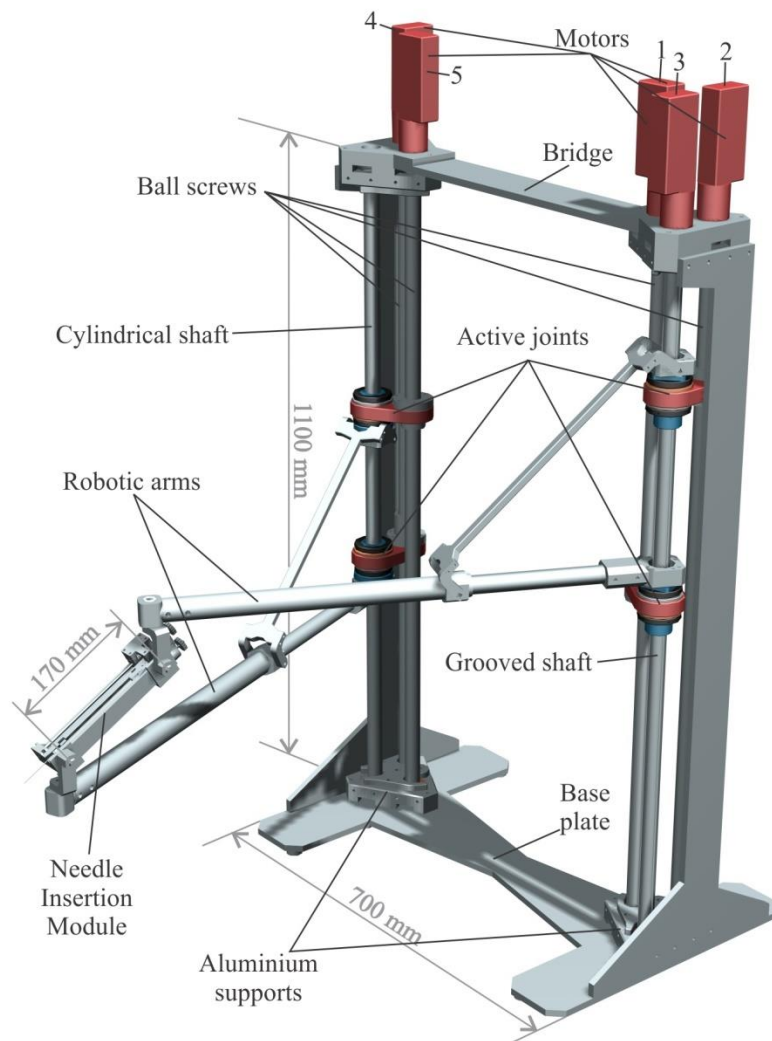


Figure 3.21. The mechanical structure of the PARA-BRACHYROB robotic system

As the needle insertion will be made always from a top position going downwards the right cylindrical module will have a larger horizontal arm by half the distance between the two Cardan joints to enable a wider orientation range of the needle insertion module. The distance between the two Cardan joints has been chosen in accordance with the available workspace of the CT and the needle length, directly influencing the orientation and positional precision of the needle, establishing a ratio between them.

The needle insertion module (figure 3.22) was designed to enable the efficient insertion and retraction of the needle for any given trajectory. Based on the conclusions presented in [STR11] regarding the needle deflection a force sensor will be integrated mechanism to monitor the force variation during the needle insertion though the body. The different types of tissue (layers of skin, fat, muscles, internal organs parenchyma) have different resistances and in case the force exceeds a certain limit the needle will deflect from the trajectory risking an unwanted damage of proximal structures, imposing a total retraction and the repeating of the procedure. A detailed experimental analysis on this issue will be presented in the next chapter.

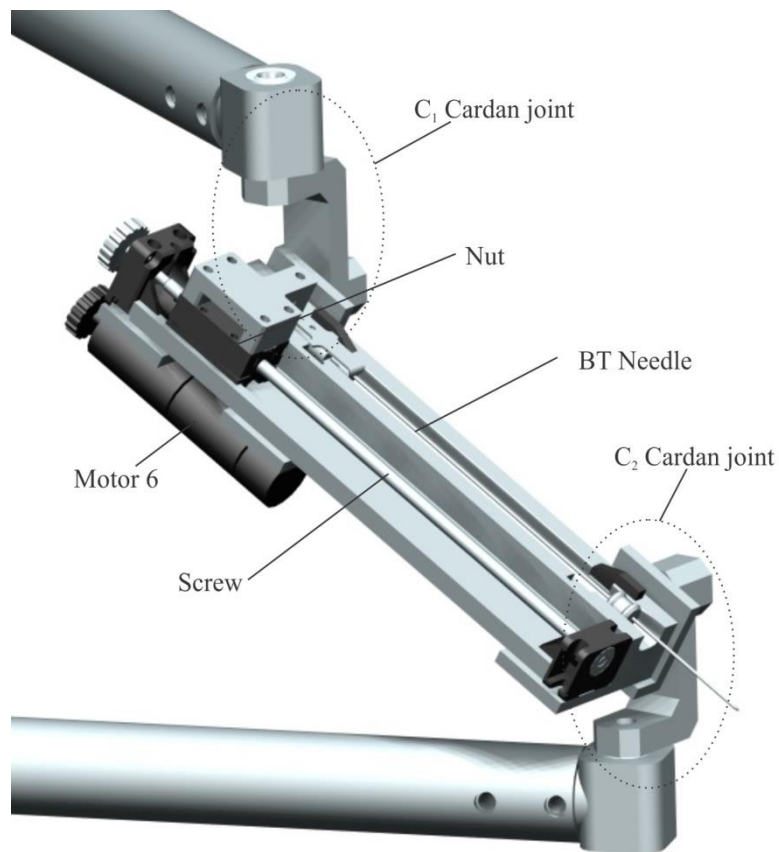


Figure 3.22. The needle insertion module

Furthermore, the mechanism uses several guiding rings to reduce (if not to eliminate) any bending of the needle during the insertion. The module has a mechanical release mechanism which enables total control of the needle length inserted inside the patient and also its safe retraction in case of an emergency. The mechanism itself consists of a linear module that moves along a screw with a fine pitch (0.8 mm per rotation) and it is actuated through a timing belt which enables the positioning of the actuator itself in parallel with the module, making it very compact. Being positioned between the Cardan joints, the mechanism is suitable for a wide variety of brachytherapy needles. In the control unit, the doctor must specify the needle length and the parameter d_{ac} will use the input given value to suit that dimension.

The control system of PARA-BRACHYROB

The control system of the robot has two main components:

- **The hardware** which integrates a PowerPanel from B&R Automation, which can be seen basically as a programmable logic controller with a display and the actuators from Maxon which are connected through a CANOpen communication interface;
- **The software** which integrate the actuator control (made based on the CanOpen communication protocol), the final equations that determine the

motion parameters that have to be sent to the actuators for a given trajectory and the user interface.

The main idea of the control system was to design a simple user-interface that could be safely manipulated by user with limited knowledge in engineering where the entire procedure is performed in a stepwise sequence (that cannot be changed) acknowledging the successful completion of each step before moving to the next. A detailed structure of the control software for PARA-BRACHYROB is presented in figure 3.23, structured on three levels:

1. **Communication protocol** level which include the data transfer for the CanOpen interface;
2. **Information exchange** level which integrates all the functions developed for the robotic structure. These include specific functions for the actuation of the motors as well as mathematical functions for the inverse and direct kinematic models of the robot along with the trajectory generation algorithm. As supplementary safety condition a workspace and singularity validation function has been added which is run before every motion.
3. **User-interface** level which integrates all the commands that can be given by user for the robot actuation.

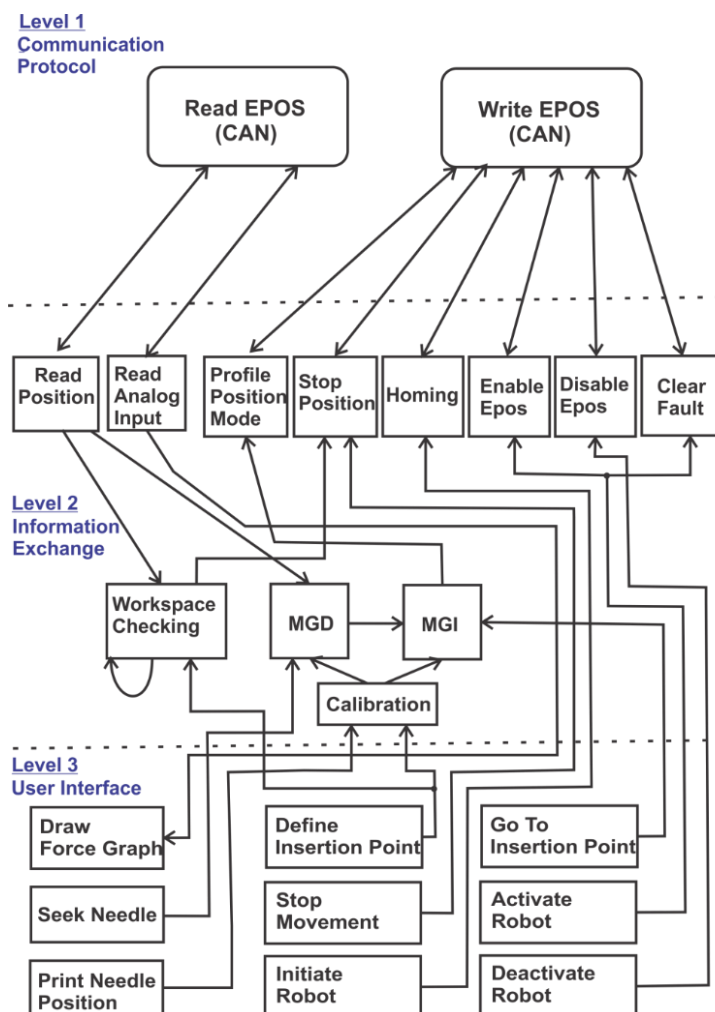


Figure 3.23. The control architecture of PARA-BRACHYROB

The interface has three control screens which integrate each a separate control. The first one provides the means to perform a fully automated procedure (figure 3.24) allowing the automated needle insertion. The use of this control solution is conditioned by an existing pre-planning and definition of the number and locations for all the Insertion-Target pairs of points. The stepwise procedure is illustrated next:

1. The robot is positioned of the CT-Scan and calibrated with respect to the laser system (using the button **Calibrate**) – this will ensure that the relative position between the robot coordinate system and the measurement system of the CT-Scan is known and the robot can use the input data given relative to that external reference system;
2. The patient is positioned on the CT-Scan mobile couch and carefully calibrated based on the external markers defined during the first scan. Once this operation is done it is confirmed on the robot using the button **Validate Patient Position**;

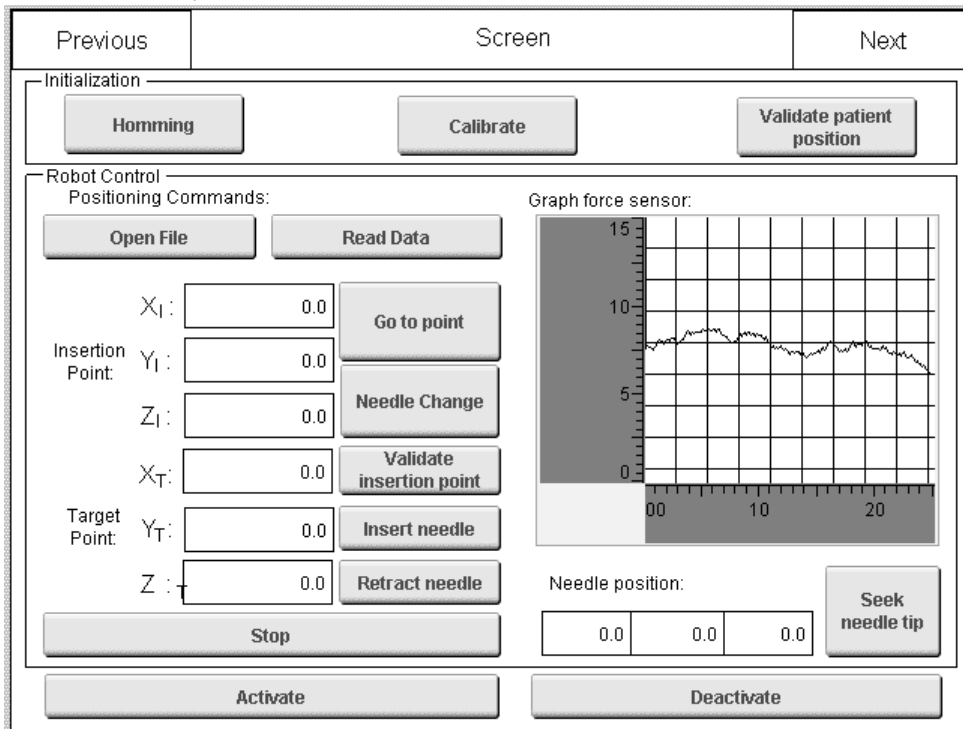


Figure 3.24. Control interface for the automated needle insertion

3. The next step is to reset all the encoders on the robot using the single active button on the interface, **Homming**. This command will reposition all the actuators on the boundary of their strokes, using external limit switches. Once all the actuators have reached their positions the next command becomes available: **Needle Change**.
4. By pressing the **Needle Change** button the robot will move in the pre-set working position (the point C).
5. Once this position is reached the interface will allow the insertion of a mobile drive in a secure USB port on which there will be a file that will store, all the

pair of points of interest (Insertion - Target). The sequential reading of the data is done with the buttons **Open File** and **Read Data**. For security reasons the **Open File** button can be used only once (it becomes disabled after the first use) and the **Read Data** will cycle through the points only once until the EOF (end of file) is reached.

6. When a pair of points is loaded, the coordinates are transmitted to the controller and the button **Go to Insertion Point** becomes active.
7. By actuating the button **Go to Insertion Point** the robot will perform the first motion sequence moving from point C to the point I (Insertion) with the needle oriented on the insertion trajectory.
8. Once the point is reached the button **Validate Insertion Point** becomes active.
9. When the medical team validates the insertion point the next button becomes active, namely **Insert Needle** that will determine the needle insertion of the needle on the distance calculated between the pair of points (I-T).
10. When the target point is reached the robot will release automatically the needle and the empty module will be retracted back to the pre-set working position (point C).
11. The needle position is validated by a quick scan and the procedure is repeated starting from step 6.
12. When all the needles have been inserted the robot is retracted in the **Homming** position not allowing any other commands, to ensure the patient safety.
13. The patient is transported in the secured treatment room where the radioactive seeds will be inserted using a special device and the robot is removed from the CT-Scan table.

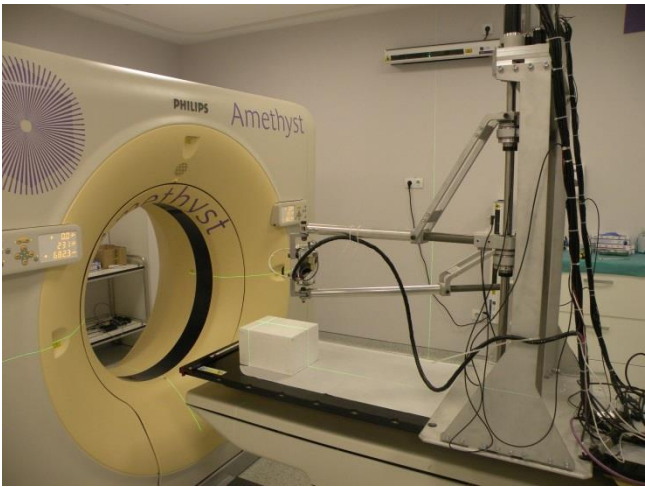
The interface has also a graphical area where the real-time resistance force for the needle is displayed. The needle insertion will stop automatically in case a certain force threshold is reached. Also the needle insertion can be stopped manually at any instance and the needle can be retracted. The robot has also a general stop button and an emergency button when power is cut, the actuators released and the robot can be removed immediately.

The other available interfaces allow a manual definition of the coordinates of the insertion and target points and the individual control of the actuators but from the medical point of view these are only for testing purposes.

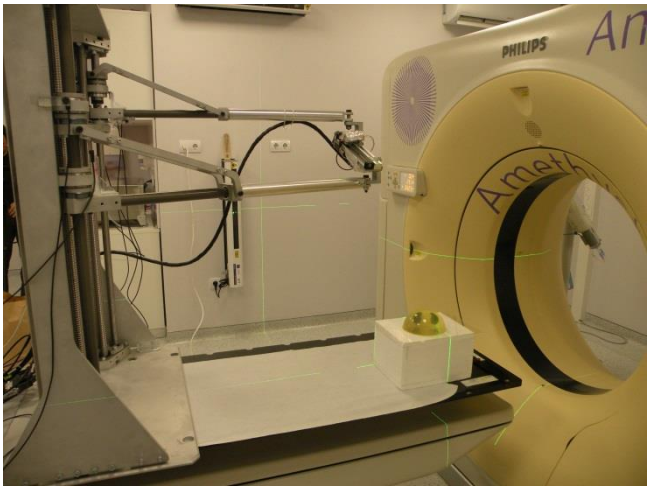
Experimental tests in a controlled environment

The experimental model of PARA-BRACHYROB was teste in November 2016 within the Amethyst Oncology Clinic, with the assistance of dr. Gabriel Kacso which provided both the access to the CT room and the necessary technical assistance to interface the two systems. Based on the agreed medical protocol a ballistic gel

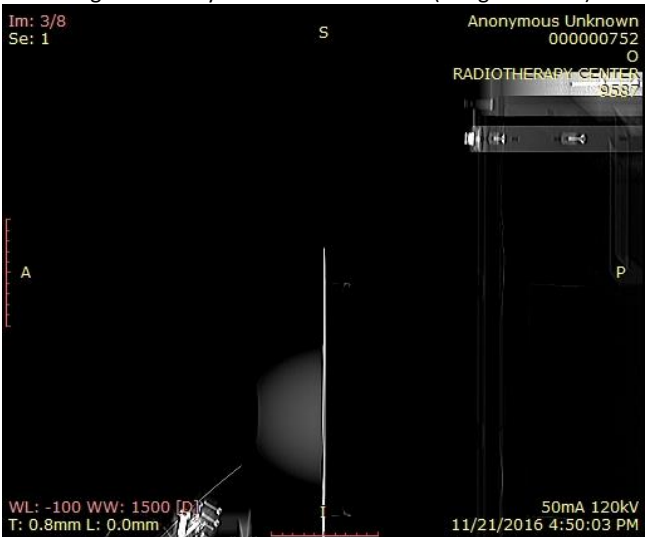
model was created inside which were inserted elements which density similar to the liver and the entire medical procedure was simulated.



a) The positioning of the robot on the CT table and its calibration using the laser system of the CT – Scan (the green lines)



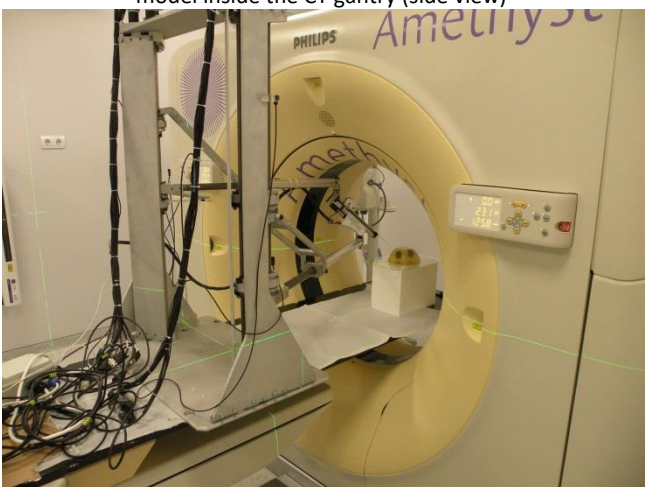
b) The positioning of the ballistic gel model on the CT and the reading of the coordinates of interest



c) Validation of the needle position with respect to the ballistic model inside the CT gantry (side view)



d) Validation of the needle position with respect to the ballistic model inside the CT gantry (top view)



e) PARA-BRACHYROB with its needle insetion module inside the CT-Scan gantry



f) Needle insertion inside the tumour under CT real-time control

Figure 3.25. Experimental tests with PARA-BRACHYROB in medically relevant environment



Needle located in the insertion point Needle motion towards the target point Needle tip in the target point

Figure 3.26. Real-time monitoring of the procedure and the validation of the needle location

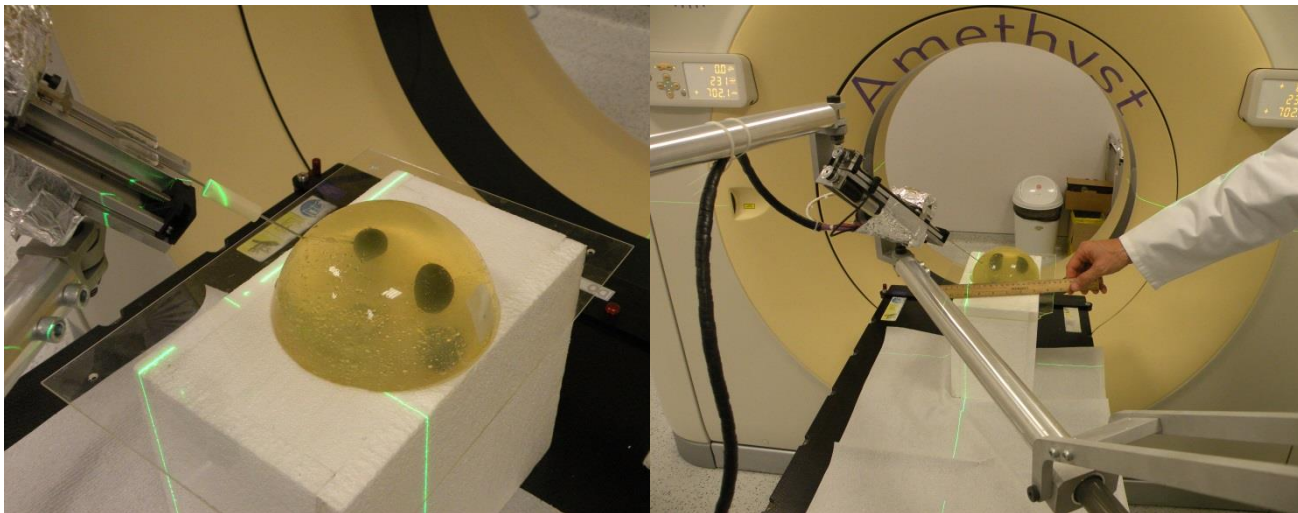


Figure 3.27. Needle position inspection at the end of the procedure and the validation of PARA-BRACHYROB as an efficient robotic solution for the treatment of malignant tumours using real-time CT Scan monitoring

In the end...

The development of robotic systems for medical applications is a very important field of work, hampered unfortunately by the limited possibility of validation of the proposed solutions due to extremely high homologation costs and limited access to proper testing conditions. The development of PARA-BRACHYROB represents a success story showing that in research the only real barriers are the limits that one imposes to himself.

However, these achievements have also set a level for the future development that must be respected once it was proven possible and also a proof that medical research can be achieved in an efficient way with limited funding.

Chapter 4. Advanced systems for minimally invasive percutaneous therapy

*“The future depends on what we do in the present.”
(Mahatma Gandhi)*

Minimally invasive percutaneous therapies

Needle placement techniques cover a wide area of medical applications, where the task can be described, in a very simple way, as the insertion of a needle (fig. 4.1) on a certain trajectory, from outside up to a target point situated in the patient body. Needle placement covers applications like biopsies, fluid extraction from internal organs (cardiac tamponade, lungs) or placement of radioactive seeds in different body organs in minimally invasive cancer therapy [STR11, BOC08].

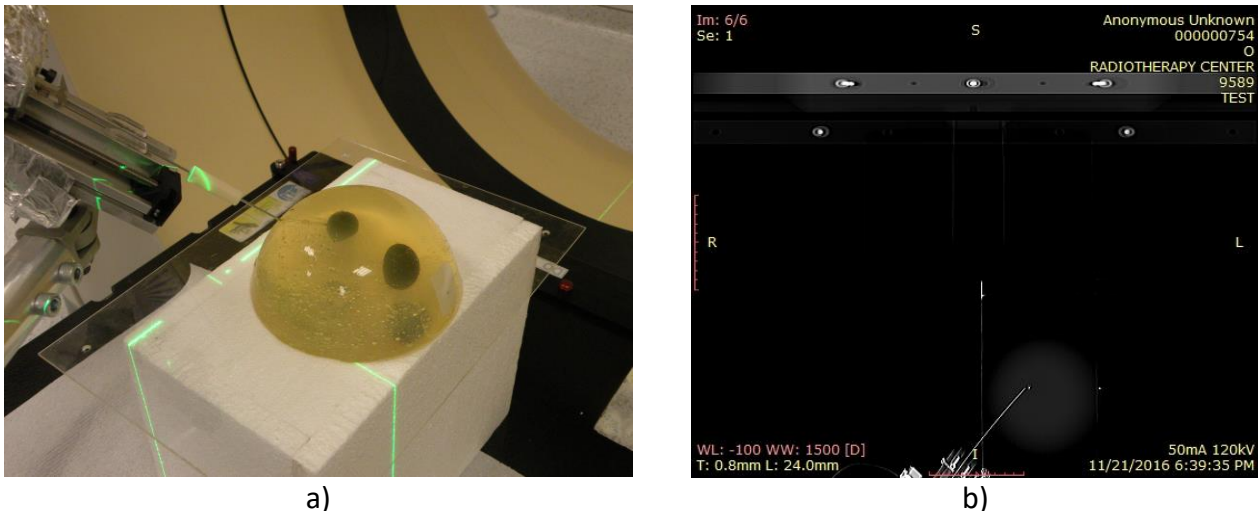


Figure 4.1. Needle insertion task, demonstrated using the PARA-BRACHYROB experimental model

This chapter will present several devices that were developed for this task:

- A robotic system developed for prostate biopsy;
- A set of three instruments that can be used as end-effectors for a robotic system, covering:
 - Prostate biopsy, using a dedicated biopsy gun;
 - Brachytherapy, enabling the successive insertion of up to 6 needles;
 - Radio-frequency ablation.

An innovative parallel robotic structure designed for transperineal prostate biopsy – PBS-BOT

A short overview of prostate cancer

Prostate cancer is the most widely spread form of cancer, generally affecting men of age over 45. Several studies showed that 80% of the men over 70 had different forms of prostate cancer, most of them not being aware of that. The latest achievements in this field have improved a lot the survival rate and life expectancy of cancer patients but the extremely high incidence of this disease places prostate

cancer on the second place as death cause, with an annual death rate of over 250.000 cases, with only pulmonary cancer being deadlier [YAC12].

The prostate is a gland in the male reproductive system and the prostate tumour begins inside the prostate and may grow to involve the entire gland having a slow evolution in time. Moreover a large percentage of the tumours located in the prostate are benign (non – cancerous) and do not require any cancer specific treatment (radiotherapy, surgery etc.). Nevertheless, several studies conducted on men that died of other causes revealed that **about 30% of the men aged 50 and over 80% of the men over 70** had different forms of **prostate cancer**, most of them not knowing about it [YAC12]. This shows that this form of cancer is not very aggressive but its high incidence rate makes it one of the most deadly diseases in the world. As in any disease, early diagnosis allows simpler curative actions, less patient trauma, better life expectancy and quality for the patient.

5 years survival rates by stage of diagnosis

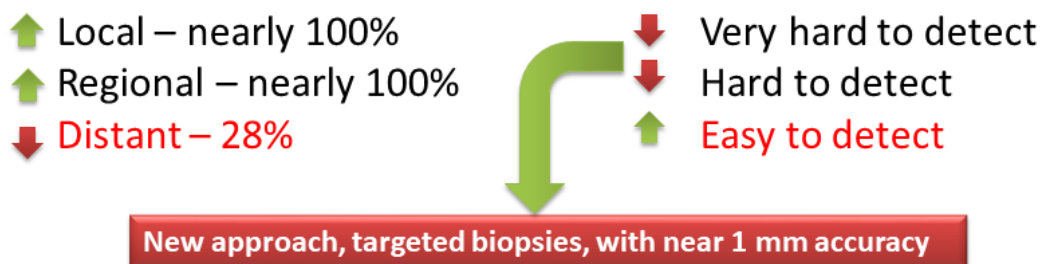


Figure 4.2. Motivation for a paradigm change in prostate cancer

Nevertheless, the diagnosis for prostate cancer is carried in the same way as it was performed 50 years ago [YAC12, GIU11]. The **preliminary investigations** for malignancy suspicion criteria impose the positive result of at least one of the following markers: **PSA** (Prostate Specific Antigen) larger than 4ng/ml, **detection of nodules** during the digital rectal examination or **positive appearance** during grey scale **TRUS** (transrectal ultrasound) [GIU11]. When suspicion arises, the **next step involves a 12-core**, TRUS guided **biopsy**, which aims to harvest tissues from every areas of the prostate to diagnose cancer [GIU11]. However, this technique is performed without knowing the exact 3D tumours location and it was proven that **more than 30%** of the cases, it provides **false-negative results**. Magnetic resonance imaging (MRI) enables a better view of the prostate with clear tumour definition, but MRI guided biopsy can be achieved only with MRI compatible materials which make the procedure prohibitive. However, it was proven by many medical research centres that mp-MRI (multi-parametric MRI) is very useful in pin-pointing the prostate tumours especially in the anterior part of the gland which suggests that a prior mapping of the biopsy target cores using the MRI would enhance the correct diagnosis rate following a biopsy, by accurately defining the targets that will be used afterwards during the prelevation procedure [PET12].

The current worldwide ultrasound guided biopsy technique, following the 2012 European Society of Urogenital Radiology (ESUR) guidelines for prostate cancer has some major drawbacks:

- Low real-time image quality;
- Blind biopsy;
- Impossibility of registering the 3D location of the biopsy cores.

These aspects make a follow-up investigation impossible as the prelevation of tissue from the same core to assess its evolution in time cannot be done.

In the same time, **the tissue biopsy** is the **only technique** which can **confirm** definitely the existence of **cancer** and it became a focus point for many research centres which proposed different approaches in order to improve its diagnostic accuracy.

In order to make a significant step ahead towards a really targeted procedure, every device shares a common requirement which conditions its development (figure 4.2): the need of a highly accurate targeting solution which could reach a defined point inside the human body with an overall accuracy of 1 mm, which is well beyond the human natural capabilities, as shown in [STR11, POD14]. The first researches in this field proposed robotic solutions which targeted a specific organ (e.g. robots for prostate brachytherapy and biopsy) but no general use solution has been developed so far. A very recent report [POD14] (August 2014) published by AAPM (American Association of Physicists in Medicine) makes a very thorough review of all achievements in robotic brachytherapy presenting 13 robotic solutions (12 for prostate and one for lung cancer) emphasizing the need of additional solutions and proposing also a guideline for their characteristics.

From the medical point of view, the prostate biopsy can be performed in two ways: transrectal (fig. 4.3) and transperineal (figure 4.4).

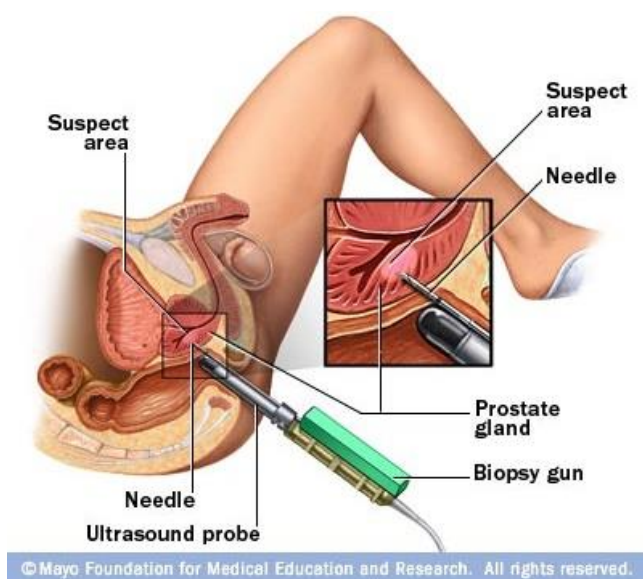


Figure 4.3. Transrectal prostate biopsy
(©Mayoclinic health library)

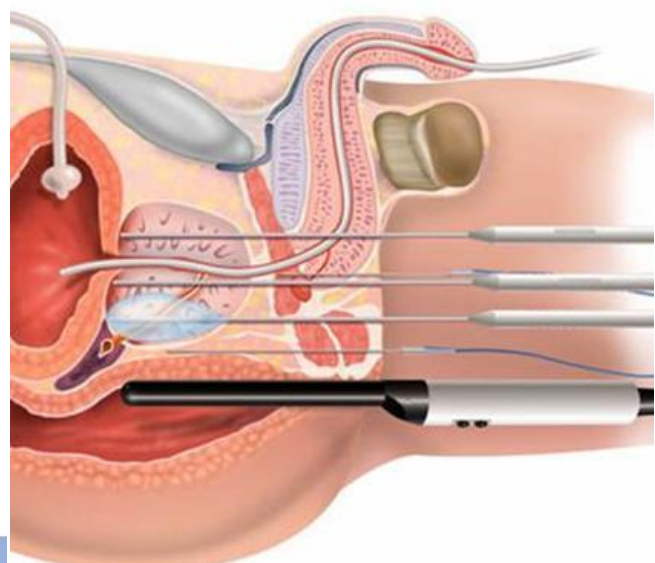


Figure 4.4 Transperineal prostate biopsy
(©AvantGardeUrology)

The transrectal approach uses an ultrasound probe inserted through the rectum, with the patient in gynaecologic position or prone sitting on one side, with the biopsy gun attached to the probe. The transperineal approach uses the ultrasound probe in the same position but the needle is inserted separately through the perineum (fig. 4.4).

The transperineal technique is less used until now in medical practice but as shown in [CHA 13] - a review article published in Nature, it has multiple **advantages**:

- ✓ improves the cancer detection rate;
- ✓ reduces the false negative results;
- ✓ improves the sampling of the anteroapical (the apex of the prostate) region;
- ✓ eliminates the sepsis risk (which appears due to the perforation of the intestine) especially for the high risk patients with diabetes.

Its underuse is determined by the longer procedural times, the slightly more expensive equipment required and the needs of high-grade anaesthesia, but globally its benefits overcome by a large margin its drawbacks.

From the medical point of view, the transperineal technique has two main approaches (schematic view illustrated in fig. 4.5):

1. The use of the needle guiding template which allows the needles to be driven on parallel trajectories in different areas of the prostate;
2. The use of a single entry port, created by a very small incision in the skin, situated on the median line of the body, driving the needles on concurrent trajectories.

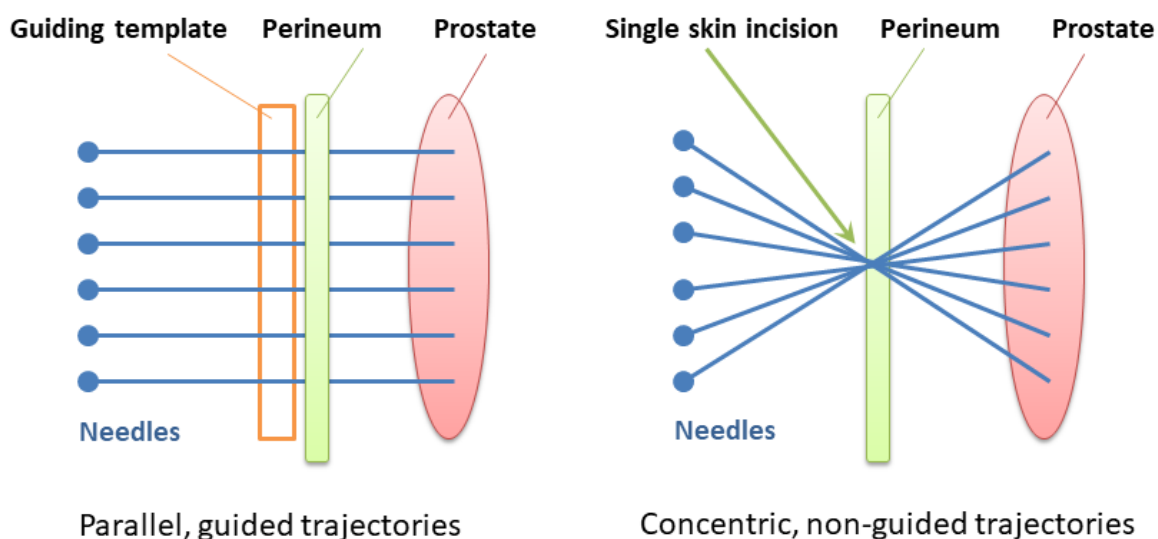


Figure 4.5. A schematic comparison between the two techniques

The **second approach is less invasive**, and even though it lacks a guiding tool for the needle, due to the lower tissue resistance it is **more accurate** and the **patient discomfort is greatly reduced**. This second technique is **more difficult** to be performed by a physician who drives the needles **manually**, by hand, but it **represents the best option for a robotic approach** where the needles are held steadily by the robot.

Transperineal prostate biopsy – a robotic task oriented application

Medical concept: *Using accurate 3D data (given as target coordinates) of the patient obtained through MRI investigations, the robot should manipulate independently the ultrasound probe and the biopsy gun, to ensure the targeted, accurate tissue prelevation from the designated locations with an error of maximum 1 mm.*

In the case of transperineal prostate, there are defined two independent access ports, the rectum for the ultrasound probe, and the incision in the perineum for the biopsy gun and for this reason a modular parallel structure with two independent kinematic chains each using its specific RCM (Remote Centre of Motion) is proposed and illustrated in fig.4.6.

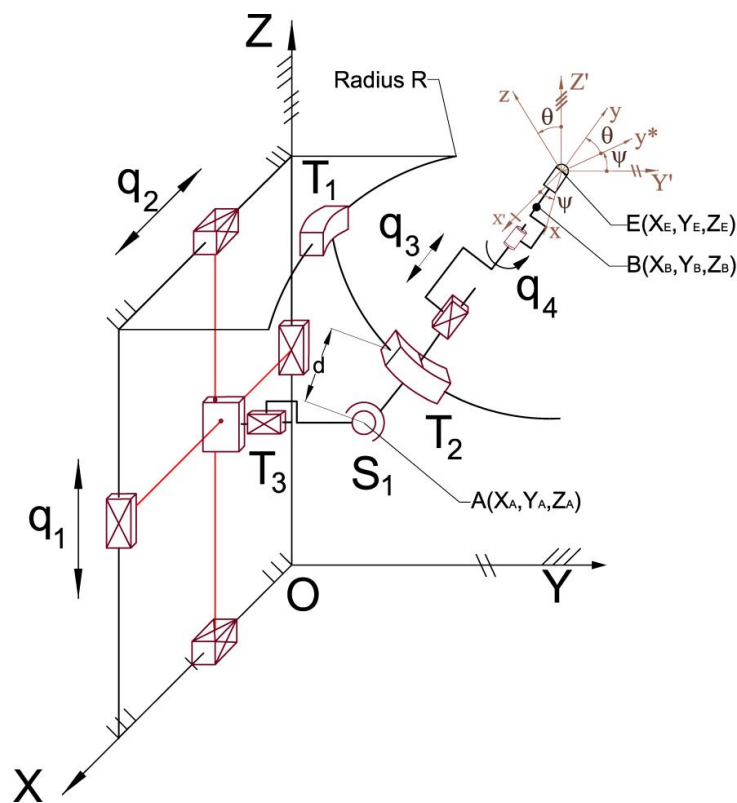


Figure 4.6. The kinematic scheme of one module of the PBS-BOT

The **first module** which is used for the manipulation of the ultrasound probe has **4 DOF** which with respect to the entry port are three rotations and a translation along the longitudinal axis of the probe. The **second module** which is dedicated for the guidance of the biopsy needle has only **3 DOF** (as the rotation of the needle around its longitudinal axes is not needed). Two coordinate systems are defined:

- OXYZ a fixed coordinate system with the three axes oriented along the axis of the human body (Z – vertical axis, X – lateral axis Y – longitudinal axis), positioned in such a way to ensure the motion of the first two active joints in the OXZ plane;

- A second, mobile coordinate system, $Exyz$, is attached to the tip of the end-effector, with the E_y axis coincident to the longitudinal axis of the medical device.

The kinematic scheme of one module of the PBS-BOT (fig. 4.6) consists of a 2-DOF translational parallel module with the active joints q_1 and q_2 which determine the position of the point **A** in a plane parallel with the OZX plane. Two passive translational joints **T1** and **T2** are moving along arcs with a common radius **R**, determining a sphere with the centre in the point **B**. The displacement of the two translational passive joints **T1** and **T2** is determined by the point **A**. Due to the fact that the two passive joints have a circular motion relative to the planar motion of the active joints q_1 and q_2 , a passive translational joint **T3** is introduced to compensate for the variation of the **Y** coordinate of the point **A**. As the orientation of the segment **d** varies with respect to the fixed coordinate system $OXYZ$, a spherical joint **S1** is used at the connection point. Thus, the active joints q_1 and q_2 will determine the motion of the segment **AE** along the radii of sphere of radius **R** ensuring the collinearity of the points **A**, **B** and **E** at all times, the point **B** representing the RCM of the robotic module. The third active joint, q_3 is a translational joint which generates a motion of the point **E** along the A-B-E line, which represents the **y** axis of the mobile system $Exyz$ attached to the end-effector (the ultrasound probe). The rotation of the end-effector around the E_y axis is achieved using the fourth active joint q_4 .

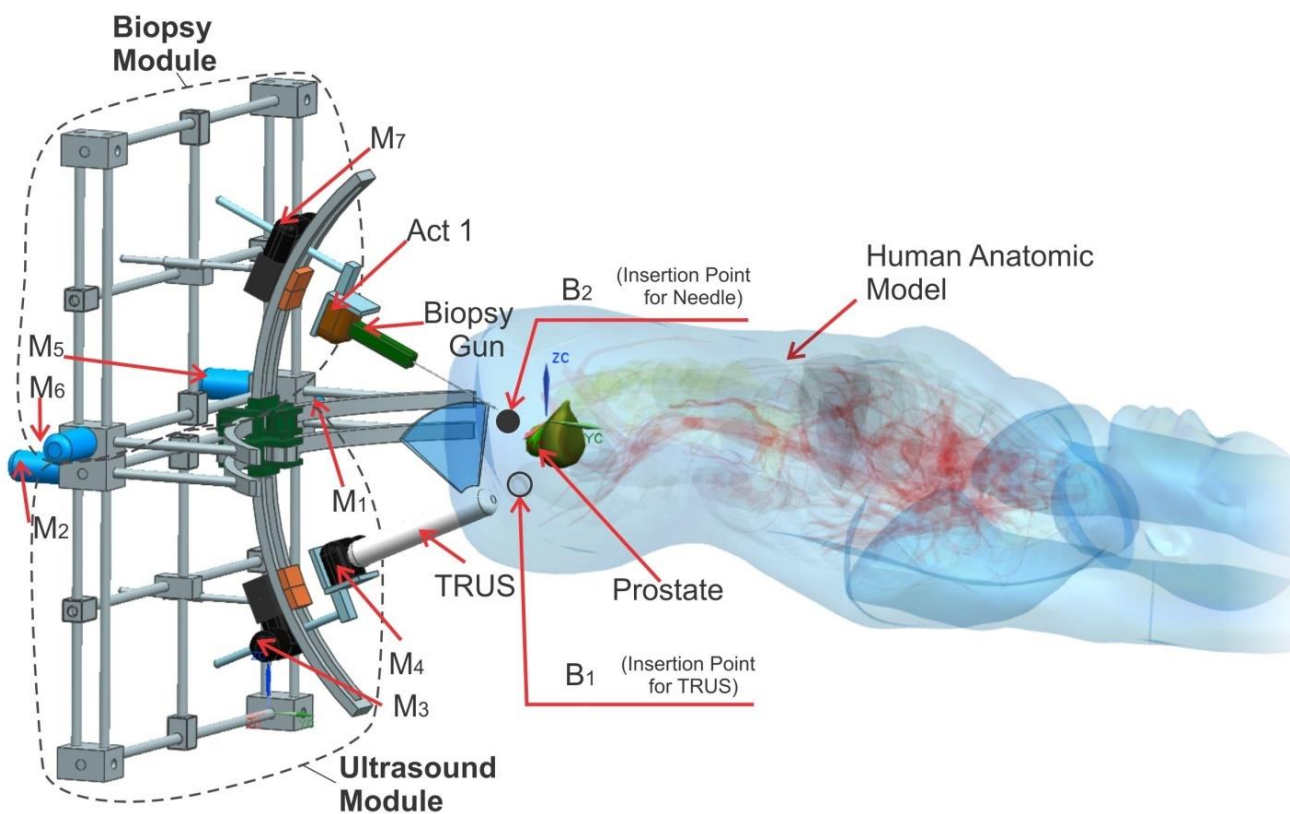


Figure 4.7. The virtual model of PBS-BOT with the human anatomical model

The second module used to guide the biopsy needle will be positioned on top of the first one, upside-down (mirrored) having the same kinematic scheme where the fourth active joint will be replaced by a simple actuation device which will trigger the biopsy gun. The use of passive circular prismatic joints will enable the construction of modules with different radii and the assembly/disassembly for sterilization will be faster and simpler.

A simplified virtual model of the robot, which illustrates the setup of the transperineal robotic system PBS-BOT, is illustrated in figure 4.7.

Structural analysis of the PBS-BOT

For the structural synthesis of the prostate biopsy robotic system the equation (3.20) introduced the previous chapter will be used.

The two modules which are used for the guiding of the ultrasound probe and the biopsy gun are mechanisms of family $F=0$. The first module, used for the guiding of the ultrasound probe, has the following inputs:

$$N = 6, C_5 = 5, C_4 = 1, C_3 = 1 \quad (4.1)$$

Using (4.1) in equation (3.20) the mobility degree of the ultrasound probe module is:

$$M_{up} = 6 \cdot N - 5 \cdot C_5 - 4 \cdot C_4 - 3 \cdot C_3 = 4 \quad (4.2)$$

The second module which does not have the rotation around the y mobile axis (the longitudinal axis of the needle) has one less mobile element and one less joint of class 5, leading to the following inputs:

$$N = 5, C_5 = 4, C_4 = 1, C_3 = 1 \quad (4.3)$$

The mobility degree of the biopsy gun guiding module is:

$$M_{bg} = 6 \cdot N - 5 \cdot C_5 - 4 \cdot C_4 - 3 \cdot C_3 = 3 \quad (4.4)$$

The geometric modelling of the PBS-BOT

Based on the constructive similarities between the modules, a single module will be analysed. A set of geometrical parameters are introduced in order to obtain a purely parametric kinematic model of the robot:

- The radius R of the arc which generates the RCM;

- The length **d** of the distance between the centre of the spherical joint **S1** and the translational joint **T2**;
- The coordinates of the point B (X_B, Y_B, Z_B) which represent the centre of the sphere on whose surface the joints **T1** and **T2** execute the motion;
- The length **l** of the insertion mechanism, when $q_3=0$.

Inverse geometrical modelling

The coordinates for the tip of the probe are defined by the vector:

$$X = [X_E \quad Y_E \quad Z_E \quad \phi_E]^T \quad (4.5)$$

All the geometrical parameters of the system are considered known. The mathematical model can be easily solved using the collinear property of the points A, B and E. Due to the fact that, with respect to the line AB the point E can be situated either between the two or beyond point B, a sign variable is introduced, when calculating the length of the segment EB.

$$ss = \text{sign}(Y_E - Y_B) \quad (4.6)$$

$$EB = ss \cdot \sqrt{(X_E - X_B)^2 + (Y_E - Y_B)^2 + (Z_E - Z_B)^2} \quad (4.7)$$

With the length of **EB** known, the joint q_3 can be determined:

$$q_3 = R - l + EB \quad (4.8)$$

With the coordinates of the points E and B known, the angles ψ and θ which define the orientation of the robot end-effector corresponding to the fixed coordinate system OXYZ can be calculated as follows:

$$\psi = \text{atan2}(X_E - X_B, Y_E - Y_B) \quad (4.9)$$

$$\theta = \text{atan2}\left(Z_E - Z_B, ss \cdot \sqrt{(X_E - X_B)^2 + (Y_E - Y_B)^2}\right) \quad (4.10)$$

Using the value of q_3 the distance between the points A and E can be calculated:

$$AE = 1 + q_3 + d \quad (4.11)$$

Using (4.9 ÷ 4.11) the coordinates of point A are:

$$\begin{cases} X_A = X_E - AE \cdot \sin(\psi) \cdot \cos(\theta) \\ Y_A = Y_E - AE \cdot \cos(\psi) \cdot \cos(\theta) \\ Z_A = Z_E - ss \cdot AE \cdot \sin(\theta) \end{cases} \quad (4.12)$$

From this point on, the values of the coordinates can be easily validated by comparison of the computed distance between points A and B in two ways:

$$AB_{(1)} = R + d \quad (4.13)$$

$$AB_{(2)} = \sqrt{(X_A - X_B)^2 + (Y_A - Y_B)^2 + (Z_A - Z_B)^2} \quad (4.14)$$

Knowing the coordinates of point A it is possible to define the active joints q_1 and q_2 .

$$\begin{cases} q_1 = Z_A \\ q_2 = X_A \end{cases} \quad (4.15)$$

The rotation of the end-effector is an independent motion which is described by:

$$q_4 = \psi \quad (4.16)$$

Direct geometrical modelling

For this approach, the coordinates of the active joints are considered known:

$$Q = [q_1 \quad q_2 \quad q_3 \quad q_4]^T \quad (4.17)$$

Using the values of the active joints and the property of points moving on a sphere, the coordinates of points A can be calculated as follows:

$$\begin{cases} X_A = q_2 \\ Y_A = Y_B - \sqrt{AB^2 - (Z_B - Z_A)^2 - (X_B - X_A)^2} \\ Z_A = q_1 \end{cases} \quad (4.18)$$

Where the length of the segment \overline{AB} is determined using the equation (4.8).

Considering the fact that the orientation of the coordinate system has to be defined using the points A and B and point E has two possible configurations on the AB line, the following conditional parameters are introduced:

$$\begin{aligned}
& \text{If } q_3+1 < R \\
& sn = \pi \text{ and } ss2 = -1 \\
& \quad \text{Else} \\
& \quad sn = 0 \text{ and } ss2 = 1 \\
& \quad \text{End}
\end{aligned} \tag{4.19}$$

The equations for the angles ψ and θ are:

$$\psi = sn + \text{atan2}(X_B - X_A, Y_B - Y_A) \tag{4.20}$$

$$\theta = \text{atan2}\left(Z_B - Z_A, \sqrt{(X_A - X_B)^2 + (Y_A - Y_B)^2}\right) - sn \tag{4.21}$$

The length of the segment AE can be easily determined geometrically using eq. (4.12), and with (4.20) and (4.21) the coordinates of the point E can be calculated as follows:

$$\begin{cases}
X_E = X_A + AE \cdot \sin(\psi) \cdot \cos(\theta) \\
Y_E = Y_A + AE \cdot \cos(\psi) \cdot \cos(\theta) \\
Z_E = Z_A + ss \cdot AE \cdot \sin(\theta)
\end{cases} \tag{4.22}$$

The rotation of the end-effector is an independent motion resulting that:

$$\psi = q_4 \tag{4.23}$$

At this point, the geometrical model of the robot is completed with all the equations depending on only three parameters: \mathbf{R} , \mathbf{d} and \mathbf{l} .

The kinematic modelling of the PBS-BOT

Using the equations from the geometrical models the implicit functions are determined in order to calculate the Jacobi matrices:

$$\begin{aligned}
f_1 &= q_1 - Z_E + (1 + q_3 + d) \cdot \frac{(Z_B - q_1)}{AB} \\
f_2 &= q_2 - X_E + (1 + q_3 + d) \cdot \frac{(X_B - q_2)}{AB} \\
f_3 &= q_3 - R + 1 - ss \cdot \sqrt{(X_E - X_B)^2 + (Y_E - Y_B)^2 + (Z_E - Z_B)^2} \\
f_4 &= q_4 - \psi
\end{aligned} \tag{4.24}$$

The following notation is introduced:

$$u = \sqrt{(X_E - X_B)^2 + (Y_E - Y_B)^2 + (Z_E - Z_B)^2} \quad (4.25)$$

Knowing that the Jacobi matrices represent the partial derivatives of the implicit functions with respect to the end-effector coordinates (matrix A) and active joints (matrix B) [MER06], their explicit form is:

$$A = \begin{vmatrix} 0 & 0 & -1 & 0 \\ -1 & 0 & 0 & 0 \\ ss \frac{(X_E - X_B)}{u} & ss \frac{(Y_E - Y_B)}{u} & ss \frac{(Z_E - Z_B)}{u} & 0 \\ 0 & 0 & 0 & -1 \end{vmatrix} \quad (4.26)$$

Respectively,

$$B = \begin{vmatrix} 1 - \frac{(l + q_3 + d)}{AB} & 0 & \frac{Z_B - q_1}{AB} & 0 \\ 0 & 1 - \frac{(l + q_3 + d)}{AB} & \frac{X_B - q_2}{AB} & 0 \\ 0 & 0 & 1 & 0 \\ 0 & 0 & 0 & 1 \end{vmatrix} \quad (4.27)$$

Singularities analysis

Based on the equations (4.26 and 4.27), the determinants of matrices A and B can be determined in an analytical form:

$$\det(A) = \frac{ss \cdot (Y_B - Y_E)}{u^3} \quad (4.28)$$

And respectively:

$$\det(B) = \frac{(d - AB + l + q_3)^2}{AB^2} \quad (4.29)$$

These two determinants share a common geometric condition when they vanish, which is described in the following three equations below:

$$\begin{aligned}
Y_B &\equiv Y_E \\
u &\equiv \overline{EB} = 0 \\
d + l + q_3 &= \overline{AB} \Rightarrow l + q_3 = R
\end{aligned} \tag{4.30}$$

The common condition described by the three relations in eq. (4.30) corresponds to the case when the end-effector tip (the point E) is located in the centre of the sphere, namely superposed over point B. In this case, the tip of the end-effector will remain fixed for any motion at the level of the active joints q_1 and q_2 . It has to be underlined that “*theoretically*” the robot loses in this point two degrees of freedom, but by actuating the joint q_3 the end-effector will be moved without any problems. In fact, this situation represents an advantage because, when the robot reaches the access port in the body, for both the ultrasound probe and the needle of the biopsy gun, the tool can be oriented freely, ensuring its positioning, before the insertion, in the best orientation without any danger for the patient. Based on the above it can be concluded that **the robot works in a singularity free configuration**, ensuring maximum safety during the entire medical procedure.

The kinematic modelling of the PBS-BOT for speed and accelerations

For solving the kinematic model at the level of speeds and accelerations, the following vectors are defined:

$$\dot{X} = [\dot{X}_E \quad \dot{Y}_E \quad \dot{Z}_E \quad \dot{\phi}_E]^T \tag{4.31}$$

$$\ddot{X} = [\ddot{X}_E \quad \ddot{Y}_E \quad \ddot{Z}_E \quad \ddot{\phi}_E]^T \tag{4.32}$$

$$\dot{Q} = [\dot{q}_1 \quad \dot{q}_2 \quad \dot{q}_3 \quad \dot{q}_4]^T \tag{4.33}$$

$$\ddot{Q} = [\ddot{q}_1 \quad \ddot{q}_2 \quad \ddot{q}_3 \quad \ddot{q}_4]^T \tag{4.34}$$

With the help of the Jacobi matrices between the velocity vectors \dot{X} and \dot{Q} , the well-known equation [MER06] can be written:

$$A \cdot \dot{X} + B \cdot \dot{Q} = 0 \tag{4.35}$$

The equation which characterizes the accelerations is:

$$A \cdot \ddot{X} + \dot{A} \cdot \dot{X} + B \cdot \ddot{Q} + \dot{B} \cdot \dot{Q} = 0 \tag{4.36}$$

The solving of inverse and direct kinematic models with unique, analytical equations will enable their future implementation in real-time control architecture for an optimized motion control.

Workspace modelling of the PBS-BOT

For the correct definition of the geometrical parameters of the PBS-BOT, workspace modelling in correspondence to the application at hand and a study of the robots accuracy is demanded.

For the precision mapping a relative coefficient between displacements of one unit at the level of the active joint and its corresponding motion at the level of the end-effector will be calculated.

For the prostate biopsy medical task, for both robot modules, the following conditions apply [YAC12]:

- the ultrasound probe can be inserted up to 150 mm inside the patient rectum;
- the prostate maximum size does not exceed the size of a sphere with a radius of 40-60 mm;
- the biopsy gun has to avoid the penetration of the urethra (fig. 4.4) where a cone with the opening angle of 5° is defined as a “no access zone”.

Considering the similarity in structures, figure 4.8 illustrates the workspace of one module, the other having the same workspace.

Figure 4.9 presents a cross-section through the workspace of the biopsy gun module, in a parallel plane with YOZ at the $X = 180$ mm, to emphasize the avoidance of the urethra using the safety cone required by the physicians, condition applied for the biopsy gun module only.

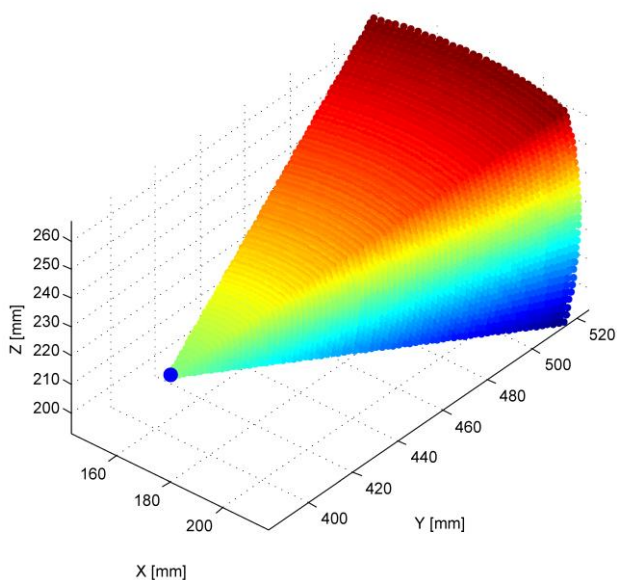


Figure 4.8. The workspace of one module of the PBS-BOT

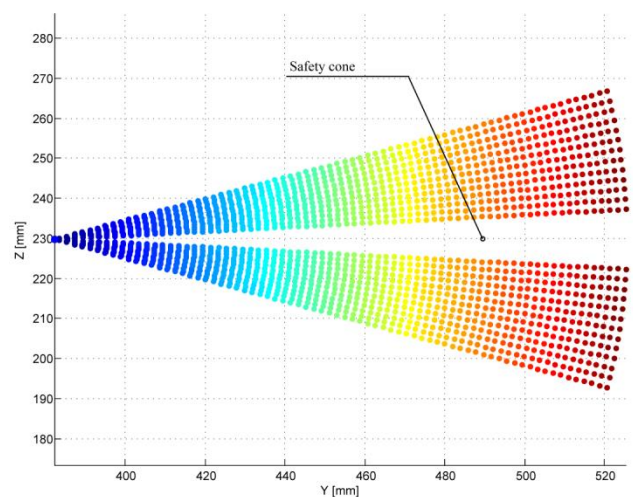


Figure 4.9. Cross-section in the workspace of the biopsy gun guiding module of the PBS-BOT

Precision Evaluation

An important requirement for any medical device used in an invasive way refers to its secure utilization and the motion accuracy becomes one of the most important features correlated with safety. For the workspace modelling the points were generated using constant increments for the advance of the point **E** for the orientation of the instrument and the translation along its longitudinal axis.

Using the data obtained during the workspace modelling a comparison between the motions of point **E** (the TCP of the medical tool) and the point **A** which is responsible for the orientation of the instruments inside the patient body, has been achieved. Knowing that the point **E** has a constant increment the ratio between two consecutive positions of the point **E** and the corresponding values of the point **A** can be calculated. Considering the motion of point **E** as a unit motion the ratio will show the corresponding motion at the level of point **A**. Figure 4.10 illustrates the simulation results, for the following parameters: $R=300$ mm, $d=32$ mm, $l=195$ mm.

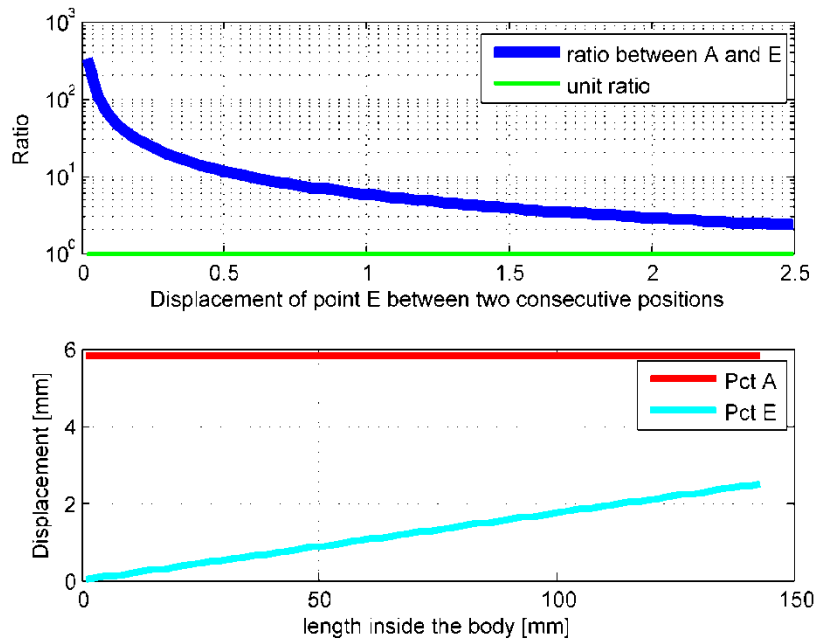


Figure 4.10. Relative motion of the points A and E within the robot workspace

The first graph illustrates the ratio between the motions of points **A** and **E** with respect to the depth of the instrument inside the human body. As the motion takes place around a fixed point (**B**) in its vicinity the ratio is clearly higher but the most important aspect is that at maximum depth is larger than **2.3** which mean that the point **E** can be accurately controlled (for a unit displacement of point E one would need 2.3 units of displacement for the point A).

The second graph represents the distance between two consecutive positions of points **A** and **E** with respect to instrument depth inside the body. It can be seen that point **A** has a **linear variation** independent with respect to the depth of the instrument, which shows that, for a given depth **the motion accuracy does not vary**

with the orientation of the instrument, meaning that for **a given depth** the robot **accuracy is the same for any orientation**.

This data is very useful for the dimensioning of the components and the selection of actuators for the experimental model in order to achieve the required precision imposed by the medical task.

The kinematic simulation of the PBS-BOT

The kinematic simulation of the PBS-BOT will be achieved according to the medical task, namely the transperineal prostate biopsy the two modules having different behaviours:

- The module guiding the ultrasound probe allows the positioning and orientation of the instrument, outside and inside the body (within specific limits) to enable the proper visualization of the prostate;
- the module guiding the biopsy gun have a motion split into two separate stages: having the current pose of the robot and target point inside the prostate, the algorithm calculates the final required needle orientation and will achieve it prior to the needle insertion, which represents the second motion stage, performed always on a linear trajectory inside the patient body.

For the determination of the needle final orientation, and the required motion at the level of the robot active joints the following parameters are given: the coordinates of the current position of the instrument tip denoted with C (X_C, Y_C, Z_C) and the coordinates of the target point, T(X_T, Y_T, Z_T).

Knowing the coordinates of the point B (X_B, Y_B, Z_B) the initial and final orientation of the robot can be modelled using the equations:

$$\psi_i = \pi + \text{atan2}(X_B - X_A, Y_B - Y_A) \quad (4.37)$$

$$\theta_i = \text{atan2}\left(Z_B - Z_A, \sqrt{(X_A - X_B)^2 + (Y_A - Y_B)^2}\right) - \pi \quad (4.38)$$

Respectively:

$$\psi_f = \text{atan2}(X_B - X_A, Y_B - Y_A) \quad (4.39)$$

$$\theta_f = \text{atan2}\left(Z_B - Z_A, \sqrt{(X_A - X_B)^2 + (Y_A - Y_B)^2}\right) \quad (4.40)$$

The numerical parameters for the kinematic simulation of the PBS-BOT are:

$$R = 300\text{mm}, d = 32\text{mm}, l = 195\text{mm} \quad (4.41)$$

- A real case scenario was defined for the biopsy gun robot module motion as follows:
- ✓ The robot has a current arbitrary position (point C) known with respect to a fixed coordinates system;
 - ✓ The robot will receive a set of coordinates for the target point inside the patient (point T);
 - ✓ The robot motion is decomposed into two parts: in the first, the robot will move from its current location to the insertion point, achieving, in the same time the final orientation for the needle (ψ_f and θ_f); in the second motion stage, the robot will drive the biopsy gun, along a linear path to the target point.

The maximum values for the speeds and accelerations for both motion stages are: $v = 10 \text{ mm/s}, a = 5 \text{ mm/s}^2$.

A numerical example is presented, for the following set of points:

$$\begin{aligned}
 X_C &= 210 \text{ mm}, Y_C = 300 \text{ mm}, Z_C = 240 \text{ mm} \\
 X_B &= 180 \text{ mm}, Y_B = 382.5 \text{ mm}, Z_B = 229.74 \text{ mm} \\
 X_T &= 220 \text{ mm}, Y_T = 450 \text{ mm}, Z_T = 250 \text{ mm}
 \end{aligned}
 \tag{4.42}$$

Figures 4.11 and 4.12 present the time history diagrams for the variation of coordinates, speeds and accelerations at the level of the needle tip (point E) respectively at the level of the active coordinates. In figure 9, the sudden change in the angle values for ψ and θ corresponds to the reach of the point B when the angles change value with π .

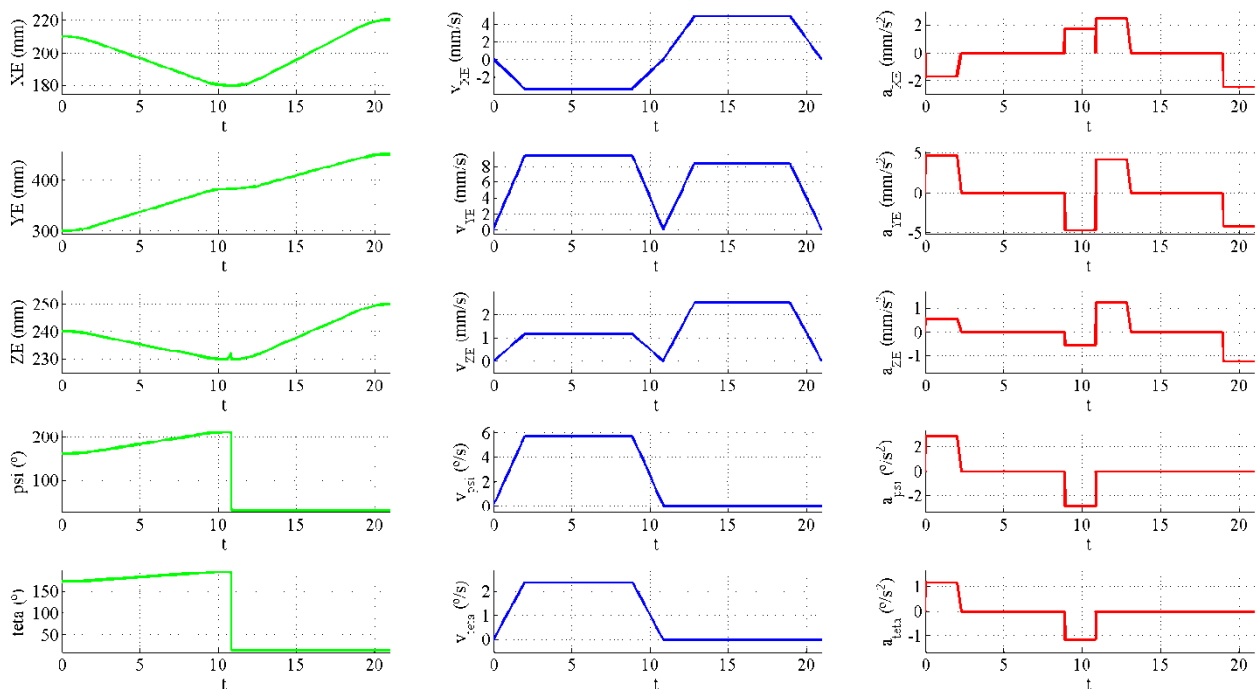


Figure 4.11 Time history diagrams for the displacement, velocity and acceleration of the instrument tip (point E)

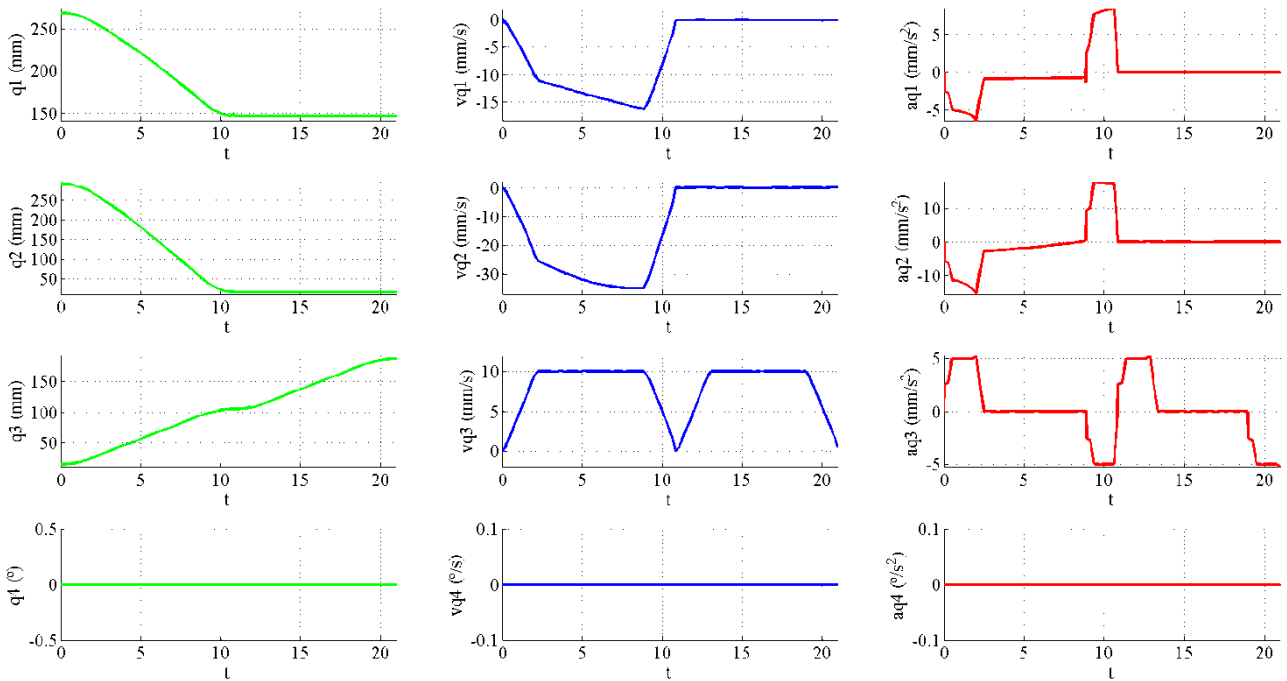


Figure 4.12 Time history diagrams for the displacement, velocity and acceleration of the robot active joints

As there is a general opinion shared by medical experts which favours whenever possible (based on the availability of the medical infrastructure) the transperineal approach, the use of either one of the transperineal approaches is not definitely decided. As it will be shown later in this chapter, an experimental study done for the measurement of the tissue reaction forces gives the motivation for favouring the single incision approach which is the technique used in the European Institute of Oncology in Milano, Italy and also by the medical experts within the Cluj-Napoca Municipal Hospital.

While an experimental model of the PBS-BOT was not build the virtual simulations give confidence that the solution is a solid option for the development of a robotic device dedicated for transperineal prostate biopsy.

A Needle Insertion Module for Robotic Assisted Transperineal Prostate Biopsy

Before introducing the design of module dedicated for operating the biopsy gun which can be used in a robotic assisted prostate biopsy, the medical protocol for such a procedure has to be defined. For transperineal prostate biopsy a 6 stepwise procedure has been proposed, considering that the robotic system used has the capability of manipulating both the biopsy gun and the TRUS probe:

Step	TRUS Module	Biopsy gun Module
1.	The module is initialised, moved into home position and calibrated with respect to the patient.	The module is initialised and moved into home position and calibrated with respect to the patient.
2.	The TRUS probe is inserted through the patient rectum and adjusted to provide proper US view of the prostate.	The robot will position the needle from the home position to a predefined position based on a pair of predefined Insertion and Target points.
3.	The US probe is adjusted to acquire the needle on its trajectory to the target point.	The needle is inserted through the perineum tissue, on a linear trajectory, into the prostate gland until the target point is reached.
4.	A final position check for the needle is performed.	The biopsy gun is fired leading to a quick actuation of the stylet (a) followed by quick actuation of the cannula (b) in order to capture the target tissue inside the needle.
5.	The US probe is kept in place.	The needle is retracted from the patient following the exact same trajectory it used for the insertion and then moved to home position.
	The US probe is kept in place.	The sample tissue is unloaded and, if necessary the gun is reloaded and placed back in the module.
	For each following required sample steps from 3 to 5 are performed for the TRUS module and steps from 2 to 5 for the Biopsy Gun module.	
6.	The US probe is retracted and the module is moved to the home position.	The module is retracted into the home position.

As the biopsy gun was mentioned several times figure 4.13 illustrate the specific instrument that was used in the module design.

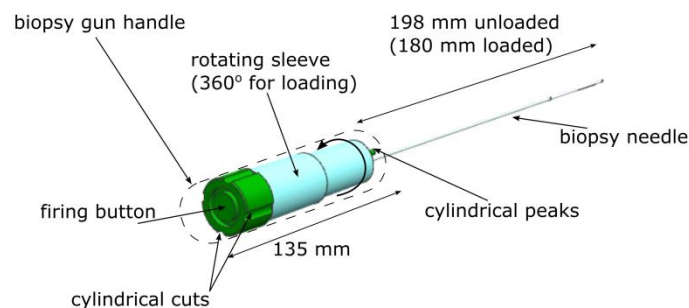


Figure 4.13. CAD illustration of the biopsy gun with geometric details

It is a BARD Monopty 22mm biopsy gun (Fig. 4.13), which contains a biopsy needle with the back side encapsulated into a plastic handle with a rotating sleeve that is used to load the gun, and a circular button behind the handle to fire the biopsy gun. The gun loading procedure is done in a sequence having two steps: by rotating the sleeve counter-clockwise about 180° the needle cannula gets retracted by about 18 mm, and next, by rotating the sleeve counter-clockwise another 180° the stylet is retracted again by 18 mm. The gun loading sequence is performed manually by the clinician, having no effect on the accuracy of the procedure, as after the biopsy gun is loaded it will be mounted in the guiding module in a fixed position. The first step of the loading sequence is used also to remove the biopsy tissue after prelevation. The internal stylet has an opening where the sample tissue is stored after the gun firing. The unloaded gun, the first loading sequence detail of the tip and the loaded gun are shown in the next figure.

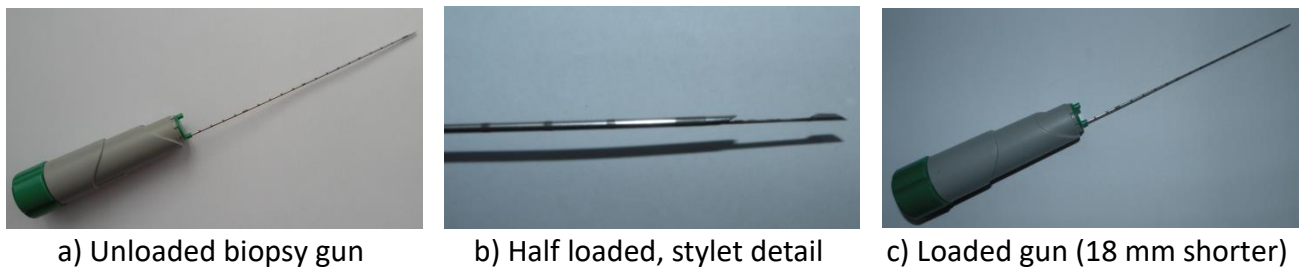


Figure 4.14. Details of the loading sequence of the BARD Monopty 22mm

A stepwise illustration of the biopsy gun behaviour during the procedure is illustrated in figure 4.15 following closely the sequence presented before.

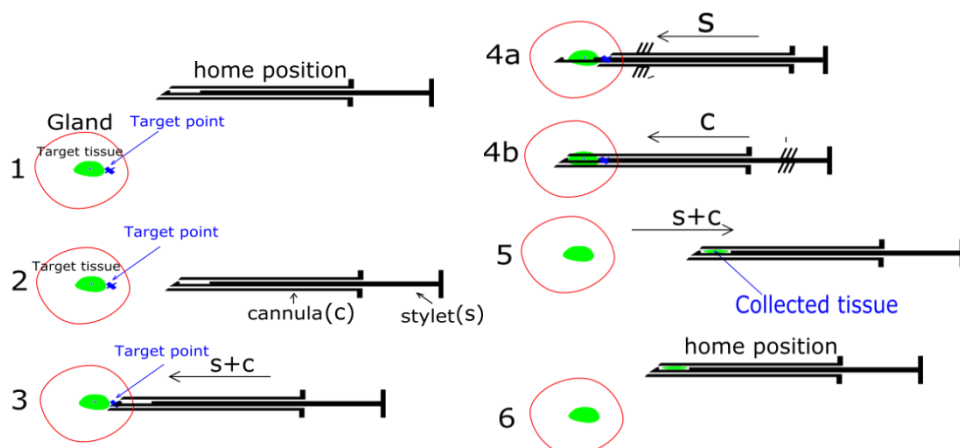


Figure 4.15. The prostate biopsy protocol with focus on the biopsy gun

The module should have the following characteristics:

1. **Efficient robot connection.** The module has to be attached to a robotic system that would perform the positioning of the module+needle assembly with the needle tip in the Insertion point and aligned on the predefined linear trajectory.

2. **Fast and reliable biopsy gun attachment.** Even in the case of a transperineal biopsy there will be multiple cores harvested from the prostate. Thus, during the procedure, after each sampling the doctor needs to detach the gun, remove the sample tissue and then reattach the gun in the module. This must be done without any misalignments between the attachments.

3. **Needle deflection avoidance.** The biopsy gun needle is almost 200 mm long and a diameter of 1.7 mm, which makes it very easy to bend in contact with an obstacle. Thus a supplementary guiding element will be used as a stiffness element close to its tip. This element, along with all the other that come into contact with the needle itself, must be either sterilisable or for single use so it has to be detachable.

4. **Total length/retraction parametrization.** In the control program the total length and retraction (when the biopsy gun is loaded) must be parametrized as the insertion has to be made in such a way that when fired the target point to reach the clearance on the stylet (which would ensure that the right tissue has been sampled).

Based on the above, the biopsy gun module has three main components, namely: a platform that is linked with the robot, a mobile (relative to the fixed platform) support that holds the biopsy gun, and a needle tip holder. The robot connection module will be achieved in two points in such a way to enable the direct mounting on either PARA-BRACHYROB (presented in chapter 3) or on another device developed in CESTER, BIO-PROS1 [TUC 18], which is a robot with two independent modules, designed especially for transperineal prostate biopsy.

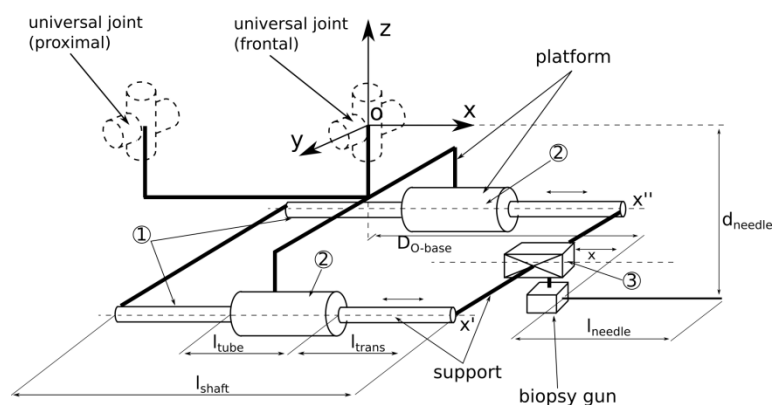


Figure 4.16. Conceptual scheme of the needle insertion module

The linkage between the fixed platform and the biopsy gun support is described in Fig. 4.16. The Cartesian coordinate system is fixed on the platform of the module into a point desired for the connection with the robot (this will make it easy to correlate the needle insertion module to the robot coordinate system). Therefore the centre of the module coordinate system will be superposed over the centre of the universal joint from the frontal part of the end effector (for the biopsy needle). The needle longitudinal axis is parallel to the OX axis and lies in the XOZ plane at distance d_{needle} . The linkage between the platform and the mobile support is created via two parallel passive cylindrical joints (using the shaft (1) from the support and

the bushings (2) from the platform). This will ensure the translation motion that will insert the needle on the linear trajectory inside the patient body.

The shaft length (l_{shaft}) and the tube length (l_{tube}) permit a total translation (l_{trans}) of the support (and needle):

$$0 \leq |l_{trans}| \leq l_{shaft} - l_{tube} \quad (4.43)$$

As the shafts slide through the bushings l_{trans} varies, i.e. if the shafts are translated along X' and X'' axes (parallel to OX) allowing the motion in both directions, i.e. the insertion and retraction of the needle.

The needle tip has the coordinates:

$$\begin{pmatrix} x_{nt} \\ y_{nt} \\ z_{nt} \end{pmatrix} = \begin{pmatrix} x_{nt} \\ 0 \\ d_{needle} \end{pmatrix} \quad (4.44)$$

Where x_{nt} can be determined as following:

$$x_{nt} = l_{needle} + l_{trans} + d_{st} \quad (4.45)$$

Where d_{st} is the distance in along the X axis from the origin O and the proximal part of the needle when translation is minimum (i.e .zero in our case) and it can be computed from:

$$d_{st} = d_{O-base} - l_{trans} \quad (4.46)$$

Where $d_{O-nbase}$ represents the distance (X coordinate) from O to the needle base (the proximal part). Finally, the needle tip coordinates are obtained:

$$\begin{pmatrix} x_{nt} \\ y_{nt} \\ z_{nt} \end{pmatrix} = \begin{pmatrix} l_{needle} + l_{trans} + d_{st} \\ 0 \\ d_{needle} \end{pmatrix} \quad (4.47)$$

The linear motion is obtained through the active prismatic joint (3) which is actuated along the X_t axis (parallel to OX) using a screw/nut mechanism.

The CAD design of the needle insertion module and its components, developed in Siemens NX, are presented in Fig. 4.17. The biopsy gun support has a fixed part (4) and a revolving part (5) (around R axis parallel to OX) to allow an open/close sequence to place and fix the biopsy gun. The biopsy gun is placed into the mobile part (5) of the support and then the support is closed by pushing it up against the fixed part (4) and locking the two parts together via a screw mechanism (6). The biopsy gun handle has a design with four cylindrical partially cut in the back side and

two cylindrical peaks in the front side (a negative mark of the external shape of the biopsy gun handle). The support design takes advantage of these geometric features, and with a back cover (7), it ensures a reliable fixed position of the pistol when the support is closed¹. On the left and right side of the support there are cylindrical shafts (1), which create cylindrical joints with the fixed platform. On the top there is a platform (8) (parallel to XOZ plane) with a carving in which a ball nut (3) is fixed to create the translation mechanism. The firing mechanism is simply a spindle drive (9) fixed into a support (10) placed and fixed behind the back cover (7) of the fixed support part (4).

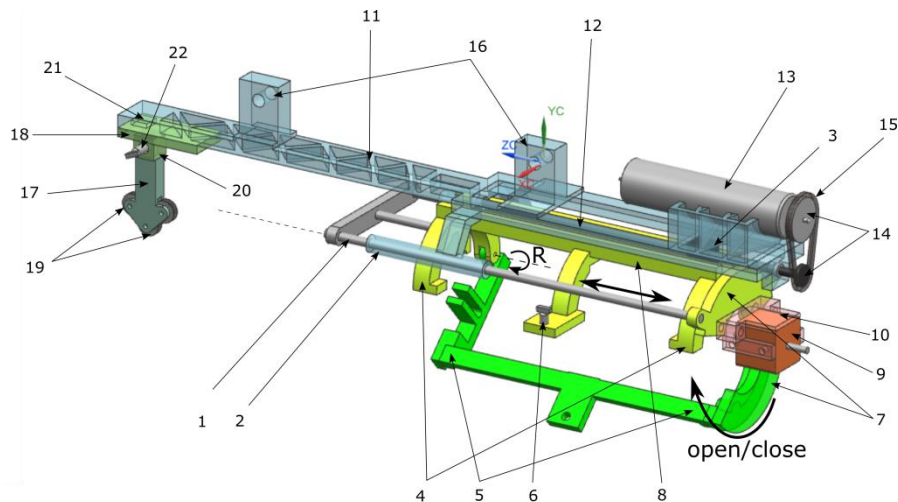


Figure 4.17. CAD design of the needle insertion module with its highlighted components.

The platform (11) (lying on a plane parallel to OXZ) is connected with the pistol support via two bushing (2) which in combination with the cylindrical shafts (1) from the support creates two parallel cylindrical joints. The translation motion of the support relative to the fixed platform is achieved with a rotating ball screw (12) (connected with the nut (3)) actuated by the motor (13) through a gear mechanism with two cogwheels (14) and a timing belt (15). Two mounting blocks (16) are fixed to the platform, in the same plane, to enable the connection between the needle insertion module and the robot.

The needle tip holder (17) is connected in the frontal part of the fixed platform (11) using a sliding sledge with springs (18). The needle tip holder has a mechanism designed with three grooved wheels (19) with spinning axes parallel with OY. The sledge purpose is to allow the motion of the holder along an axis parallel to the needle axis, motion that is needed when the clinician mounts the gun into the support. I.e. the holder must be moved away from the gun when the pistol is being mounted, and moved back after the support is closed so the needle goes through the holder. The holder is removable from the sledge for sterilization related issues (or it can be made out of plastic for single-use). The holder (17) is fixed into its plug

¹ This design is valid only for the Bard biopsy gun. Such an adaptation has to be achieved individually for each type/size of gun used.

(20) using either a magnet or a compression spring (21) for exact positioning and a screw (22) for stiffness. The needle holder is fixed relative to the insertion point, and the biopsy needle slides through it in the insertion stage. The wheels mechanism reduces friction in comparison with a fixed needle holding mechanism, which helps especially on the pistol firing stage when the needle instantaneous acceleration is high. The space between the wheels is 1.7 mm i.e. the mechanism is designed for the standard 1.7 mm diameter biopsy needles found within the Monopty 22mm biopsy gun².

For a needle insertion correlated with the clinical specifications presented in section 2, the length of the cylindrical shafts is chosen to be 175 mm while the length of the cylindrical counterparts from the platform is 60 mm. This offers a total of 115 mm translation of the needle tip, which allows certain flexibility in determining the needle distance relative to the insertion point, and allows the reach of the target point from various needle positions and orientations.

The total mass of the needle insertion module is:

$$m_{\text{module}} = m_{\text{fix}} + m_{\text{move}} \quad (4.48)$$

Where m_{fix} is the mass of the parts that are not actuated by the modules motor (platform, needle holder, motor), and m_{move} is the mas of the motor actuated parts (support, biopsy gun, firing mechanism).

The formula needed to calculate the thrust generated when torque is applied is:

$$F_a = \frac{2\pi \cdot \eta_1 \cdot T}{Ph} \quad (4.49)$$

With:

$F_a =$	Thrust generated by the torque (N);
$Ph =$	Feed screw lead (mm);
$\eta_1 =$	Positive efficiency of the feed screw (%);
$T =$	Driving torque (Nmm).

F_a can be viewed as the frictional resistance on the guided surface (i.e. friction inside the cylindrical joints of the module):

$$F_a = \mu \cdot m_{\text{move}} \cdot g \quad (4.50)$$

Assuming perfect surface contact in the cylindrical joints, and taking into account the tissue resistance on needle insertion, using Eq. (4.49) the net thrust when torque is applied is defined as:

² For other needle diameters the wheels have to be changed in order to ensure an efficient guiding contact.

$$F_{total} = F_a + F_{tissue} \quad (4.51)$$

Where F_{tissue} = tissue resistance.

The torque needed to maintain a linear motion (constant velocity) of the biopsy gun in the insertion stage is:

$$T = F_{total} \cdot \frac{Ph}{2\pi \cdot \eta_1} \quad (4.52)$$

The torque needed to accelerate the needle has to be computed by accounting all the moments of inertia of the rotating parts:

$$T_{acc} = J \cdot \dot{\omega} \quad (4.53)$$

Where:

J – total moment of inertia ($\text{kg} \cdot \text{m}^2$)

$\dot{\omega}$ – angular acceleration ($\text{rad} \cdot \text{sec}^{-2}$)

The total moment of inertia is calculated from:

$$J = m_{move} \cdot \left(\frac{P}{2 \cdot \pi} \right)^2 + J_s + J_a + J_b \quad (4.54)$$

Where:

J_s – moment of inertia of the screw

J_a – moment of inertia of the gear attached to the screw

J_b – moment of inertia of the gear attached to the motor shaft

$$J_a = J_b = m_{pul} \cdot d^2 \cdot \frac{1}{8} \quad (4.55)$$

Where:

m_{cog} – mass of the pulleys from the gear (10 grams)

d – outer diameter of the pulleys (15 mm)

The angular acceleration can be calculated from:

$$\dot{\omega} = \frac{d(2 \cdot \pi \cdot N)}{dt} \quad (4.56)$$

With:

N – number of rotations per sec.

A very important aspect related to the overall module design and the accuracy of the procedure is the analysis of the needle behaviour when inserted through the different layers of tissue up to the target point. A special attention will be given to the skin penetration which is a very tough and elastic layer of tissue.

As the literature data is somewhat inconclusive regarding the resistance forces for needle insertion techniques and the different surveys [JIA14, YAN18] report many approaches but inconstant values, an experimental setup has been created to measure the tissue resistance forces for the specific needles that are used for the

minimally invasive non-surgical techniques, in a configuration as close as possible to a real case scenario. An important aspect that has been overlooked by many scientists is the effect of the neighbouring tissues, thus a setup where a small piece of tissue is used can lead to false information as its behaviour can be totally different when the overall forces are distributed over a large volume.

Thus, for the experimental tissue an ex vivo large pork leg with all the internal structures intact has been used as a test sample (figure 4.18). The needle was inserted into the tissue using the ZWICK/ROEL testing equipment (basically a calibrated press with force sensors in the moving head, which can perform motions on the vertical axis with different velocities setups) while the reactive force was continuously registered. The results obtained from 5 experimental trials, as well as the mean of those trials are presented in Fig. 4.19 for biopsy needle insertion, with and without skin incision. The point of insertion was carefully selected not to be closer than 5 mm than the previous insertion point to avoid following a needle path that was already used, therefore measuring lower forces since the tissue was already penetrated. However with this approach it is easy to observe the variations in the force curve since the needle, most likely, penetrated through different tissue (fat, muscle etc.) for every experimental trial. The velocity during needle insertion was 10 mm/sec and the force was registered for 8 sec. This leaves a variable interval of depth length of about 70 mm. As illustrated in Fig. 4.19, the resulted tissue resistance to needle insertion was in less than 10 N.

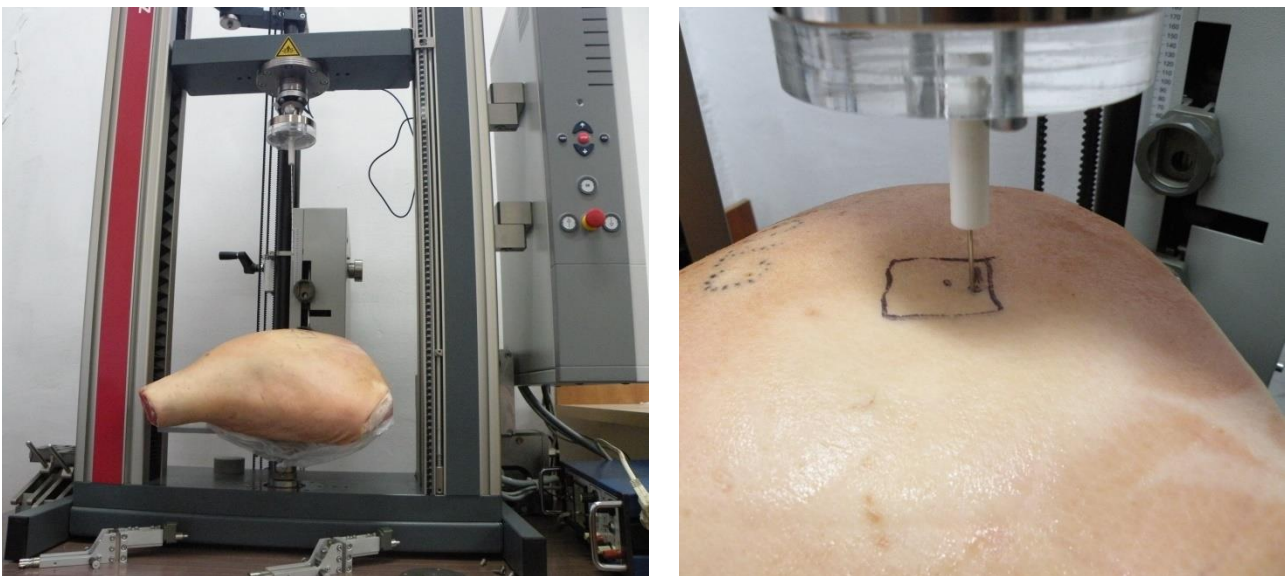


Figure 4.18. Tissue resistance on needle insertion experimental setup. Overview on the left; close view on right.

The experimental results validated also a medical variation of the transperineal procedure performed by specialists from the European Institute of Oncology, Italy, which perform a small incision in the perineum skin and insert the needle in a cone shape through a single port, rather than using parallel trajectories, as presented also in the first part of this chapter (see figure 4.5) [COB15].

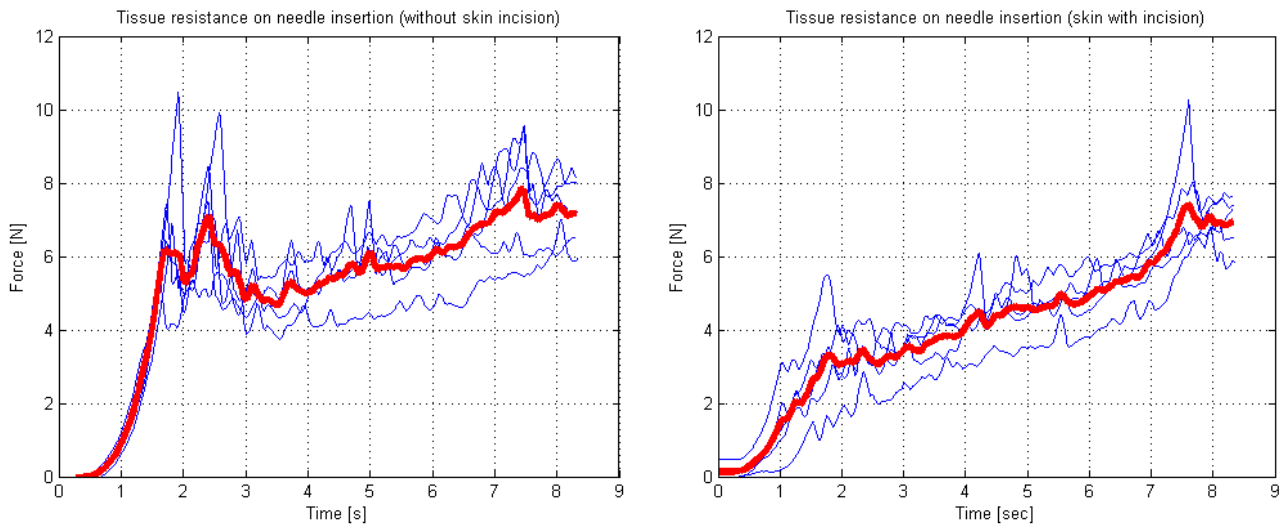


Figure 4.19 Reported tissue resistance for needle insertion using ex vivo animal tissue without skin incision (on the left) and with skin incision (on the right).

With this approach, where a skin incision was performed, the resistance force of the tissue has a more linear evolution, eliminating the spike which appear when the skin is penetrated which leads to an increased accuracy due to the elimination of the needle deflection. This approach eliminates the use of a guiding template making the manual needle insertion somewhat more difficult, but using a robotic arm for the needle guidance this drawback is eliminated. Simulation using Siemens NX™ software showed a mass of the mobile parts of the needle insertion module ≈ 175 grams (using Al 5086). The biopsy gun mass is ≈ 50 grams, and by considering the nut and the spindle drive masses, the total moving mass of the module is ≈ 240 grams. The friction coefficient in the cylindrical joints is 0.04 (steel to teflon since teflon bushings are used inside the joints). By using equation (9) the torque value required for needle insertion (at constant velocity) of ≈ 0.0017 Nm is obtained. Using equations (11-14), with the screw moment of inertia $\approx 0.0285 \cdot 10^{-6}$ ($\text{kg} \cdot \text{m}^2$), the pulleys moments of inertia $\approx 0.2813 \cdot 10^{-6}$, the required needle velocity $= 10 \text{ mm} \cdot \text{sec}^{-1}$ and acceleration $= 10 \text{ mm} \cdot \text{sec}^{-2}$ (thus the acceleration time is 1 sec), and finally the rotational velocity $10 \text{ rot} \cdot \text{sec}^{-1}$, the extra torque required for accelerating motion is obtained $\approx 37.52 \cdot 10^{-6}$ Nm.

The force needed to fire the biopsy gun was experimentally determined by pressing the loaded biopsy gun firing button against a force sensor FSR® from Interlink Electronics™, while the data was acquired using National Instruments™ hardware (NI USB-6210) and MatLab™ software (Fig. 7). The experimental bench was developed inside CESTER research center. Output data from 31 experimental trials showed a normal distribution with a mean of 2.689 V (at gun firing instance) and a standard deviation of 0.11. The force sensor was calibrated using standardized weights to determine the characteristic curve that describes volt to force conversion (Fig. 7). Out of this curve, a force of 7.84 N resulted to be de mean value at the gun firing instance.

An electromagnet or a spindle drive that offers a force of 10 N is recommended since it gives an extra $\approx 25\%$ interval to ensure the gun firing. In the selection of the actuation solution weight is a critical parameter which has to be minimized.

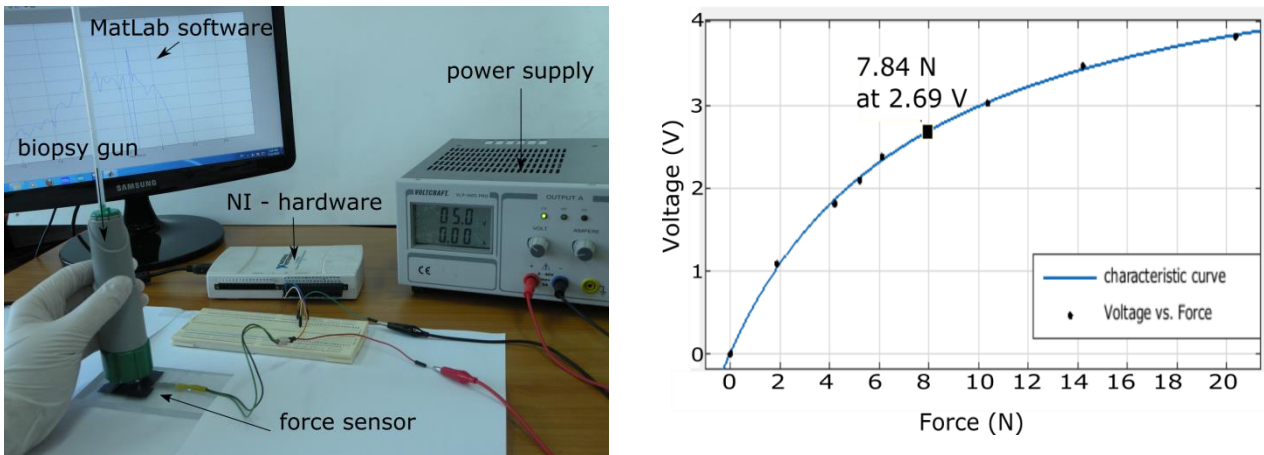


Figure 4.20. Experimental setup for the gun firing needed force (left). Voltage to force characteristic curve of the force sensor (right).

Following the above results (calculated and experimentally determined) the proposed actuators (motor and spindle drive) for the needle insertion module and the screw/nut mechanism are the following:

- The Spindle Drive GP 6 S $\varnothing 6$ mm from Maxon Motor™; max continuous force of 10 N, max intermittent force 18 N, with a mass of 4 grams.
- The motor, ECX SPEED 8 M $\varnothing 8$ mm, and the planetary gearhead GPX 8 $\varnothing 8$ mm from Maxon Motor™; offer continuous torque of 0.008 Nm and a maximum intermittent torque of 0.012 Nm with a mass of 9 grams.
- The ball screw and the ball nut from THK, screw model MDK 0401-3 with its afferent nut. The mechanism has the lead of 1 mm, efficiency of 0.95 and it works well at a rotating speed of 600 RPM. The mass of the screw is 10.15 grams while the mass of the nut is 10 grams.

The total mass of the needle insertion module with the biopsy gun mounted is around 560 grams. The compact solution proposed for the needle insertion module makes this device suitable for a wide variety of biopsy procedures, extending its utilization to other organs as well: liver, kidneys, breast, and thyroid. The overall size makes this device also capable of performing CT-Sim guided biopsies, working as the end-effector of a robotic arm which works inside the gantry of the imaging device, such the PARA-BRACHYROB robot [19]. The modular design allows, with minimal changes its conversion towards another biopsy gun, imposing as a single restriction the presence of the release mechanism at the end of the proximal head of the medical instrument.

A Multi-Needle Insertion Module for Robotic Assisted Brachytherapy

Before introducing the design of module dedicated for robotic assisted brachytherapy, the procedural steps are described below:

Step Preplanning

1. The patient undergoes a complete non-invasive imagistic investigation (CT – compulsory and MRI – if needed) for the exact definition of the tumour(s) location.
 2. The CT images are analysed and the following parameters are defined:
 - a. The radiation dosage and type.
 - b. The number of needles.
 - c. The matrix distribution of the needles.
 - d. The linear trajectories which have to avoid the proximity of high risk areas (organs penetration, blood vessels, nerves) and high density tissues (cartilages, bones).
 3. Using a CT-Scan equipment which has an external laser-based fixed coordinate system (see figure 3.3), the patient position for the procedure is established to enable:
 - a. Comfortable fixed patient position during the entire procedure (as only local anaesthesia will be used);
 - b. Easy access to all the predefined trajectories for the robot with the needle insertion module positioned above the patient.
 4. A set of markers is positioned on the patient to enable:
 - a. An accurate reproduction of the patient position with respect to the external laser based coordinate system;
 - b. A clear view of the needle insertion points achieved through:
 - i. Markers highly visible under the CT-Scan;
 - ii. A needle guiding plate where the holes of interested are marked.
 5. Using the CT-Scan the patient is scanned again and all the markers are validated making if needed the final fine adjustments.
 6. The relative robot-patient position is optimized to ensure that all the targeted points can be reached (are located within the robot workspace) and the final trajectories are validated.
- CT guided robotic assisted brachytherapy**
7. Using the numbered mounting holes the robot is positioned on the mobile CT-Scan couch followed by the patient, whose position will be reproduced using the existing markers (step 4). The patient and robot are calibrated with respect to the laser coordinate system and the transformation matrix for the transformation of the patient coordinates into the robot coordinates is introduced.
 8. The robot performs the homing and then positions the needle insertion module in a predefined point, above the patient, but not very far from the area of interest.
 9. The coordinates of the pairs of points (Insertion – Target) are loaded using a secured USB drive to avoid any human errors.
 10. The first needle is positioned from the current (neutral point) into the Insertion point oriented on the linear trajectory defined by the first pair of points. Due to the external markers the doctors will be able to see any misalignments before any invasive action has been performed.

11.	The needle is introduced into the patient at a depth of 40-50 mm followed by a quick scan aimed to validate the trajectory.
12.	If needed, small trajectory corrections are applied.
13.	In case the trajectory has an error higher than 0.2° - 0.5° (depending on the target depth) the needle is retracted and introduced again.
14.	The needle is introduced until the targeted point and then released from the insertion module.
	For each following needle the steps 10 – 14 are repeated until all the needles are in place.
15.	The robot is retracted into the home position to allow full access to the inserted needles.
16.	The needles are connected to dedicated equipment that will delivered the radioactive seeds based on the treatment protocol.
17.	After the treatment the needles are extracted from the patient body and the patient is removed from the CT-Scan mobile couch.
18.	The robot is removed and the procedure is completed.
	Patient follow-up
19.	The patient evolution is monitored and based on his/her evolution sub-sequent treatments are scheduled.
20.	All the information is stored in a database recording the robot parameters, procedural times as well as all the medically relevant data such as needle accuracy and treatment efficiency.

The procedural steps described below are somewhat autonomous, based on the careful preplanning even though they require a stepwise validation. The only human intervention during the procedure would be the loading of a new needle in the insertion module of the robot. This can be seen as a potential source of errors motivating the idea of developing a multi-needle module that would perform an automated loading of the sub-sequent needles.

The multi-needle insertion module has two main mechanical subsystems: one designed to load one needle at a time, from a magazine that can hold up to 6 needles and one which performs the insertion on a linear path until the calculated depth. The first subsystem is the needle storage mechanism (Fig. 3) with a total capacity of 6 brachytherapy needles and the second subsystem is the loading/insertion mechanism (with the main component being the needle gripper).

The two subsystems (actuated by two motors) work together with a synchronized motion as follows:

1. With the actuation of motor 1, both the needle storage airscrew element, and the needle loading gripper will rotate. The needle is guided (by the storage airscrew element) through a circular channel (Fig. 4.21) and at the end of the channel it is grabbed by the gripper. This synchronous motion is provided by the actuation of two shafts simultaneously (using the motor 1). The two shafts rotate in opposite directions with different speeds (1:6) the different ratio being achieved using a

planetary gear. This makes possible the loading stage of a single needle, and the storage of up 6 needles (displayed on circular pattern at equal angles).

2. After the loading stage, the needle is fixed in the gripper, and the pre-insertion stage begins (actuated by motor 2 through a screw/nut mechanism), i.e. the needle is moved on a linear path until it enters from through the needle tip guiding element (Fig. 4.22). From here the insertion stage is performed based on the preloaded coordinates, followed by the release of the needle with the actuation of motor 1 (30° rotation opposite of the loading direction). The shaft that guides the gripper allows both the translation on a linear path and the rotation of the gripping claws.

3. With the needle inserted the loading mechanism is actuated back (motor 2) to the needle loading position. To load another needle the motor 1 is actuated 390° (to compensate for the 30° motion used during the release needle stage).

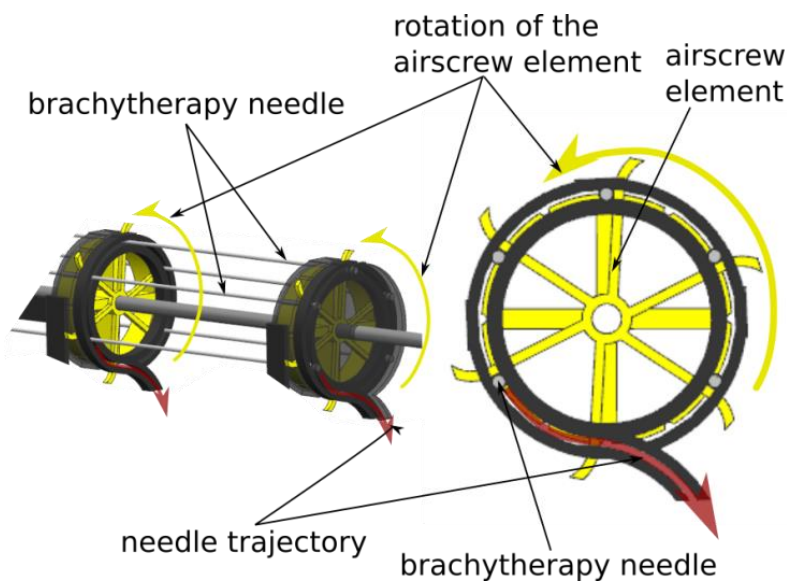


Figure 4.21. The needle magazine sub-system

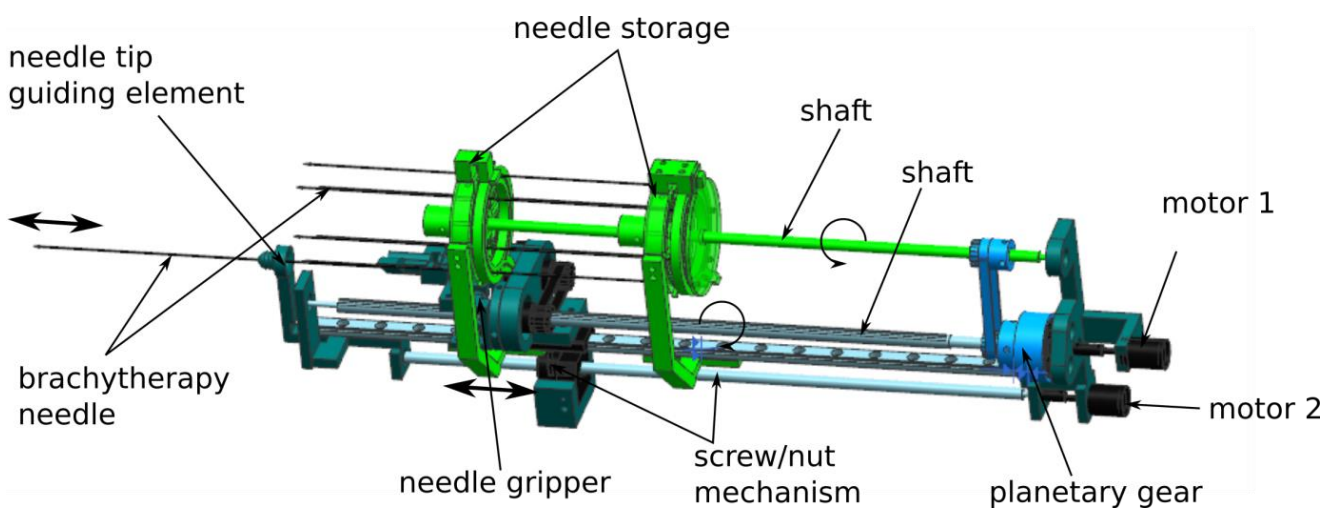


Figure 4.22. CAD model of the multi-needle insertion module

One critical aspect that has to be pointed out is that after the needle is released, the robot has to retract the medical instrument on the same linear path that has been used for the needle insertion until the needle exits the needle tip guiding element hole, in order to leave the needle inside the tissue without causing trauma.

An experimental model for the multi-needle insertion module has been achieved using commercial off-the-shelf motors, bearings and a linear rail. All the other components have been manufactured using 3D print manufacturing technology from ABS (Fig. 4.23).

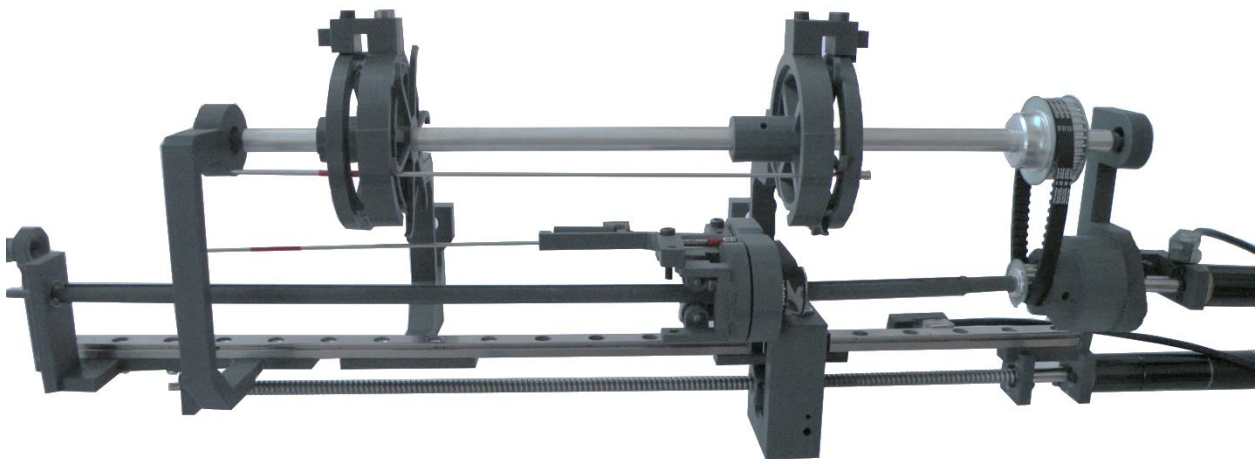


Figure 4.23. Experimental model of the multi-needle insertion module

As in the case of the prostate biopsy module a set of experiments has been performed:

1. The tissue resistance: the experimental measurements performed with the same setup (see figure 4.18) revealed a similar behaviour with a slight increase in the maximum force (12 N) for the skin penetration. As this procedure is performed in the a CT room and the fact that the needles will be inserted through different points of entry into the body the use of local skin incisions is a bit more difficult but the overall benefits recommend this approach.

2. The needle loading: 50 experimental trials were conducted by only testing the needle loading stage. Out of the 50 trials 45 were successful (90% success rate), while in the other trials the needle loading failed due to various reason (friction between the needle and the circular path in which is guided, improper gripping due to elasticity of the ABS). This aspect issued a series of optimizations for the final design of the instrument.

3. Experimental procedure on a phantom: A set of experiments were performed based on a medical scenario using a human torso phantom and ballistic gel (to simulate the tissue resistance). As shown in Fig. 4.24 a breast cancer procedure and a hepatic carcinoma treatment were simulated where the instrument was mounted on PARA-BRACHYROB.

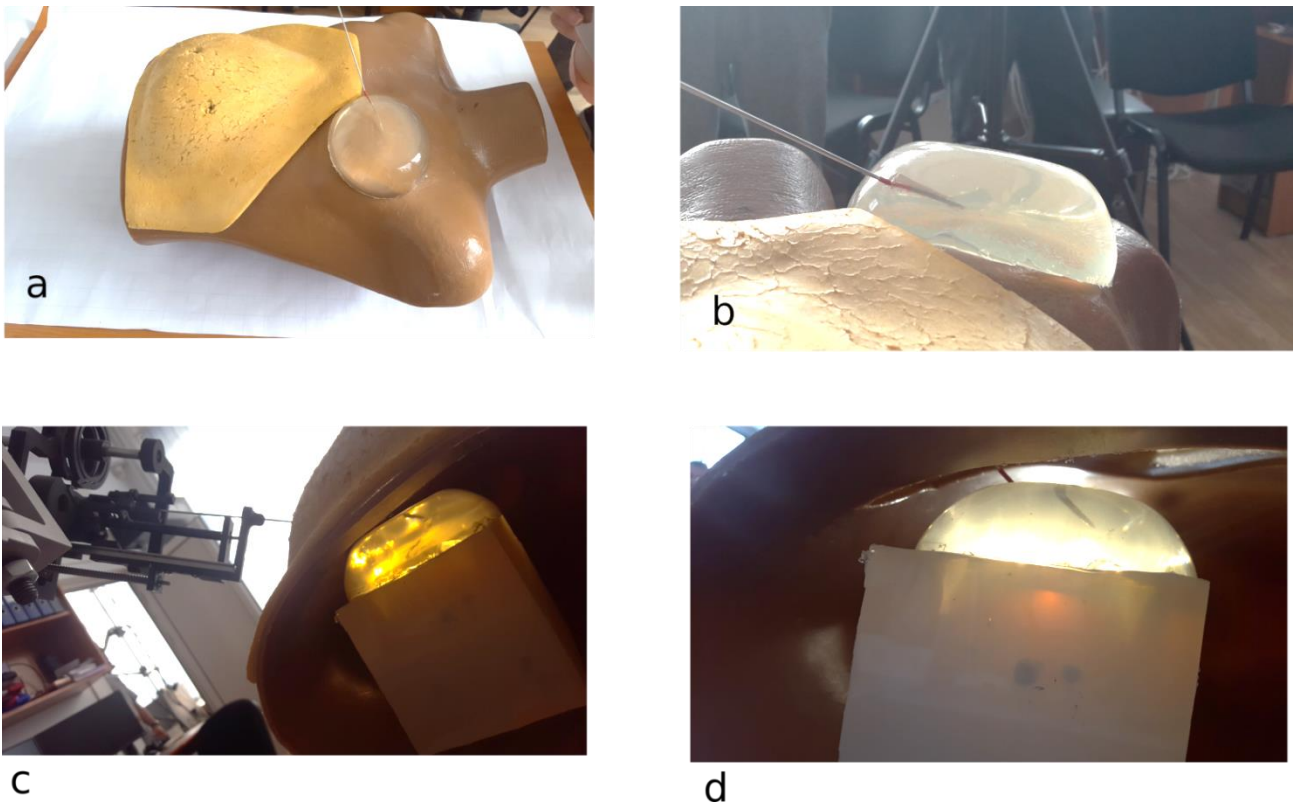


Fig. 4.24. Brachytherapy experiments a) - b) breast brachytherapy (general and close-up view); c) – d) liver brachytherapy (general and close-up view).

A module for robotic assisted Radio-Frequency Ablation

Percutaneous radiofrequency ablation (RFA) is one of the thermal ablation procedure used in radiation oncology as a treatment method for liver cancer [BAR 14, BAR15, GRA06, RAD13]. RFA scope is to heat the tumour in a controlled way, until the liver cancer cells reach necrosis. One way the clinicians use to achieve RFA of the liver tumours, is with a special needle (containing a set of electrodes) that is inserted through the patient abdomen, within the tumour, and is able to deliver an adjustable dose of electromagnetic radiation in the radio spectrum (generated by specialized medical equipment). Limitations of RFA are mainly because of the position inaccuracies of the needle or electrodes [BRA07]. Medical imaging is required in order to overcome the limitations, e.g. the clinician is able to confirm the correct needle placement (before starting the RFA), and the degree of the therapy success (after the RFA is complete). Moreover, robotic assisted needle placement may improve upon the accuracy of the needle and electrode positioning within the tumour.

Starting from the description of the manual procedure [GRA06, RAD13] a protocol for the robotic assisted percutaneous RFA procedure is defined using a RITA RFA needle manually mounted in the RFA module which will be guided using the robotic system PARA-BRACHYROB.

The RITA RFA needle [ANG18] is presented in Fig. 4.25, with examples of two different handle actuation levels to illustrate the shape and the volume that the electrodes cover (when the electrodes are inserted they take an umbrella like shape). The volume is adjustable to offer flexibility on the tissue ablation procedure, i.e. the electrodes are inserted based on the tumour size (at this stage it is important that the clinician validates the electrodes position).

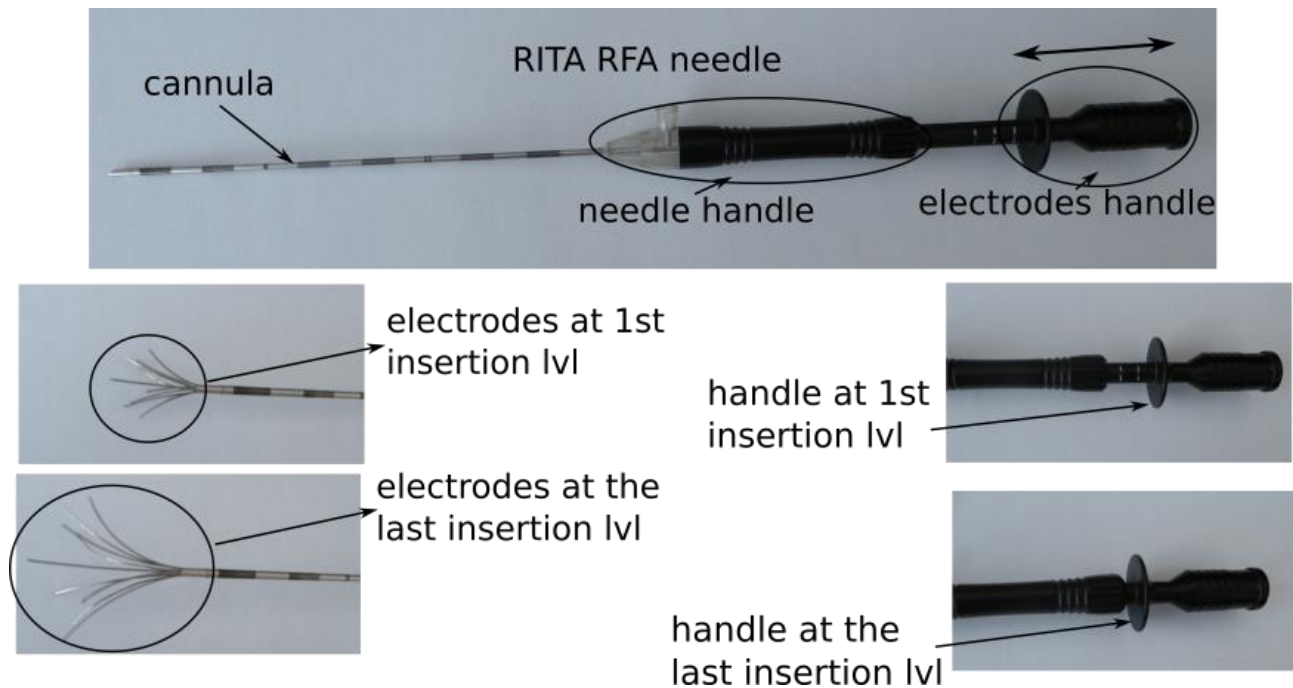


Fig. 4.25. RITA RFA needle with different electrodes insertion levels

The RFA robotic assisted procedure protocol is defined as follows:

Step Action

1.	The patient undergoes a complete non-invasive imagistic investigation (CT – compulsory and MRI – if needed) for the exact definition of the tumour(s) location and size.
2.	The CT images are analysed and the following parameters are defined: <ul style="list-style-type: none"> a. The insertion and target point; b. The insertion level of the electrodes; c. The patient position during the procedure based on the tumour location and the pair of insertion and target points.
3.	Using a set of external markers the robot is calibrated with respect to the patient.
4.	The robot will move from the homing position to the insertion point defined previously. (Fig. 4.26. – step 1)
5.	The needle is inserted following a linear path to a predefined depth - the target point (Fig. 4.26. – step 2); the insertion is monitored using an ultrasound (US) probe manually manipulated by the doctor;
6.	The electrodes within the needle are inserted by actuating the needle handle on a linear path until a predefined level (Fig. 4.26. – step 3)

7. Once the position is validated by the doctor (through US) the RFA procedure is started by delivering the radiofrequency through the electrodes (Fig. 4.26. – step 4); at this stage the clinician is constantly monitoring the therapy progress to ensure that all the electrodes heat up to a certain value to provide medical efficiency
8. After the therapy is over the electrodes are retracted inside the needle cannula (Fig. 4.26. – step 5)
9. The needle is retracted from the patient (Fig. 4.26. – step 6)
10. The robot is sent into Homing position (Fig. 4.26. – step 7) and the needle is dismantled from the instrument
11. The patient follow-up is performed at clear intervals to establish the treatment efficiency.

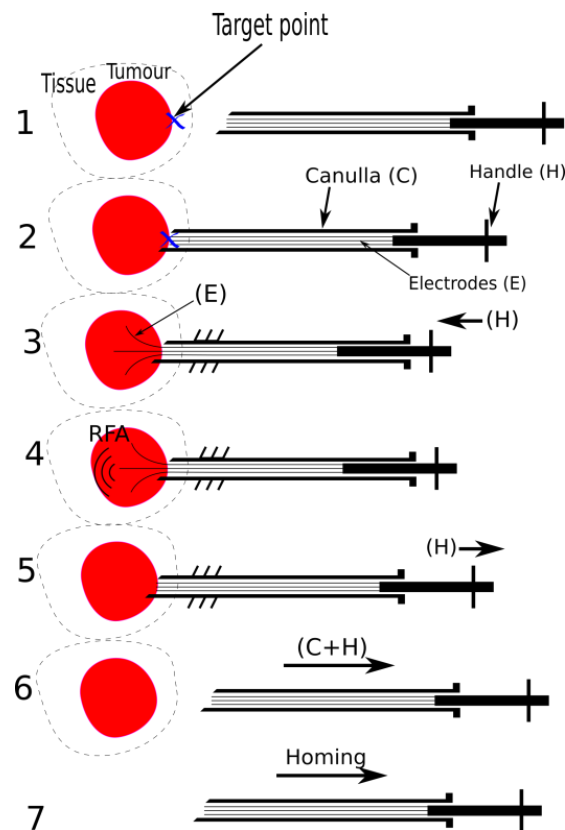


Fig. 4.26. The RITA needle manipulation during the RFA procedure

Following the FRA protocol the instrument should have two degrees of freedom (namely two independent motions), one for needle insertion/retraction and the other for electrodes insertion/retraction. Both motions are linear and have to be precise, with a good resolution, to ensure the accuracy for reaching the target point in the tissue, and covering the desired volume with the electrodes (based on the tumour size).

Fig. 4.27 illustrates the medical instrument with its components. To achieve the two linear motions of the instrument, a rail (1) was used together with two mounted sledges (2,3) that hold two motion independent handles (one attached to the needle for the needle insertion 4 and the other attached to the needle handle for electrodes insertion 5). The linear motion for the needle insertion is performed with a ball screw/nut mechanism (6), where the screw is rotated by a motor (7), and the

nut is linearly actuated on the screw rotation axis. The electrode insertion/retraction is also done with a second ball screw/nut mechanism (8), actuated by another motor (9). A frame that holds both nuts is used, to ensure the motion requirements of the instrument, i.e. with the actuation of motor (7), both sledges (with both handles) are moved, thus obtaining the needle insertion stage, and with the actuation of motor (9) only the sledge (3) is moved for the electrodes insertion retraction stage. To increase precision and decrease the needle bending risk, the needle (10) is held by a needle holder (11) at its tip (the needle slides through the holder at the insertion/retraction stage).

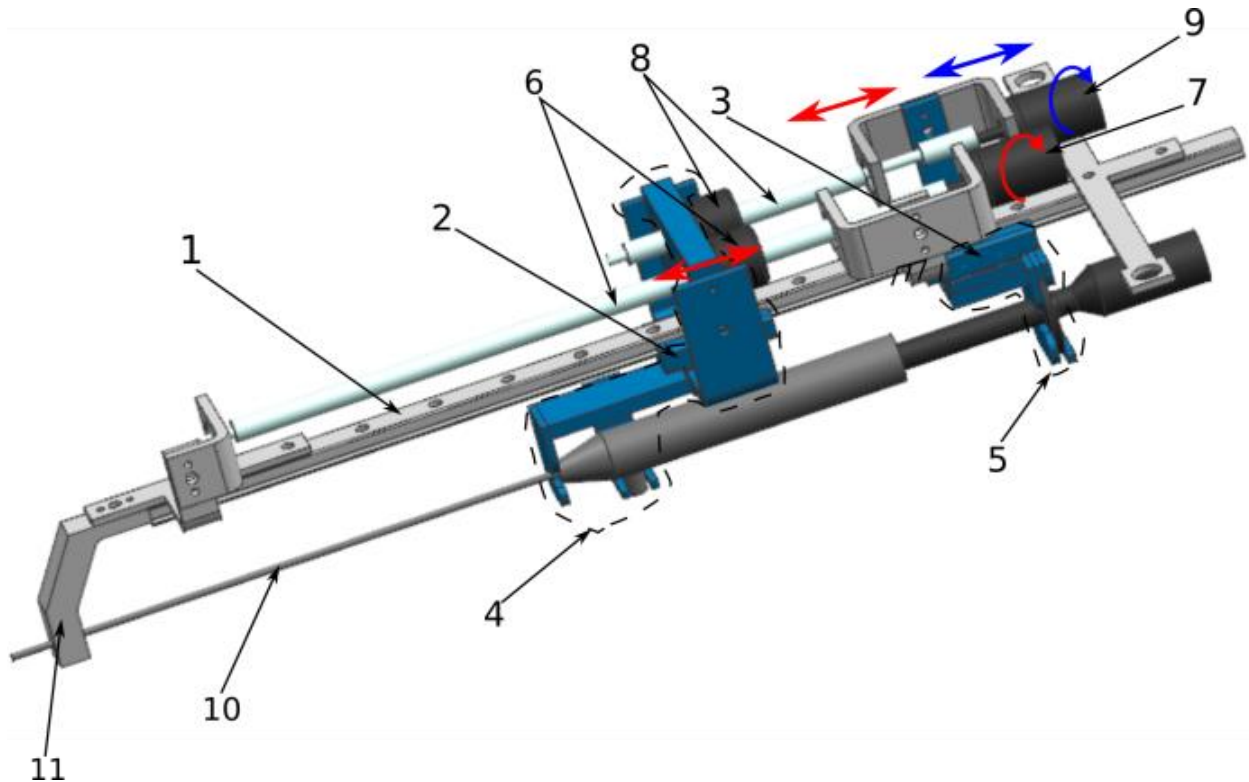


Fig. 4.27. The CAD model of the FRA instrument

For the experimental behaviour of the needle, the same experimental setup as for the other two types of needle was used. The experiment was performed with and without a small skin incision (five trials for each). Fig. 4.28 shows the experimental results, where the needle was inserted 8 sec at a constant speed of $10 \text{ mm}\cdot\text{sec}^{-1}$. It is shown that a small skin incision reduces the force required for the insertion stage. This should improve the procedure precision since the needle bending due to resistance should be lower.

A set of experiments has also been conducted using the designed module mounted on the PARA-BRACHYROB robotic system, to validate the overall procedure. The experimental model of the instrument and the experimental trial with the robotic system are illustrated in Figure 4.29.

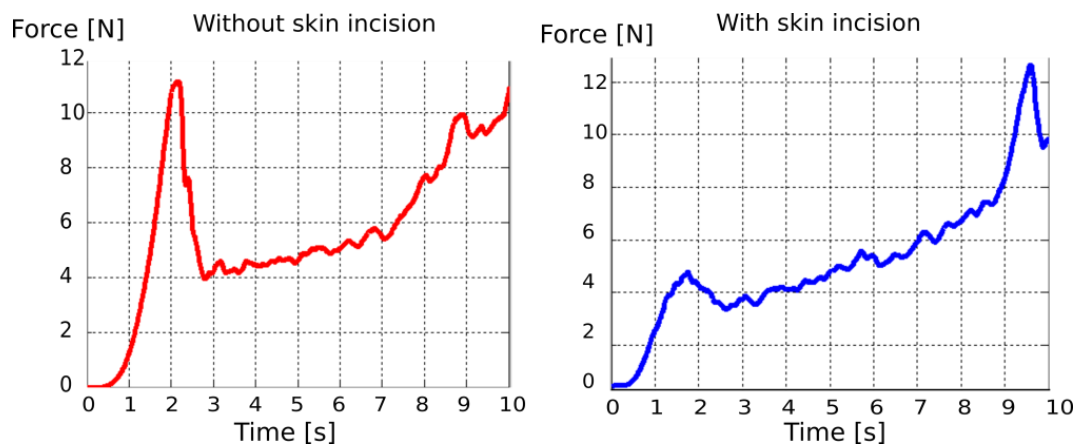


Fig. 4.28. Tissue resistance during needle insertion.

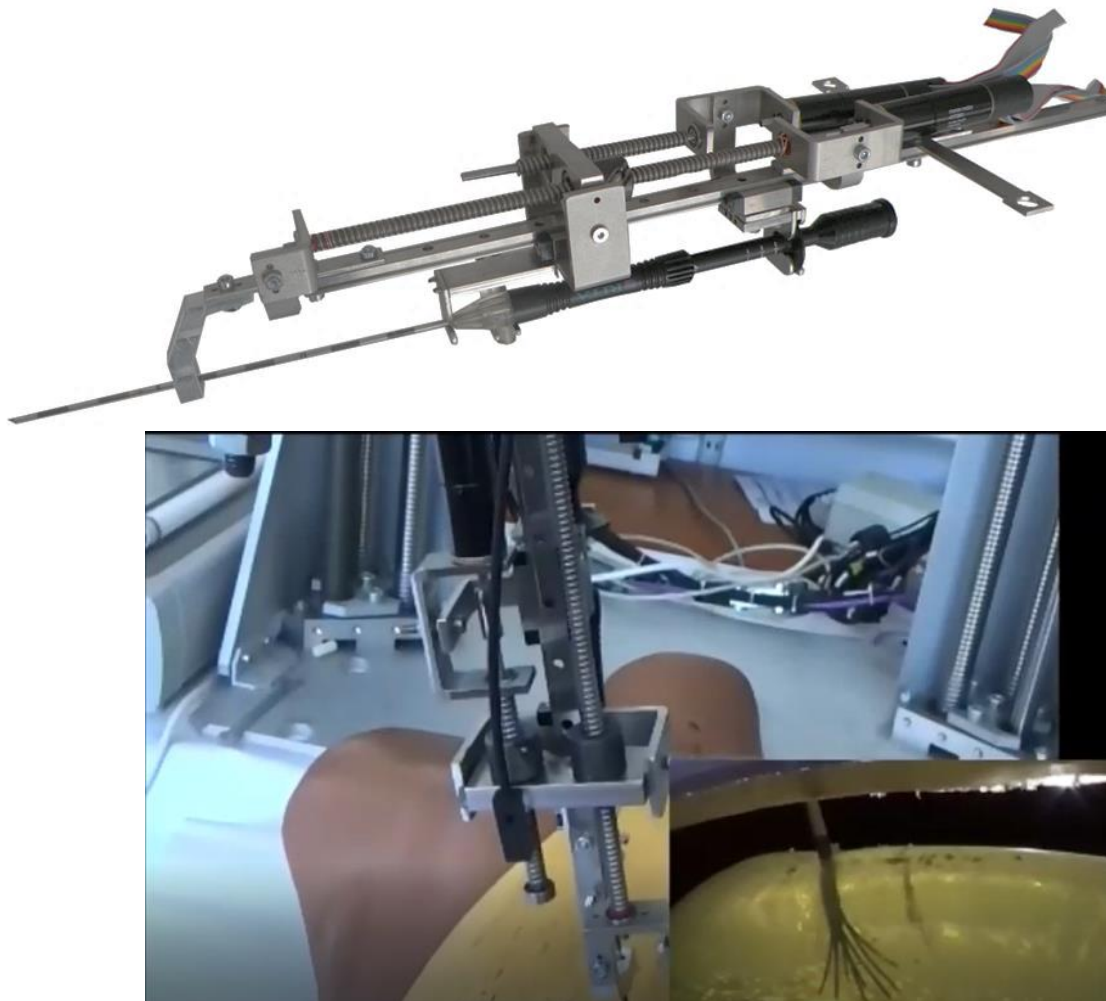


Fig. 4.29. Experiments with the RFA module guided by PARA-BRACHYROB

In the end...

The fight against cancer is far from being won but each day research centres all over the world make important steps in the development of new techniques which aim to improve if not to cure more and more forms of cancer. A challenging task with great responsibility beautiful and scary in the same time, **the fight against cancer will end** but only when a cure will be found.

Chapter 5. Robotic rehabilitation of the upper limb

“Strength doesn't come from what you can do. It comes from overcoming the things you couldn't.” (Rikki Rogers)

A short overview on the post-stroke rehabilitation

Based on the data presented in the first chapter there are several aspects that not only encourages but imposes the development of robotic devices capable of providing an efficient aid in the rehabilitation of a post-stroke patient:

- The EUROSTAT population projections estimates that in the European Union (EU) the percentage of population aged over 65 will increase from a value of 17.1% in 2008 to 30% in 2060 while the population aged over 80 will rise from 4.4% to 12.1% for the same period;
- One of the major disability causes among elderly people is neurological with emphasis on stroke;
- The incidence of the first stroke in Europe is 1.1 million and prevalence around 6 million;
- The post-stroke one year survival rate is around 75% with 80% of the survivors experiencing long-term reduced manual dexterity.

Based on this data, MAR defines an acute demand for the development of new methodologies in rehabilitation that will allow physicians to treat, with better perspective, a larger number of patients. Furthermore, current projections in neurologic rehabilitation point out the following critical aspects:

- Stroke is one of the major diseases which target especially the elderly population;
- Stroke incidence will increase with the increase of average life span of the population;
- In less than 20 years the medical system will be unable to supply sufficient medical personnel to attend stroke patients;
- Due to lack of economical sustainability and unavailable technologic solutions there are no devices specialized in the acute post stroke rehabilitation.

The robotic systems represent a viable solution which can allow physical therapists to develop patient-oriented rehabilitation programs that can maximize the therapeutic effects aiming towards an increased quality of life in the framework of Activities of Daily Living (ADL).

The rehabilitation management differs for the different stages of stroke follow-up, the scientific and medical community accepting largely the time based classification proposed in [PET11]. Thus, the post-stroke stages are:

- **Acute phase:** covers the period of less than three months post-stroke;

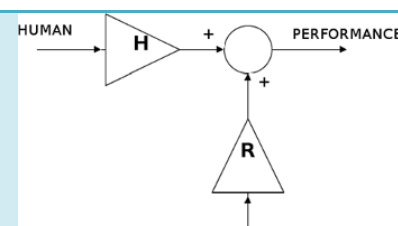
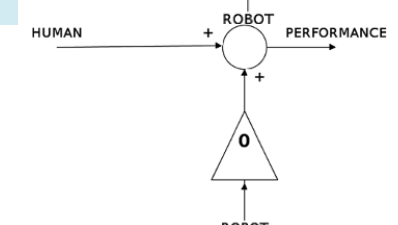
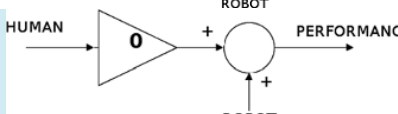
- **Sub-acute phase:** covers the period between three and six months post-stroke;
- **Chronic phase:** covers the period of more than six months post-stroke, spreading up to two years, after which further patient progress is low and rehabilitation has only conservative role.

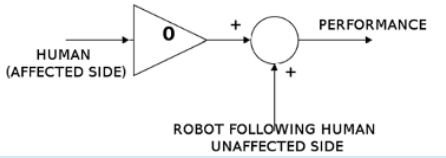
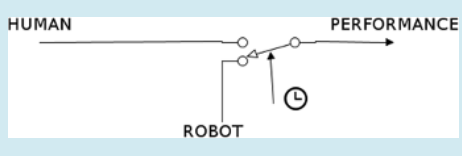
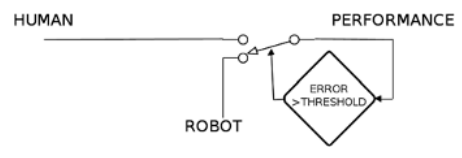
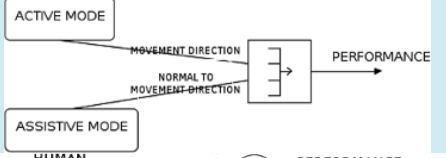
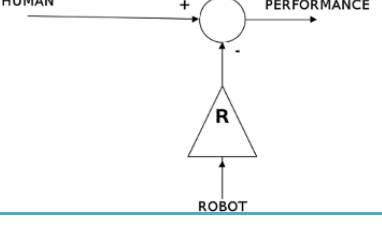
The literature has also emphasized cases where patients that experienced long time disability (> 2 years) have achieved outstanding progress when a newly developed technique was used and this is why, based on the information exchange capability of nowadays, extensive databases should be created to allow patients to benefit from the positive results of other cases as, especially in physical rehabilitation, there is absolutely no therapy that will work in 100% of the cases.

Human Robot interaction – a must in robotic assisted rehabilitation

Robotic rehabilitation for the upper limb has its origin in the 1990s, with multiple devices becoming commercially available. The existing patient oriented studies have proven their efficiency in increasing upper limb motor scores and muscle strength, however very often these improvements had little to no effect upon the patient performance increase in ADL. Based on this general view, multiple reviews that covered a wide number of medical and technical papers (over 400 publications) have been analyzed to identify the weak spots in the current approaches. Based on this data, a classification of the interaction modalities in robot assisted rehabilitation is defined as result of the existing literature information [BAS14a, GOP16, KAN11, LO12, LOU11, POS10] and presented in the following table (Table 5.1).

Table 5.1. Interaction modalities review

Control modality	Specifications	Control scheme
Assistive	The patient voluntary movement is required. The robot assists the patient by providing partial weight support or forces that lead to the task completion.	
Active	The robotic system acts only as a measurement device without providing any forces upon the limb.	
Passive	The robot performs the movement without any contribution from the patient.	

Control modality	Specifications	Control scheme
Passive mirrored	A bimanual configuration where the unimpaired limb is guiding (through an active device) the exact/mirrored passive motion for the affected limb.	
Active assistive	- The task is completed by the robotic device only when the subject cannot achieve it completely. From this stage, the robot acts in a passive mode.	
Corrective	The subject motion is stopped when a certain error level is reached from the given task, afterwards the task is reissued and the robot works in an active mode.	
Path-guidance	The robot will assist the motion on a given trajectory by performing corrections when a deviation occurs.	
Resistive	The robot applies resistive forces against the given motion task.	

Based on this classification it is clear that not all human-robot interactions can be applied for every patient and it is the physical therapist task to identify correctly the best possible treatment for a patient based on the motor evaluation scoring such as: the Fugl-Meyer score [CHE14, GLA02, WEI11], Action Research Arm Test [NOR14, WEI11], Motor Activity Log [WEI11] and others [LYL81]. The existing HRI modalities emphasize the idea that a robotic device would not replace the human therapist, instead would allow him to individually assess patient progress, determine personalized rehabilitation regimes, and to use multiple motivational tools to encourage and support patient progress, to attend multiple subjects and many more.

An in-depth analysis of the current studies and reports reveal the following conclusions [ABD14, BAS14a, COL16, DIP12, KLA14, LO10, NOR14, POS10, YAD16, YOO15, WEI11]:

- To the current day the existing data has shown that no physical therapy seem as preferable and the selection of the best rehabilitation plan depends on the physical therapist and the patient evolution;

- Most of the robotic devices that reached a maturity level of hospital testing provide a selection among the following four modalities for training: active, active-assisted, passive and resistive;
- Several studies illustrated that in some cases robotic structures have improved the motor scores and muscle strength but without positive influence on ADL;
- One possible reason for the limited transfer of motor gains to ADL is that the earlier studies on robot mediated therapy have only focused on the proximal joints of the arm, while integration of distal with proximal arm training has been recognized as essential to enhance functional gains.
- A second problem identified as progress limitation is the lack of physiological activities – some robotic systems perform only repetitive motions without any feedback from the patient, lacking a real HRI.

For acute patients the modalities with better outcome on body functions were active (2 out of 3 groups, 67%), assistive (4 out of 6 groups, 67%), active-assistive (5 out of 10 groups, 50%) and passive (6 of 13 groups, 46%). [BAS14a]

For subjects in acute phase, inclusion of passive mirrored and resistive modality did not lead to improvements in body functions (in none of the 4 and 3 groups, respectively). [BAS14a]

In chronic phase instead, the inclusion of passive-mirrored modality led to improvement in 75% of the groups (6 out of 8), while the inclusion of resistive modality was effective on 71% of the groups (12 of 17). [BAS14a, PER16]

The path guidance modality led to the best results for chronic patients (6 out of 6 groups improved on body functions). Results for other modalities are similar among them, with all the other modalities being effective on about 60% of the groups. [BAS14a, SQU 14]

Additionally, it is known that post-stroke training should include exercises that are as “task-specific/functional” as possible to stimulate motor relearning, which further supports inclusion of the hand and with proximal arm training. [BAS14a, DIP12]

Motion amplitudes at the level of the upper limb

In order to enable the proper design of a robotic system that will enable the performing of these motions, a set of measurements were achieved on a number of 21 patients [MAJ16], compared to other literature results and corroborated with several standards that evaluate the weight and length of each body segment. This data enables the definition of the technical specifications of a new robotic system with proper motion scaling and link dimensioning and load capacity. Three widely accepted metrics were used for limb weight and length estimation:

1. The Plagenhoef model [PLA13];
2. The R.L. Huston model [HUS08];
3. The Contini model [CON66].

For the motions description the anatomic planes of the body are used, as defined by the medical community:

1. The Coronal (Frontal) plane: divides body into anterior and posterior portions;
2. The Sagittal plane: divides the body into left and right portions;
3. The Transverse (Cross-Sectional) plane: divides the body into superior and inferior portions.

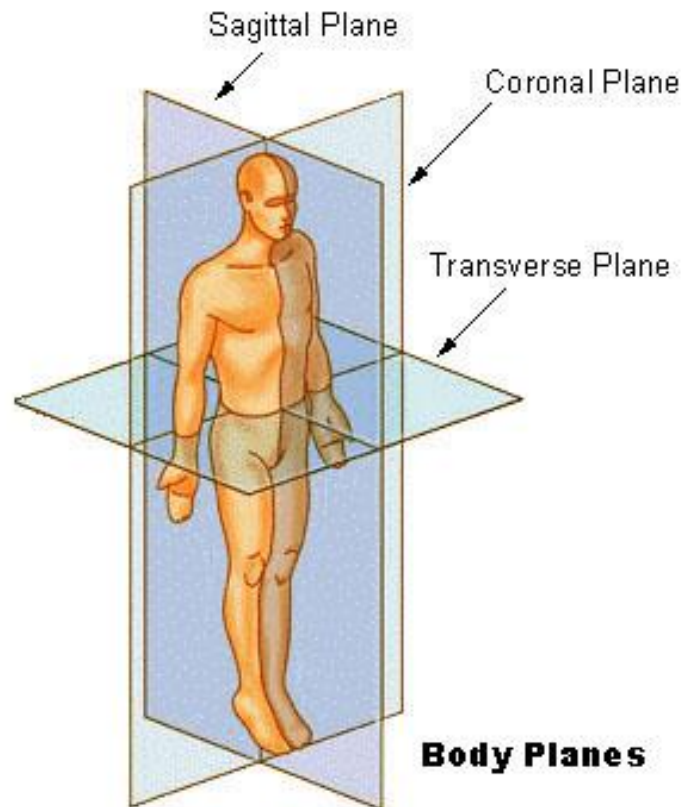


Figure 5.1. The planes of the body [WIK18]

With respect to the body planes, a corresponding Cartesian system is defined for the robotic system, as illustrated in figure 2.

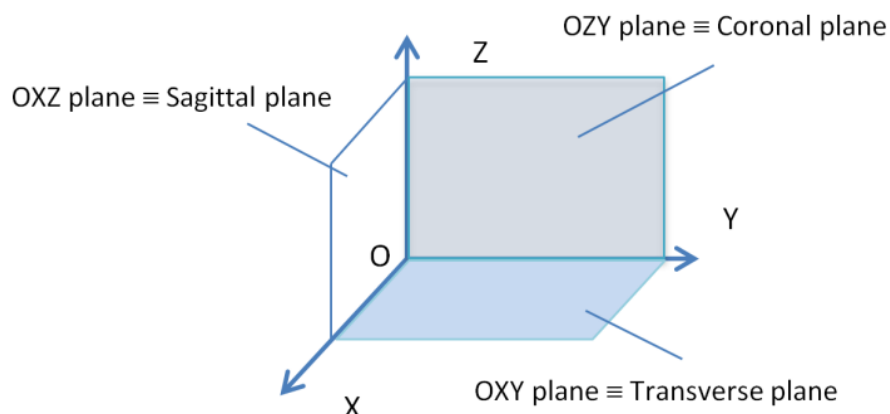


Figure 5.2. Cartesian coordinate system correlated with the body planes

Shoulder Motions

At the level of the shoulder, four motions are defined, each of them described in the following lines:

- a) **Shoulder flexion and extension** is performed in a plane parallel with the sagittal plane of the body:

Starting position: patient in standing/sitting, the upper limb is placed parallel with the body and the palm faces the sagittal plane.

- **Shoulder flexion without rotation:** the upper limb, with the elbow extended is raised from the starting position towards the front of the patient without any rotation from the shoulder joint.

- **Shoulder extension:** the upper limb is rotated backwards, until possible, keeping the elbow extended.

- b) **Shoulder abduction and adduction** is performed in a plane parallel with the coronal or frontal plane:

Starting position: patient in standing/sitting, the upper limb is parallel with the body and the palm faces the coronal plane.

- **Shoulder Adduction:** from the starting position the upper limb is moved with a lateral motion and brought in front of the body

- **Shoulder Abduction:** from the starting position the upper limb is raised with a lateral motion until the maximum possible angle is reached in the shoulder, palm faces the floor.

The measurements performed on 21 patients involved in the study revealed the data presented in Table 5.2.

Table 5.2. Motion amplitudes in degrees [°] for the shoulder motions measured from the starting position

Motion type	Maximum Value		Mean Value		Minimum value	
	Left	Right	Left	Right	Left	Right
Shoulder flexion	120	114	98.3	93.75	72	72
Shoulder extension	65	72	48.77	48.66	30	29
Shoulder abduction	114	102	90.9	89.15	68	74
Shoulder adduction	44	44	25.3	24.55	7	8

Elbow motions

At the level of the elbow three motions are defined, all performed in a plane parallel with the sagittal one.

- a) **Elbow flexion** is performed alone, without the flexion as some people cannot (naturally) perform the elbow extension.

Starting position: patient in sitting/standing, the upper limb in extension, 90 degrees flexion in the shoulder, elbow fully extended, palm faces upwards.

➤ **Elbow flexion:** from the starting position the elbow is flexed to maximum, bringing the forearm over the arm.

b) Elbow supination/pronation.

Starting position: patient in sitting/ standing, the arm is parallel with the trunk, elbow is flexed to 90 degrees, and palm faces the sagittal plane:

- **Elbow supination:** the forearm and the hand is rotated, with the palm pointing upwards
- **Elbow pronation:** the forearm and the hand is rotated, with the palm pointing down.

The measurements performed in the study are summarized in Table 5.3.

Table 5.3. Motion amplitudes in degrees [°] for the elbow motions measured from the starting position

Motion type	Maximum Value		Mean Value		Minimum value	
	Left	Right	Left	Right	Left	Right
Elbow flexion	150	152	131.1	137.7	56	122
Elbow pronation	92	104	77.75	81.1	54	40
Elbow supination	100	128	84.55	81.55	60	62

Wrist Motions

For the wrist two motions are defined.

Starting position: patient in standing/sitting, the upper limb is flexed to 90 degrees in the shoulder joint, elbow and the wrist are fully extended, the arm being situated in a plane parallel with the transverse one.

- **Wrist Flexion:** the patient flexes the wrist upwards;
- **Wrist Extension:** the patient extends the wrist downwards.

The measurements performed in the study are summarized in Table 5.4.

Table 5.4. Motion amplitudes in degrees [°] for the wrist motions measured from the starting position

Motion type	Maximum Value		Mean Value		Minimum value	
	Left	Right	Left	Right	Left	Right
Wrist flexion	98	90	60.7	58.9	22	27
Wrist extension	72	62	45.1	45.1	18	24

Robot specifications

Robot design has been widely addressed in literature, such as in [CAR06, CAR08, GOM12], as in first design stage one has to set up design specifications (PDS) in terms of functions, performance, operation, manufacturing, environment, materials and control interfaces. The robot structure is defined based on the number of degrees of freedom required for each upper limb joint with the definition of the link lengths and associated limb weight based on the anthropometric body data.

a) Shoulder Motions

It is considered an OXYZ coordinate system placed with the origin in the rotating centre of the shoulder (the tip of the humerus) where two degrees of freedom are required:

- one rotation around the OY axis for flexion/extension;
- one rotation around the OX axis for abduction adduction;

For the shoulder mobilization the robot can use the following two anchor points (AP) positioned on the upper limb:

- the main (actuated) anchor in the distal third of the arm;
- the support anchor in the area of the hand and the wrist.

When moving the arm from the shoulder the robot has to support the entire weight of the arm which has the following percentages of the total body weight, based on two different models, Plagenhoef [PLA13] (Table 5.5) and Houston [HUS08] (Table 5.6):

Table 5.5. Calculated weight for the upper limb; Plagenhoef model.

Plagenhoef (shoulder)		
	Males	Females
Total weight	5.7%	4.97%
Examples calculated in kilograms [kg]		
70 kg	3.99	3.48
80 kg	4.56	3.98
90 kg	5.13	4.47
120 kg	6.84	5.96

Table 5.6. Calculated weight for the upper limb; Houston model.

RL Houston (shoulder)			
Males			
Distribution	5th%	50th%	95th%
Total weight	3.41%	4.14%	4.96%
Examples calculated in kilograms [kg]			
70 kg	2.387	2.898	3.472
80 kg	2.728	3.312	3.968
90 kg	3.069	3.726	4.464
120 kg	4.092	4.968	5.952
Females			
Distribution	5th%	50th%	95th%
Total weight	2.59%	3.15%	3.81%
Examples calculated in kilograms [kg]			
70 kg	1.813	2.205	2.667
80 kg	2.072	2.52	3.048
90 kg	2.331	2.835	3.429
120 kg	3.108	3.78	4.572

When fixing the anchor points, the limb length must be taken into consideration, with some average data being presented below, extracted from two different studies (Plagenhoef [PLA13] in table 5.7 and Contini [CON66] in table 5.8) and completed also with the specific values for most common total body height.

Table 5.7. Calculate anchor points for the shoulder; Plagenhoef model.

Plagenhoef (shoulder)				
Male – calculated value for different heights				
Segment	TBH [%]	160 cm	170 cm	180 cm
Upper arm	17.2	27.52	29.24	30.96
Forearm	15.7	25.12	26.69	28.26
Hand	5.75	9.2	9.775	10.35
Active AP	11.47	18.35	19.49	20.64
Passive AP	36.72	58.76	62.43	66.10
Female – calculated value for different heights				
Segment	TBH [%]	150 cm	160 cm	170 cm
Upper arm	17.3	25.95	27.68	29.41
Forearm	16	24	25.6	27.2
Hand	5.75	8.625	9.2	9.775
Active AP	11.53	17.30	18.45	19.61
Passive AP	37.14	55.72	59.43	63.15

Table 5.8. Calculated anchor points for shoulder, Contini model.

Contini (shoulder)				
Male – calculated value for different heights				
Segment	TBH [%]	160 cm	170 cm	180 cm
Upper arm	18.9	30.24	32.13	34.02
Forearm	14.5	23.2	24.65	26.1
Hand	12.8	20.48	21.76	23.04
Active AP	12.60	-20.16	-21.42	-22.68
Passive AP	37.60	-60.16	-63.92	-67.68
Female – calculated value for different heights				
Segment	TBH [%]	150 cm	160 cm	170 cm
Upper arm	19.3	28.95	30.88	32.81
Forearm	15.2	22.8	24.32	25.84
Hand	11	16.5	17.6	18.7
Active AP	12.87	-19.30	-20.59	-21.87
Passive AP	38.79	-58.18	-62.06	-65.94

b) Elbow Motions

It is considered an OXYZ coordinate system placed with the origin in the rotating center of the elbow having the OZ axis along the upper arm (when the arm is positioned along the body the OZ axis will point upwards), defining the two degrees of freedom for the elbow motions:

- one rotation around the OY axis for the flexion/extension;
- one rotation around the OX axis, considering a 90° angle between the arm and the forearm, having the arm along the OZ axis and the forearm along the OX axis.

The anchor points for the forearm are:

- active anchor point in the distal third of the forearm;
- the passive anchor point, in the distal third of the arm.

When moving the forearm, the robot has to support the weight of the forearm and the hand which has the following percentages of the total body weight based on two models, Plagenhoef [PLA13] (Table 5.9) and Houston [HUS08] (Table 5.10).

Table 5.9. Calculated weight for the forearm and hand; Plagenhoef model

Plagenhoef (forearm)		
	Males	Females
Total weight %	2.52%	2.07%
Examples calculated in kilograms [kg]		
70 kg	1.76	1.45
80 kg	2.02	1.66
90 kg	2.27	1.86
120 kg	3.02	2.48

Table 5.10. Calculated weight for the forearm and hand; Houston model.

RL Houston (forearm)			
Males			
Distribution	5 th %	50 th %	95 th %
Total weight	1.57%	1.91%	2.29%
Examples calculated in kilograms [kg]			
70 kg	1.099	1.337	1.603
80 kg	1.256	1.528	1.832
90 kg	1.413	1.719	2.061
120 kg	1.884	2.292	2.748
Females			
Distribution	5 th %	50 th %	95 th %
Total weight	1.18%	1.44%	1.74%
Examples calculated in kilograms [kg]			
70 kg	0.826	1.008	1.218
80 kg	0.944	1.152	1.392
90 kg	1.062	1.296	1.566
120 kg	1.416	1.728	2.088

When fixing the anchor points, the limb length must be taken into consideration, with some average data being presented below, extracted from two different studies (Plagenhoef [PLA13] in Table 5.11 and Contini [CON66] in Table 5.12) and completed also with the specific values for most common total body height.

Table 5.11. Calculated anchor points for forearm; Plagenhoef model.

Plagenhoef (forearm)				
Male – calculated value for different heights				
Segment	TBH [%]	160 cm	170 cm	180 cm
Upper arm	17.2	27.52	29.24	30.96
Forearm	15.7	25.12	26.69	28.26
Hand	5.75	9.2	9.775	10.35
Active AP	10.47	16.75	17.79	18.84
Passive AP	-5.73	-9.17	-9.75	-10.32
Female – calculated value for different heights				
Segment	TBH [%]	150 cm	160 cm	170 cm
Upper arm	17.3	25.95	27.68	29.41
Forearm	16	24	25.6	27.2
Hand	5.75	8.625	9.2	9.775
Active AP	10.67	16.00	17.07	18.13
Passive AP	-5.77	-8.65	-9.23	-9.80

Table 5.12. Calculated anchor points for forearm; Contini model.

Contini (forearm)				
Male – calculated value for different heights				
Segment	TBH [%]	160 cm	170 cm	180 cm
Upper arm	18.9	30.24	32.13	34.02
Forearm	14.5	23.2	24.65	26.1
Hand	12.8	20.48	21.76	23.04
Active AP	9.67	15.47	16.43	17.40
Passive AP	-6.30	-10.08	-10.71	-11.34
Female – calculated value for different heights				
Segment	TBH [%]	150 cm	160 cm	170 cm
Upper arm	19.3	28.95	30.88	32.81
Forearm	15.2	22.8	24.32	25.84
Hand	11	16.5	17.6	18.7
Active AP	10.13	15.20	16.21	17.23
Passive AP	-6.43	-9.65	-10.29	-10.94

The negative values of the Passive AP state that the anchor point is positioned behind the origin of the coordinate system, in opposite sense with respect to the Active AP.

c) Wrist Motions

It is considered an OXYZ coordinate system placed with the origin in the rotating center of the wrist with the OX axis pointing towards the fingers (when the forearm is positioned horizontally the OZ axis will point upwards), defining the one degree of freedom for the hand motions:

- one rotation around the OY axis for the wrist flexion/extension.

The anchor points for the wrist mobilization are:

- active anchor point: the palm and the dorsal side of the hand;
- passive anchor point: the distal third of the forearm.

When performing the wrist mobilization, the robot has to support the weight of the hand which has the following values with respect to the total body weight based on two different models, Plagenhoef [PLA13] (Table 5.13) and Houston [HUS08] (Table 5.14):

Table 5.13. Calculated weight for the hand; Plagenhoef model.

Plagenhoef (hand)		
	Males	Females
Total weight %	0.65%	0.5%
Examples calculated in kilograms [kg]		
70 kg	0.46	0.35
80 kg	0.52	0.40
90 kg	0.59	0.45
120 kg	0.78	0.60

Table 5.14. Calculated weight for the hand; Houston model.

RL Houston (hand)			
Males			
Distribution	5 th %	50 th %	95 th %
Total weight	0.43%	0.52%	0.63%
Examples calculated in kilograms [kg]			
70 kg	0.301	0.364	0.441
80 kg	0.344	0.416	0.504
90 kg	0.387	0.468	0.567
120 kg	0.516	0.624	0.756
Females			
Distribution	5 th %	50 th %	95 th %
Total weight	0.34%	0.42%	0.50%
Examples calculated in kilograms [kg]			
70 kg	0.238	0.294	0.35
80 kg	0.272	0.336	0.4
90 kg	0.306	0.378	0.45
120 kg	0.408	0.504	0.6

For the positioning of the anchor points, the limb length must be taken into consideration, with the average data being presented below, extracted from two different studies (Plagenhoef [PLA13] in Table 5.15 and Contini [CON66] in Table 5.16) and completed also with the specific values for most common total body heights.

Table 5.15. Calculated anchor points for hand; Plagenhoef model.

Plagenhoef (hand)				
Male – calculated value for different heights				
Segment	TBH [%]	160 cm	170 cm	180 cm
Upper arm	15.7	25.12	26.69	28.26
Forearm	5.75	9.2	9.775	10.35
Hand	2.88	4.60	4.89	5.18
Active AP	-5.73	-9.17	-9.75	-10.32
Passive AP	15.7	25.12	26.69	28.26
Female – calculated value for different heights				
Segment	TBH [%]	150 cm	160 cm	170 cm
Upper arm	16	24	25.6	27.2
Forearm	5.75	8.625	9.2	9.775
Hand	2.88	4.31	4.60	4.89
Active AP	-5.77	-8.65	-9.23	-9.80
Passive AP	16	24	25.6	27.2

Table 5.16. Calculated anchor points for hand; Contini model

Contini (hand)				
Male – calculated value for different heights				
Segment	TBH [%]	160 cm	170 cm	180 cm
Upper arm	14.5	23.2	24.65	26.1
Forearm	12.8	20.48	21.76	23.04
Hand	6.40	10.24	10.88	11.52
Active AP	-6.30	-10.08	-10.71	-11.34
Passive AP	14.5	23.2	24.65	26.1
Female – calculated value for different heights				
Segment	TBH [%]	150 cm	160 cm	170 cm
Upper arm	15.2	22.8	24.32	25.84
Forearm	11	16.5	17.6	18.7
Hand	5.50	8.25	8.80	9.35
Active AP	-6.43	-9.65	-10.29	-10.94
Passive AP	15.2	22.8	24.32	25.84

The negative values of the Passive AP state that the anchor point is positioned behind the origin of the coordinate system, in opposite sense with respect to the Active AP.

As it can be seen for the complete set of motions of the upper limb, a set of three anchor points are defined which are either active or passive depending on the motion performed:

- the distal third of the arm;
- the distal third of the forearm;
- the palm and the dorsal side of the hand.

The defined set of anchor points enables the development of a robotic device that can perform a wide variety of motions for multiple joints of the upper limb. Based on the data presented in section 2, this approach should have an increased impact on the post-stroke patient rehabilitation with positive impact upon ADL.

Medical protocols for robotic assisted post-stroke patients

Due to the different management of the patient in the post-stroke stages, two separate protocols are defined:

a) Medical protocol for robotic assisted rehabilitation in acute post-stroke patients

1. In order to start rehabilitation, in the acute phase, the patient must be conscious, hemodynamically stable, without fever and with CT/MRI confirmation of the brain lesion (to exclude other diseases).
2. The patient is initially assessed by a physical therapist (both mechanical and dynamical) and assigned an initial post-stroke score. One of the above mentioned scoring tests can be used and are repeated in a periodic cycle following the stroke, as follows: Month 1, Month 3, Month 6, Month 12. As an alternative to classical scores an evaluation chart can be developed, to cover properly the entire limb evaluation.
3. The robot motion amplitudes are adjusted based on the initial data from point 2.
4. The patient is positioned sitting on the side of the bed or on a chair if possible. For more severely affected patients, the exercises will be performed with the patient lying in bed.
5. The robotic device is attached to the patient.
6. The rehabilitation procedure is initiated, based on the physical therapist's recommendations – programmed mode - predefined exercises (5 repetitions each), or in one of the following working modes:
 - A. passive;
 - B. EMG proportional driven;
 - C. Direct nerve potential driven;
 - D. ECoG (ElectroCorticoGram) driven.
 - E. For exercises, the following motion sets are defined, in different sequences and in advanced rehabilitation stages in different combinations, attempting to replicate ADL similar motions, performed in a passive HRI:
 - I. Shoulder – Flexion, Extension, Abduction, Adduction (optional Rotation);
 - II. Elbow – Flexion, Extension, Supination, Pronation;
 - III. Wrist – Flexion, Extension;
 - IV. Fingers - Flexion, Extension. (3 joints for fingers 2-5 and 2 for finger 1).

7. The device is detached.
8. The physical-therapist evaluates the integrity of muscles and ligaments
9. The steps 2-8 are repeated for each rehabilitation session.

b) Medical protocol for robotic assisted rehabilitation in sub-acute and chronic post-stroke patients

1. In the sub-acute and chronic phases, the patient has a well-known hemiparesis level with clear indication and an assessment score.
2. The patient is evaluated by the physical therapist that establishes, based on the score the rehabilitation therapy, conditioned by the limb mobility and patient overall state.
3. The robot motion amplitudes are adjusted based on the initial data from point 2.
 4. The patient is positioned in an orthostatic position, sitting on a chair, where possible. This allows focus on the upper limb rehabilitation, avoiding the balance and gait problems. For more severely stroke patients which cannot support this stance, an alternative position will be used, depending on the subject capability.
5. The robotic device is attached to the patient.
6. The rehabilitation procedure is initiated, based on the -therapist recommendations in one of the following working modes:
 - A. predefined exercises (5 repetitions each)
 - B. passive-mirrored motions;
 - C. EMG proportional driven;
 - D. Direct nerve potential;
 - E. ECG (ElectroCorticoGram) driven;
 - F. Path Guidance: The patient must follow a trajectory on a computer screen, with the robot acting as a partial guide when the patient cannot complete the motion or as a resistive guide in later recovery stages.

For the predefined set of exercises, the HRI modalities use are Resistive, Active, Active-Assistive, for the following motions:

- I. Shoulder – Flexion, Extension, Abduction, Adduction (optional Rotation);
 - II. Elbow – Flexion, Extension, Supination, Pronation;
 - III. Wrist – Flexion, Extension;
 - IV. Fingers - Flexion, Extension. (3 joints for fingers 2-5 and 2 for finger 1).
Path Guidance
7. The patient performs multiple exercises based on the therapeutic program.
 8. At the end of the procedure the device is detached.
 9. The physical therapist evaluates the integrity of the muscles and ligaments of the patient, if necessary.
 10. The steps 2-8 are repeated for each rehabilitation session.

11. Based on the patient progress recorded by the robotic system the exercises are adjusted for the next session.
12. The evaluation of a new robot performance must be correlated to the potential patient progress following the robotic assisted therapy and it can be achieved in two ways:
 - A. Use a single group of patients, evaluate them before and after the therapy using a standard scoring procedure (such as Fugl-Meyer score, Action Research Arm Test, Motor Activity Log) and compare the results with the literature;
 - B. Split the group in two, using normal therapy on the control group and robotic assisted exercises on the other comparing the FM scores before and after therapy. (This option would be preferred being conditioned only by a sufficient number of patients which would generate statistically relevant data).

An innovative robotic device for upper limb rehabilitation – ASPIRE

Targeted amplitudes and motions

The ASPIRE robotic device is developed with the purpose of reproducing the necessary motions used in the rehabilitation of the upper human limb, more specifically at the level of the shoulder and the forearm joints. Following a number of discussions and sampling procedures carried by kinetotherapists and neurologists at the Municipal Hospital of Cluj-Napoca, both motions that are used in rehabilitation procedures, and the angular dimensions that need to be achieved when defining the operational workspace of the robotic system were determined.

For the purpose of achieving shoulder rehabilitation, two motions need to be reproduced. These motions are as follows:

- 1) **Shoulder flexion/extension.** In rehabilitation, the patient must start with the midline of arm parallel to the body's vertical midline (neutral position). The arm is then rotated using the shoulder joint forward (in front of the patient) for flexion and backwards (behind the patient) for extension, all of these rotations must be done while maintaining the arm in the same plane as it was in the neutral position.
- 2) **Shoulder abduction/adduction.** In this case, the patient must yet again start with the arm in the same neutral position. The arm is then moved away from the body (abduction) via a rotation from the shoulder joint, adduction represents the arm being moved towards the body and in front of it in the same notion as it was moved away.

For the purpose of achieving forearm rehabilitation, a single motion is being implemented within the design of the robotic structure, mainly forearm pronation/supination.

- 1) **Forearm pronation/supination.** For this motion the patient must hold the arm parallel to the body, while keeping the elbow flexed at a 90 degrees. The pronation/supination is obtained by rotating the hand around the midline of the forearm.

As mentioned before, a sampling procedure was carried out on patients from the Municipal hospital of Cluj-Napoca. Measurements (i.e. goniometry performed by the kineto-therapist on post stroke subjects) were made on 21 patients (11 females and 10 males), ranging between the ages of 43 years and 83 years. The measurements taken are showcased in Table 5.17.

Table.5.17. Mean angular amplitudes measured on patients

Joint_Side_Movement	Mean	Std.Error	Std.Dev.
Shoulder_R_FL	93.75	2.32	10.38
Shoulder_L_FL	98.3	3.28	14.68
Shoulder_R_EXT	48.67	3	12.73
Shoulder_L_EXT	48.78	2.62	11.1
Shoulder_R_ABD	89.15	1.69	7.57
Shoulder_L_ABD	90.9	2.03	9.07
Shoulder_R_ADD	24.55	2.08	9.3
Shoulder_L_ADD	25.3	1.78	7.95
Elbow_R_PRON	81.1	3.33	14.89
Elbow_L_PRON	77.75	2.95	13.21
Elbow_R_SUP	81.55	3.91	17.48
Elbow_L_SUP	84.55	2.08	9.31

Legend: FL-flexion; EXT-extension; ABD-abduction; ADD-adduction; PRON- pronation; SUP-supination; R-right arm; L-left arm; Std.Error-Standard error; Std.Dev.-Standard Deviation

It should also be mentioned that while achieving **the flexion motion**, upon **surpassing a 90-98 degrees amplitude**, the patient, depending on whether the left or right limb is used, **has to begin the pronation/supination motion of the forearm**, in order to make sure that the muscles actuating the shoulder joint does not suffer unnecessary strain.

2.2 Kinematic representation of the ASPIRE robotic system

The ASPIRE robotic system is a 3 DOF spherical robot with hybrid architecture (with spherical motion of the moving platform guided by a parallel mechanism and a rotation of the moving platform around its O'X' axis – Fig. 5.3). The kinematic scheme of the robot is presented in Fig. 5.3. with the general representation in Fig. 5.3.a and the mechanism representation in Fig. 5.3.b. A fixed coordinate frame OXYZ is defined at the centre of the spherical motion with Z axis pointing up (vertically)

and the X axis pointing in front of the patient. Consequently Z and Y axis are the rotation axes of the two active joints q_1 and q_2 . The ASPIRE spherical robot is composed of 2 kinematic chains, kinematic chain 1 (KC_1 actuated by q_1) which will perform the motion of abduction/adduction around the shoulder, and kinematic chain 2 (KC_2 actuated by q_2) which will perform the motion of flexion/extension around the shoulder. The two kinematic chains are geometrically represented by geodesic curves on the sphere that defines the motion, and intersect at the origin of the moving platform coordinate frame $X'Y'Z'$ at a distance R as shown in [BIR 18]. It should be noted that when the two kinematic chains are actuated, the angle between the geodesics (G_1 and G_2) changes, which makes it necessary to have a rotation motion between the two kinematic chains (r_f). The third rotation actuated by q_3 (which has the same rotation axis as r_f) is introduced to maintain the orientation of the arm during the rehabilitation exercise and to allow the pronation/supination of the forearm (around the elbow joint).

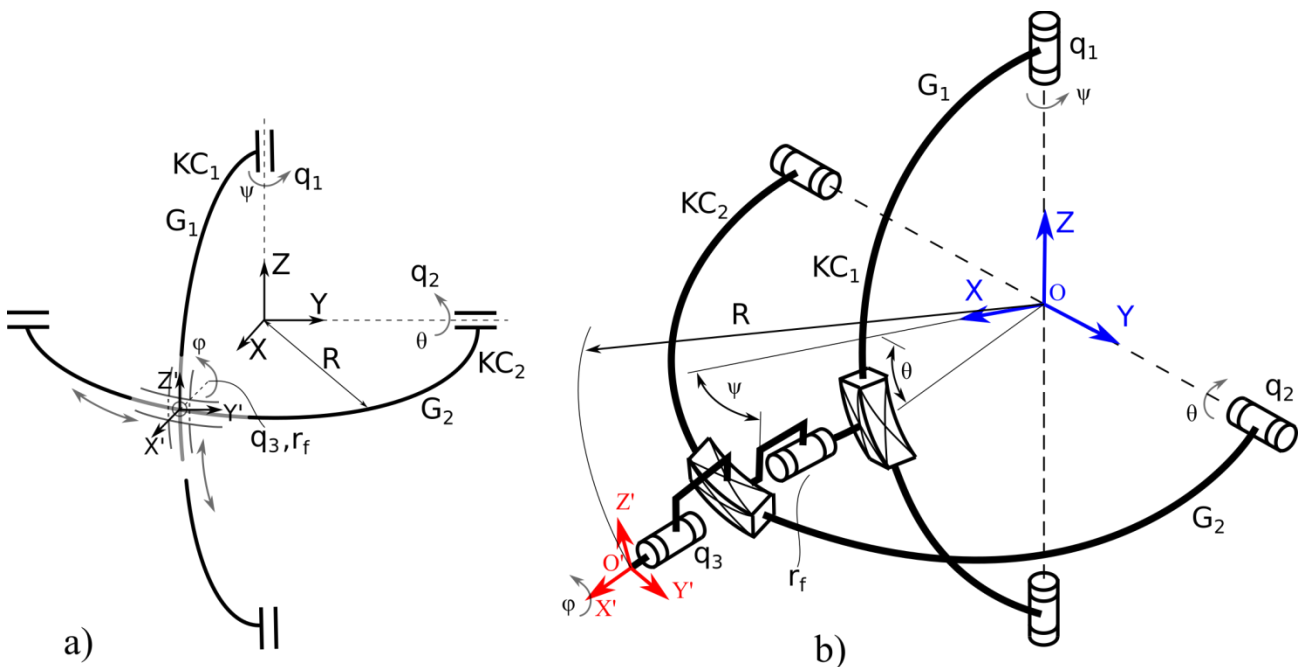


Figure 5.3. Kinematic scheme of the ASPIRE parallel robot

The advantages of the 3-DOF ASPIRE parallel robot over the 2-DOF one which has a free rotation at the intersection of the 2 kinematic chains previously introduced in [PLI18] are: **i)** it allows fine control over the flexion/extension, abduction/adduction exercises of the arm by controlling the forearm orientation (which reduces the risk of injury), and **ii)** it allows the pronation/supination of the forearm (which is also part of upper limb rehabilitation exercise).

Kinematic modelling of the ASPIRE robotic system – a methodical approach

The kinematic modelling and singularity conditions are two important aspects in robotics since they allow motion control based on the kinematic equations, and avoid specific configurations (singularities), where the robot loses control by gaining or losing one or more DOFs. The mathematical modelling of these problems greatly benefits the safety of using the robotic structures, especially when they are designed for medical purposes. This section presents the mathematical modelling of the ASPIRE robot structure starting from the kinematic modelling, followed by deriving the singularity conditions from the kinematic models.

ASPIRE kinematic model

The kinematic model was derived in Cartesian coordinates. The motion of the moving platform coordinate system $O'X'Y'Z'$ relative to the fixed coordinate system $OXYZ$, is constrained by the two geodesic curves G_1 and G_2 (see Fig. 5.3) defining the kinematic chains KC_1 and KC_2 . Each geodesic is contained in a plane; the plane equations for each geodesic curve intersect in a line (which is actually the radius R):

$$\begin{cases} P_1 : \sin(q_1)x + \cos(q_1)y = 0 \\ P_2 : \sin(q_2)x + \cos(q_2)z = 0 \end{cases} \quad (5.1)$$

with P_1 intersecting OZ axis and P_2 intersecting OY axis. By adding the final constraint equation, the sphere equation centered in the origin of the fixed coordinate frame and radius R ($x^2 + y^2 + z^2 = R^2$) and by solving Eq. 5.1 for x' , y' , z' (using the Maple software) the coordinates of the moving platform origin are obtained:

$$\begin{cases} x' = \sqrt{\left(\frac{1}{\sin(q_2)^2 \cdot \cos(q_1)^2 + \cos(q_2)^2 \cdot \sin(q_1)^2 + \cos(q_2)^2 \cdot \cos(q_1)^2} \right)} \cdot \cos(q_1) \cdot \cos(q_2) \cdot R \\ y' = \sqrt{\left(\frac{1}{\sin(q_2)^2 \cdot \cos(q_1)^2 + \cos(q_2)^2 \cdot \sin(q_1)^2 + \cos(q_2)^2 \cdot \cos(q_1)^2} \right)} \cdot \sin(q_1) \cdot \cos(q_2) \cdot R \\ z' = -\sqrt{\left(\frac{1}{\sin(q_2)^2 \cdot \cos(q_1)^2 + \cos(q_2)^2 \cdot \sin(q_1)^2 + \cos(q_2)^2 \cdot \cos(q_1)^2} \right)} \cdot \sin(q_2) \cdot \cos(q_1) \cdot R \end{cases} \quad (5.2)$$

Eq. 5.2 represents only one of the two resulted solutions (since the line computed from the intersection of P_1 and P_2 will in fact intersect the sphere in two points). However, only this solution is of interest due to the mechanism intended

functionality (Fig. 5.3 shows the mechanism working with positive values of X). Furthermore, Eq. 5.2 describes the constraints of the mechanism in the flexion/extension and abduction/adduction motions of the shoulder joint. To add the pronation/supination motion of the forearm, the angle between the two geodesics (and P_1 , P_2 respectively) must be considered. Let α be the angle of the pronation supination of the forearm (dependent on the active joint q_3). Due to the ever-changing angle (β) between the two geodesics (at the actuation of q_1 and q_2), the angle α is computed as:

$$\alpha = q_3 + \beta \quad (5.3)$$

where:

$$\beta = \arccos\left(\frac{\mathbf{v}_1 \cdot \mathbf{v}_2}{\|\mathbf{v}_1\| \cdot \|\mathbf{v}_2\|}\right) \quad (5.4)$$

With \mathbf{v}_1 being a vector normal to the plane containing G_1 , and \mathbf{v}_2 being a vector normal to the plane containing G_2 :

$$\begin{aligned} \mathbf{v}_1 &= \sin(q_1)\vec{i} + \cos(q_1)\vec{j} \\ \mathbf{v}_2 &= \sin(q_2)\vec{i} - \cos(q_2)\vec{k} \end{aligned} \quad (5.5)$$

Eq. 5.2 and 5.3 represent the constraints of the moving platform origin and are dependent on the active joints q_i . By setting $q_i = q_i(t)$ the time derivatives may be computed obtaining thus the kinematic equations for velocities and accelerations.

Singularities within the robot workspace

The singularity conditions are derived based on the kinematic model presented so far. A Jacobian may be computed from 2 out of the 3 equations from Eq. 5.2 (only 2 equations are needed since there is a dependency between the 3). For our computation Y' and Z' coordinates are used and a Jacobian is computed by differentiating with respect to q_1 and q_2 :

$$J = \begin{vmatrix} \frac{\partial y'}{\partial q_1} & \frac{\partial y'}{\partial q_2} \\ \frac{\partial z'}{\partial q_1} & \frac{\partial z'}{\partial q_2} \end{vmatrix} \quad (5.6)$$

Computing the determinant yields the singularity conditions for the ASPIRE robotic structure (a singularity occurs when the determinant vanishes):

$$R = 0 \quad (5.7)$$

$$\cos(q_1) = 0 \quad (5.8)$$

$$\cos(q_2) = 0 \quad (5.9)$$

Eq. 5.7 implies that the robot is in singular configuration when the radius of the sphere is 0 (which is physically impossible). Eq. (5.8) – (5.9) implies that singularities occur when q_1 and/or q_2 have a value of $\pm\pi/2$ (poses at the edge of the workspace according to Fig.5.3 and should be avoided by mechanical constraints or active joint stroke limits).

Fig. 5.3 illustrates the relevant singularities in the ASPIRE robot workspace. When one of the active joints q_1 or q_2 are actuated by $\pm\pi/2$ the robot loses one DOF which corresponds to a gimbal lock. When both active joints q_1 and q_2 are actuated by $\pm\pi/2$ the moving platform acquire self-motion (the robot becomes totally uncontrollable which may harm the patient).

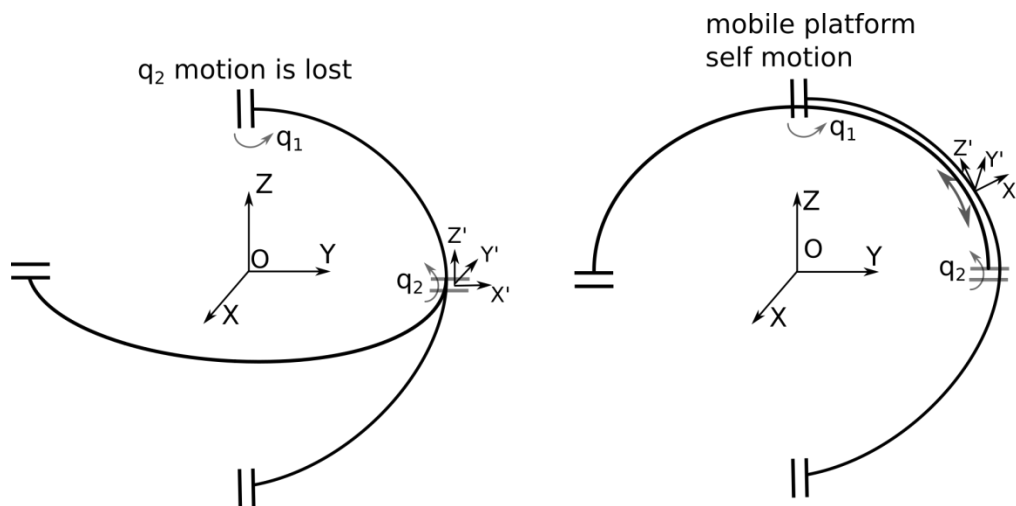


Fig. 5.3. Singular poses for the ASPIRE robotic structure

Preliminary design of the ASPIRE robot

The ASPIRE robotic rehabilitation device has adopted a parallel structure with a spherical architecture. The reasoning behind this comes firstly from the fact that the rehabilitation motion amplitudes that need to be used on the patients have to be accurate, assuring that the patient's joints limits are not surpassed, as this could lead to unwanted muscular strain and/or tissue damage (it should be noted that the muscular structure of the patient can be weakened after a stroke). Secondly, due to the fact that all of the joint motions targeted by the system can be equated via the usage of rotation joints, it was determined that the complexity of the design of the device can be kept at a minimum, by adopting a spherical structure, this in turn would also accommodate the implications of a parallel structure outputting a high

precision of motion. Furthermore, as some patients suffer from complete loss of muscle control, the architecture must be able to support the entire limb weight with anchor points for each body segment, including the hand.

Initially, two different versions of the ASPIRE structure have been modelled using 3D CAD software. One of these is aimed towards choosing a less demanding actuation solution, and the other towards providing greater user friendliness.

The initial design of the ASPIRE robot included only the two rotation joints targeting the shoulder joint motions, but as it was mentioned before, fully executing the flexion of the shoulder above a certain angular value, requires an additional rotation to be introduced under the form of forearm pronation/supination. As a result a third rotational joint was introduced, which not only enables the flexion to be carried fully and correctly but it also allows the device to achieve another rehabilitation motion at the level of the forearm. The addition of the third rotation joint also enabled the necessity of making several modifications and additions to the device structure, mainly in the form of new gripping elements for each of the upper limb segments. Initially within the system, the arm would have to be maintained in a stretched position, with the proximal part of the forearm serving as the active anchor and the back of the shoulder joint serving as the support anchor. Following the addition of the third joint, two new gripping points are added, and these are located on the wrist and respectively the hand, between the thumb and the fingers. Following further analysis the addition of more gripping points also improves the patient's experience with the device overall, as the arm is more safely secured within the device, and the additional mobility of the arm due to the added joint can confer a more natural motion to the human arm.

The two ASPIRE solutions

Following the medical and demographic data analysis, mentioned in previous sections, it is quite clear that rehabilitation devices are becoming a necessity. Despite that, currently there are no standards that define the system characteristics, safety conditions and behaviour of such a device. For this purpose an ISO standardization is under development at this moment with the code IEC/CD 80601-2-78, but until finished we have to rely on other methods of defining the characteristics that will influence the design of the robot. Therefore, several aspects that are considered important to the development process have been assessed in [VAI 17] and these have led to the development of two robotic structures (Fig.5.4).

One important aspect that needs to be mentioned is how the integration of the patient within the robotic structure affects the overall structure of the device. Due

to the large diameter of the arm and as a result the guided platform, it is impossible to maintain the alignment of the axes (as opposed to a single point on the surface of the sphere), as such it was observed that a rotation between the two axes needs to be permitted. The following two versions of the device will present two methods of maintaining axis alignment for this particular robot.

The first version of the robot has what can be defined as a closed architecture. The alignment of the axes is achieved via a modification in the guiding element, as this is no longer unitary but divided in two different components (Fig. 5.4.a), each one attached to its corresponding spherical rail. During motion these two components rotate relative to each other thus maintaining the collinearity of their axes as well as alignment between the vertical and horizontal axes of the shoulder joint.

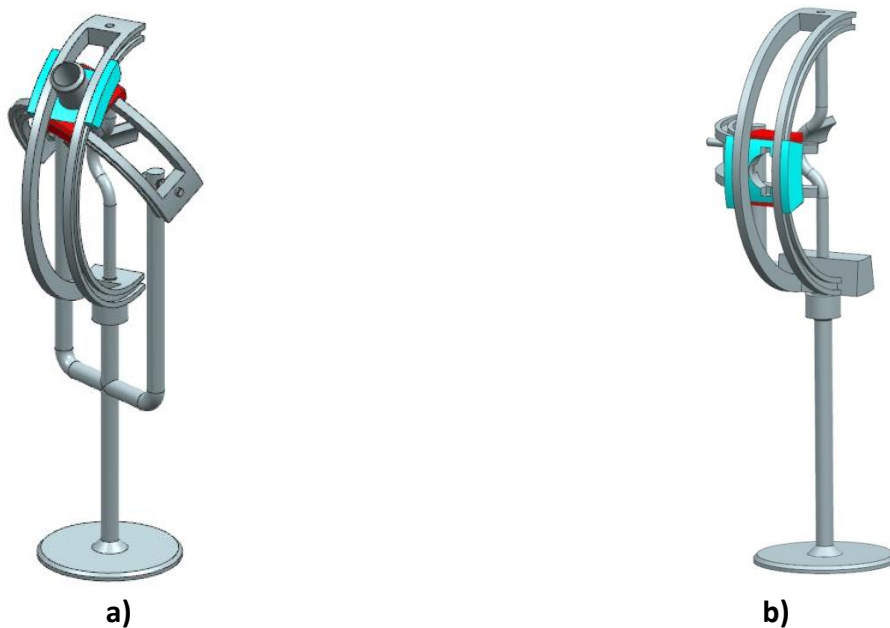


Figure 5.4 The two ASPIRE versions. a) closed version; b) open version.

The closed design also permits the actuators responsible for the shoulder motions to maintain their position during operation as such the only actuator related masses and forces that need to be taken into consideration during motion are the pronation/supination motor generated ones.

The second version of the ASPIRE device (Fig.5.4.b) adopts a more open design. This form of the robot approaches the axis alignment problem by rotating the entire assembly around the vertical axis as such the horizontal axis keeps its position relative to the vertical one, at all times. This modification to the design also permitted the horizontal guide to be reduced in size considerably, almost by half, as such the robot design has become relatively one sided. This has permitted the modification of the arm gripping elements in order to allow easier patient mounting and offer the device a more user friendly design by removing as many obstructive elements from the patient's field of view. One disadvantage that this version

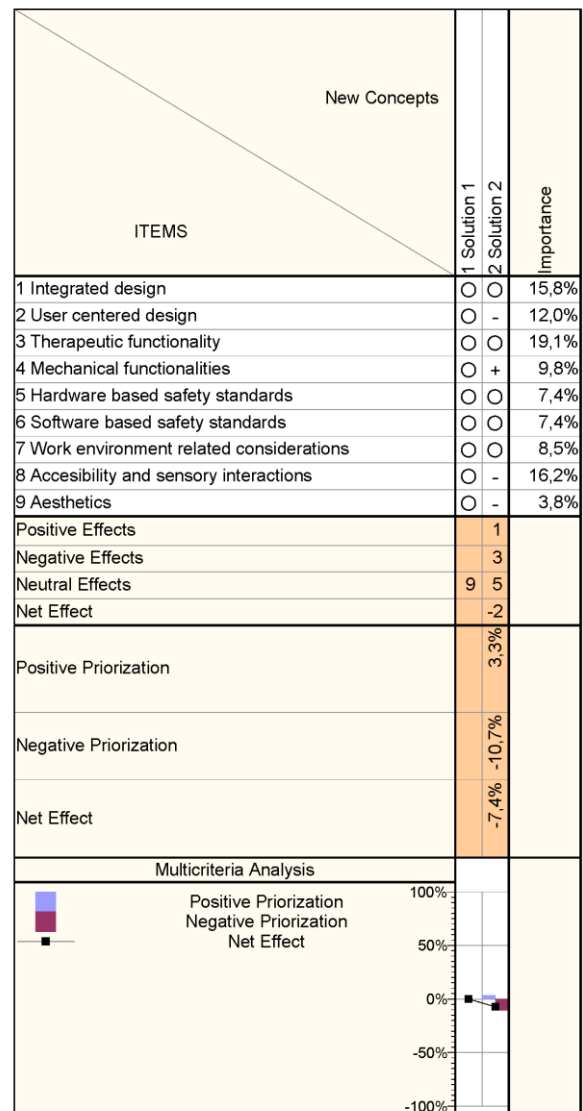
presents as it is compared to the first one has to do with its actuators, and how these will be affected by the new modifications. Due to the fact that the vertical rotation motion includes all of the device's components aside from support elements, the actuator responsible for this respective motion will have to handle a greater load overall when compared to the previous version where it only needed to carry the guide, the mobile platform, the human arm and the gripping elements, as opposed to all that plus the horizontal guide and its associated elements.

Another advantage of the open structure is that its open design will allow the medical specialist to have easier access to the patient and visual confirmation of the patient's wellbeing, and the execution of the rehabilitative motions during operations, as one side of the patient is permanently visible, with the gripping zones being the only portions of the human body that are obstructed.

Group:	Top Level ITEMS	Output	Completed:
	AHP Toplevel Matrix 1		<input checked="" type="checkbox"/>
	9 9,00 an order of ... ¼ 0,14 demonstrat...		
	8 8,00 absolutely ... ¼ 0,13 absolutely l...		
	7 7,00 demonstrat... ¼ 0,11 an order of ...		
	6 6,00 demonstrat...		
	5 5,00 essentially ...		
	4 4,00 essentially ...		
	3 3,00 considerabl...		
	2 2,00 twice as im...		
	+ 1,50 somewhat ...		
	○ 1,00 Equally imp...		
	- 0,67 somewhat l...		
	½ 0,50 half as impo...		
	¼ 0,33 clearly less ...		
	¼ 0,25 essentially l...		
	¼ 0,20 essentially l...		
	¼ 0,17 demonstrat...		
		1 Integrated design	
		2 User centered design	
		3 Therapeutic functionality	
		4 Mechanical functionalities	
		5 Hardware based safety standards	
		6 Software based safety standards	
		7 Work environment related considerations	
		8 Accessibility and sensory interactions	
		9 Aesthetics	
		Importance in group	
Input	1 Integrated design	○ ○ + 2 2	14,1%
	2 User centered design	○ ○ + + 0 0	11,7%
	3 Therapeutic functionality	○ ○ + + 2 2	16,2%
	4 Mechanical functionalities	○ ○ ○ ○ + + 3 3	10,3%
	5 Hardware based safety standards	○ ○ ○ ○ - - +	8,7%
	6 Software based safety standards	○ ○ ○ ○ - - +	8,7%
	7 Work environment related considerations	○ ○ ○ ○ + ½ 2	9,4%
	8 Accessibility and sensory interactions	○ ○ ○ ○ + 2	14,4%
	9 Aesthetics	○ ○ ○ ○ + 2	6,4%



ITEMS	Importances	Calculated Importa...	Final importance %
1 Integrated design		14,1%	15,8%
2 User centered design		11,7%	12,0%
3 Therapeutic functionality		16,2%	19,1%
4 Mechanical functionalities		10,3%	9,8%
5 Hardware based safety standa...		8,7%	7,4%
6 Software based safety standards		8,7%	7,4%
7 Work environment related con...		9,4%	8,5%
8 Accessibility and sensory intera...		14,4%	16,2%
9 Aesthetics		6,4%	3,8%
Most important item:		16,2%	
Least important item:		6,4%	



(a) Importance

(b) Multicriteria analysis of the two versions

Figure 5.5. Assessment of the two ASPIRE conceptual solutions

In terms to accomplishing the rehabilitation of the upper arm safely and efficiently, both versions are on par with each other but as mentioned before, these devices have several differences between themselves. In [VAI17] a set of nine (9) technical characteristics required by a robotic structure for rehabilitation were weighted, with respect to the application, their final importance being a criteria of structure efficiency. Figure 5.4.a illustrate the obtained results that have been used to compare the two conceptual solutions proposed for ASPIRE using the Pugh selection criteria. (Fig. 5.4.b). Assessing with neutral effect the first solution a comparison of each individual characteristic has been made with respect to the second one. Thus, the closed version has lower aesthetics, provides less accessibility and makes the use of an external sensor system more difficult but due to its architecture it has better mechanical functionalities based on the even distribution of loads. The final result point out that the first solution is more efficient for robotic rehabilitation and will represent the starting point for the development of the constructive model of ASPIRE but the final design will provide also a solution of the uneven load distribution while keeping the architecture opened.

Numerical simulations for the ASPIRE robot – An exercise oriented trajectory

This section presents numerical simulations for the ASPIRE proposed models. The motion ranges of both models is the same, i.e. both moving platforms are constrained on a sphere with same radius. Consequently the kinematics (the dependency of the moving platform position relative to the active joints) is the same. Four sets of coordinates were chosen (for both the proposed module) based on spherical values. The motivation is that the spherical motion definition (using angular values rather than Cartesian coordinates for the TCP) has a direct correspondence with the way the medical experts will define a therapeutic exercise:

$$(A): \begin{cases} \psi_A = 0^\circ \\ \theta_A = 0^\circ \end{cases}; (B): \begin{cases} \psi_B = -30^\circ \\ \theta_B = 30^\circ \end{cases}; (C): \begin{cases} \psi_C = -30^\circ \\ \theta_C = -60^\circ \end{cases}; (D): \begin{cases} \psi_D = 60^\circ \\ \theta_D = 30^\circ \end{cases} \quad (5.10)$$

As the motion is performed on the surface of the sphere, the angle and arc length can be computed using the following equations (illustrated for the A-B motion):

$$\begin{cases} DX = \cos(\theta_B) \cdot \cos(\psi_B) - \cos(\theta_A) \cdot \cos(\psi_A) \\ DY = \cos(\theta_B) \cdot \sin(\psi_B) - \cos(\theta_A) \cdot \sin(\psi_A) \\ DZ = \sin(\theta_B) - \sin(\theta_A) \end{cases} \quad (5.11)$$

Thus resulting that:

$$\begin{cases} \alpha = 2 \cdot \text{asin} \left(\frac{\sqrt{DX^2 + DY^2 + DZ^2}}{2} \right) \\ l_\alpha = R \cdot \alpha \end{cases} \quad (5.12)$$

The motion time is computed based on the angle and imposed maximum speed and calculated acceleration in order to achieve a trapezoidal profile for the speed:

A) Maximum speed is achieved, resulting in a three stage motion having the time intervals denoted with t_1 – acceleration time, t_2 – motion time until deceleration, t_3 – full motion, and their corresponding equations for the acceleration value:

$$t_1 = \frac{\omega}{\varepsilon}; \quad t_2 = \frac{|\alpha|}{\omega}; \quad t_3 = \frac{|\alpha|}{\omega} + \frac{\omega}{\varepsilon} \quad (5.13)$$

$$\varepsilon_\psi = \frac{\psi_B - \psi_A}{2 \cdot t_1 \cdot t_3 - t_1^2 - (t_3 - t_2)^2}; \quad \varepsilon_\theta = \frac{\theta_B - \theta_A}{2 \cdot t_1 \cdot t_3 - t_1^2 - (t_3 - t_2)^2} \quad (5.14)$$

The trajectory from point to point was computed with an angular velocity $\omega = 10^\circ / s$ and an angular acceleration of $\alpha = 5^\circ / s^2$ for a period of $t = 30s$. The variation of the active joints, velocity, and acceleration, as well as the arc length variation, and the Cartesian displacement is illustrated in Fig. 5.6.

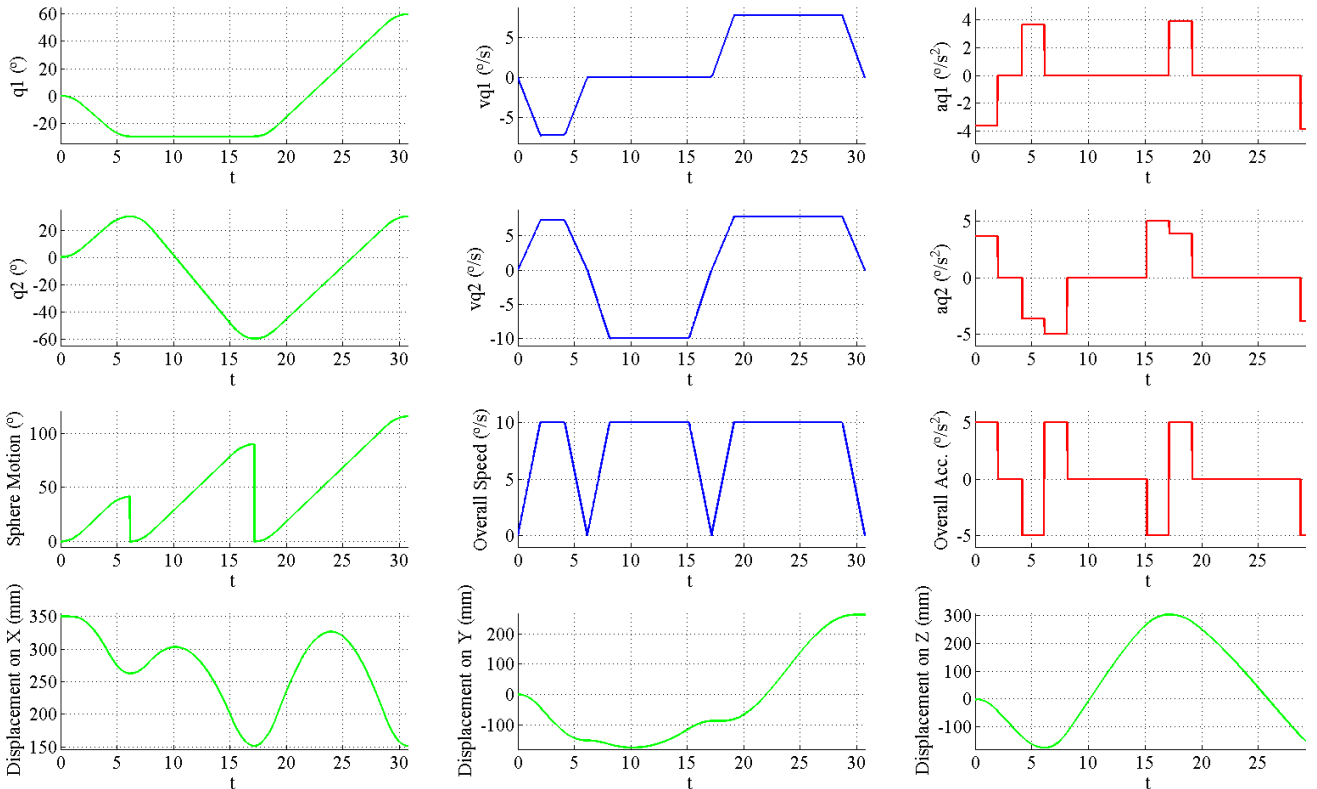


Fig. 5.6. Motion simulation of the Aspire robot

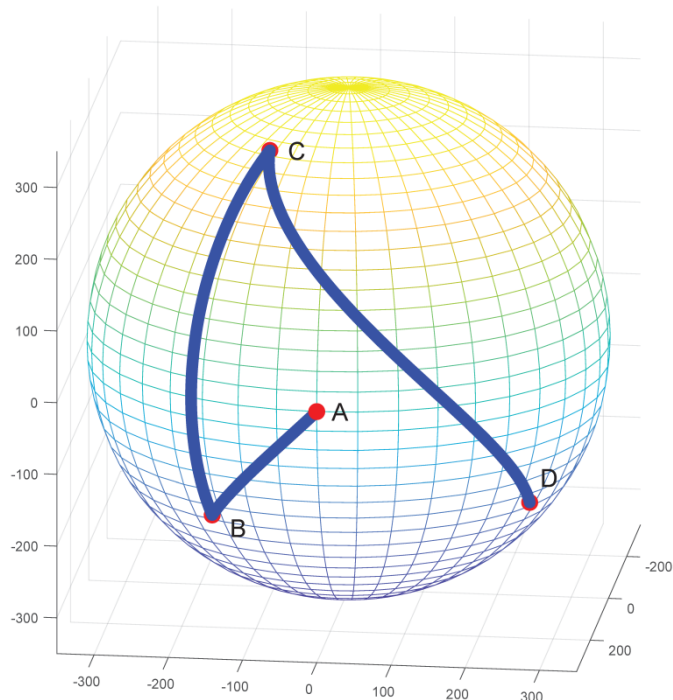


Figure 5.7. Trajectory representation on the sphere

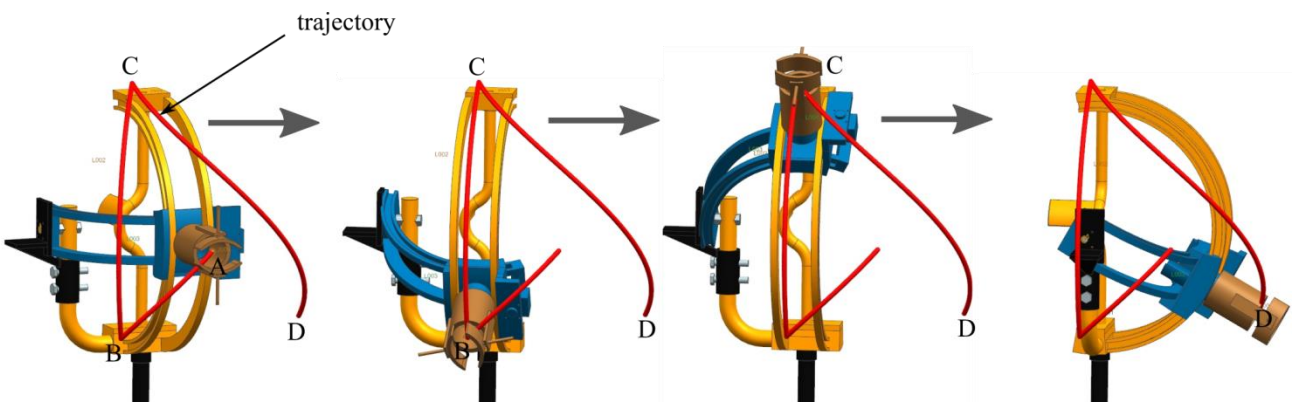


Figure 5.8. Siemens NX trajectory simulation for the open architecture ASPIRE module

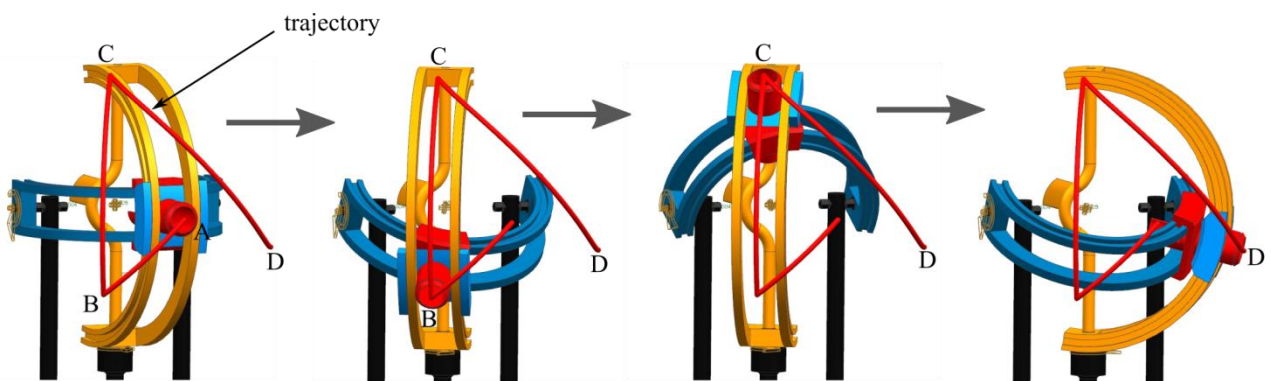


Figure 5.9 Siemens NX trajectory simulation for the closed architecture ASPIRE module.

The corresponding motion on the sphere is presented in figure 5.7. The computed trajectories were validated with Siemens NX software, and they are illustrated for both ASPIRE modules (Fig. 5.8 for the open module, and Fig.5.9 for the closed module).

In the end...

Robotic assisted rehabilitation is a critical field of research which will become increasingly integrated as a common therapeutic practice in the next decade due to the natural age shifting of the population, where the role of the physical therapist will shift from the performing of the exercises with each patient to the development, programming and setup of personalized treatment plans for the post-stroke patients, thus **defining a new paradigm in this medical field.**

Research will have to address also safety issues which relate to the possibility of using such devices without the physical presence of a medical expert whereas any improper setup can lead to harming the patient without even realising it.

The simple setup and the possibility of adapting a robotic device to an as high as possible percentage of the population will enable the large scale use of such a system increasing also the acceptance, enlarging the patient database, improving and optimizing the exercises.

Whether we like it or not, in 10 to 15 years a change will have to be made in the post-stroke patient management and until then researchers will have to deliver mature, tested, validated and more importantly efficient solutions that will have a positive impact on the quality of life of the post-stroke patients.

Chapter 6. Some final thoughts

“Scientists have become the bearers of the torch of discovery in our quest for knowledge” (Stephen Hawking)

Scientific, professional and academic career development

Personally, I consider that the **Habilitation** title represents an important step in my academic career, an element that certifies the reach of a level of maturity from scientific point of view, when younger scientists, at the beginning of their research activity will rely on my experience to complete their doctoral studies. This title honours me and in the same time obliges me to a continuous evolution in research and education. As a personal opinion, as member of a research centre, I placed the two terms in that specific order as, in order to educate the new generation of scientific researchers in an environment connected to the social and economic current context, it is critical that us, the senior researchers to understand these realities and to find ways towards progress through **research** but also to have the skills and wisdom to communicate them to our younger colleagues through **education**.

Regarding the research activity I would like to continue to work on the topics that defined my development in the last 15 years, namely robotics in medicine. With respect to the above, I commit myself to contribute to the continuous development and evolution of the CESTER Research Centre through:

- ✓ Continuous study and development of the research topics of interest at European level in the field of medical robotics;
- ✓ The dissemination of research results with valuable original contributions in prestigious journals and scientific conferences;
- ✓ Identification and active involvement in attracting research funds through national and European projects that will provide the necessary funds to achieve valuable research results;
- ✓ Achievement of new competences and skills in the development of parallel robots;
- ✓ Improvement of the communication skills at scientific and personal level.

As the next step in my personal evolution I look forward towards the fulfilment of my moral duties as a future PhD coordinator and learn how to guide young engineers in their pursuit to become scientific researchers.

Academic development plan

As members of the academic staff of one of the most prestigious Technical Universities in Romania, we are committed to contribute to its evolution but also to the support of its role within society. Again, I find here a strong synergy between **research** and **education**. The evolution and progress of our University is supported through recognized results in **research** achieved by its members but its main role towards society is the **education** of new generations of engineers. So, through

research we remain connected towards the current societal needs being thus able to **educate** the young in the right direction.

Personally, with respect to my academic development I commit to:

- ✓ Continuously improve my teaching skills to create an attractive and stimulating environment for the students;
- ✓ Continuously improve my communication skills to understand the specific needs of the younger generations;
- ✓ Continuously update the contents of my lectures;
- ✓ Prepare a new didactic material for the lecture Modelling and Simulation of Robots with focus on parallel architectures;
- ✓ Learn to develop interpersonal skills in the relation with PhD students.

I will also contribute to the development of the human resource in our research centre by identifying bachelor and master students with aptitudes and passion for research and their integration in our structure as apprentices, young researchers and later on PhD students.

Scientific and professional development plan

As a member within CESTER since the beginning of my PhD studies I always valued research considering it a cornerstone in the evolution of society. As a natural consequence, valuing also the Continuous Learning paradigm, I will work towards improving my knowledge in:

- ✓ Kinematic modelling of parallel robots;
- ✓ Design optimization approaches;
- ✓ Autonomous systems;
- ✓ Internal and external sensors;
- ✓ Control and information flow.

Professionally I must learn to find a balance between everything valuable in life because this equilibrium will not only enable me to focus on all aspects of life but also to be more efficient in each of them.

The Organization of Economic Cooperation and Development estimates that by 2020 the knowledge stock will double each 73 days. In this context, we, as teachers for the young generations will have to commit ourselves to a continuous evolution, to educate the future engineers in an evolving world, where education becomes both factor and effect. And the key towards high level education in engineering is research. And research must be the outcome of passion, stubbornness, denial of fail and continuous evolution.

Some closing remarks

It seems that this book, this thesis, this collection of ideas, this summary of years of work, has reached its **inevitable end...**

An End which is also *A Beginning* as it represents the commitment of responsibility towards the younger generation of researchers which aim towards perfecting themselves, towards the creating of knowledge, towards the quest of discovery.

It took me a while to decide how should I end this work, and I've decided that everyone who had the curiosity and patience to reach this part is entitled to some sincere words about **Research** regarded as **a Beauty** and **a Beast**.

I've always considered that *Impossible is Nothing*, but I have realized that I don't have the necessary personal abilities to change the system, as this implies a good knowledge of politics and the mastering of the art of compromise. So I will try to express my beliefs and my thoughts with hope that someone will take up the fight and create a better environment for us, the researchers.

The dark side of research

Our greatest adversary in our quest towards new discoveries is **time**. Why is that so? Because, in the current system we dedicate much to less **time** for the actual research while investing too much effort in side quests with little to none added value but unfortunately necessary for our survival.

In order to be able to do research one needs resources, both human and material and the value of these resources will have an impact on the quality of research. Of course, this means that one needs to fight for these resources and dedicate **time** to receive them. This means that one needs to invest **time** in *attracting funds* (that will improve the material resource) and *educate the younger generation* (that will improve the human resource). But this is not the issue here. The real problem(s) refer to accessibility for these resources.

The sub-financing level of research

Our country still trails way behind Europe (I don't even want to mention USA or Japan) regarding the amount of money invested in research. Putting the personal well-being in front, slowly but steadily we managed to destroy our industry followed closely by the national network of research institutes which represented the bridge between universities and industrial companies the two sides complaining very often that "*universities are doing research without relevance for the industry*" and "*the industry is just production without innovation*". The funding of research has also

decreased creating a **hunger** and many times transforming **collaboration** into **competition** between groups of researchers. But all these things are well-known, many choosing not to speak about them, however the question that arises is: **What can we do? Should we just criticise or act?**

In my opinion the big issue is the **loss of confidence and trust**. The society has lost its confidence in the capability of us, researchers, to produce added value which in the end should turn into increases revenues, the industry does not trust us, researchers, of being capable of creating industrial innovation and finally, we, the researchers, do not trust ourselves anymore for being capable of breaking the barriers of knowledge.

So, for this particular problem, I believe that is us, the researchers, who have to make the first step. We need **to become unsatisfied** with our situation and we need **to want more**. We have to regain that trust, step by step, search for new opportunities, learn, evolve and the rewards will start coming. But unless we can prove that we can provide more value for the funds we receive we will get nothing.

The brain drain and the competition with industry

As in many other fields the lower income countries are facing a big threat whereas the younger generation is attracted towards two main directions:

1. Leaving the country and work abroad for a much higher income, without a major concern on the personal development and carrier;
2. Starting to work early in a company, which in most cases, means a reduced amount of time invested in the studies, which supported also by the early income will not encourage the students to pursue a carrier in research.

The companies are, of course, interested in attracting the best students because a good worker will have a greater added value for the company while the mirage of working abroad is a generalized problem in all the countries from Central and East Europe.

What can we do? Should we just watch passively and complain that we cannot get good students to work in research anymore?

Again, I think that this matter is completely in our hands. We should **fight fire with fire**. **The companies advertise their jobs? We can do the same**. We can also find, with the help of the university and research grants, means to **provide a financial benefit** for the young students even before they graduate.

In my opinion there is no greater satisfaction for an engineer than to see something real and functional coming out as a result. So, by carefully integrating students in our teams, encourage them to do their master studies (in an active way) we have a great chance of having skilled, competent and I would say even a bit experienced PhD students that will generate, of course, greater added value for the research.

The paperwork around the research activities

I have reached now what I consider to be the greatest thread against our efficiency in research. In the last 5 years the amount of paperwork that needs to be prepared in more and more complicated ways has increased multiple times, consuming a lot of time and adding a continuous frustration. After being awarded a grant (where theoretically the financing authority has decided to **trust** a certain team in their capability of generating innovation through the awarded funds), a researcher must become an expert accountant, human resources manager and a public acquisitions specialist. Everyone working as a senior researcher in a grant understands this frustration.

What can we do? I believe that here we need institutional help. And I don't refer here to assistance in preparing the paperwork, but rather in a paradigm change where there will be less restrictions and more trust. Once a grant is awarded the manager should be allowed to perform the assumed tasks without further justifications for each step. Just take a look at acquisitions. In research, most of the time one needs the state-of-the-art equipment which of course is produced by a certain company. But you have to go through fire and hell to get that equipment and always prepare a tonne of documentation to avoid the sharks hunting for a "deal". We are considered outlaws in case we favour the only manufacturer that meets our demands but all the shell companies that hunt these deals are never to be blamed. The persons with decisional power in both universities and research institutes could develop a joint strategy and as a whole to convince the authorities to reduce the burden of documents which has only a negative impact on the performance, available time, state of mind all leading towards lower added research value.

I started with the "*dark side*" to be able to finish in a positive manner. Why? Because I still believe that we can achieve great things, because I believe in research, I believe in our power to improve and I want to contribute to that.

I consider myself very fortunate to be part of a great team which slowly became more than a group of co-workers, more than a group of friends, it became family. Of course, families do argue, do complain sometimes, BUT they stick together and fight together for the ultimate goal: innovation through commitment, dedication, desire and joint effort.

However, behind all the criticism above, I don't see defeat I don't see despair; I see opportunity, challenge and hope that if we don't sit back, we can make things better.

Research, engineering and education

*“If we knew what it was we were doing, it would not be called research, would it?” –
Albert Einstein.*

In today’s society which is dominated by achievements, knowledge and evolution, **innovation is no longer achieved by joining desire and opportunity, but by exploiting the grey matter of the engineer behind the novelty.**

Research represents **the cornerstone of engineering** and the ultimate source of personal integration in the current trends representing maybe the most important component in the daily activity as engineers and teachers. **Research** however, must be performed with **wisdom**, awarded as a continuous effort of **self-improvement, pushing the frontiers of knowledge and denial of impossible.**

Now as an older person, I look back in time and I see all the people that have contributed to my development both as a researcher and as human being. It seems that inevitability has struck and this is the point where I have to start giving back. A good friend of mine once told me: *“In order to be a righteous man, never forget where you started from!”* In my opinion this means that once we get higher in ranks, with longer titles than the name itself, it does not mean that we are smarter or superior. All this is just the benefit of time. However what we do get is experience and this experience has to be put up for the greater good, passing the knowledge that was once given to us to the next generation, closing the circle of evolution and becoming better researchers.

With the completion of this book, I will probably be granted the responsibility of guiding other researchers in becoming specialists in a certain field showing them the meaning of research, innovation, effort and stubbornness towards the ultimate goal: making a small contribution to the evolution of knowledge in a form that society awards a PhD title for it.

This is it...

– The End –

“Nemo vir est qui mundum non reddat meliorem!”

References

“I do believe that something very magical can happen when you read a good book” (J.K. Rowling)

- ABD 14 Abdollahi F, et al: Error augmentation enhancing arm recovery in individuals with chronic stroke: a randomized crossover design. *Neurorehabil Neural Repair* vol. 28(2):120–128, 2014
- ADH 03 Adhami, L., Coste-Maniere, E.: Optimal planning for minimally invasive surgical robots. *IEEE Trans Robot Autom* 19(5):854–863, 2003
- ANG 18 Angiodynamics, <http://www.angiodynamics.com/products/what-is-rfa>, Accessed: 04.11.2018
- BAR 14 Basri, J.J.A., et al: Robot-assisted radiofrequency ablation of primary and secondary liver tumours: early experience. In: *INTERVENTIONAL, Eur Radiol* (2014) 24:79–85
- BAR 15 Basri, J.J.A., et al: Robotic-assisted thermal ablation of liver tumours. In: *INTERVENTIONAL, Eur Radiol* (2015) 25:246–257
- BAS 14 Basteris A et al.: Error augmentation enhancing arm recovery in individuals with chronic stroke: a randomized crossover design, *Neurorehabil Neural Repair* vol. 28(2):120–128, 2014
- BAS 14a Basteris, A., et al., Training modalities in robot-mediated upper limb rehabilitation in stroke: a framework for classification based on a systematic review, *Journal of NeuroEngineering and Rehabilitation*, vol. 11: 111, pp. 15, 2014
- BES 10 Bessler, M., et al.: Pure natural orifice transluminal endoscopic surgery (NOTES) cholecystectomy, *Surgical Endoscopy*, Vol. 24, pp. 2316-2317, 2010.
- BIN 14 Bingener, J., Ibtahim-zada, I.: Natural orifice transluminal endoscopic surgery for intra-abdominal emergency conditions, *Br J Surg*. 2014 Jan; 101(1): e80–e89. doi: 10.1002/bjs.9352
- BIR 14 Birsen, O. et al: A Critical Analysis of Postoperative Morbidity and Mortality After Laparoscopic Radiofrequency Ablation of Liver Tumors, *Annals of Surgical Oncology*, vol. 21(6), DOI: 10.1245/s10434-014-3526-8, 2014
- BIR 18 Birlescu, I., Vaida, C., Pisla, A., Carbone, G., Pisla, D., Singularity analysis of a spherical robot used in upper limb rehabilitation. Third Conference on Interdisciplinary Applications in Kinematics, IAK 2018. Lima, Peru, 5-7 May. 2018
- BOC 08 Boctor, E. et al: Three-dimensional ultrasound-guided robotic needle placement: an experimental evaluation, *Int J Med Robotics Comput Assist Surg*, 4(2), (2008), 180-191.
- BRA07 Bradford, J.W., et al: Technologies for Guidance of Radiofrequency Ablation in the Multimodality Interventional Suite of the Future. In: *Vasc Interv Radiol*. 2007 January ; 18(1 Pt 1): 9–24.
- BRI 17 Brierley, J.D.; Gospodarowicz, M.K.; Wittekind, Ch., eds.: *TNM classification of malignant tumours* (8th ed.). Chichester, West Sussex, UK: Wiley-Blackwell. ISBN 978-1-4443-3241-4., 2017
- CAR 06 Carbone, G., Lim, H.O., Takanishi, A., Ceccarelli, M., Stiffness Analysis of the Humanoid Robot WABIAN-RIV, *Mechanism and Machine Theory*, vol.41, n.1, pp.17-40, 2006.
- CAR 08 Carbone, G., Ceccarelli, M., Oliveira, P.J., Saramago, S.F.P., Carvalho, J.C.M., Optimum Path Planning of CaPaMan (Cassino Parallel Manipulator) by Using Inverse Dynamics, *Robotica: An International Journal*, vol.26, n.2, pp.229-239, 2008.

- CHA 13 Chang, D. T. S., Challacombe, B., Lawrentschuk, N.: Transperineal biopsy of the prostate--is this the future? *Nat. Rev. Urol.* advance online publication 24 Sept. 2013; doi:10.1038/nrurol.2013.195, 2013
- CHE 14 Chen, K.L., Chen, C.T., Chou, Y.T., Shih, C.L., Koh, C.L., Hsieh, C.L., Is the long form of the Fugl-Meyer motor scale more responsive than the short form in patients with stroke? *Arch Phys Med Rehabil.* vol. 95(5):941-9, 2014
- CLA 09 Clarke, J.R.: Designing safety into the minimally invasivesurgical revolution. *Surg Endosc* 23:216–220, 2009
- COB 15 Cobelli, O., et al. Predicting Pathological Features at Radical Prostatectomy in Patients with Prostate Cancer Eligible for Active Surveillance by Multiparametric Magnetic Resonance Imaging, *PLoS ONE* 10(10):e0139696. doi:10.1371/journal.pone.0139696, 2015
- COC 16 Cocorean, D.: Development of innovative parallel robots for brachytherapy, PhD thesis, 2016
- COL 16 Colomer, C., Noe, E., Llorens, R., Mirror therapy in chronic stroke survivors with severely impaired upper limb function: a randomized controlled trial. *European Journal of Physical and Rehabilitation Medicine*, vol. 52(3):271-8, 2016
- CON 66 Contini, R., Body Segment Parameters, Part II, *Artificial Limb*, vol. 16(1):1-19, 1966
- DAG 10 Daghia, F., Fabrizio, M., Grandi, D.: A non isothermal Ginzburg-Landau model for phase transitions in shape memory alloys. *Meccanica* 45:797–807, 2010
- DEN 46 Denoix, P. F.: Enquete permanent dans les centres anticancereaux. *Bull Inst Nat Hyg* 1946;1:70–5
- DIP 12 Dipietro L, et al: Learning, not adaptation, characterizes stroke motor recovery: evidence from kinematic changes induced by robot-assisted therapy in trained and untrained task in the same workspace. *IEEE Trans Neural Syst Rehabil Eng*, vol. 20(1):48–57 2012
- EHL 13 European Health and Life Expectancy – EHLEIS Country Reports, Issue 6 – April 2013, Health Expectancy in Romania
- EVA18 Evans, C.R., Medina, M.G. & Dwyer: Telemedicine and telerobotics: from science fiction to reality *A.M. Updates Surg* (2018). <https://doi.org/10.1007/s13304-018-0574-9>
- FIL 14 Filson, P.C., Improvement in Clinical TNM Staging Documentation Within a Prostate Cancer Quality Improvement Collaborative, *Urology*, vol. 83, <http://dx.doi.org/10.1016/j.urology.2013.11.040>, 2014
- GHE 10 Gherman B et al. (2010) Singularities and workspace analysis for a parallel robot for minimally invasive surgery. In: 2010 IEEE international conference on automation quality and testing robotics (AQTR), Cluj-Napoca, Romania
- GIU 11 Giurgiu, C., Manea, C., Crisan, N., Bungardean, C., Coman, I., Dudea, S. Real-time sonoelastography in the diagnosis of prostate cancer. *Medical Ultrasonography*, 13(1): 5-9, 2011
- GLA 02 Gladstone, D., Danells, C., Black, S., The Fugl-Meyer Assessment of Motor Recovery after stroke: A Critical Review of Its Measurement Properties. *Neurorehabil Neural Repair* 16:232-240, 2002

- GOM 12 Gómez-Bravo, F., Carbone, G., Fortes, J.C. Collision free trajectory planning for hybrid manipulators. *MECHATRONICS*, vol. 22, p. 836-851, ISSN: 0957-4158, 2012
- GOP 16 Gopura, R., Bandara, D., Kiguchi, K., Mann, G., Developments in hardware systems for active upper-limb exoskeleton robots: A review. *Robotics and Automation Systems*, vol. 75, pp. 203-220, 2016
- GRA 06 Graur, F., et al: Radiofrequency ablation of liver tumors: technique and preliminary results. In: *Chirurgia (Bucur)*. 2006;101(2) 159-167. PMID: 16752682
- GUP 05 Gupta, S. et al, Imaging-guided percutaneous biopsy of mediastinal lesions: different approaches and anatomic considerations, *RadioGraphics*, 25, (2005), 763-788
- HIM 02 Himel, H.S.: Minimally invasive (laparoscopic) surgery – the future of general surgery, *Surg Endosc* (2002) 16: 1647–1652, DOI: 10.1007/s00464-001-8275-7
- HUS 07 Husty, M. L., Pfurner, M., Schröcker, H.-P. and Brunthaler, K.: Algebraic Methods in Mechanism Analysis and Synthesis. *Robotica*, 25(6):661–675 (2007).
- HUS 08 Huston, R.L., Principles of Biomechanics, CRC Press, ISBN 9780849334948, 2008
- JIA 14 Jiang, S., Li, P., Yu, Y., Loiu, J., Yang, Z., Experimental study of needle–tissue interaction forces : Effect of needle geometries, insertion methods and tissue characteristics, *J. Biomechanics*, 45, pp. 3344-3353, 2014
- JUB 15 Jubran A.: Pulse oximetry, *BioMed Central*, 19:272, DOI 10.1186/s13054-015-0984-8, 2015
- KAM 11 Kamran, A., Patel, V. et al: The role of single-incision laparoscopic surgery in abdominal and pelvic surgery: a systematic review, *Surgical Endoscopy*, Vol. 25, No. 2, pp. 378-396, 2011.
- KAN 11 Kan, P., Huq, R., Hoey, J., Goetschalckx, Mihailidis, A., The development of an adaptive upper-limb stroke rehabilitation robotic system, *Journal of NeuroEngineering and Rehabilitation*, vol 8: 33, 2011
- KEL 01 Kelling, G.,: Die Tamponade der Speiseröhre und des magens mit beigsamen instrumenten. *Verhandlungen der Gesellschaft Deutscher Naturforscher und Aerzte*. Vogel verlag (1901), Leipzig 73, pp 117–119
- KEN 13 Kennedy, T. et al.: Laparoscopic radiofrequency ablation for the management of colorectal liver metastases: 10-year experience, *Journal of Surgical Oncology*, vol. 107(4), DOI: 10.1002/jso.23268, 2013
- KHA 14 Kharofa, J. et al., 3-T MRI-based adaptive brachytherapy for cervix cancer: Treatment technique and initial clinical outcomes, *Brachytherapy*, Vol. 13(4), doi:10.1016/j.brachy.2014.03.001, 2014
- KLA 14 Klamroth-Marganska V., et al. Three-dimensional, task-specific robot therapy of the arm after stroke: a multicentre, parallel-group randomised trial. *Lancet Neurol*. Vol.13(2):159–66, 2014
- LEE 13 Lee-Kong, S., Feingold, D.,: The History of Minimally Invasive Surgery, *Semin Colon Rectal Surg* (2013) 24:3-6
- LEE 14 Lee, Y. N. et al: Core biopsy needle versus standard aspiration needle for endoscopic ultrasound-guided sampling of solid pancreatic masses: a randomized parallel-group study, *Endoscopy* vol. 46(12), DOI: 10.1055/s-0034-1377558, 2014

- LIT 98 Litynski, G.S.: Erich Muhe and the rejection of laparoscopic cholecystectomy: a surgeon ahead of his time. *J Soc Laparosc Surg*, (1998) ,2: 341–346
- LO 12 Lo, H.S., Xie, S.Q., Exoskeleton robots for upper-limb rehabilitation: State of the art and future prospects. *Medical Engineering & Physics* vol. 34: 261– 268, 2012
- LOU 11 Loureiro, R. C. V., Harwin, W., Nagai, K., Johnson, M., Advances in upper limb stroke rehabilitation: a technology push. (Review) *Med Biol Eng Comput* vol. 29: 1103-1118, 2011
- LYL 81 Lyle, R.C. A performance test for assessment of upper limb function in physical rehabilitation treatment and research. *Int J Rehabil Res* vil.4: 483–492, 1981
- MAJ 16 Major, K.A., Major, Z.Z., Carbone, G., Pisla, A., Vaida, C., Gherman, B., Pisla, D. Ranges of motion as basis for robot-assisted post-stroke rehabilitation. *HVM Bioflux* vol;8(4):192-196, 2016
- MAR 17 Multi Annual Roadmap, https://www.eu-robotics.net/sparc/upload/Newsroom/Press/2016/files/H2020_Robotics_Multi-Annual_Roadmap_ICT-2017B.pdf
- MER 06 Merlet, J.P.:Parallel Robots. Second Edition, Kluwer, Dordrecht. 2006
- MEE 13 Meerbeeck, J.P. and Janssens, A., The seventh tumour–node–metastasis staging system for lung cancer: Sequel or prequel? *European J of Cancer Suppl.*, vol. 11(2), 2013
- MOR 09 Morvan, T. et al: Collision detection and untangling for surgical robotic manipulators. *Int J Med Robot Comput Assist Surg* 5:233–242, 2009
- MOU 96 Mouret, P.: How I developed laparoscopic cholecystectomy. *Ann Acad Med Singapore* (1996), 25: 744–747
- NEA 11 Neagos, H., Graur, F. et al.: The Contribution of Technology in Cholangiocarcinoma Treatment, *IFMBE Proceedings*, vol. 36, DOI: 10.1007/978-3-642-22586-4_39, 2011
- NII 15 Niiniluoto, I.: "Scientific Progress", *The Stanford Encyclopedia of Philosophy* (Summer 2015 Edition), Edward N. Zalta (ed.), <https://plato.stanford.edu/archives/sum2015/entries/scientific-progress/>
- NOR 14 Nordin, A., Alt Murphy, M., Danielsson, A., Intra-rater and inter-rater reliability at the item level of the Action Research Arm Test for patients with stroke. *J Rehabil Med. Sep*; vol. 46(8):738-45, 2014
- OTT 01 Ott, D.O.: Ventroscopic illumination of the abdominal cavity in pregnancy. *Z Akush Zhenskikl Boleznei*, (1901), 15: 7–8
- PER 16 Pérez-Cruzado, D., Merchán-Baeza, J.A., González-Sánchez, M., Cuesta-Vargas, A.I. Systematic review of mirror therapy compared with conventional rehabilitation in upper extremity function in stroke survivors. *Aust Occup Ther J.* doi: 10.1111/1440-1630.12342., 2016
- PET 11 Peter O., Fazekas G., Zsiga K., Denes Z. Robot-mediated upper limb physiotherapy: review and recommendations for future clinical trials. *Int J Rehabil Res*, vol. 34(3):196–202, 2011
- PET 12 Petralia, G., et al. Anterior prostatic tumours are difficult to diagnose without MRI, *Ecancermedalscience*. 6: 252, 2012
- PIS 10 Pisla, D., et al: PARAMIS parallel robot for laparoscopic surgery, *Chirurgia*, Vol. 105, pp. 677-683, 2010.

- Pisla, D., Cocorean, D., Vaida, C. (c.a.), Gherman, B., Pisla, A., Plitea, N: Application Oriented Design and Simulation of an Innovative Parallel Robot for Brachytherapy, Proceedings of the ASME 2014 International Design Engineering Technical Conferences & Computers and Information in Engineering Conference IDETC/CIE 2014, Buffalo, New York, USA, DETC2014-35047
- PIS 14
- Plagenhoef S., Gaynor Evans F., Abdelnour T.. Anatomical Data for Analyzing Human Motion. J. Research Quarterly for Exercise and Sport, vol. 54, 1983, republished on-line in 2013
- PLA 13
- Plitea, N. et al.: Innovative Development of Parallel Robots and Microrobots, Acta Tech. Napoc. Ser. Appl. Match Mech. 46(I), 15-26 (2006)
- PLI 06
- Plitea, N., Pisla, D., Vaida, C et al.: On the Kinematics of a New Parallel Robot for Brachytherapy, Proceedings of the Romanian Academy, Series A, **15**(4), 2014, pp. 354–361
- PLI 14
- Plitea N., Vaida C., Carbone G., Pisla A., Ulinici I., Pisla D. On the Kinematics of an Innovative Spherical Parallel Robot for Shoulder Rehabilitation. In: Carvalho J., Martins D., Simoni R., Simas H. (eds) Multibody Mechatronic Systems. MuSMe 2017. Mechanisms and Machine Science, vol 54. Springer, Cham, 2018
- PLI 18
- Platten, D. et al: GE LightSpeed RT CT scanner technical evaluation, Report 05070, National Health Service (NHS), 2005
- PLA 05
- Protection of Disabled Persons, Evolution in the field of Protection of Disabled Persons, 2014 Report of the Romanian Ministry of Labour
- PDP 14
- Podder, TK., et al., AAPM and GEC-ESTRO guidelines for image-guided robotic brachytherapy: Report of Task Group 192, Med. Phys. 41, 10150; <http://dx.doi.org/10.1118/1.4895013>, 2014
- POD 14
- Posteraro, F., et al: Upper limb spasticity reduction following active training: a robot-mediated study in patients with chronic hemiparesis. J Rehabil Med, vol. 42(3):279–281 2010
- POS 10
- Radu, P., et al.: Treatment of hepatocellular carcinoma in a tertiary Romanian center. Deviations from BCLC recommendations and influence on survival rate. In: Journal of Gastrointestinal & Liver Diseases. 22.3 (2013)
- RAD 13
- Rajih, E., et al: Error reporting from the da Vinci surgical system in robotic surgery: A Canadian multispecialty experience at a single academic centre, Can Urol Assoc J. 2017 May; 11(5): E197–E202.
- RAJ17
- Saumoy, M., Guenthart, B., Madanat, L., Ahaneh, C., Kahaleh, M., Robotic-assisted endoscopic full-thickness resection of a gastrointestinal stromal tumor: the tip of the iceberg. Endoscopy. 2018 Aug;50(8):E216-E217. doi: 10.1055/a-0624-1644.
- SAU 18
- Semm, K.: Endoscopic appendectomy. Endoscopy, (1983), 15: 59–64
- SEM 83
- Sharma, D.N. et al: Computerized tomography-guided percutaneous high-dose-rate interstitial brachytherapy for malignant lung lesions, J of Cancer Research and Therapeutics, vol. 7(2), 2011
- SHA 11
- Shah, C. et al.” The American Brachytherapy Society consensus statement for accelerated partial breast irradiation, Brachytherapy, Vol. 12(4), doi:10.1016/j.brachy.2013.02.001, 2013
- SHA 13

- SCH 18 Schadlbauer J., Vaida C., Tucan P., Pisla D., Husty M., Plitea N. (2018) A Complete Analysis of Singularities of a Parallel Medical Robot. In: Lenarčič J., Merlet JP. (eds) *Advances in Robot Kinematics 2016*. Springer Proceedings in Advanced Robotics, vol 4. Springer, Cham
- SNS 14 Strategia Nationala de Sanatate 2014 – 2020, Ministerul Sanatatii din Romania, 2014
- SON 11 Song D.Y., et al., Robotic needle guide for prostate brachytherapy, *Clinical testing of feasibility and performance*, *Brachytherapy*, vol. 10, pp. 57-63, 2011.
- SQU 14 Squeri, V., Masia, L., Giannoni, P., Sandini, G., Morasso, P.: Wrist rehabilitation in chronic stroke patients by means of adaptive, progressive robot-aided therapy. *IEEE Trans Neural Syst Rehabil Eng* vol. 22(2):312–325, 2014
- STR 11 Strassman G. et al: Advantage of robotic needle placement on a prostate model in HDR brachytherapy, *Strahlenther Onkol.* 187(6), (2011), 367-272
- STU1903 Study, E.: *Geometrie der Dynamen*. Teubner (1903).
- SUC 11 SuciM(2011) Contributions for the development of a new active parallel robot for minimally invasive surgery. PhD thesis, Cluj-Napoca, Romania, 203 pp
- TAY 95 Taylor, R. H. et al: A Telerobotic Assistant for Laparoscopic Surgery, *IEEE Engineering in Medicine and Biology*, 1995,14: 279-287.
- TIL 14 Tilborg, Van M. et al.: Long-term results of radiofrequency ablation for unresectable colorectal liver metastases: a potentially curative intervention, *The British Journal of Radiology*, vol. 84 (1002), <http://dx.doi.org/10.1259/bjr/78268814>, 2014
- TRE 07 Trejos, A.L., Patel, R.V., Ross, I. et al: Optimizing port placement for robot-assisted minimally invasive cardiac surgery. *Int J Med Robot* 3(4):355–364, 2007
- TUC 18 Tucan, P., Development of new parallel robots for prostate biopsy, PhD Thesis, Technical University of Cluj-Napoca, Romania, 2018
- VAI 09 Vaida C (2009) Contributions to the development and kinematic-dynamic modeling of parallel robots for MIS. PhD thesis, Cluj-Napoca, Romania, 213 pp
- VAI 11 Vaida, C., Plitea, N., Pisla, D., Gherman, B., Suci, M.: Orientation module with modular structure with multiple curvatures. Patent pending no. A10113/2011, Romania
- VAI 12 Vaida, C., Gherman, B., Pisla, D., Plitea, N.: A spherical robotic arm for instruments positioning in minimally invasive medical applications, *The 2nd IFToMM Asian Conference on Mechanism and Machine Science* November 7 -10, 2012, Tokyo, Japan
- VAI 12a Vaida, C. et al: Family of spherical robots for minimally invasive medical applications, patent pending no A10213/2012.
- VAI 13 Vaida, C., Gherman, B., Pisla, D., Plitea, N., A CT-Scan compatible robotic device for needle placement in medical applications, (2013) In *Advanced Engineering Forum*, Trans Tech Publications, pp. 574-583, DOI 10.4028/www.scientific.net/AEF.8-9.574
- VAI 16 Vaida, C., Pisla, D., Schadlbauer, J., Husty, M., Plitea, N: Kinematic Analysis of an Innovative Medical Parallel Robot using Study parameters, *New Trends in Medical and Service Robots. Mechanisms and Machine Science*, vol 39. Springer, Cham, 2016
- VAI 17 Vaida C et al.: On Human Robot Interaction Modalities in the Upper Limb Rehabilitation After Stroke Patients, *Acta Tehnica Napocensis, Series AMMM*, vol. 60(1):91-102, 2012

- VER 12 Verma, S. et al: Overview of Dynamic Contrast- Enhanced MRI in Prostate Cancer Diagnosis and Management, AJR Am J Roentgenol. Vol. 198(6). DOI: 10.2214/AJR.12.8510, 2012
- VOG 13 Vogl, T., et al.: Thermal ablation therapies in patients with breast cancer liver metastases: A review, European Radiology, Vol. 23(3), DOI: 10.1007/s00330-012-2662-4, 2013
- WAL 10 Walter, D. R. and Husty, M. L.: On Implicitization of Kinematic Constraint Equations. Machine Design & Research, 26:132–151 (2010).
- WEI 11 Wei XJ, Tong KY, Hu XL: The responsiveness and correlation between Fugl-Meyer Assessment, Motor Status Scale, and the Action Research Arm Test in chronic stroke with upper-extremity rehabilitation robotic training. Int J Rehabil Res, vol. 34(4):349–356 2011
- WIK 18 [33] Wikipedia, [https://en.wikipedia.org/wiki/ Anatomical_terms_of_location](https://en.wikipedia.org/wiki/Anatomical_terms_of_location), accessed on 04/11/2016
- YAC 12 Yacoub, J., Verma, S., Moulton, J.S., Eggner, S., Oto, A. Imaging-guided Prostate Biopsy: Conventional and Emerging Techniques, RadioGraphics 32:819–837, 2012
- YAD 16 Yadav, R.K., Sharma, R., Borah, D., Kothari, S.Y., Efficacy of Modified Constraint Induced Movement Therapy in the Treatment of Hemiparetic Upper Limb in Stroke Patients: A Randomized Controlled Trial., J Clin Diagn Res. vol. 10(11):YC01-YC05. 2016
- YAN 18 Yang, C., Xie, Y., Liu, S., Son, D., Force Modeling, Identification, and Feedback Control of Robot-Assisted Needle Insertion: A Survey of the Literature, Sensors, 18(2): 561, 2018
- YOO 15 Yoo, D. H., Kim, S. K., Effects of upper limb robot-assisted therapy in the rehabilitation of stroke patients, J. Phys. Ther. Sci. vol. 27: 677-679, 2015